DUPLICATE ALSO

Advanced Lectures 1988

The physics and dynamics of the climate system

Part 1

LONDON, METEOROLOGICAL OFFICE.
Advanced Lectures 1988

The physics and dynamics of the climate system.
Part 1.

00211088 551.583 FG2
551.588
551.513.1

ORGS UKMO A

National Meteorological Library
FitzRoy Road, Exeter, Devon. EX1 3PB

uarters, Bracknell

DUPLICATE ALSO

METEOROLOGICAL OFFICE
152898
23 SEP 1988
C
LIBRARY

Advanced Lectures 1988

The physics and dynamics of the climate system Part 1

P.R. Rowntree

S.J. Foreman

H. Cattle

J.F.B. Mitchell

Permission to quote from this document must be obtained from the Principal, Meteorological Office College, Shinfield Park, Reading RG2 9AU

The physics and dynamics of the climate system
Part 1

1. **Introduction to the climate system**
   P.R. Rowntree
2. **The role of waves in the general circulation of the atmosphere and oceans. Part I: Wave characteristics**
   S.J. Foreman
3. **The role of waves in the general circulation of the atmosphere and oceans. Part II: Non-linear aspects**
   S.J. Foreman
4. **Atmospheric response to asymmetric forcing**
   P.R. Rowntree
5. **Observed atmospheric circulation**
   P.R. Rowntree

THE PHYSICS AND DYNAMICS OF THE CLIMATE SYSTEM

THE ROLE OF WAVES IN THE GENERAL CIRCULATION OF THE ATMOSPHERE AND OCEANS

PART I: WAVE CHARACTERISTICS

S J Foreman

Met O 20, Meteorological Office, Bracknell

ERRATA

Page 2.3: replace equation 2.3 with

$$\frac{\partial Q}{\partial y} = \beta - \frac{\partial^2 U}{\partial y^2} - \frac{1}{\rho}\frac{\partial}{\partial z}\left(\frac{f^2}{N^2}\rho\frac{\partial U}{\partial z}\right); \qquad (2.3)$$

Page 2.6: replace last line with

vertical (**large** scale orography) or decay with height (**short** scale orography).

Page 2.9: replace (2.14) with

$$\iiint |\psi^2|\left\{\chi^2 + \frac{(f/N)^2}{(2H)_s^2}\right\} - \frac{1}{2H_s}\left|\frac{\partial\psi}{\partial z}\right|^2 \, dV \; +$$

$$\iiint \frac{(\mathbf{U}.\mathbf{k} + ck)}{|\mathbf{U}.\mathbf{k} - ck|^2}|\psi|^2\{(-l,k).\nabla Q + \frac{\delta}{2fH_s}\left[f|\mathbf{U}.\mathbf{k} - ck|^2 + N(-l,k).\nabla h - \right. \qquad (2.14)$$

$$\left. - \mathbf{k}.(\partial\mathbf{U}/\partial z)\right]\} dV = 0$$

and the correct expression for B is:

$$B = (-l,k).\nabla Q + \frac{\delta}{2fH_s}\left[f|\mathbf{U}.\mathbf{k} - ck|^2 - N(l,-k).\nabla h - \mathbf{k}.(\partial\mathbf{U}/\partial z)\right]$$

Page 2.10: Second para of §2.3.1 second from last line.

The velocity must have a turning point within the region for instability to be possible.

THE PHYSICS AND DYNAMICS OF THE CLIMATE SYSTEM

THE ROLE OF WAVES IN THE GENERAL CIRCULATION OF THE ATMOSPHERE AND OCEANS
PART II: NON-LINEAR ASPECTS

S J Foreman

Met O 20, Meteorological Office, Bracknell

ERRATA

Page 3.2: replace second line of text with

slope **westwards** with increasing latitude ($l/k>0$) and northwards if ($l/k<0$) (fig.

Page 3.5: replace (3.3) with

$$ZAPE = \tfrac{1}{2}c_p \int \gamma[T']^2 \, dm \qquad (3.3)$$

Page 3.7: replace third from last line of first paragraph with

levels momentum was being transferred polewards, or up the potential vorticity

Page 3.8: the line above the summations should read

solutions of $\nabla^2\psi_q + a_q\psi_q = 0$) with amplitudes b_q results in the constraints

Page 3.12: The following figure caption should be substituted for that in the text.

Fig. 3.5 E-vectors for the northern hemisphere during winter 1979/80. Regions of convergence correspond to westerly acceleration of the mean flow by the eddies. From Hoskins *et al.* (1983).

PHYSICS AND DYNAMICS OF THE CLIMATE SYSTEM

Corrections and additions to Advanced Lectures 1, 4 and 5

Lecture 1

p. 1.5, 1.13 (i.e. page 1.5, line 13): REPLACE 'barotropically' BY 'inertially'.

p. 1.5, line before 1.3.2: REPLACE 'barotropic' BY 'inertial'.

p. 1.5, before 1.3.2, INSERT:

The condition for inertial instability is that the 'dynamical' zonally averaged zonal wind u_D satisfy:

$$u_D < u_M \equiv a\Omega \sin^2\theta / \cos\theta$$

(Williams, 1988) which, from eq. (1.3), demands of the temperatures that:

$$-\partial T_D/\partial\theta < 2a^2T_D\Omega^2\sin^3\theta / gH \cos\theta$$

This gives maximum gradients ΔT_D in K / 5° latitude as below.

Latitude	7½	12½	17½	22½
Maximum $\Delta T/5°$	.175	.81	2.2	4.7
Observed Dec-Feb 600 HPa ΔT	-.05	.75	1.85	3.1

Figures 1.3, 1.9(a): the Fig/Eq references in the captions are to the source text.

Lecture 4

p. 4.2, 5 lines from bottom: REPLACE '$\nabla^2\chi$' BY '$-\nabla^2\chi$'.

3 lines from bottom: INSERT AFTER 'oceanic' 'lower tropospheric'.

p. 4.3, line after equ. (4.1), REPLACE 'ζ' BY '(negative ζ)'.

p. 4.3-4.4: the last 13 lines of p. 4.3, starting 'One approach' should be moved to form a new paragraph after the first paragraph on p. 4.4.

p. 4.4, section 4.3, 1.4: INSERT AFTER '1985': ', shows the effects of warm anomalies, centred at the black spots, on the 200 HPa geopotential'

Figure 4.10 caption: REPLACE '9.20', BY '4.9';

Figure 4.18 caption: REPLACE '6.19-6.23', BY '4.18-4.20'.

Figures 4.19, 4.22: the Figure references in the captions are to the source text.

Lecture 5

p. 5.2, 1.4: REPLACE 'minima' BY 'maxima'.

p. 5.4, third paragraph, 1.2: REPLACE '. Despite' BY ', despite'.

1.3: REPLACE 'ocean,' BY 'ocean, because'.

p. 5.10, before 1.9 ['Wallace and...'], START NEW PARAGRAPH.

p. 5.12, 1.5: INSERT 'atmospheric' BEFORE 'storage'.

1.9: INSERT 'from observations' AFTER 'storage in the ocean'.

p. 5.13, 6th line from bottom: INSERT 'as calculated from the model' AFTER 'terms'.

p. 5.14, section 5.5: REPLACE 'P_z' BY 'P_M' AND 'K_z' BY 'K_M'.

THE PHYSICS AND DYNAMICS OF THE CLIMATE SYSTEM

INTRODUCTION TO THE CLIMATE SYSTEM

P R Rowntree

Met O 20, Meteorological Office, Bracknell

1.1 INTRODUCTION

The climate system can be regarded as consisting of the interacting atmosphere, hydrosphere, cryosphere, lithosphere and biosphere. In the hydrosphere we consider the ocean, water in lakes and rivers on land, and water within the soil. The cryosphere includes the sea-ice on the ocean, land-ice in the form of glaciers and icecaps, and water frozen in the soil both on a seasonal basis and perennially in permafrost regions. Of the lithosphere, we should include the soil to a sufficient depth to include thermal and hydrological interactions on the timescales we are considering, and also, if timescales are long enough, rises and falls of the mantle. Most of the biosphere is relevant on the longest timescales, even the chemical and biological processes in the deep ocean (and the word is perhaps too narrow as it should include mankind's bricks and concrete!)

These lectures will not be as wide-ranging as this. There is no precise restriction to timescales but, typically, we shall confine ourselves to consideration of the parts of the climate system necessary for understanding its present state and its variations for a few thousand years into the past and a hundred years or so into the future (roughly, this corresponds to the present capabilities of climate models.) This allows us to omit considerations of changing mantle heights, expanding icesheets and radically altered atmospheric composition, except as we may prescribe them. Vegetation changes are not modelled, though they may be prescribed. We do include simple changes in soil moisture, sea-ice and snow cover and detailed modelling of ocean temperatures.

In this first lecture, the radiative forcing of climate and the response of symmetric atmospheres to this forcing will be considered, leading to an appreciation of the need for transports of energy. The second and third lectures will investigate some of the mechanisms both for achieving these energy transports and for satisfying other requirements of the atmosphere and ocean circulation systems. Lectures 4 and 5 will review both theories and observations relevant to the atmospheric general circulation. The sixth and seventh lectures are concerned with the ocean - its forcing and the observed circulation - and

the eighth considers some of the longer timescale aspects of climate and climate change. Finally, lectures 9 and 10 review the simulation of climate and climate change, with particular emphasis on the effects of increasing carbon dioxide.

1.2 RADIATIVE FORCING AND HEAT BALANCE

1.2.1 Radiation

It is possible to conceive of an atmosphere in which there are no meridional transfers of heat and a radiative equilibrium is maintained. In the vertical this requires that the radiative equilibrium state is convectively stable. There would be no net radiative heating rates. This radiative equilibrium is easily determined using a one-dimensional (1-D) model with the convective parametrization omitted (Fig 1.1) (from Manabe and Strickler, 1964) The equilibrium lapse rate turns out to be highly unstable to convective perturbations at lower levels. By imposing a maximum lapse rate of 6.5K/km, close to the moist adiabatic lapse rate, and allowing for clouds (Fig 1.2), a vertical structure similar to the observed global mean is obtained.

The structure is also realistic in the stratosphere where radiative equilibrium does obtain. Absorption of solar radiation (Fig 1.3), mostly due to ozone, near the top of the stratosphere together with cooling (most importantly by CO_2 though water vapour and ozone also contribute) maintain a stable lapse rate. The troposphere is different because of the presence of gases (water vapour and carbon dioxide) which are more important in the longwave than the solar, and of a surface which absorbs a large fraction of incident solar radiation - i.e. there is heating at the base in contrast to the stratosphere which is heated at the top. It is a common oversimplification to say that the atmosphere cools because of longwave radiation and the surface is heated by solar radiation. A quantitative study shows that there is substantial solar heating of the troposphere (Fig 1.4) (from Mason (1976)), mainly through water vapour though again CO_2 is significant.

Fig 1.4 contains much instructive information which, though global, can be usefully interpreted in a local context. For example, it reminds us of the surface energy balance equation

$$R_{N*} - G = H + LE$$

where R_{N*} is the surface net radiation and H and LE are the upward sensible and latent surface heat fluxes. G is the downward heat flux through the surface which, in the annual mean, vanishes over land apart from geothermal heat fluxes ($<<0.1$ W m^{-2}) but, over the ocean, equals the heat flux divergence by ocean

currents. The total atmospheric dry static energy ($c_pT + gz$) gain is

$$R_{NT} - R_{N*} + H + LP = R_{NT} + L(P-E) - G$$

where P is precipitation and R_{NT} is the net radiation at the top of the atmosphere. This must be balanced by lateral export of energy. Taking the more broadly defined moist static energy ($m \equiv gz + c_pT + Lq$), the moisture convergence (P-E) drops out and we see that regions with positive (negative) (R_{NT}-G) must export (import) energy. As discussed later, in the atmosphere this export is mainly either by vertical circulations or by eddies, or in oceanic regions the ocean currents may achieve the required transfers.

The spectral structure of incoming and outgoing solar and outgoing longwave radiation is instructive (Fig 1.5) (from Barry and Chorley, 1976). The solar spectrum is much eroded before it reaches the surface due to the water vapour absorption in the infra-red beyond 0.9μm. The longwave spectrum is better shown by actual observations from space (Fig 1.6) (from Houghton, 1977). Particularly evident in the longwave are the strong minima corresponding to CO_2, indicating that the emissions at those wavelengths are from the low temperature upper atmosphere rather than the lower troposphere responsible for the emission in the window region near 11μm (900 cm^{-1}). Note that over Antarctica, the CO_2 bands lead to maxima in the spectrum because of the low surface and tropospheric temperatures.

In the solar, both the quantity and the spectral signature of the outgoing flux is strongly affected by the nature of the reflecting surface. Clouds tend to reflect most strongly in the visible and absorb most in the near infrared, where there are strong liquid water and water vapour absorption bands. Land surface spectral reflectivity depends on the nature of the surface and the zenith angle h_o (Fig 1.7) (from Kondratyev, 1982). Snow reflects most in the visible and soil has little spectral variation, whereas green plants have low reflectivity in the visible, with a weak maximum near their colour, and a marked maximum in the very near infrared, where albedos of 30-40% are common. It is these features which have led to the development of vegetation indices, based on this contrast between the visible and the near infrared reflectivities as seen from space (Fig 1.8).

1.2.2 Heat balance

For a vertical column of atmosphere and surface, the heat balance in the absence of horizontal motions is:

$$C dT/dt = (1-\alpha)\, S - \sigma\, T_E^4 = (1-\alpha)\, S - \varepsilon\, \sigma\, T_*^4 \qquad (1.1)$$

Here S is the average solar radiation at the top of the atmosphere (1372 ÷ 4 = 343 W m^{-2}), α is the planetary albedo, ε is an effective emissivity for the black body radiation at surface temperature T_*, and σ is Stefan's constant. T_E, the effective emitting temperature is on average over 30K lower than T_* because of the emission from clouds at temperatures below T_*, and because of the emission from greenhouse gases, notably water vapour and carbon dioxide (Fig 1.6). In the presence of dense high cloud, T_E is close to the cloud temperature while, for a very dry, cloudfree atmosphere, it approaches the surface temperature; more typically it is a middle troposphere temperature. With appropriate choices of α, S and T_E, this equation represents the global heat balance and forms the basis of simple zero- or one-dimensional climate models.

Note that the above equation is for atmosphere and surface. By surface we mean here the medium which interacts with the atmosphere on relevant timescales. Over land even for timescales of a year, this is a layer only a few metres deep, with heat capacity similar to that of the atmosphere. For the ocean, even for timescales of a few days, the layer interacting with the atmosphere is tens of metres deep except perhaps during sunny calm periods in summer while, for the annual timescale, it is commonly at least 50 metres deep, with heat capacity twenty times that of the atmosphere; in regions such as the western north Atlantic and Pacific, exposed to strong winter cooling, it is several hundred metres deep. This has interesting implications for the transient response of climate to perturbations of the forcing, with a more rapid response expected in regions of relatively low thermal capacity.

1.3 GENERAL CIRCULATION ON A SYMMETRIC EARTH

1.3.1 Latitudinal temperature structure

We have seen that radiative equilibrium is not a possible vertical structure for the atmosphere. Is a global atmosphere with a horizontal structure determined by radiative equilibrium unstable to horizontal perturbations? The analysis by Stone (1978) is an instructive treatment of this question. Fig 1.9(a) shows his comparison of three temperature gradients calculated for annual mean conditions:

(a) radiative equilibrium mid-tropospheric temperature gradients calculated from (1.1):

$$T_E = (S\,(1-\alpha)\,/\sigma)^{1/4}$$

(b) critical gradients for baroclinic instability which are proportional to β/f, where f is the coriolis parameter and β is df/dy, so that $\beta/f \propto \cot\theta$, θ being latitude. (Baroclinic and barotropic instability are discussed by Dr Foreman in Lectures 2 and 3)

(c) observed 600 HPa temperature gradients for the northern hemisphere.

The observed temperature gradients are very similar to the critical gradients north of about 40°N and well below the radiative equilibrium gradients at all latitudes. The same calculations for each of the seasons give similar results except that in summer the radiative equilibrium gradients are small south of 40°N. An interesting question is why the observed gradients are well below radiative equilibrium at low latitudes. As discussed by Williams (1988), winds satisfying the geostrophic thermal wind balance for radiative equilibrium temperatures are barotropically unstable, having negative absolute vorticity, at low latitudes. At height H, this 'radiative' geostrophic zonal wind u_E is, relative to the wind at the surface:

$$u_E = \frac{-gH}{aT_0 f}\frac{\partial T_E}{\partial \theta} \qquad (1.2)$$

using the approximation $\delta\varphi = gH\,\delta T/T_0$, where φ is geopotential, T_0 is a global mean temperature and a is earth's radius. The condition for the absolute vorticity $(f-(\partial u/\partial\theta)/a)$ to be positive

$$\partial u_E/\partial\theta < fa \qquad (1.3)$$

leads, using (1.2) to

$$\frac{gH}{T_0}\left(\frac{\beta}{f^2}\frac{\partial T_E}{\partial\theta} - \frac{1}{af}\frac{\partial^2 T_E}{\partial\theta^2}\right) < fa \qquad (1.4)$$

It is not obvious how to obtain any general constraint for the zonal mean flow from (1.4), as the two terms tend to oppose each other. It is however clear for spatially varying flows in general that large temperature gradients will induce barotropic instability in some part of the flow.

1.3.2 Mechanisms for poleward transports

It is evident from the above discussion that heat transport is required if the radiative equilibrium gradient becomes large, especially in low latitudes in view of the strong dependence on f in equ. (1.4). Because baroclinic instability criteria relate temperature gradients to β/f and minimum eddy scale to $1/f$ (e.g. Williams, 1988) and so are less relevant at low latitudes (Fig 1.9), this heat transfer is mostly achieved in the tropics by vertical circulations, in which energy is converted from the latent to the sensible form through condensation, and then to potential energy, in the upward branch, with conversion back to

sensible heat in the downward branch. In these conversions, the total energy m is conserved apart from sources and sinks, mainly surface fluxes and radiative cooling.

The actual vertical profile of m in the tropics has a minimum in the middle troposphere (Riehl, 1979, p. 70), and deep convection conveys energy from the shallow near-surface inflow layer to a shallow outflow layer just below the tropopause where the environmental m is close to its surface value. Held and Hoskins (1985, p.9) found that m/c_P in the outflow layer exceeded its inflow value by about 15K in each of three experiments with different solar forcing. The intensity of the minimum in m and the height of the outflow both rose with the solar constant (Fig 1.10). They were unable to explain the value of 15K.

It is clear from the above discussion that the real atmosphere is not in radiative equilibrium at most latitudes. The extent of the actual disequilibrium is shown in Fig 1.11 (from Winston et al, 1979). The mechanisms for the poleward transfer of heat required to make good this radiative imbalance are mainly either the vertical circulations just discussed or, where temperature gradients are large enough, baroclinic eddies.

Williams (1988) has investigated the relative importance of these mechanisms by simulating the general circulation of a symmetric earth for a wide range of rotation rates. The meridional circulations he obtained (Fig 1.12) show a gradual contraction of the Hadley cell from near-global extent at small rotation rates ($\Omega_* = \Omega/\Omega_E$ where Ω_E is the actual earth rotation rate). to much narrower than observed for Ω_* of 4 and 8. This is as expected from the strong dependence on f in equ. (1.4). At low rotation rates, baroclinic instability is inhibited either by the requirement that eddy scales are proportional to 1/f and so become too large to be effective on earth, so allowing large temperature gradients (Fig 1.13) or, for very small Ω_*, by the weak temperature gradients allowed by equ. (1.4), all the heat transfer then being carried by the Hadley cell. These results are consistent with observations of planetary circulations; for example, Venus rotates very slowly and has a very extensive Hadley cell, while Jupiter and Saturn rotate faster than Earth and their circulations have a more banded structure. Since the eastward flow accelerates poleward throughout the Hadley cell regime, the subtropical jet forms near its poleward limit, near 30° latitude for $\Omega_*=1$ (Fig 1.14). The wind strengths tend to increase with decreasing rotation rate for a given temperature gradient, leading to the intense jets of the small Ω_* cases.

1.3.3 Interactions between eddies and the mean meridional circulation

At the observed rotation rate, the near-surface winds are easterly in the Hadley cell region to a much greater extent than for the stronger Hadley cell found with very low rotation rates (Fig 1.12). This is because of the effect of the baroclinic eddies, as discussed by Williams (1988, p 237). As illustrated in the upper two panels of Fig 1.15, these eddies generate poleward heat fluxes peaking at 40-70°N, as is necessary to remove the baroclinic instabilities, and also poleward momentum fluxes at a somewhat lower latitude (20-40°N). These momentum fluxes are concentrated in the upper troposphere and produce changes in zonal wind u as shown, so tending to weaken the vertical shears on their equatorward side and strengthen them to poleward. Combined with the effect of the heat fluxes which are weakening the temperature gradients in middle latitudes and strengthening them in the subtropics - i.e. the opposite of what is required for consistency with the momentum changes! - the eddies thus tend to destroy the thermal wind balance. Vertical circulations must be generated to maintain the balance; what is required is shown in the lower panel of the figure: the indirect (i.e., with equatorward heat transport) circulation in middle latitudes seen in Fig 1.12, called the Ferrel cell, and a strengthening of the Hadley cell.

One can imagine a midlatitude circulation driven largely by the Ferrel cell - misleading of course in view of the role of the eddies in generating it but perhaps instructive nonetheless. Near the surface, the divergence below the descent in the Ferrel cell helps to maintain the subtropical anticyclones while the convergence below its ascending branch likewise contributes to the positive vorticity of the subpolar low; the associated pressure gradients support the westerlies generated at low levels through conservation of angular momentum by the surface poleward flow, while the surface drag removes eastward momentum to maintain the momentum balance against the dominating contribution (the generation of eastward momentum by the convergence of the eddy momentum flux in the upper troposphere). We shall return to the poleward fluxes and heat and momentum balances in Lecture 5. The mechanisms by which the baroclinic eddies transport heat and momentum will be discussed in Dr Foreman's lectures.

1.4 A SIMPLE CLIMATE MODEL

We can study the transient and equilibrium responses to perturbations of forcing by using a simple 1-D model based on equ (1.1). We shall consider deviations from an equilibrium state, following the analysis by Schlesinger (1986). The analysis is conveniently made in terms of the net radiation at a level where

other non-radiative fluxes such as largescale or convective motions are small. This could be the tropopause or the top of the atmosphere though the latter has some disadvantage if it is the tropospheric heat balance which is being studied, since the stratospheric and tropospheric responses may be in opposite senses as in the case of CO2. At this level, the net flux N may be written

$$N = N(\underline{E}, T_s, \underline{I}) \qquad (1.5)$$

where $\underline{E}$ and $\underline{I}$ are vectors representing external variables (e.g. solar intensity, earth's orbit) and internal variables (e.g. water vapour content, surface albedos) respectively and T_s is the temperature of the surface layer.

The effect of a perturbation ΔQ on N may be written as

$$\Delta N = \Delta Q + \underbrace{\frac{\partial N}{\partial T_s}}_{[-G_o^{-1}]} \Delta T_s + \underbrace{\left\{\sum_J \frac{\partial N}{\partial I_J} \frac{\partial I_J}{\partial T_s}\right\}}_{[F]} \Delta T_s \qquad (1.6)$$

Then, if there are no internal feedbacks, at equilibrium ($\Delta N = 0$)

$$\Delta T_s = G_o \Delta Q \qquad (1.7)$$

We can estimate G_o by considering the unperturbed equilibrium:

$$N = S(1-\alpha) - \varepsilon \sigma T_s^4 = 0 \qquad (1.8)$$

Then
$$-G_o^{-1} \equiv \partial N/\partial T_s = -4\varepsilon\sigma T_s^3 = -4S(1-\alpha)/T_s \qquad (1.9)$$

(note that this assumes that ε is constant; calculations by Manabe and Wetherald (1967, Fig 7) for radiative convective equilibrium with fixed absolute humidity indicate errors in this assumption of less than 1% for a 25% change in solar constant)

Taking observed values, $S \approx 343$ W m^{-2}, $\alpha_p \approx 0.3$ and $T_s \approx 288$K, we obtain $G_o = 0.3$ K (W m^{-2})$^{-1}$. For the particular case of doubling of CO_2, the increase of downward flux at the tropopause is ≈ 4 W m^{-2}, so the response in the absence of internal feedbacks or zero feedback response is

$$(\Delta T_s)_o = G_o \Delta Q \cong 1.2K$$

With internal feedbacks, at equilibrium, (1.6) gives

$$\Delta T_s = \frac{\Delta Q}{G_o^{-1} - F} = \frac{G_o \Delta Q}{1 - G_o F} = \frac{(\Delta T_s)_o}{1-f} \qquad (1.10)$$

where $f = G_o F$ is Schlesinger's feedback factor (not to be confused with the dynamic use of f earlier in this lecture).

A positive feedback is obtained with $0 < f < 1$. The feedback parameter f may be estimated from experiments with 3-D or general circulation models (GCMs). Recent GCM results with interactive cloud suggest that $f \cong 0.7$, with an equilibrium

warming for a doubling of CO_2 of 4K. Note however that the models do not yet include all relevant feedbacks. (In Advanced Lecture 10, Dr. Mitchell uses a similar approach in terms of a feedback parameter λ where $\lambda = G_0^{-1}\ (1-f)$)

Of the contributions to f in the GCMs, the largest ($\approx$0.4) is from water vapour combined with changes in lapse rate, clouds contribute 0.1 to 0.2 and snow/ice feedback about 0.1. An interesting application is to the case of a decreasing solar constant S. As S decreases, the extent of snow (and ice) would increase and hence also the length of the snowline and the area of new snow generated by a given cooling if the meridional temperature gradient near the snowline were unchanged. Thus the snow/ice contribution f_I to f would increase. Only a quadrupling of f_I would be needed to create an unstable climate with f$\approx$1 if other feedbacks remained unchanged. GCM experiments do show an increase in sensitivity as the icecap becomes larger (Spelman and Manabe, 1984). (see Held et al (1981) for a discussion of climate sensitivity for a low order spectral GCM) (see also the final lecture in the Climate of the World series)

A predictive equation for temperature in this system is, from (1.6):

$$C\partial(\Delta T_s)/\partial t = \Delta Q - G_0^{-1}\ (1-f)\ \Delta T_s \qquad (1.11)$$

This may be integrated with prescribed time-dependent ΔQ. The right hand side is the perturbed top of the atmosphere or tropopause flux, and may be taken as the upper boundary condition of a multi-layer model of arbitrary vertical resolution. If the seasonal cycle is not to be represented, it is sufficient for illustrative purposes to regard T_s as the temperature not only of the surface but also of the seasonally well mixed layer of the ocean, about 100m in depth. As discussed by Schlesinger et al (1985), analysis of coupled GCMs and of the observed penetration of bomb-produced tritium and C_{14} into the ocean both indicate that a good approximation to the global mean surface temperature change can be obtained with vertical mixing in the deeper ocean represented by a diffusive formulation using a diffusion coefficient of 2.25-2.5 $m^2\ s^{-1}$.
(N.B. It must be stressed that this is only a first approximation to the transfer of heat into the ocean; for further discussion see Bryan and Sarmiento (1985)).

A simple climate model with these assumptions and structure has been used to study the transient response to increasing trace gas concentrations (e.g. CO_2, CH_4 and CFCs). The response for a sudden doubling of CO_2 is compared with the Schlesinger et al (1985) results in Fig 1.16, using f=0.58 (their estimate of the

feedback), a mixed layer depth of 125m, and κ=2.25 $m^2 s^{-1}$ in a 9 layer ocean. As found by Schlesinger et al, this value of κ gives a good simulation of the surface change. However, the transfer of heat to lower levels is deficient, probably because of the neglect of deep convection in higher latitudes. In Lecture 10, Dr Mitchell shows the response of this model to a transient increase of CO_2.

1.5 REFERENCES

Barry, R. G. and Chorley, R.J., 1976, Atmosphere, weather and climate. Methuen, London, 432 pp.

Bryan, K. and Sarmiento, J. L., 1985, Modeling ocean circulation. In: Issues in atmospheric and oceanic modeling; Part A: Climate Dynamics. Advances in Geophysics, Vol. 28, Academic Press, pp. 433-459.

Held, I. M. and Hoskins, B. J., 1985, Large-scale eddies and the general circulation of the troposphere. ibid, 3-31.

Held, I.M., Linder, D. I. and Suarez, M. J., 1981, Albedo feedback, the meridional structure of the effective diffusivity, and climatic sensitivity: Results from dynamic and diffusive models. J Atmos Sci, 38, 1911-1927.

Houghton, J. T., 1977, The physics of atmospheres. Cambridge University Press, 203 pp.

Kondratyev, K. Ya., Korzov, V. I., Mukhenberg, V. V. and Dyachenko, L. N., 1982, The shortwave albedo and the surface emissivity. In 'Land surface processes in atmospheric general circulation models', Cambridge University Press, pp. 463-514.

Manabe, S. and Strickler, R. F., 1964, Thermal equilibrium of the atmosphere with a convective adjustment. J Atmos Sci, 21, 361-385.

Manabe, S. and Wetherald, R. T., 1967, Thermal equilibrium of the atmosphere with a given distribution of relative humidity. J Atmos Sci, 24, 241-259.

Mason, B.J., 1976, Towards the understanding and prediction of climatic variations. Quart J R Met Soc, 102, 473-498.

Riehl, H., 1979, Climate and weather in the tropics. Academic Press, 611 pp.

Schlesinger, M. E., 1986, Equilibrium and transient climatic warming induced by increased atmospheric CO_2. Climate Dynamics, 1, 35-51.

Schlesinger, M. E., Gates, W. L. and Han, Y.-J., 1985, The role of the ocean in CO_2-induced climate change: preliminary results from the OSU coupled atmosphere-ocean general circulation model. In: Coupled ocean-atmosphere models (Ed. J. C. J. Nihoul), Elsevier Oceanography Series, 40, pp. 447-478.

Spelman, M. J. and Manabe, S., 1984, Influence of oceanic heat transport upon the sensitivity of a model climate. J Geoph Res, 89, 571-586.

Stone, P. H., 1978, Baroclinic adjustment. J Atmos Sci, 35, 561-571.

Williams, G. P. 1988, The dynamical range of global circulations - I. Climate Dynamics, 2, 205-260.

Winston, J. S., Gruber, A., Gray, T.I., Varnadore, M. S., Earnest, C. L. and Mannello, L. P., 1979, Earth-atmosphere radiation budget analyses derived from NOAA satellite data June 1974-February 1978. NOAA, NESS, Washington, D.C.

WMO, 1985, The global climate system. World Climate Data Programme.

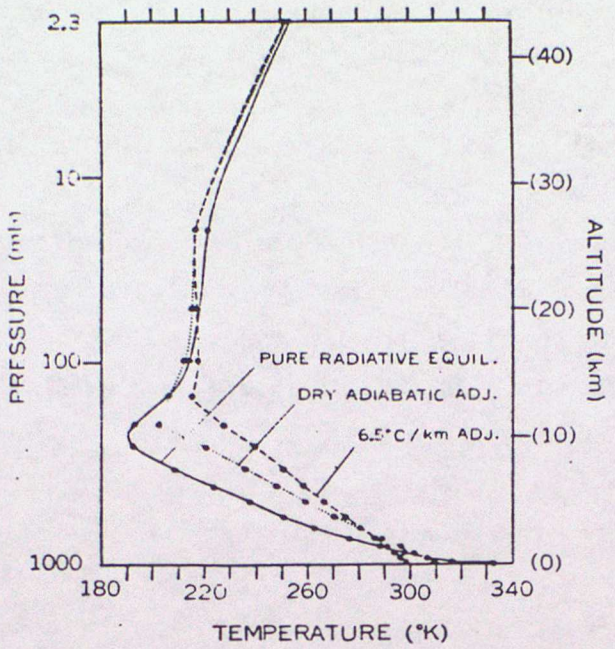

The dashed, dotted, and solid lines show the thermal equilibrium with a critical lapse rate of 6.5 deg km^{-1}, a dry-adiabatic critical lapse rate (10 deg km^{-1}), and pure radiative equilibrium.

Figure 1.1

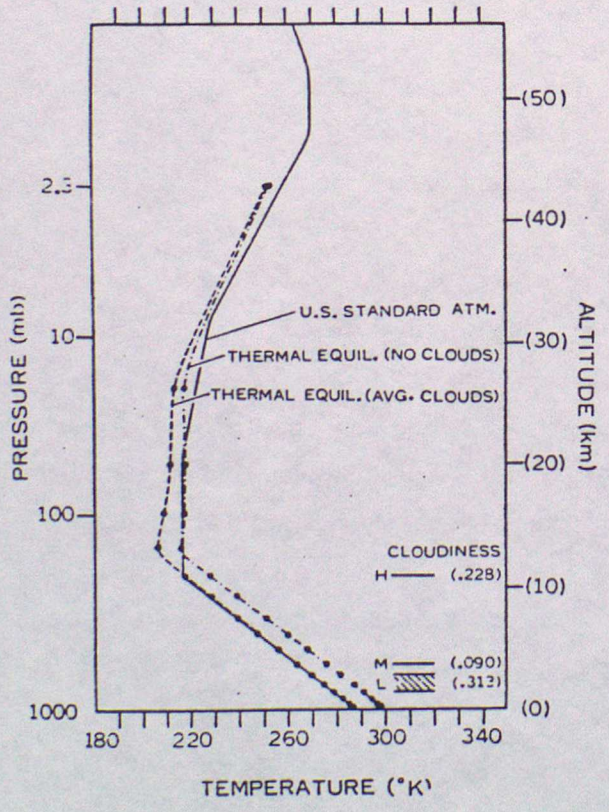

Dash-dotted and dashed lines show the thermal equilibrium of the atmosphere with and without cloudiness. The critical lapse rate for convection is 6.5 deg km^{-1}. The cloud amounts and cloud heights are shown on the right hand side. The solid line shows the U. S. Standard Atmosphere.

Figure 1.2

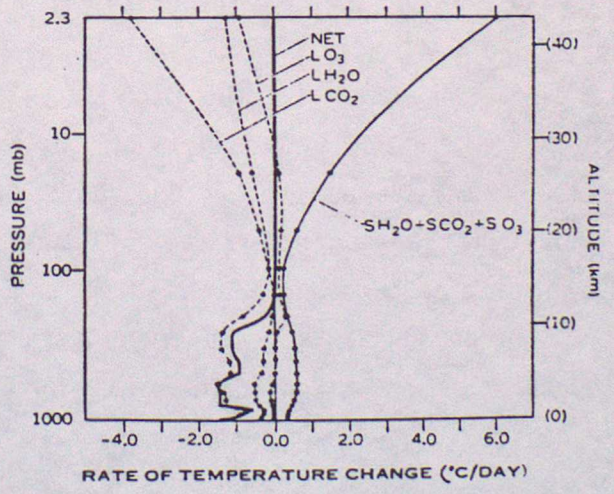

Vertical distributions of radiative balance components for the thermal equilibrium of the atmosphere with the average cloudiness shown in Fig. 7 "Net" means the net rate of temperature change due to all of these components.

Figure 1.3

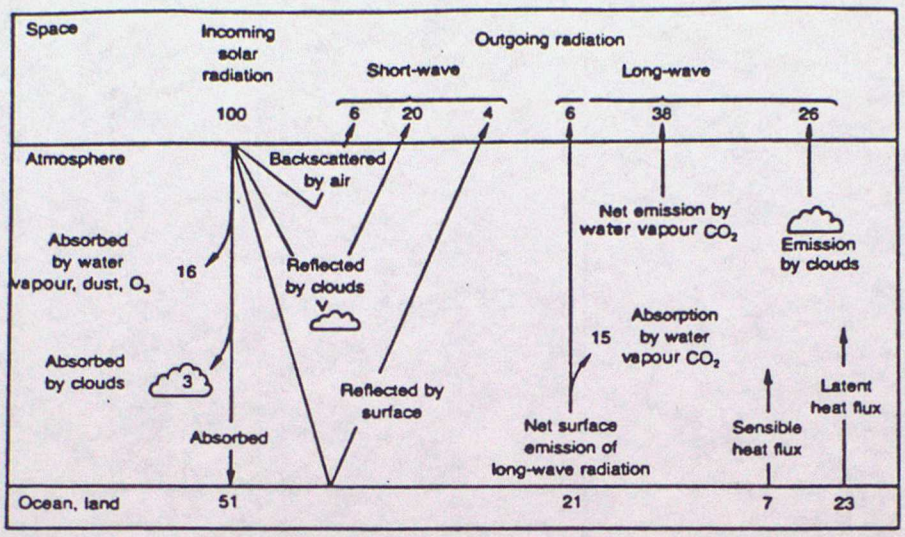

The radiation balance of the atmosphere–earth system showing the redistribution of the incoming solar radiation and the mechanisms by which these are effected. (From the US National Academy Report, 'Understanding Climatic Change', 1975.)

Figure 1.4

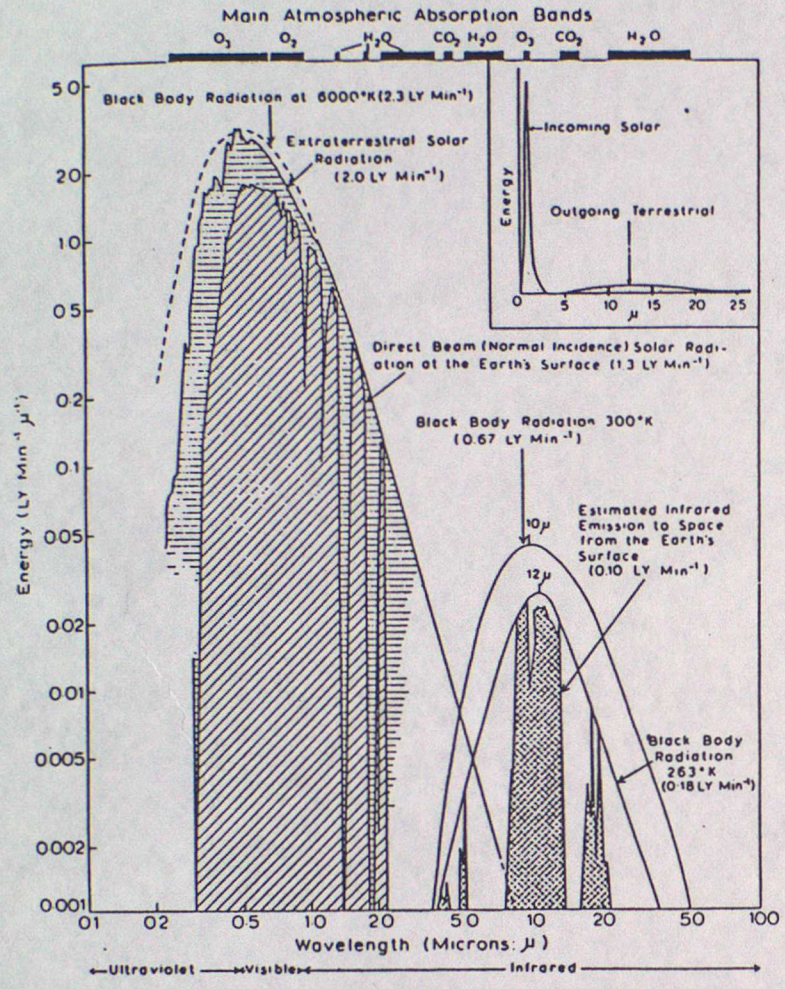

Spectral distribution of solar and terrestrial radiation, plotted logarithmically, together with the main atmosphere absorption bands. The black body radiation at 6000°K is that proportion of the flux which would be incident on the top of the atmosphere. The inset shows the same curves for incoming and outgoing radiation with the wavelength plotted arithmetically (*mostly after Sellers 1965*). (μ is now denoted as μm.)

Figure 1.5

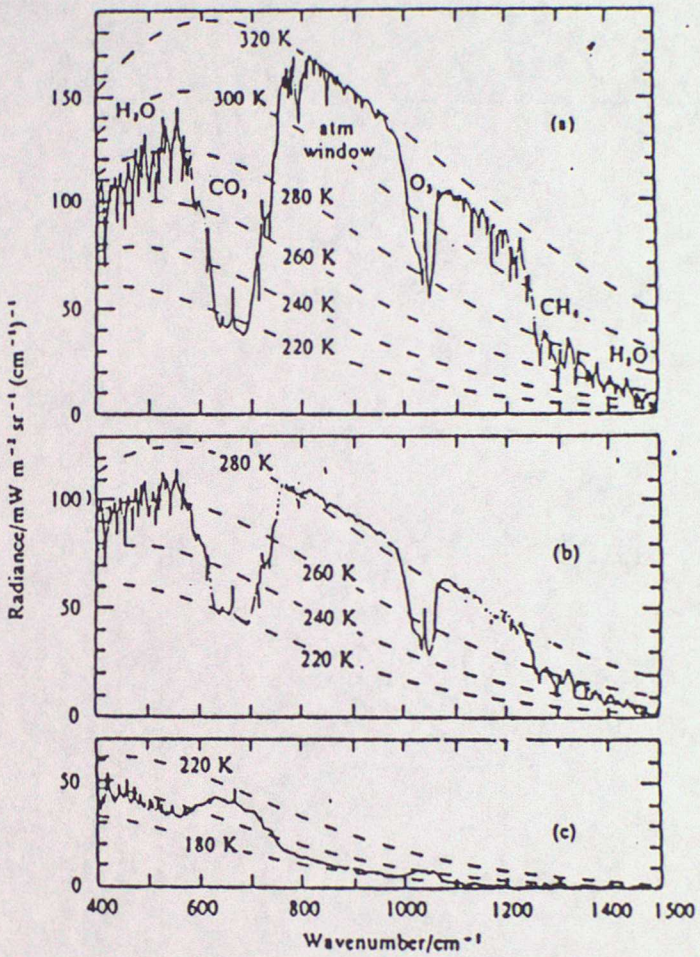

Thermal emission from the earth plus atmosphere emitted vertically upwards and measured by the infrared interferometer spectrometer on Nimbus 4, (a) over Sahara, (b) over Mediterranean, (c) over Antarctic. The radiances of black bodies at various temperatures are superimposed. (From Hanel *et al.*, 1971)

Figure 1.6

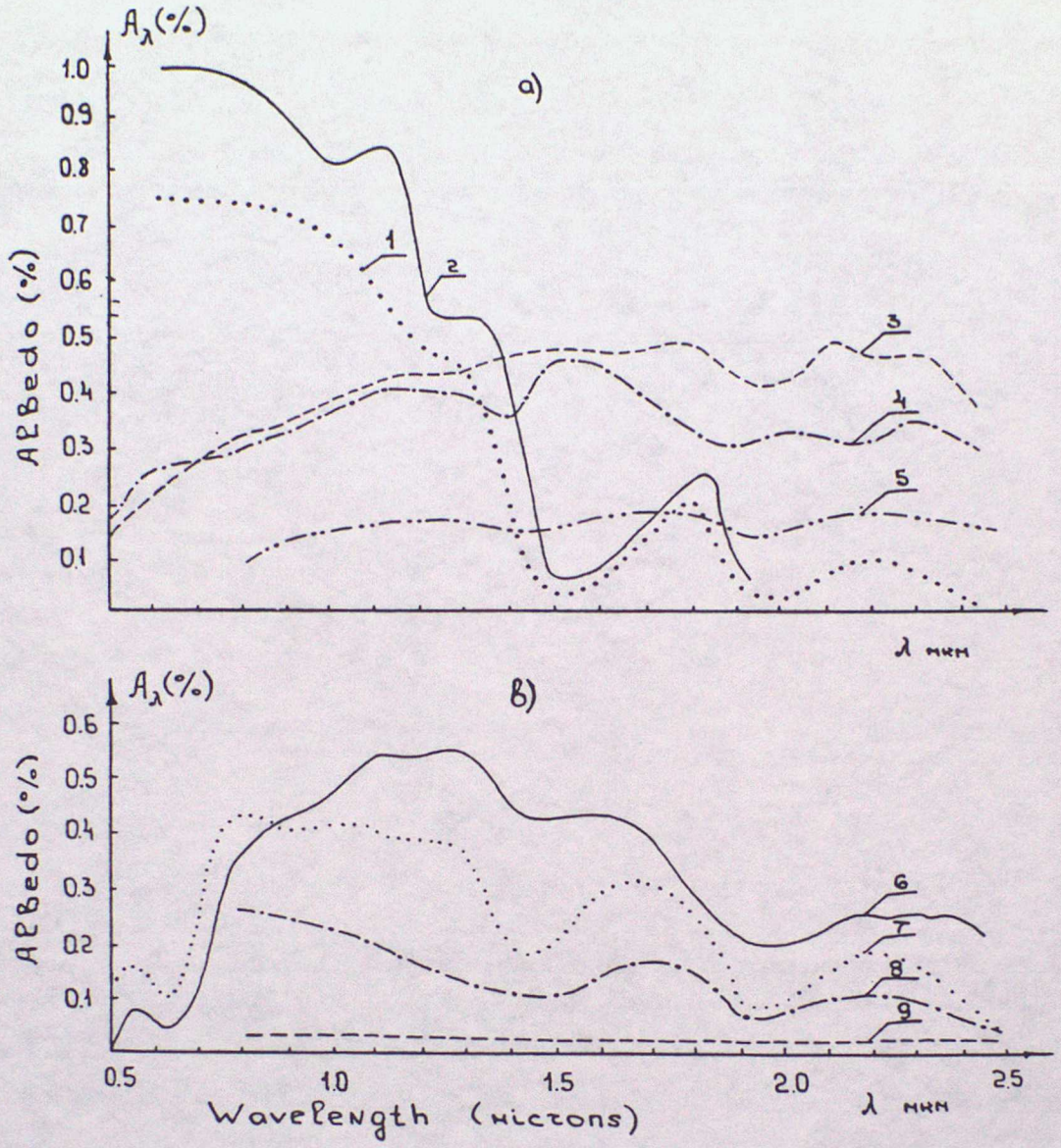

- The wavelength dependence of the spectral albedo for some natural formations:

1 - new snow, h_o = 20-25°
2 - snow cover
3 - sandy loam, h_o = 25-30°
4 - dry sand, h_o = 40-45°
5 - chernozem, sandy loam
6 - blossoming meadow. h = 40-45°
7 - green leaf
8 - green coniferous forest
9 - water surface

Figure 1.7

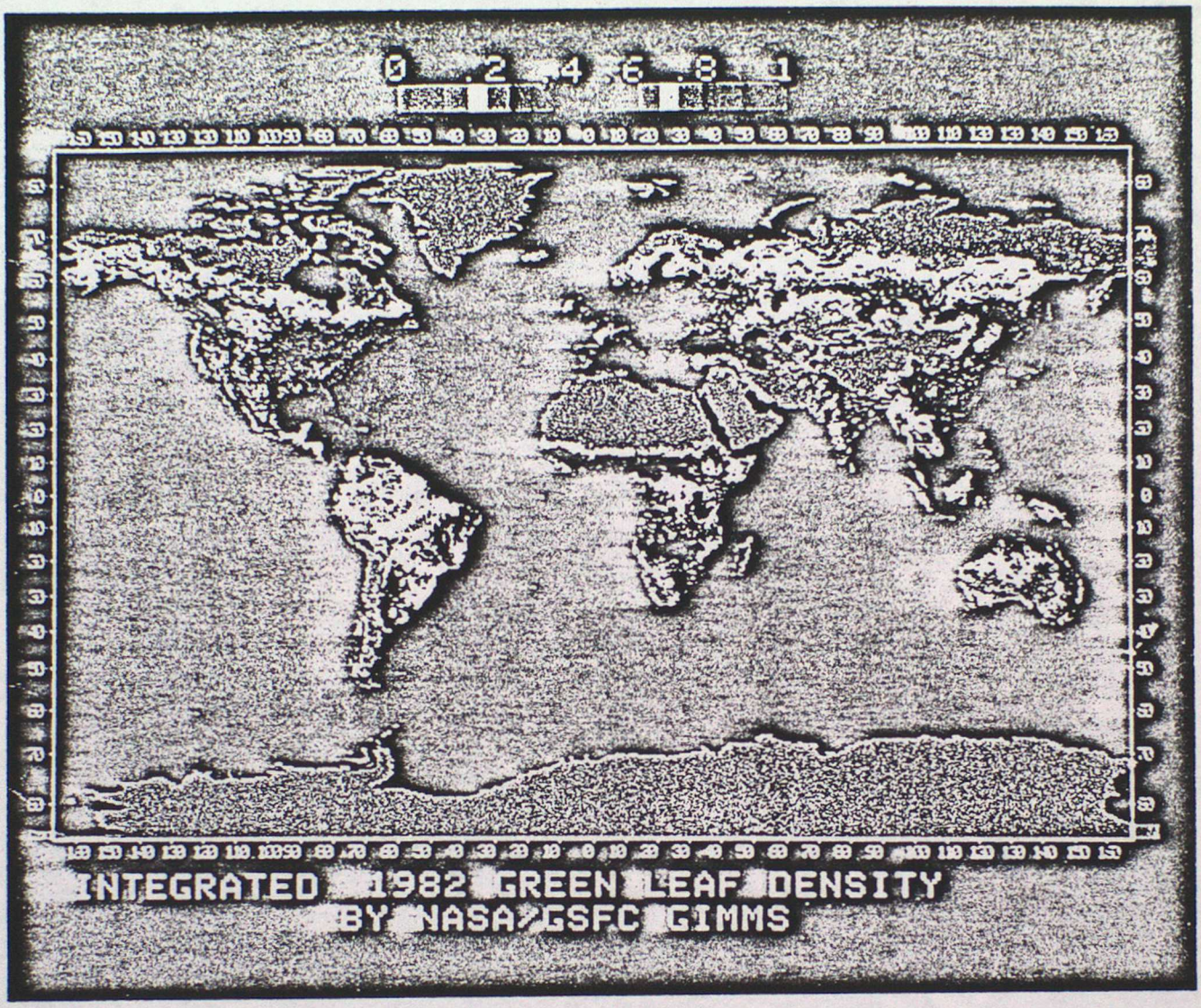

Figure 1.8: Vegetation index based on $(\alpha_1 - \alpha_2)/(\alpha_1 + \alpha_2)$, where α_1 and α_2 are reflectivities in the near infrared (near 0.7-0.75μm) and visible (about 0.6μm). Though some information is lost in the copying from the original colour picture (WMO, 1985), (the white areas over the tropical forests of Africa, South America and S.E.Asia and Indonesia have a value of about 0.7, whilst other white areas are just below 0.2), the figure still portrays well the asymmetries of the land surface. To some extent, these are forced by other asymmetries, such as the nearby warm water for western China, but also they force asymmetries in the climate as with the Sahara desert.

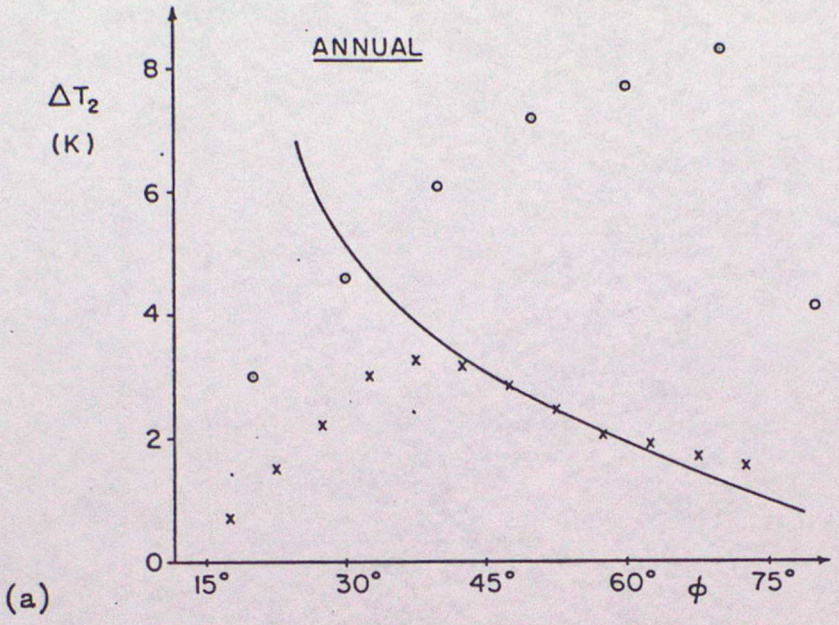

(a)

Various zonal mean meridional temperature gradients at 600 mb vs latitude, evaluated for annual mean conditions. The solid curve gives the critical gradient [Eq. (7)], the X's indicate the observed gradient and the O's indicate the radiative equilibrium gradient.

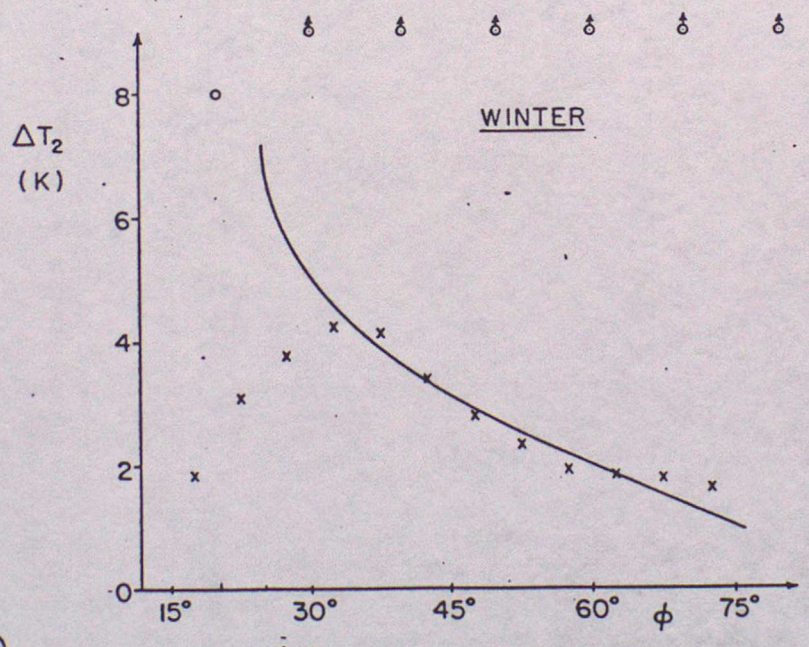

(b)

As in (a) except for winter mean conditions (December, January, February).

Figure 1.9

ΔT_2 is the temperature gradient in degrees Kelvin per 5° latitude

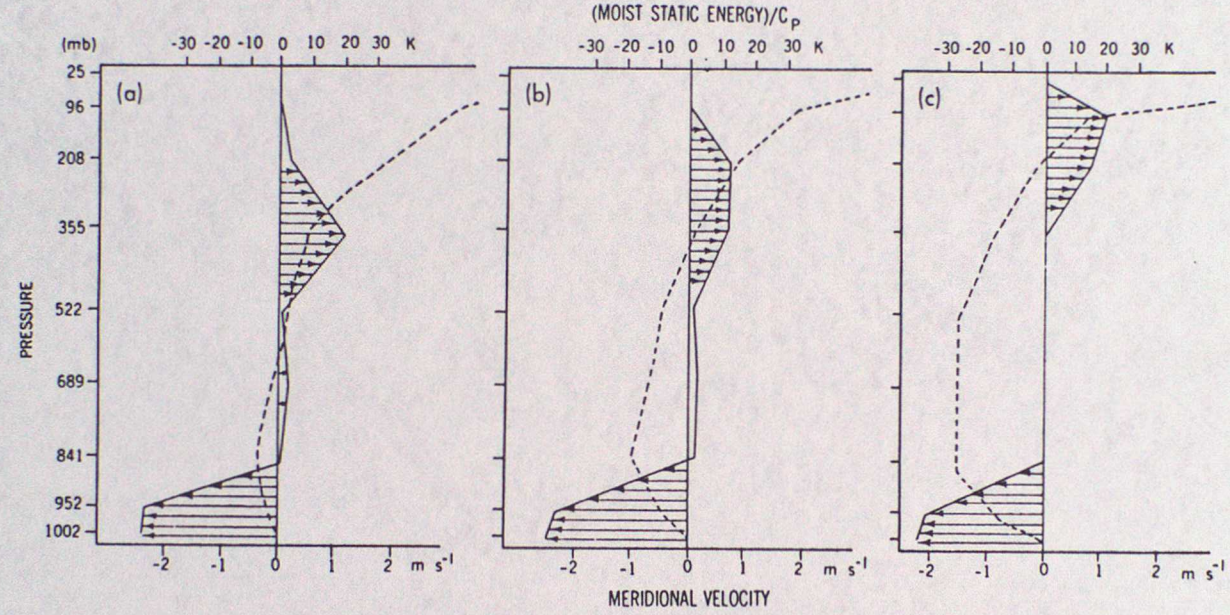

Meridional wind (arrows) and moist static energy profile $m(p)-m(p_s)$ as functions of pressure at the latitude of maximum mass transport in the Hadley cell, for three different values of the solar constant: (a) −10%, (b) 0%, (c) +10%.

Figure 1.10

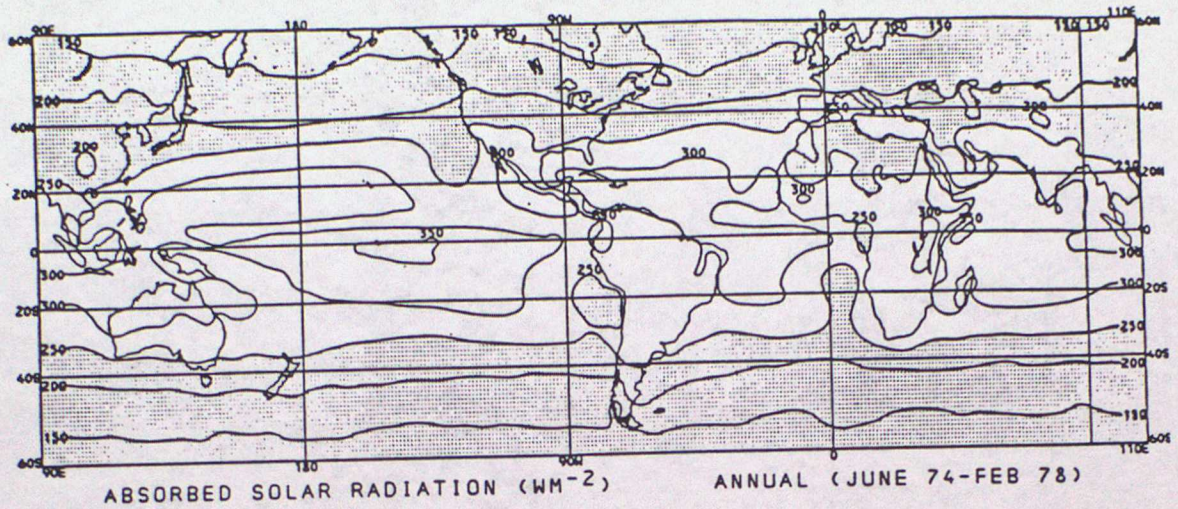

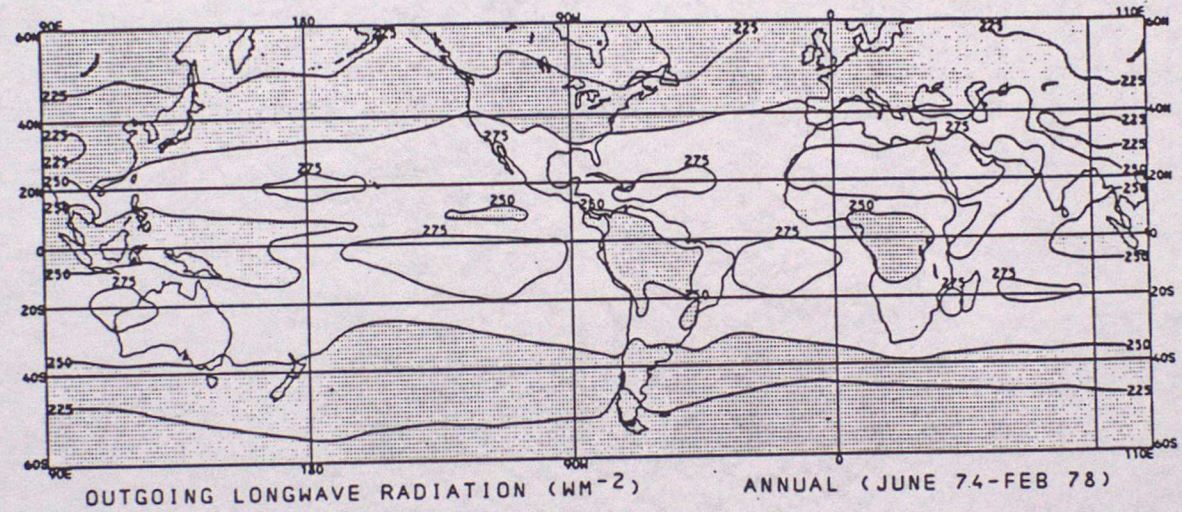

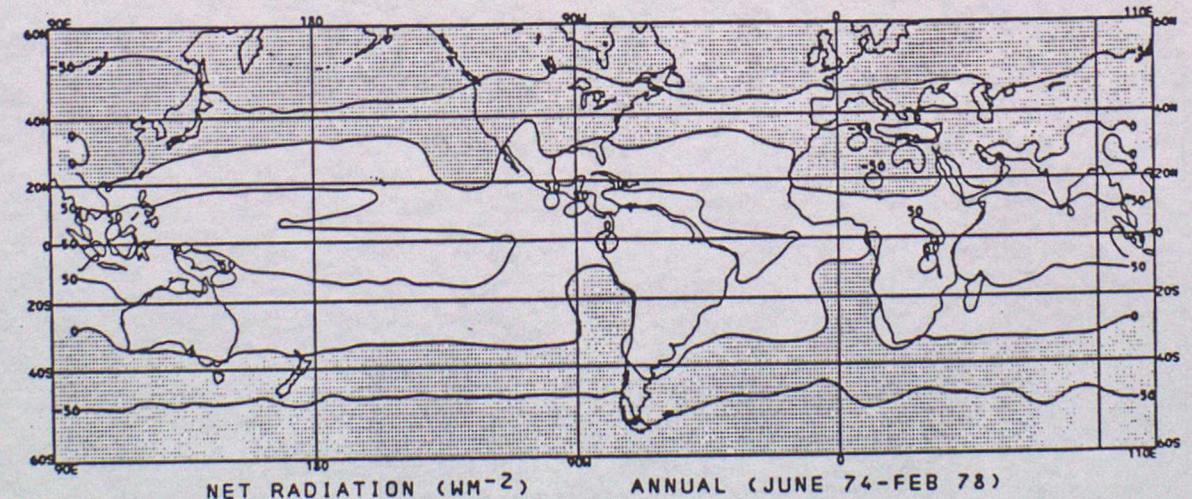

Figure 1.11 Annual-mean maps of absorbed shortwave, outgoing longwave and net radiation for the Earth-Atmosphere system, as observed from NOAA satellites between 1974 and 1978

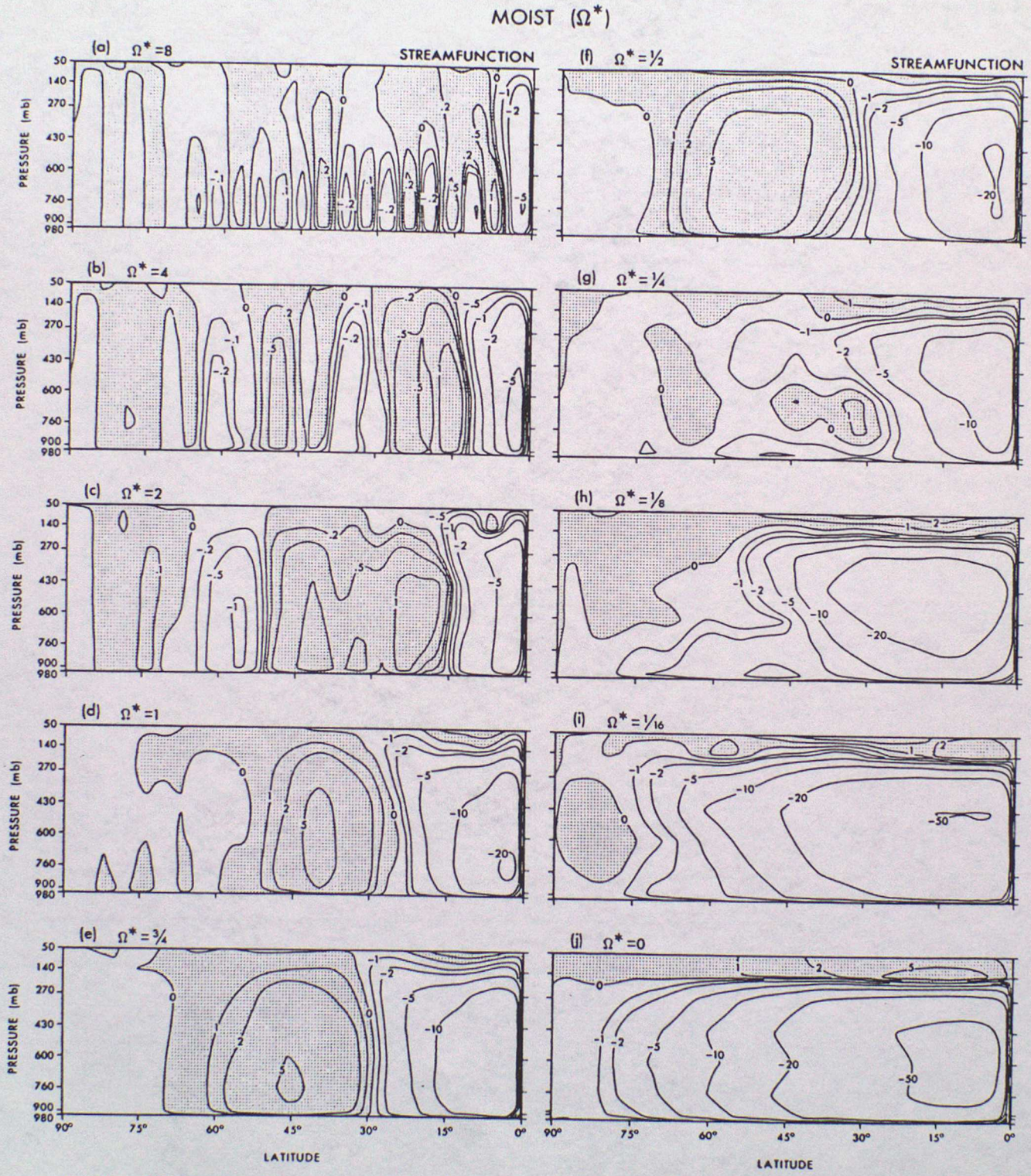

Meridional distribution of the mean stream function for the MOIST model with $\Omega^* = 0$-8. Units: 10^{13} g s^{-1}

Figure 1.12

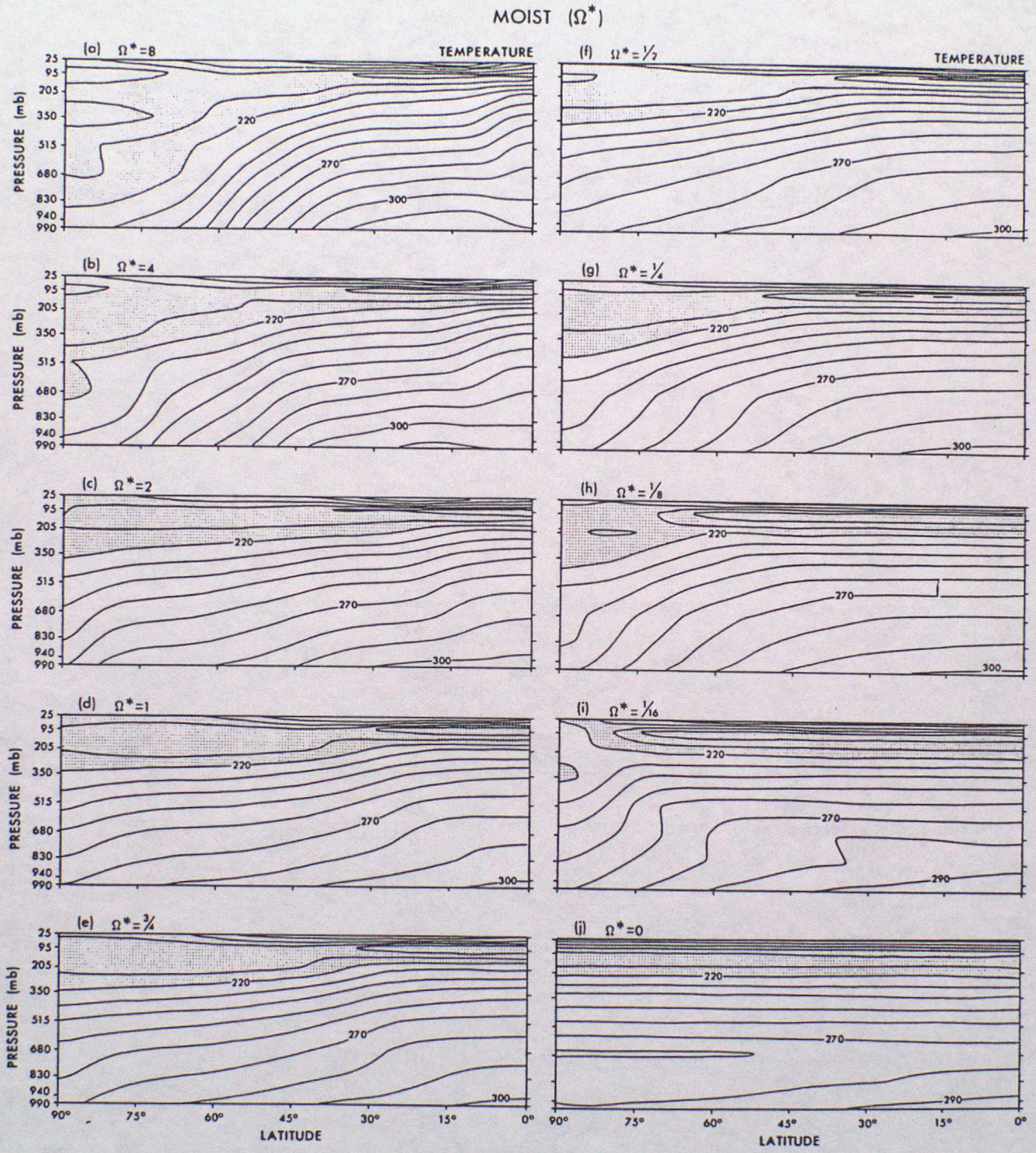

Meridional distribution of the mean temperature for the MOIST model with $\Omega^* = 0$–8. Units: K

Figure 1.13

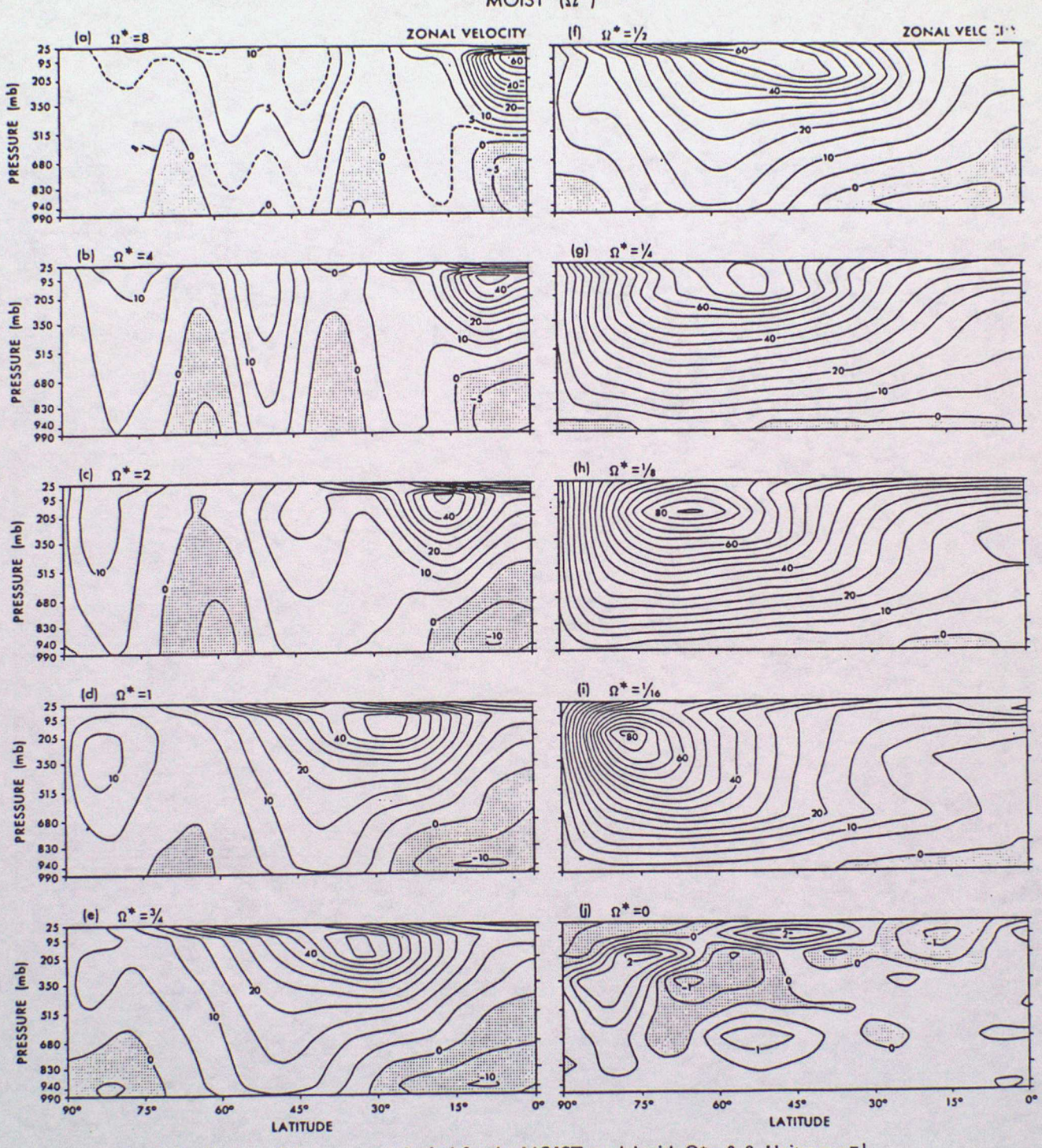

Meridional distribution of the mean zonal wind for the MOIST model with $\Omega^* = 0$–8. Units: m s^{-1}

Figure 1.14

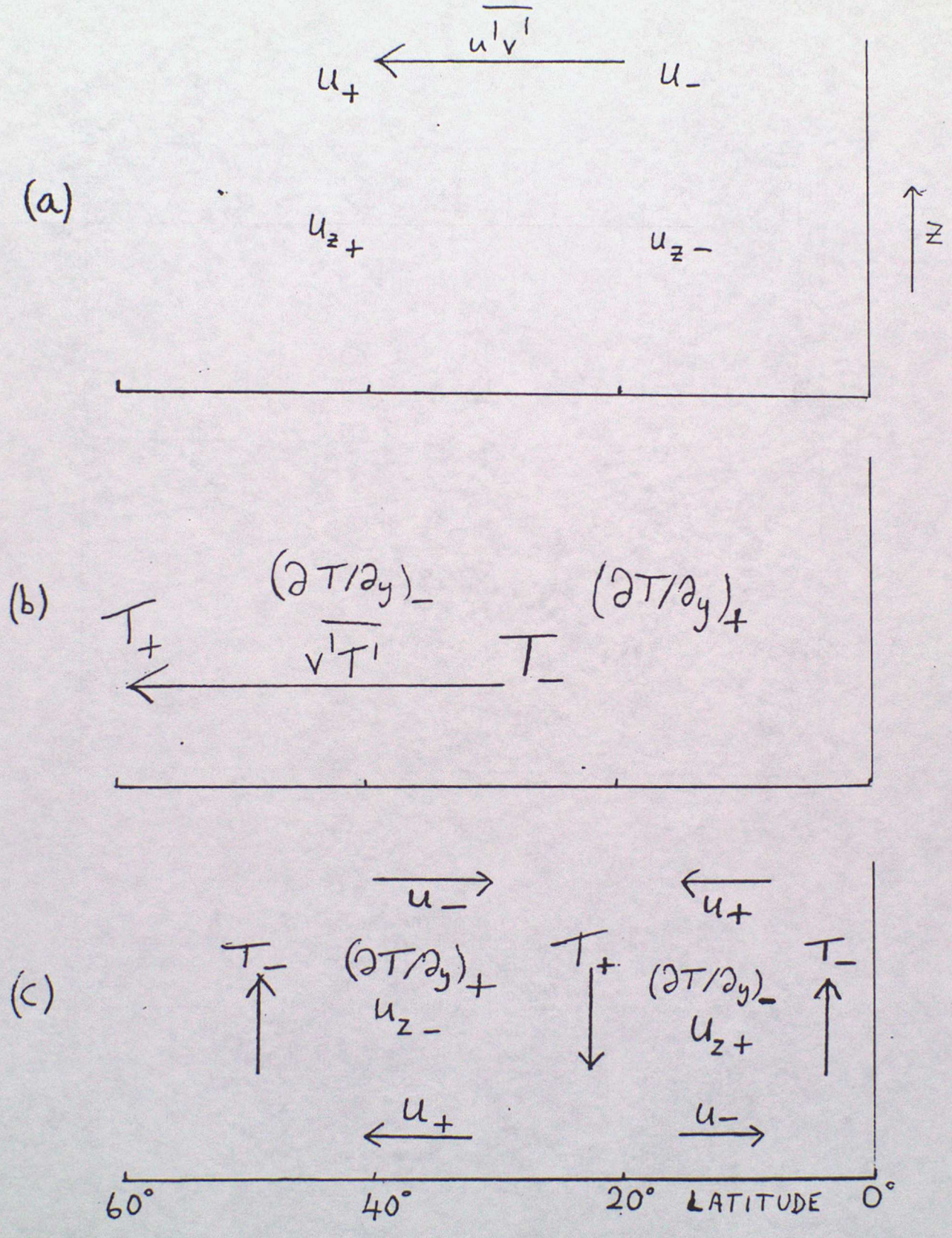

Figure 1.15: Schematic representation of the interactions between the baroclinic eddies (and the associated fluxes) and the meridional circulation: (a) the effects of eddy momentum fluxes, (b) the effects of eddy heat fluxes, (c) the compensating effects of the meridional (Ferrel and Hadley) cells (see text).

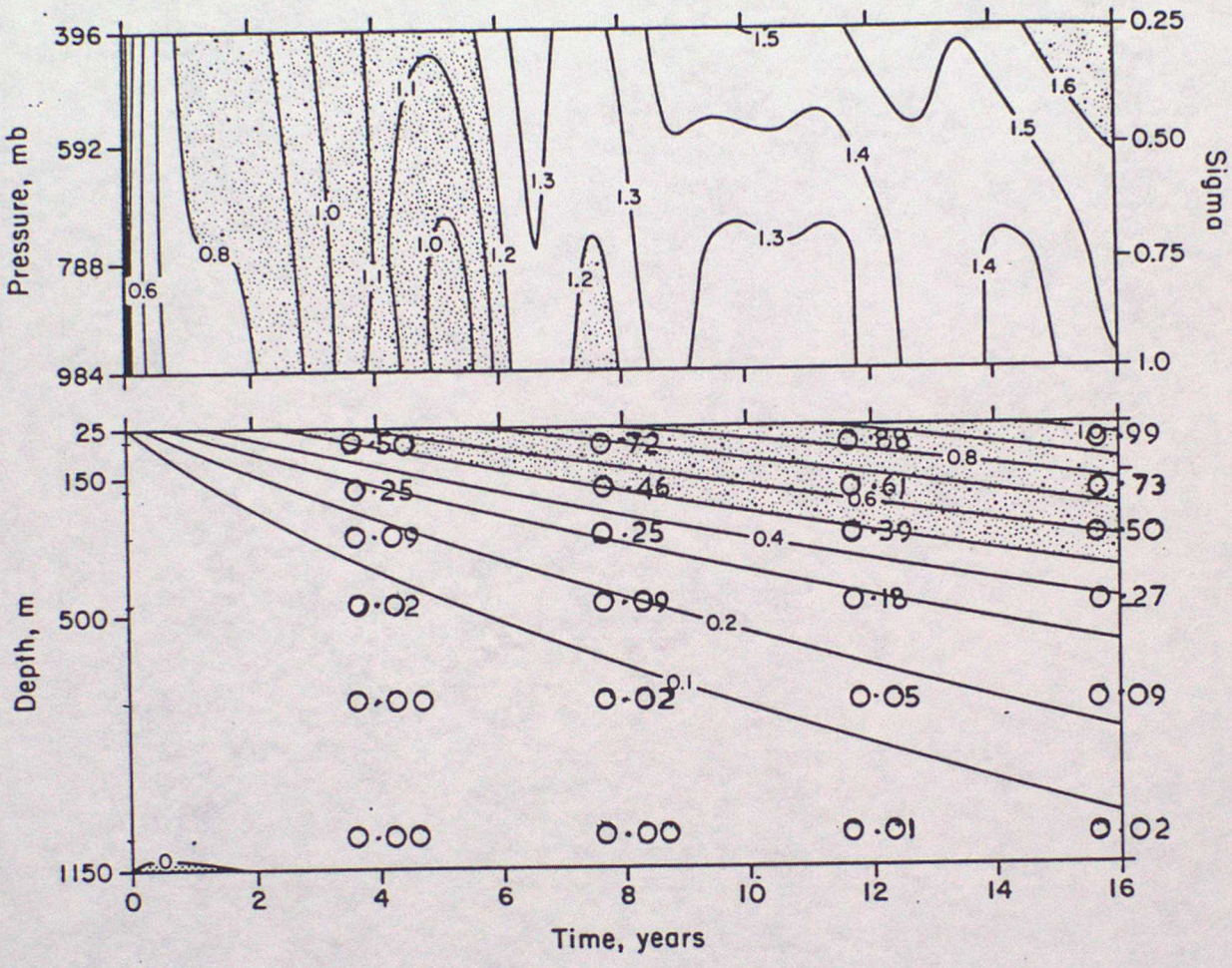

Fig.1.16 Time-vertical distribution of the $2xCO_2$-$1xCO_2$ difference in monthly-mean global-mean temperatures (°C) of the atmosphere (above) and ocean (below). The temperature differences have been filtered using a symmetric 12-pole, low-pass recursive filter with a 24-month cutoff period. Atmospheric warming between 0.8-1.2°C and larger than 1.6°C is indicated by light stipple, as is oceanic warming of 0.5-1.0°C, while oceanic cooling is shown by heavy stipple.

The plotted numbers are the warmings simulated using the one dimensional model described in the text

THE PHYSICS AND DYNAMICS OF THE CLIMATE SYSTEM

THE ROLE OF WAVES IN THE GENERAL CIRCULATION OF THE ATMOSPHERE AND OCEANS
PART I: WAVE CHARACTERISTICS

S J Foreman

Met O 20, Meteorological Office, Bracknell

2.1 INTRODUCTION

It is well known that motions of the atmosphere and ocean take place on a broad range of time and space scales. In order to understand the mechanisms generating and maintaining this chaotic regime it is necessary to make use of simplifications of the governing equations.

A technique frequently used is to analyse the motion in terms of waves. This involves separating the state of the fluid into a **mean state** and a **perturbation**. Typically the field will be assumed to have a structure of the form

$$\psi(x,y,t) = \Psi_{mean} + \Psi(y)\exp\{i(kx-\omega t)\}$$

where ψ is the perturbed quantity, Ψ_{mean} its mean value, $\Psi(y)$ the **amplitude** of the wave (which varies in one of the spatial directions in this example), k the **wave number** (equal to 2π/**wavelength**), and ω the **frequency**. It is conventional in discussing waves to assume the real part of complex expressions. Such a wave has **phase speed** (c) equal to ω/k, the speed of translation of a given **phase** of the wave form. These terms are illustrated in fig. 2.1. The value of the phase speed is determined by the dynamic constraints of the system. These may be determined by assuming the perturbations to be small enough that second order terms (arising, for example, from advection of a wave property by the wave motion) may be ignored (linearising the equations). This introduces an equation, known as the **phase relationship**, which determines the permissible combinations of wave number and frequency:

$$\omega = f(\Psi_{mean},k)$$

from which the velocity at which wave energy propagates, the **group velocity** (c_g), may be derived:

$c_g = \partial\omega/\partial k$

If the motion is truly linear (ie the approximations used to derive the structure of the wave are unconditionally valid) the wave motions may be seen in their pure form. Provided that the permissible waves form a mathematically complete description of the system, any state of the system may be described in terms of the component waves and their propagation. If either of these constraints is relaxed (most motions are not exactly described by linear theory), the decomposition into waves is only an aid to understanding. Although it may still be mathematically possible to decompose an observed field into wave components, its evolution may differ markedly from that which would be deduced from separate consideration of the component waves. An illustration of this may be found in surface water waves (fig. 2.2). A wave field may be described by a combination of waves, each of which is of small enough amplitude to be considered linear. In combination they may produce regions in which the combined amplitude is sufficiently large for non-linear processes to become important, for example the formation of cusps. Once this stage has been reached the motion of the component waves no longer describes the evolution of the total field: cusps may form and the waves may break. Wave theory, and linear theory in particular, must therefore be used with caution as an aid to understanding; if used inappropriately the results may not apply to the real world.

The remainder of this lecture describes the properties of several types of wave motion, suggesting mechanisms for their generation and maintenance, and relating them to aspects of the general circulation. Discussion of the ways in which the waves affect the mean state is delayed until the next lecture.

2.2 TRAVELLING STEADY WAVES

2.2.1 A Quasi-Geostrophic Wave Equation

One of the dominant modes of motion in the atmosphere and ocean is the planetary wave. The governing equation for such modes is the linearised quasi-geostrophic vorticity equation (see, eg, Gill, 1982, §12 for a derivation and further discussion). This takes the form

$$\frac{\partial q}{\partial t} + U\frac{\partial q}{\partial x} + v\frac{\partial Q}{\partial y} = 0 \qquad (2.1)$$

where q is the quasi-geostrophic potential vorticity of the perturbation,

defined by

$$q = \frac{1}{f}\left(\frac{\partial^2\Phi}{\partial x^2} + \frac{\partial^2\Phi}{\partial y^2} + \frac{1}{\rho}\frac{\partial}{\partial z}\left\{\frac{f^2}{N^2}\rho\frac{\partial\Phi}{\partial z}\right\}\right) \qquad (2.2)$$

Φ is the quasi-geostrophic stream function, and N the Brunt-Väisälä frequency multiplied by the rate of change of geometric height with the log pressure coordinate z. The height coordinate is defined by $z = -H_s \log(p/p_{ref})$. H_s is a scale height and p_{ref} a reference pressure (see Gill, 1982, §6.17). The "density", ρ, is defined by $\rho = \rho_r \log(-z/H_s)$, ρ_r being the density at the reference pressure. $U(y,z)$ is the zonal component of the mean flow, and v the meridional component of the perturbed flow ($v = f^{-1}\partial\Phi/\partial x$); the meridional gradient of the quasi-geostrophic potential vorticity of the mean state ($\partial Q/\partial y$) is given by

$$\frac{\partial Q}{\partial t} = \beta - \frac{\partial^2 U}{\partial y^2} - \frac{1}{\rho}\frac{\partial}{\partial z}\left(\frac{f^2}{N^2}\rho\frac{\partial U}{\partial z}\right); \qquad (2.3)$$

f is a reference value of the Coriolis parameter, and β its meridional gradient.

Any partial differential equation requires boundary conditions for its solution. In this case they can be derived from the equation for the vertical motion:

$$N^2 w + \left(\frac{\partial}{\partial t} + U\frac{\partial}{\partial x}\right)\frac{\partial\Phi}{\partial z} - \left(\frac{\partial U}{\partial z}\right)\frac{\partial\Phi}{\partial x} = 0 \qquad (2.4)$$

which is applied at the top and bottom of the domain to be modelled. The derivation of this equation is given by Gill (1982, §12.9).

Following Gill, seeking solutions with the form

$$\Phi = \psi(z)\exp\{z/2H_s + ily + ik(x-ct)\} \qquad (2.5)$$

leads to the equation for the vertical structure

$$\partial^2\psi/\partial z^2 + m^2\psi = 0 \qquad (2.6)$$

where $$m^2 = (N/f)^2\left\{(U-c)^{-1}\partial Q/\partial y - \kappa^2\right\} - (2H_s)^{-2} \qquad (2.7)$$

and the square of the horizontal wavenumber is given by

$$\kappa^2 = (k^2 + l^2). \qquad (2.8)$$

Note that, as is customary in discussing waves, the real part of complex quantities is implicitly assumed. The boundary conditions for (2.6) must be derived from (2.4), so that

$$N^2 w + ik(U-c)\partial\psi/\partial z + ik\{(U-c)/2H_s - \partial U/\partial z\}\psi = 0 \qquad (2.9)$$

which relates the phase speed to the vertical structure. This constraint must be applied at both the upper and lower boundaries of the atmosphere or ocean.

2.2.2 Travelling Waves On A Uniform Flow

Consider now some major simplifications of (2.5) to (2.9). Firstly, assume that the horizontal boundaries are flat so that $w=0$ on $z=0, z_{top}$. Also ignore any variation of the mean flow, so that U is a constant, and the potential vorticity gradient of the mean flow reduces to β. The boundary conditions (2.4) reduce to

$$\partial\psi/\partial z + \psi/2H_s = 0$$

and the phase relationship may be derived from (2.7) as

$$c = U - \frac{\beta}{\left\{k^2 + \frac{(m^2 + [1/2H_s]^2)}{N^2/f^2}\right\}} \qquad (2.10)$$

in which the phase speed is related to the horizontal and vertical wave numbers. For the external mode (φ constant with height) the phase speed is that of the external Rossby wave. In the absence of a mean flow, the wave propagates westwards with the speed increasing for longer waves (smaller k,l).

The value of m determines the phase speed of the waves. Positive values of m^2 indicate a sinusoidal structure to the vertical modes (2.6), larger values of m denoting modes with more structure (nodes) in the vertical, whereas negative values indicate an exponential change with height. Although it is possible for m^2 to attain complex values with both real and imaginary parts, these would imply (from (2.7) and (2.5)) that the wave was growing or decaying: this section is concerned with steady waves. In addition to the vertical structure arising from m, there is an exponential increase of amplitude implied by the form chosen for the wave (2.5).

Increasing the spatial scale of the waves (or decreasing the values of k and m) results in an increase of the phase speed of the waves relative to the mean

wind. In the absence of a mean wind, these planetary waves propagate westwards. In their simplest form these waves have uniform vertical structure ($m^2 = -(1/2H_s)^2$). Such an external Rossby wave with zonal wavelength 5000km, which is uniform in the meridional direction, propagates westwards at a speed of 10 m s^{-1} relative to the mean flow at 45°N. (SA table giving the phase speeds of a selection of Rossby waves is given in the Forecaster's Reference Book.) Modes oscillating more rapidly in the vertical have slower speeds. The fastest external mode in the tropical oceans is found in the equatorial Pacific, and has phase speed of order 100 m s^{-1}.

Inspection of (2.1) to (2.3) for the case when there is no vertical structure to the modes indicates the principal mechanism for the existence of these waves. The only terms remaining in the equation are the advection of the relative vorticity of the perturbation by the mean flow, and the meridional advection of planetary vorticity by the wave. As a parcel of fluid moves polewards, it moves into a region of increased magnitude of the planetary vorticity, and must thus decrease that of its relative vorticity. Similarly a parcel moving towards the equator must increase the magnitude of its relative vorticity. This induces a restoring motion, at the same time causing the pattern of motion to propagate westwards as in fig. 2.3

For $m^2<0$ the waves are sinusoidal in the vertical, and propagate in that direction as well as zonally. For $m^2>0$ the waves must be evanescent in the vertical (ie their kinetic energy must remain bounded at all heights).

Neither the equation for the motion in the interior of the fluid, nor the boundary conditions, imposes a constraint on the sign for $|m^2|^*$. This must be chosen on physical grounds: energy must be transferred away from the source, or the kinetic energy of the waves must remain bounded. Some method of determining the direction of energy propagation is thus required. The group velocity provides such a discriminant (eg Lighthill, 1978). For the waves considered here, this has the value

$$c_g = c + \left(2k\beta/(x^2 + \{m^2+[2H_s]^{-2}\}/\{N/f\}^2)^2\right)\left(k,l,-im/(N/f)^2\right) \qquad (2.11)$$

which, in the zonal direction, corresponds to westward propagation (relative to the mean flow) for long waves (k small) and to eastward propagation for short waves (k large).

2.3 STEADY FORCED WAVES

Although the travelling, transient, waves are of importance to the general circulation, there is another class of wave motions which makes a significant contribution to the climatologies of the atmosphere and ocean. These are the forced modes which arise from asymmetries of the boundaries, for examplesurface orography and differential heating. In the real world both effects occur simultaneously, but it is convenient to consider them separately.

2.3.1 Orographically Forced Waves

The Rockies represent a major obstacle to the atmospheric circulation of the northern hemisphere, as do the Himalayas.

Consider (2.4) in the presence of small, zonally sinusoidal, orography, so that the linearised lower boundary condition may be assumed to apply at z=0. In order for there to be no flow through the surface the waves must satisfy

$$w = \mathbf{u}.\nabla h$$

at z=0, where h is $-(p_r/\rho_r H_s g)$ times the amplitude of the orography (from 6.17.28 of Gill, 1982). The interior equation for waves of the form (2.5), (2.6), is unchanged, but the boundary condition (2.9) now includes a term due to the vertical velocity at the surface. This modifies the permissible vertical structures and places a constraint on the phase speed and zonal structure of the waves, which must remain stationary relative to the orography (so that c=0) and which must vary on the same spatial scale. Equation (2.9), applied at z=0, thus becomes

$$N^2 h + U(\partial\psi/\partial z + \psi/2H_s) = 0$$

(where the orography has wavelength k, the same as that of the waves), which determines the amplitude and phase of the waves at the surface; the vertical structure is governed by (2.10):

$$m^2 = (N/f)^2 \{\beta/U - k^2\} - (2H_s)^{-2}.$$

Depending on the scale of the orography the waves are either sinusoidal in the vertical (short scale orography) or decay with height (large scale orography).

The wavenumber for which the change from evanescence to vertical propagation occurs is determined by

$$k = (|U|/\beta)^{\frac{1}{2}}$$

which corresponds to wavelengths of 1000km in the atmosphere and 30-100km in the ocean (Gill, 1982, p525). Evanescent waves have constant phase with height; vertically propagating waves have a phase tilt with height. Figure 2.4 shows the observed deviations from zonal symmetry for the atmosphere.

2.3.2 Thermally Forced Waves

Heating of the column of fluid implies a change in its temperature at the levels of heating. This implies a source term in (2.1) in the interior (or on the boundaries) of the fluid, derived through the equation for the evolution of heat (2.4). This extra term will modify the form of (2.6), thus influencing the vertical structure of the waves.

Consider a heat source which is introduced into the fluid. Waves generated by the heating must propagate away from the source, transporting wave energy. The appropriate direction of propagation is thus not that of the phase velocity (and the individual waves) but of the group velocity (of the wave train). In the real atmosphere, the winds vary with both latitude and longitude, resulting in variations of the group velocity of the waves on long space scales. A physical property of the waves which is conserved as they propagate is the frequency (eg Lighthill, 1978). Tracing the path of waves of constant frequency away from the source of heating in a direction always parallel to their group velocity enables the evolution of the wave pattern to be determined.

Figure 2.5(a) illustrates the response of a model atmosphere to a local heat source in the tropics. One of the dominant anomaly patterns of the atmosphere is known as the Pacific North America (PNA) pattern (Wallace and Gutzler, 1981); fig. 2.5(b) shows a similar anomaly pattern induced by the introduction of the 1982/3 Pacific sea surface temperature anomaly into a general circulation model experiment.

It may be seen in fig. 2.5(a) that the wave train is distorted by the mean flow characteristics. This is analogous to the refraction of light by media of

varying refractive index, and the equivalent quantity for planetary waves is κ_L defined by

$$\kappa_L^2 = \frac{1}{U}\frac{\partial Q}{\partial y} - \left(\frac{f}{2NH_s}\right)^2$$

a quantity discussed by Matsuno (1970) in relation to stratospheric waves. The planetary waves are refracted in the direction of $\nabla\kappa_L$, so that regions of maximum κ_L act as a waveguide, and those of minimum κ_L act as barriers to wave propagation. Both these features may be seen in fig. 2.5(a). Since κ_L varies, and the waves may propagate, in all three space dimensions this conclusion applies to both the horizontal and the vertical propagation of modes.

2.3 INTERNAL INSTABILITIES OF THE FLOW

Discussion of planetary waves has so far been confined to stable waves, although the forced waves discussed in §2.2.2 need not be steady. The discussions have been based on the assumption that c, the phase velocity, is real. This need not be the case; an imaginary component of the phase speed results in growth (or decay) of the wave.

Consider the generalisation of (2.3) in which the potential vorticity of the basic state varies in all three space dimensions, and the horizontal velocity field has both zonal and meridional components. Equation (2.1) then becomes

$$\frac{\partial q}{\partial t} + \mathbf{U}.\nabla q + \mathbf{u}.\nabla Q = 0 \qquad (2.12)$$

and the boundary conditions (2.7) may be written

$$N^2 w + \left(\frac{\partial}{\partial t} + \mathbf{U}.\nabla\right)\frac{\partial \varphi}{\partial z} - \left(\frac{\partial \mathbf{U}}{\partial z}\right).\nabla\varphi = 0. \qquad (2.13)$$

Following Dutton (1976 pp 531-540) a wave of the form (2.5) is substituted into (2.12), the result multiplied by the complex conjugate of ψ and then integrated throughout the region of interest. It is possible, by integrating by parts and substitution of the boundary conditions (2.13), to obtain

$$\iiint |\psi^2| \{ \kappa^2 + \frac{(f/N)^2}{2H_s^2} \} - \frac{1}{2H_s} \left| \frac{\partial \psi}{\partial z} \right|^2 \quad dV \quad +$$

$$\iiint \frac{(\mathbf{U.k} + ck)}{|\mathbf{U.k} - ck|^2} |\psi|^2 \{ (-l,k).\nabla Q + \frac{\delta}{2fH_s^2} [f|\mathbf{U.k} - ck|^2 - N(-l,k).\nabla h + \mathbf{k}.(\partial \mathbf{U}/\partial z)] \} dV = 0 \qquad (2.14)$$

where $\delta(z)$ has the property

$$\int_{z_{bot}}^{z_{top}} \delta(z) a(z)\, dz = [a(z_{top}) - a(z_{bot})].$$

Only the second integral of (2.14) contains an imaginary part, arising solely from c_i, the imaginary part of the phase speed, corresponding to the growth rate. If c_i is to be non zero, the remainder of the integral must be zero for some wave vector $\mathbf{k}=(k,l)$. For this to be possible

$$B = (-l,k).\nabla Q + \frac{\delta}{2fH_s^2} [f|\mathbf{U.k} - ck|^2 - N(-l,k).\nabla h + \mathbf{k}.(\partial \mathbf{U}/\partial z)]$$

must change sign in the region of interest (or on the boundaries) for some $\mathbf{k}$. This forms a necessary condition for instability (but it is not sufficient; sufficiency requires the integral to be zero, placing constraints on the spatial distribution of B). The contribution to B from $|\mathbf{U.k} - ck|$ is always positive, and thus of limited interest. The remaining terms may be split into those dependent on k and those on l. Considering the "k-terms" alone results in the condition

$$\frac{\partial}{\partial y} \{ Q - \frac{N}{2fH_s} h\delta \} - \frac{1}{2fH_s} \frac{\partial U}{\partial z} \delta < 0 \qquad (2.15)$$

somewhere in the domain (to counteract the always positive contribution from $|\mathbf{U.k} - ck|$), and a similar condition relating the (negative of) zonal gradient of Q and the vertical gradient of V arises if the "l term" is considered. Equation (2.15) is the conventional stability condition for quasi-geostrophic flow.

Dutton (1976) demonstrates how the integral technique used here to determine the necessary conditions for stability may be generalised, for zonally uniform

mean flow, to place constraints on the phase speed and growth rate of unstable waves.

2.3.1 Barotropic Instability

Consider (2.14) for barotropic flow in a region without orography and in which the mean flow is independent of height, as is the perturbation, ψ. The terms involving δ cancel requiring that $(-1,k).\nabla Q$ change sign in the region. If the mean flow is purely zonal this reduces to the condition: $\beta - U_{yy}$ changes sign in the domain. For a non-zonal mean state, instability may be possible if the zonal gradient of $(V_x - U_y)$ is negative somewhere in the region (since β is positive).

For a zonal flow, instability thus requires the magnitude of the curvature of the wind profile in the horizontal to be larger than a value determined by the variation of Coriolis parameter. On an f-plane ($\beta=0$) the condition reduces to the requirement for U_{yy} to change sign: thus on a f-plane it is necessary for the velocity to attain a maximum within the region for instability to be possible.

Waves generated by the instability resulting from the horizontal shear of the mean flow are said to result from barotropic instability.

2.3.2 Baroclinic Instability

Consider now the situation in which the potential vorticity is uniform within the interior of the region, bounded by flat rigid surfaces at the top and bottom, in which the zonal mean flow increases with height, and motion occurs on an f-plane. The only contribution to (2.24) arises from the vertical shear of the mean flow at the boundaries which is of the correct sign to permit instability. A vertical shear of the mean flow can thus result in instability. The example given here is the "Eady" problem, first studied by Eady (1949). A related problem, for which β is not zero and the upper boundary was taken to be at infinity, was studied by Charney (1947).

Although three approaches to the analytic study of baroclinic waves are used in the literature (based on papers by Eady (1949), Charney (1947), and Phillips (1954)), only the Eady problem is discussed in detail here. The other theories include the effects which, although of interest, are secondary to the principal mechanism which generates the waves. It is instructive to examine the solution

of the Eady problem in terms of the wave structure. It is possible to solve (2.2) in the case of uniform vertical shear of the mean wind, and to use the boundary conditions (2.4) to determine the phase speed and growth rates of the waves. It is convenient to use a vertical coordinate which is centred at the mid-level of the domain, so that the horizontal boundaries are at $z=\pm H$. This results in a solution of the form

$$\varphi = A(x,y,t)\sinh(z/H_R) + B(x,y,t)\cosh(z/H_R)$$

where $H_R = f/Nx$ (see, eg, Gill 1982 for a fuller discussion). Solutions exist for A and B proportional to

$$\cos(ly)\exp(ik(x-ct))$$

which have

$$c^2 = (DU/Dz)^2(H\tanh(H/H_R) - H_R)(H\coth(H/H_R) - H_R).$$

Wave growth corresponds to positive values of c_i which may be shown to occur for $H\tanh(H/H_R) < H_R$ or

$$NxH < 1.1997\ f$$

The maximum growth rate occurs in a domain which is unbounded to the north and south in which a wave with l=0 is possible (in this special case the Eady wave is a solution of the nonlinear quasi-geostrophic equations). The zonal wavenumber of such a wave is given by

$$NkH = 0.8031f$$

and the maximum growth rate is

$$kc_i = 0.3098(f/N)\ dU/dz.$$

Substituting typical values for the shear of the mean flow and the static stability into these relationships enables the size and growth rates of the most unstable modes to be calculated for the atmosphere and the ocean. Gill (1982) quotes representative values for the wavelength of 4000km (wave number 6) for

the atmosphere, and 200km for the ocean. The associated growth rates are an e-folding time of 2-3 days for the atmosphere and 100 days for the ocean.

The structure of the Eady wave may shown to have a westward phase tilt of geopotential (and thus perturbation velocity) with height, while the temperature tilts eastwards. The resulting phase differecne is such as to produce a net transport of heat polewards, arising from the net effect of upward, poleward moving warm fluid parcels and corresponding downward, equatorward moving cold parcels. This erodes the available potential energy gradient of the mean flow, which is the source of energy for the wave. These processes are illustrated in fig. 2.6.

The Eady solution does not include the effects of β or variations in the vertical shear. Other simple models of baroclinic instability are able to do so. Perhaps the next simplest is the two level model (Phillips, 1954), which includes the β-effect, and exhibits both the short wave cut-off for instability of the Eady solution and a long wave cut-off. In addition, the model exhibits a minimum vertical shear below which instability is not possible.

The term "baroclinic" instability is used to describe the instability arising from gradients in potential energy. In most situations the instability is a mixture of barotropic and baroclinic processes.

2.4 ADJUSTMENT PROCESSES

In the preceding sections the presence of a mean state has been assumed. This assumption disguises the mechanisms responsible for setting up that state and maintaining it. The adjustment problem is concerned with the response of a fluid to a change in the applied forcing. Three aspects are discussed in the remainder of this lecture: the adjustment of the extra-tropical oceans to the wind stress; the response of the equatorial oceans to changes in wind-stress; and the maintenance of geostrophic balance.

2.4.1 Rossby Wave Adjustment

Large scale ocean gyres result from the wind stress at the surface (as will be discussed in lecture 6). Rossby waves may be used to understand the processes involved. Initially the ocean is at rest. Imposing the windstress generates motion in the ocean, which organises itself into Rossby waves. Long waves propagate information westwards rapidly (2.11), setting up the Sverdrup balance

throughout the ocean interior (lecture 7). At the western boundary, westward propagation is not possible, and the energy must be organised into the shorter waves with eastward group velocity. These slowly propagate east from the boundary, generating the western boundary current. This is clearly demonstrated in fig. 2.7, taken from Anderson and Gill (1979), in which a baroclinic mode is considered (ie a mode sinusoidal in the vertical), since the diagnostic being portrayed is the thermocline depth, a feature of the vertical structure of the ocean.

2.4.2 Combined Rossby and Kelvin Wave Adjustment

In the interior of middle latitude oceans there are no wave modes which propagate information rapidly eastwards. The equator, though, acts as a boundary for modes which depend on f. This results in equatorial Kelvin waves. This may be examined using the equatorial β-plane in which $f=\beta y$, resulting in the linear equations

$$\partial u/\partial t - \beta y v = -g\partial\eta/\partial x$$

$$\partial v/\partial t + \beta y u = -g\partial\eta/\partial y$$

$$\partial\eta/\partial t + \partial(Hu)/\partial x + \partial(Hv)/\partial y = 0$$

H being the depth of the fluid and η the surface displacement (see Gill, 1982, §11.5). Solving these for a translating pattern G(x-ct) results in the solution

$$\eta = \exp(-\beta y^2/2c)\, G(x-ct)$$

$$u = (g/c)\exp(-\beta y^2/2c)\, G(x-ct)$$

$$v=0$$

and the phase speed for sinusoidal waves is $c=(gH)^{1/2}$, corresponding to 20-80 m s^{-1} in the atmosphere (for internal modes) and 0.3-3 m s^{-1} for the ocean. These waves are non dispersive, so that their group velocity is the same as their phase velocity. The waves travel eastwards, keeping the equator on their right in the northern hemisphere and on their left in the southern. Waves with the same properties are supported by any barrier in the fluid; they travel

at the same speed and in the same direction, with the barrier taking the role of the equator. Such waves have been observed in the atmosphere, eg Gill (1982, fig. 10.23).

A further mode, the Yanai wave, is possible at the equator. This is closely related to the Rossby modes, but has no nodes in the meridional direction. Unlike the Kelvin mode it is antisymmetric about the equator, and has a major role to play in the reflection of waves at boundaries, permitting the meridional structure of an incident wave of given frequency to be matched by reflected waves of the same frequency consisting of a combination of Rossby, Yanai, and Kelvin modes.

A Kelvin wave can traverse the Pacific from west to east in 50 days; a returning baroclinic Rossby mode is slower. The combination of these waves forms a major part of the oceanic contribution to an El Niño event. Weakened winds in the western tropical Pacific generate an area of warm water locally, which causes a Kelvin wave to propagate eastwards (aided by a positive feedback from the atmosphere). On reaching the eastern coast, the wave reflects as a Rossby mode, further warming the water in the eastern Pacific through a shoalled thermocline, which propagates westwards at the group speed of the dispersive Rossby modes.

2.4.3 Geostrophic Adjustment

The quasi-geostrophic theory used in much of this lecture assumes that the fluid is close to geostrophic balance. Such a theory cannot explain the mechanisms which maintain this. To do so it is necessary to consider a system which permits gravity modes. Such a system is provided by the shallow water equations. The following discussion follows that of Haltiner and Williams (1980, §2.8). The meridionally uniform Cartesian shallow water equations for a basic state at rest on an f-plane may be written as

$$\begin{aligned} u_t - fv + gh_x &= 0 \\ v_t + fu &= 0 \\ h_t + Hu_x &= 0 \end{aligned}$$

where H is the scale height of the fluid and h the surface displacement. This may be shown, using Fourier analysis, to have equilibrium solution with wave components of meridional velocity (v_*) and height (h_*) given by

$$v_a = (1/(1+R^2))\ (R^2 v_o + i\mu g h_o/f)$$

and

$$h_a = (1/(1+R^2))\ (\ R^2 f v_o/i\mu g + h_o)$$

for wave number μ and $R=L_R/L$, $L=1/\mu$ and $L_R=(gH)^{1/2}/f$. Subscript 0 indicates the initial value of the component. R determines the relative sizes of the terms in these equations, for large R (waves short compared with the Rossby radius) the equilibrium solution is such that only the v_o terms are retained: the mass field adjusts to the momentum field. This is the case for motion on small space scales, or motion near the equator which has large Rossby radius due to the small Coriolis parameter. In the reverse case (R small), the only remaining terms are those in h_o: the momentum adjusts to the height field. This is the case for the ocean gyres (due to the small Rossby radius) and for mid-latitude synoptic systems in the atmosphere.

The mechanism for this adjustment arises from the local nature of the assumed deviations from geostrophy. The solutions correspond to wave triplets consisting of a Rossby mode and two gravity waves in the shallow water system. In this case of no potential vorticity gradient of the mean state ($\beta=0$) the Rossby mode is stationary and non-dispersive: it cannot propagate wave energy away from the disturbance. The gravity waves, however, are able to propagate energy away from the initial disturbance, dissipating it and ensuring adjustment to geostrophy. It is for this reason that an initialisation technique is required for atmospheric weather prediction models. The large deviations from geostrophy introduced by the analysis process can generate gravity wave modes on the large scale of the atmosphere model grid, which may be far larger than the scale of the waves which perform the adjustment in reality. These are removed by the initialisation scheme. Bryan (1984) made use of the rapid adjustment to geostrophy in the oceans by introducing a distortion to the physics of the internal gravity modes in an ocean model. This increased their amplitude, and the rate of temperature advection, in the deep ocean, thus decreasing the time required for the ocean model to approach equilibrium with the surface conditions.

2.5 REFERENCES

Anderson, D L T, and Gill, A E 1979 Beta-dispersion of inertial waves. J. Geophys. Res., 84, 1836-1842.

Bryan, K

1984 Accelerating convergence to equilibrium of ocean climate models.

Charney, J G

1947 The dynamics of long waves in a baroclinic westerly current.
J. Meteor., 4, 135-162.

Dutton, J A

1976 The ceaseless wind: an introduction to the theory of atmospheric motion.
McGraw Hill.

Eady, E T

1949 Long waves and cyclone waves.
Tellus, 1, 33-52.

Gill, A E

1982 Atmosphere-ocean dynamics
Academic Press

Haltiner, G J, and
Williams, R T

1980 Numerical prediction and dynamic meteorology.
John Wiley and Sons.

Hoskins, B J, and
Karoly, D J

1981 The steady response of a spherical atmosphere to thermal and orographic forcing.
J. Atmos. Sci., 38, 1179-1196.

Lighthill, J

1978 Waves in Fluids
Cambridge University Press

Lau, N-C

1979 The observed structure of tropospheric stationary waves and the local balance of vorticity and heat.
J. Atmos. Sci., 36, 996-1016.

Matsuno, T

1970 Vertical propagation of stationary planetary waves in the winter northern hemisphere.
J. Atmos. Sci., 27, 871-884.

Palmer, T N, and Mansfield, D A 1986 A study of the wintertime circulation anomalies during past El Niño events, using a high resolution general circulation model. II: Variability of the seasonal mean response. Quart. J. Roy. Meteorol. Soc., 112, 639-660

Phillips, N A 1954 Energy transformations and meridional circulations associated with simple baroclinic waves in a two-level, quasi-geostrophic model. Tellus, 6, 273-286.

Wallace, J M, and Gutzler, D S 1981 Teleconnections in the geopotential height field during the Northern Hemisphere winter. Mon. Wea. Rev., 109, 784-812.

2.6 FIGURE CAPTIONS

Fig. 2.1 Illustration of terms used to describe wave motion.

Fig. 2.2 An example of the breakdown of linear theory for surface water waves. The upper panel shows a Fourier decomposition of the amplitude of the wave field versus wavenumber. The middle panel shows the waves in physical space at an initial time. The lower panel shows the wave field a short time afterwards. The dotted line shows the evolution which might have been expected from linear theory; the solid line shows that linear theory has broken down and the waves have broken. On all three panels, the amplitude at which linear theory might be expected to break down is illustrated by a dashed line. This diagram is schematic.

Fig. 2.3 Schematic representation of the mechanism for the propagation of a Rossby wave. For convenience a northern hemisphere example is used. As a parcel moves northwards, it experiences a weakened planetary vorticity ($\partial f/\partial y > 0$), and must therefore develop decreased relative vorticity (ζ decreases,

producing relative anticyclonic motion). The larger the parcel displacement, the greater the relative vorticity. The induced relative vorticity of the parcel results in a velocity field (the circles in the diagram) which acts on the neighbouring parcels. Since the parcels displaced furthest from their initial (rest) positions (on the straight line) have largest perturbation relative vorticity, the residual velocity field acting on the fluid parcels is as shown by the bold arrows. This results in the wave pattern being propagated towards the west (relative to the mean flow).

Fig. 2.4 Longitude-height cross sections of the departure of geopotential height from the zonal mean. Orography is indicated by the shading at the bottom of each diagram. The contour interval is 50m. (a) 60°N; (b) 45°N; (c) 25°N. (From Lau, 1979, figs. 2a-2c). The phase variation with height can be seen, indicating that the waves propagate vertically; the phase does not reverse in a vertical column, indicating that the largest vertical mode is excited.

Fig. 2.5 (a) Paths of planetary waves generated by a tropical heat source. The marks are at equal intervals of time. (From Hoskins and Karoly, 1981). (b) 250mb geopotential height anomaly response to 1982/3 sea surface temperature anomalies in the tropical Pacific produced by a general circulation model of the atmosphere. (From Palmer and Mansfield, 1986).

Fig. 2.6 Schematic illustration of the energy source for baroclinic waves. The isentropes (surfaces of constant potential temperature) of the mean state are inclined to the horizontal. Parcel displacements (arrows) are to lie between the slope of the isentropes and the horizontal, thus transporting heat polewards and eroding the potential energy of the mean state.

Fig. 2.7 Evolution of the thermocline depth in response to the introduction of surface windstress. East is towards the right. Lines are numbered with increasing time. Rapid westward group velocity of long waves enables the Sverdrup balance to be set up quickly, but the slower eastward group velocity of the short waves results in a much slower set up for the western boundary currents.

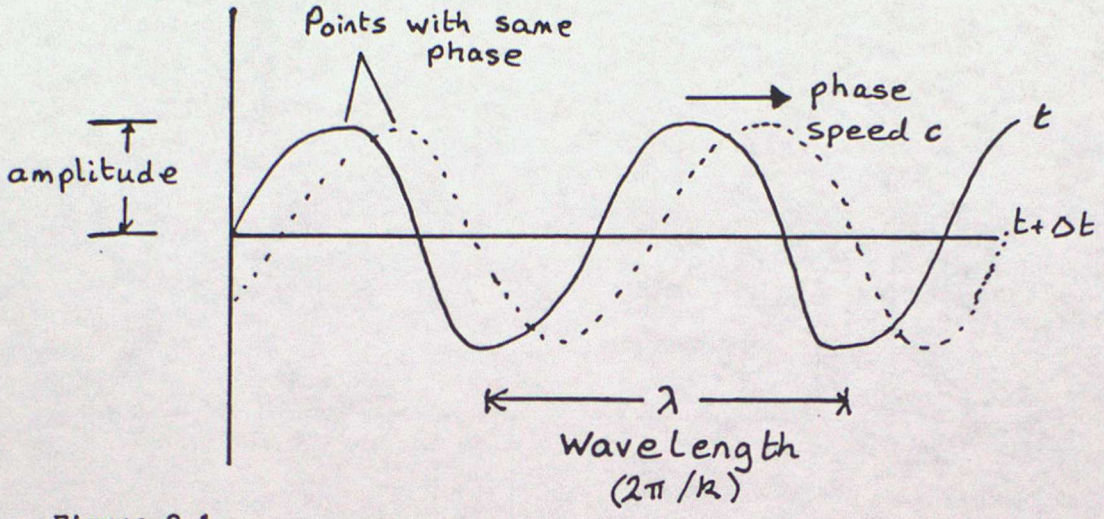

Figure 2.1

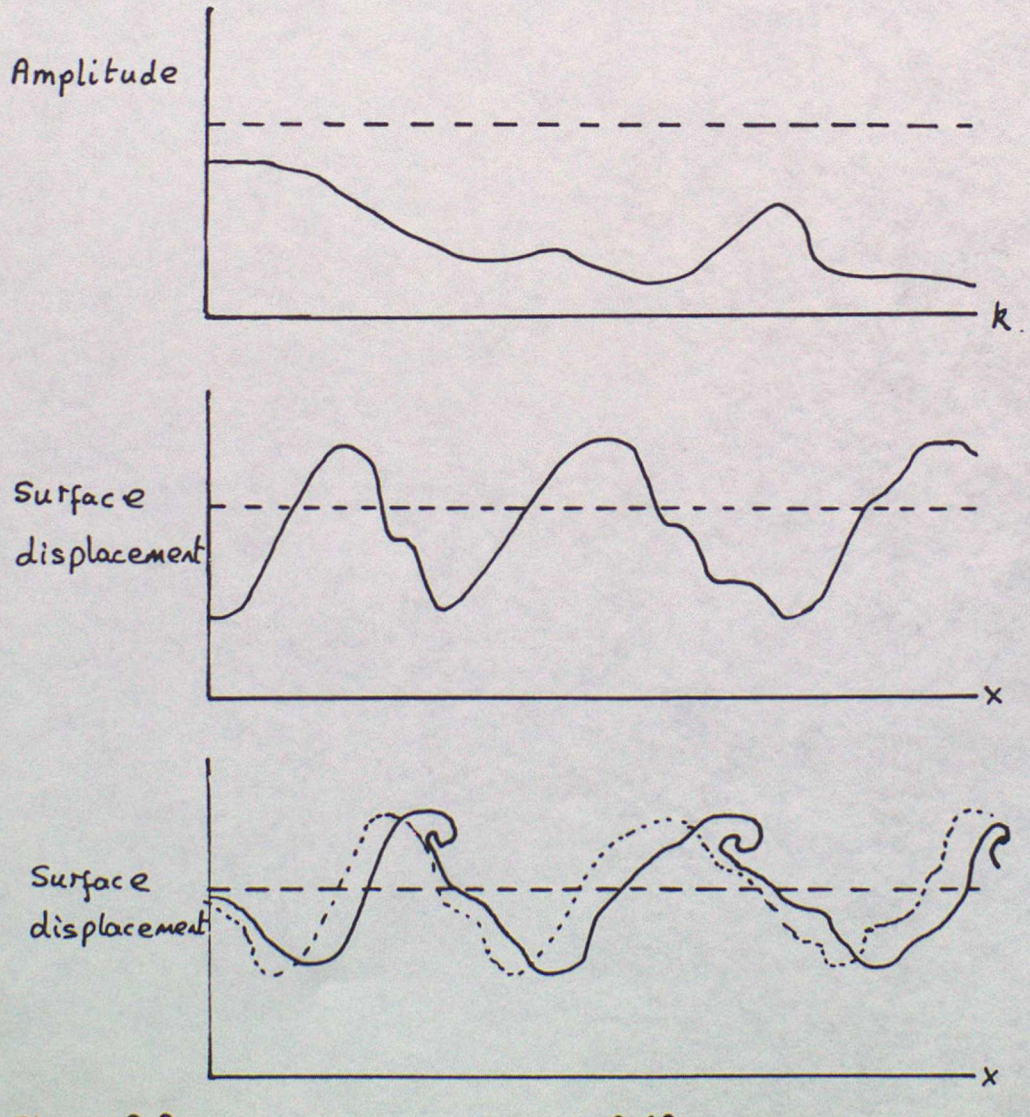

Figure 2.2

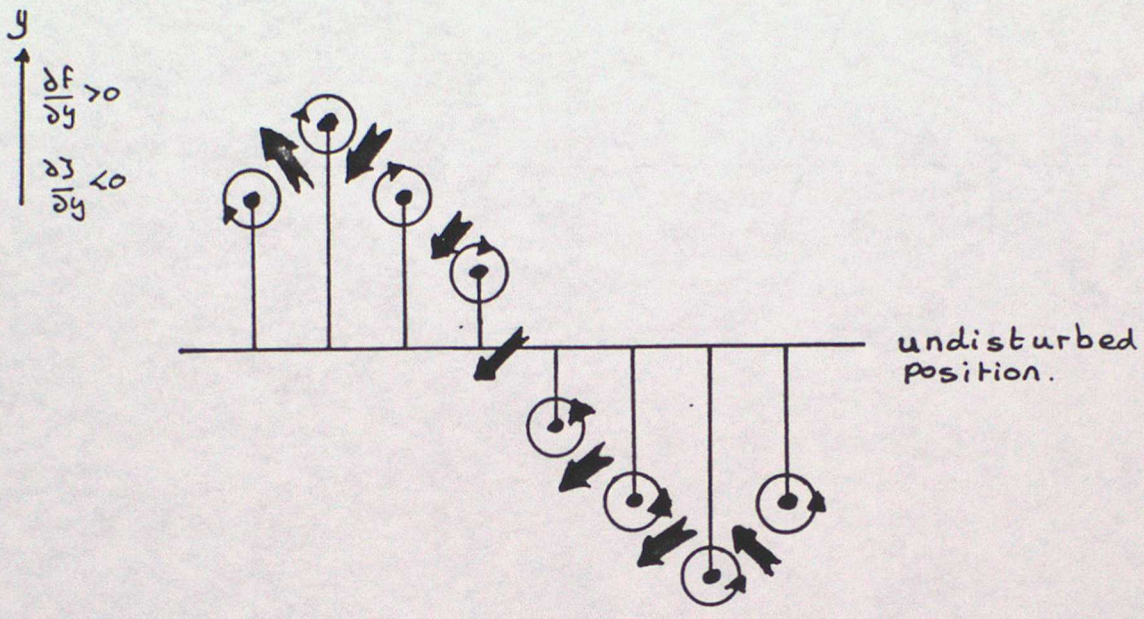

Figure 2.3

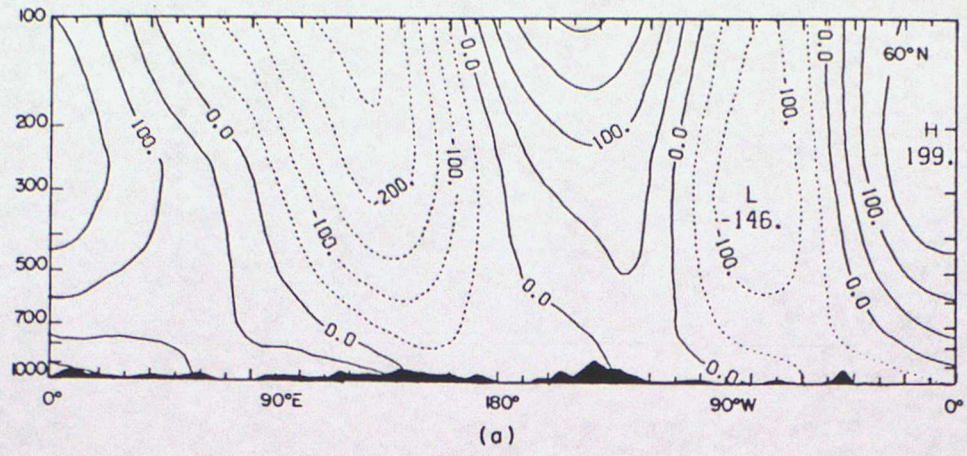

(a)

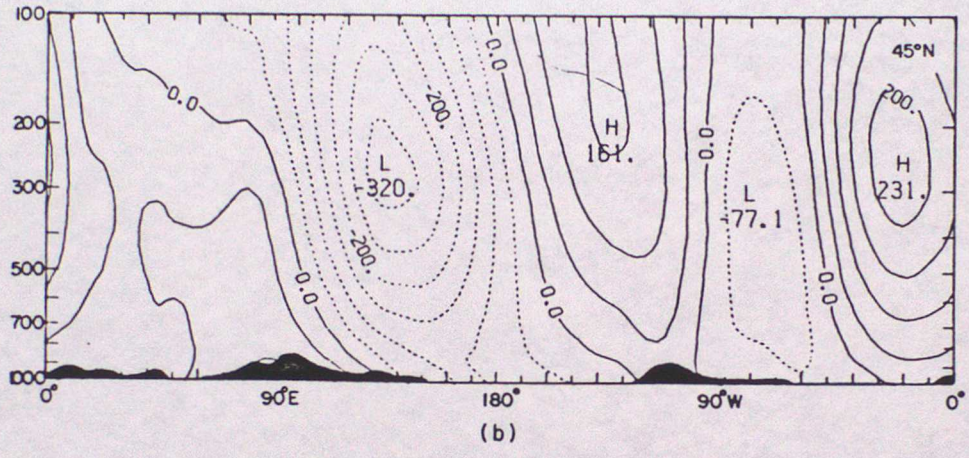

(b)

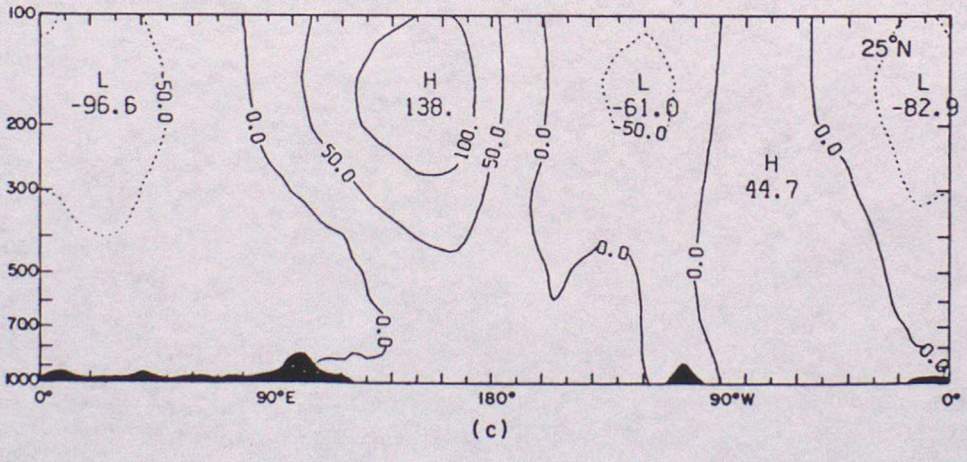

(c)

Figure 2.4

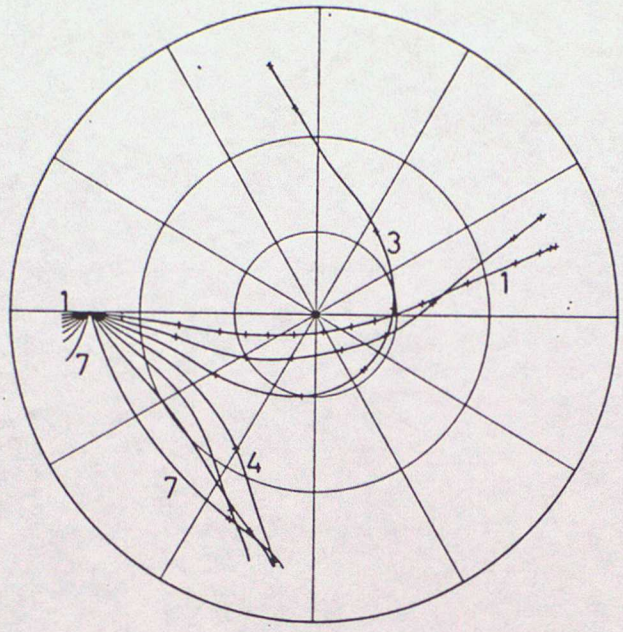

(a)

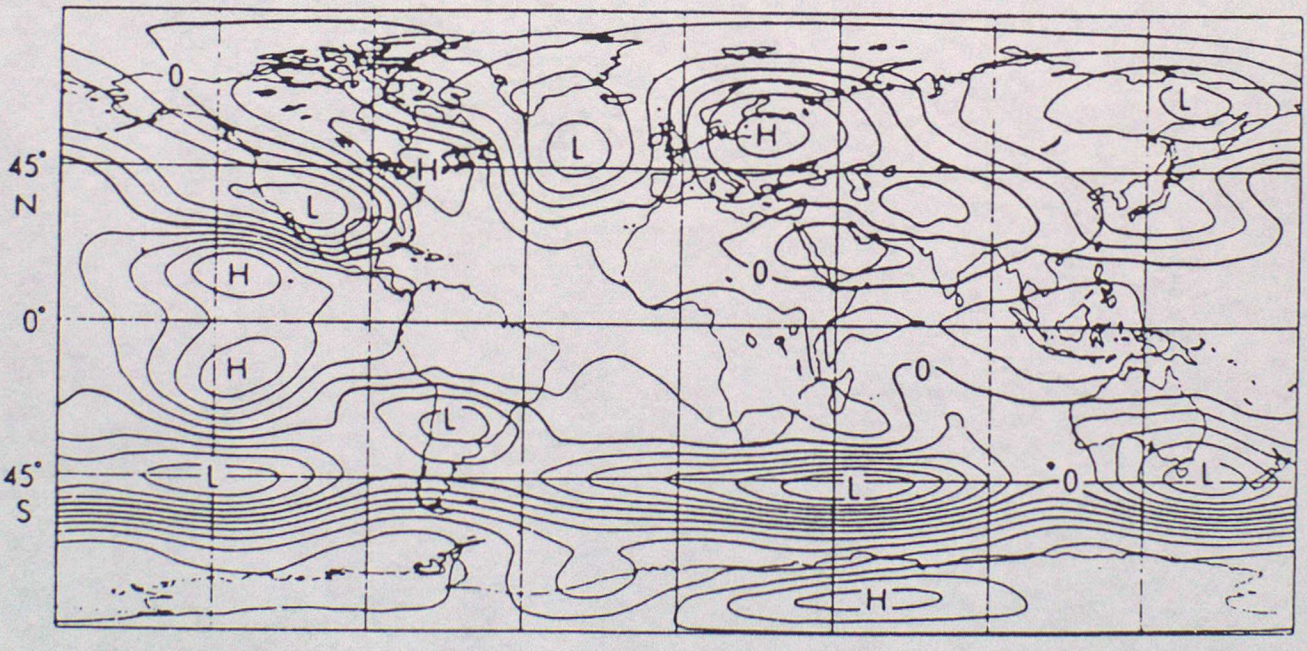

(b)

Figure 2.5

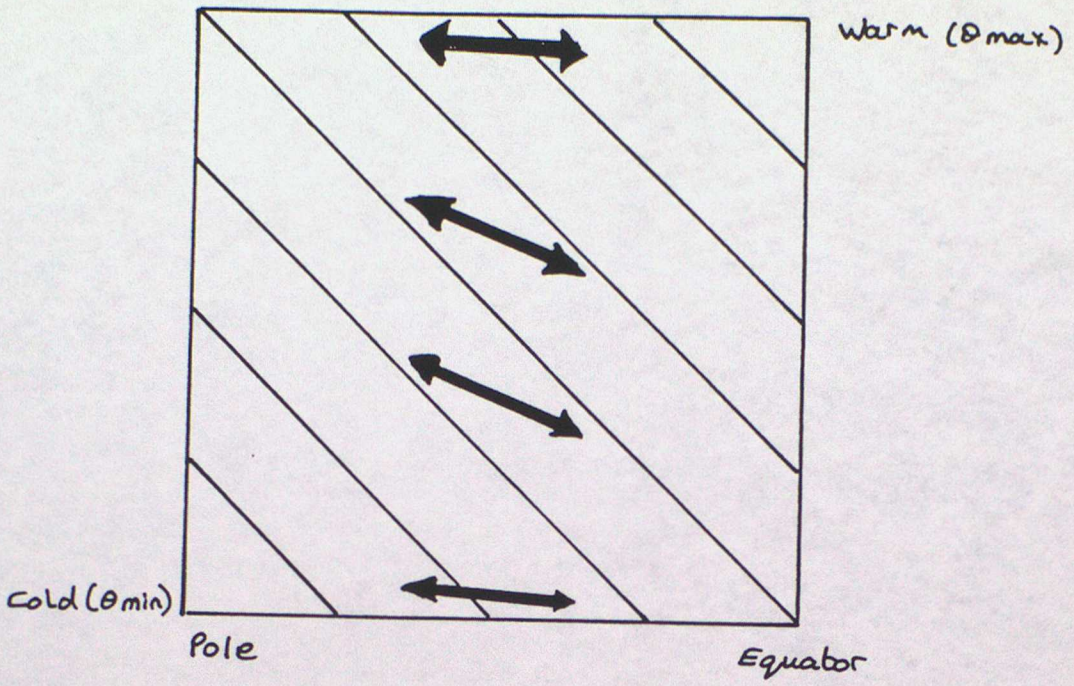

Figure 2.6

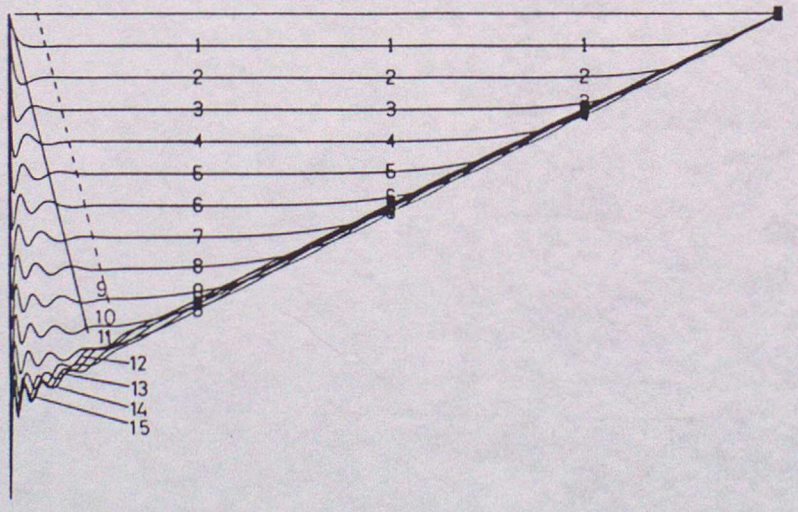

Figure 2.7

THE PHYSICS AND DYNAMICS OF THE CLIMATE SYSTEM

THE ROLE OF WAVES IN THE GENERAL CIRCULATION OF THE ATMOSPHERE AND OCEANS
PART II: NON-LINEAR ASPECTS

S J Foreman

Met O 20, Meteorological Office, Bracknell

3.1 INTRODUCTION

In the previous lecture the linear dynamics of several waves were discussed. It was suggested that waves may be of importance in determining the mean general circulation. Stationary waves, forced by orography, provide a clear example of persistent features which may be evident in a long term climatology, but it is less obvious that transient eddies produce a lasting influence on the mean flow. It is necessary to examine nonlinear properties of the waves to determine their impact on the mean flow and on each other. This lecture explores aspects of wave mean-flow and wave-wave interaction.

3.2 SPATIAL STRUCTURE OF WAVES AND THEIR TRANSPORT PROPERTIES

Consider two wave components (eg temperature and meridional velocity) which, at a given latitude, height, and time have structure

$$\psi(x) = A \cos(kx)$$
$$\varphi(x) = B \cos(kx + \varepsilon)$$

There is a phase difference of ε between the components. Their correlation is thus

$$AB \int \cos(kx).\cos(kx + \varepsilon)\, dx \;/\; \int dx$$

$$= \tfrac{1}{2}AB \cos(\varepsilon).$$

If ψ represents the meridional component of velocity and φ any other component, the correlation represents the mean northward transport by the wave.

Rossby waves have velocity components of the form

$$u = -lA\cos(kx + ly - kct)$$

and

$$v = kA\cos(kx + ly - kct)$$

so that the meridional transport of momentum ($-lkA^2$) is southwards if the waves slope eastwards with increasing latitude ($l/k>0$) and northwards if ($l/k<0$) (fig. 3.1(a)). This correlation remains the same at all latitudes for a simple Rossby wave on a uniform mean flow

Waves on a mean flow which has a jet structure in the horizontal often adopt a "banana" shape (eg McIntyre, 1970), in which the correlation between the two velocity components changes sign either side of the jet axis, transporting momentum in different directions. (fig. 3.1(b)). For baroclinically unstable waves, Held and Andrews (1983) demonstrated that for mean flows with jets varying on a larger scale than the radius of deformation of the waves the momentum transport is up-gradient, increasing the strength of the jet, while for small scale jets the transport is down-gradient, eroding the jet. This may be understood in terms of the potential vorticity gradient of the mean flow. In the region of the jet maximum $U_{yy}<0$, so that $\beta - U_{yy}>0$, and increasing the curvature further can stablise the flow. Provided that the jet is broad enough, the baroclinic waves (whose spatial scale is determined by the deformation radius) can modify their structure to transport momentum up the gradient. This requires the scale of the jet to be at least that of the waves.

Eady waves have a velocity field which slopes westwards with height while the temperature field slopes eastwards. It may be shown (eg Gill, 1982, p558) that there is a positive correlation of temperature with poleward velocity at all levels: the waves transport warm air polewards and cool air equatorwards. For this special form of baroclinic instability the heat transport is the same at all heights. A similar correlation may be found between the vertical velocity and the temperature, so that warm air is transported upwards and cold air downwards by the waves. A wave with constant phase in the meridional direction (eg one of the form $A.\cos(ly).\cos(k[x-ct])$) does not transport westerly momentum meridionally.

3.3 IMPACT OF WAVES ON THE MEAN FLOW

3.3.1 Baroclinic Instability

One of the examples used in the previous section was the Eady wave. It was found that the wave transports heat polewards. This heat must be extracted from the mean flow. For all but the case of a meridionally uniform, unbounded, mean flow there is a finite source of heat available for redistribution. The waves act to erode the temperature gradient of the mean flow which gave rise to the instability, and the growth rate slows as a result. Eventually the mean state is modified to such an extent that wave growth ceases, and other mechanisms become of importance. In simple models (eg the two-layer model as investigated by Pedlosky, 1970) the waves transport enough heat to reverse the temperature gradient in the centre of the channel. This causes the waves to decay, transporting heat in the opposite direction and re-creating the original temperature gradient if dissipation is neglected. Numerical experiments with primitive equation models have investigated this further. Simmons and Hoskins (1978) discussed the decay phase of mature baroclinic eddies and found that it was associated with mainly barotropic processes, converting the energy contained in the wave into a strengthening and narrowing of the upper level jet in their model which later decayed slowly through other barotropic processes.

A two layer quasi-geostrophic model of baroclinic instability exhibits a minimum vertical wind shear below which instability is not possible. This is determined by the relative magnitudes of the variation of the Coriolis parameter and the static stability. Sufficient shear is needed to ensure that the meridional gradient of potential vorticity is negative (§2.3.2). Stone (1978) argued that baroclinic waves would decrease the temperature gradient of the mean flow whenever it exceeded the minimum value corresponding to the critical wind shear, and thus ensure that the temperature gradients observed are close to those corresponding to this minimum vertical shear. It was shown in lecture 1 that, at mid-latitudes, the observed temperature gradient is indeed close to the limit suggested by Stone.

3.3.2 Critical Layers And Gravity Waves

In deriving (2.14) it was assumed that the imaginary part of the complex phase speed (c_i) was non-zero. This avoided a singularity of the equation when the real component of the phase speed equalled the speed of the mean flow (a critical line or layer).

Charney and Drazin (1961) clearly demonstrated in the theorem named after them that Rossby waves are unable to penetrate a critical layer. This theorem is used in the interpretation of stratospheric circulations. Linear theory indicates that the wave energy is absorbed at the critical level, suggesting that large changes to the mean flow may be expected there. The importance of the theorem for stratospheric studies is the asymmetry which occurs between easterly (for which a critical line is possible) and westerly mean flows. Easterlies may therefore act as a barrier to the propagation of Rossby waves.

Another feature of stratospheric dynamics is the Quasi-Biennial Oscillation (the QBO). This consists of a reversal of the equatorial stratospheric winds every two years or so, and is thought to result from planetary wave forcing and its interaction with the mean flow. Although not directly related to critical layers, the process is a clear indication of the importance of wave mean-flow interactions. A simple analogue for the process was suggested by Plumb and McEwan (1978) in an experiment in which a fluid initially at rest was forced from below by oscillating membranes. These induced a pattern of standing gravity waves consisting of a pair of waves propagating in opoposite horizontal dirctions, and each propagating upwards (fig 3.2(a)). This mimicked the eastward Kelvin waves and westward Rossby waves in the atmosphere. The process depended upon the viscous dissipation of the waves, which was related to the difference between the velocity of the mean flow and that of the wave; the closer the velocities the stronger the dissipation. In the experiment (and inthe atmosphere), dissipation of the waves accelerated the mean flow in the direction of the wave phase speed. After a time, random instabilities in the flow generated an asymmetry in the mean velocity profile (fig. 3.2(b)). This resulted in enhanced dissipation of one of the waves and in further acceleration of the mean flow at that level. As time progressed the level of maximum mean speed lowered (fig. 3.2(c)), trapping one set of waves below it. The other wave train was able to propagate through the wind maximum, to experience its maximum dissipation higher in the fluid, and induce a reverse flow near the top of the container. This process continued until the lower wind maximum reached the base of the container, when the mean flow was eroded by bottom friction. The second set of waves was then free to produce a second wind maximum in the opposite direction, so the process continued (3.2(d,e)).

3.4 ENERGY CONVERSIONS IN WAVES

One perspective of the climate system is to regard it as a system for transforming energy. Suitable manipulation of the equations of motion enable the energetics of the system to be derived. It is useful to divide the energy into several components and examine the exchanges between these. A full derivation of the quantities concerned may be found in Oort (1964), but in order to illustrate the process one of the "conversion" terms is derived here for the case of spatial variations only. Before doing so, it is necessary to define the basic quantities involved. The kinetic energy is defined to be K where

$$K = \tfrac{1}{2}\int u^2 + v^2 \, dm = ZKE + EKE$$

$$ZKE = \tfrac{1}{2}\int [u]^2 + [v]^2 \, dm \qquad (3.1)$$

$$EKE = \tfrac{1}{2}\int [u^{*2}] + [v^{*2}] \, dm \qquad (3.2)$$

[a] denoting the zonal mean of a and a^* the deviation from [a]. The integrals are over the mass of the atmosphere.

Potential energy of the atmosphere is not a useful concept since it is not all available for conversion. Available potential energy (APE) is a concept that has been introduced to enable comparisons of the energy components to be made. It may be thought of as the increase of potential energy over a state in which the atmosphere has been rearranged to eliminate horizontal gradients of potential energy. Denoting the deviation of a variable, a, from its average on a pressure surface, $\tilde{a}$, by a', the APE may be defined as

$$APE = \tfrac{1}{2}c_p \int \gamma T'^2 \, dm = ZAPE + EAPE$$

$$ZAPE = \tfrac{1}{2}c_p \int \gamma [T']2 \, dm \qquad (3.3)$$

$$EAPE = \tfrac{1}{2}c_p \int \gamma [T^{*2}] \, dm \qquad (3.4)$$

where c_p is the specific heat capacity, and γ a lapse rate given by

$$\gamma = -\left(\frac{\Theta}{T}\right)^2 \frac{R}{c_p p_0} \int_0^{p_0} \left(\frac{T}{\theta}\right)\frac{1}{p}\left(\frac{\partial\tilde{\theta}}{\partial p}\right)^{-1} dp \qquad (3.5)$$

Here p_0 is a reference pressure. Forming equations for the rates of change of ZAPE and EAPE results in the following terms (among others):

$$\frac{\partial ZAPE}{\partial t} = -c_p \int \gamma [v^* T^*] \frac{\partial [T]}{a\partial\varphi} \, dm - \underset{3.5}{c_p} \int \left(\frac{T}{\theta}\right)[\omega^* T^*] \frac{\partial [\theta]'}{\partial p} \, dm + \cdots$$

and

$$\frac{\partial EAPE}{\partial t} = + c_p \int \gamma [v^* T^*] \frac{\partial [T]}{a \partial \varphi} \, dm + c_p \int \left(\frac{T}{\theta}\right) [\omega^* T^*] \frac{\partial [\theta]'}{\partial p} \, dm + \cdots$$

It is readily seen that the same terms occur in the two equations with opposite sign. These are known as the conversion term: C(ZAPE,EAPE). Similar analyses determine the form of the expressions which govern the exchanges between other energy components, a full list being given in the appendix to Oort (1964). In addition to the terms themselves, there are generation and dissipation terms arising from diabatic heating and friction.

The results of an energy analysis are frequently presented in diagrams of the form in fig. 3.3, in which the total of each form of energy is represented by the quantities in the boxes and the conversion terms by the values on the connecting arrows. This example is for middle latitudes (20°N to 80°N), taken from Holopainen (1983) and examines the role of baroclinic eddies by considering the contributions to the energy budget from time varying eddies.

3.5 DIAGNOSING THE IMPACT OF EDDIES ON THE MEAN FLOW

3.5.1 The EP-Flux

Transport properties of eddies may be examined by consideration of the "E-P Flux", a concept introduced by Eliassen and Palm (1961) and whose importance was emphasised by Edmon *et al.* (1980). Using quasi-geostrophic theory in (x,y,p) space (and accepting its limitations) define the vector quantity **E** as

$$\mathbf{E} = \left(0, \; -[u^* v^*] \; , \; f_o [v^* \theta^*] / [\theta_p] \right)$$

where subscript p refers to differentiation with respect to pressure, θ is the assumed mean temperature profile. Means and deviations from these are as in the previous section. Note that **E** is in the y-p plane. The divergence of **E** is then

$$\nabla . \mathbf{E} = -[u^* v^*]_y + f_o \left\{ [v^* \theta^*] / [\theta]_p \right\}_p$$

$$= [v^* q^*]$$

following Hoskins (1983), the eddy transport of eddy potential vorticity; the original vector represents the meridional momentum transport and heat fluxes.

Differentiation of (2.7) with respect to meridional and vertical wave numbers (l and m) shows that the group velocity of quasi-geostrophic planetary waves in the y-z plane is parallel to the E-P vector, so that the vector also provides information on the direction of propagation of wave energy. Using a numerical model, Edmon *et al.* (1980) investigated the E-P vectors during the life cycle of baroclinic disturbances (fig. 3.4). During the initial growth phase the E-P vectors were vertical, indicating that the waves were transporting heat but not momentum (fig 3.4(a)). During the decay phase (after eight days) the importance of the heat transport in the lower atmosphere had decreased, while at upper levels momentum was being transferred equatorwards, or up the monentum gradient. This is consistent with the decay of the waves (Hoskins, 1983, p171 eq 7.7).

3.5.2 E vectors

Whereas the E-P vector uses spatial variations to diagnose the transports due to spatial variations of the flow, the E-vector uses deviations from the time mean fields to derive information about the influence of time variation on the mean flow. In §3.2 it was shown that the shape of the eddies determines the direction of their momentum and vorticity transport, and in particular it is their orientation and departure from circular symmetry which enables these transports. Hoskins *et al.* (1983) demonstrated that, for mean flows which are "almost zonal, the shape of the eddies may be diagnosed from the "vector"

$$\mathbf{E}' = \left([v'^2 - u'^2] , - [u'v'] , f_o[v'\theta']/\theta_p \right)$$

which also determines the direction and magnitude of the potential vorticity transport after simplifying assumptions are made. Square brackets now indicate a time mean and the prime a deviation from this. A consequence of this is that areas of convergence of $\mathbf{E}'$ correspond to regions in which the westerly momentum of the mean flow is being increased (eg a westerly jet accelerated), and regions of divergence correspond to deceleration of the (westerly) mean flow. $\mathbf{E}'$ may be thought of as a extension of the E-P vector although it does not have the correct properties to enable it to transform as a true vector under coordinate changes (because of the approximations in its derivation).

In analysing the effects of time variation it is convenient to apply a numerical filter to the data to separate the effects due to synoptic eddies and those due

to more persistent events (eg blocking). Figure 3.5 shows an analysis of the E-"vectors" for norhtern winter taken from Hoskins *et al.* (1983).

3.6 MODIFICATION OF EDDY GROWTH BY MOISTURE

Diabatic effects have so far been ignored in this lecture. Latent heat release provides an important source of energy for growing waves. Baroclinic waves grow faster when the effects of moisture are considered (eg Golding, 1984).

Between 1°N and 15°N over eastern Africa the meridional gradient of potential vorticity becomes negative (Riehl, 1979). Unstable eddies develop with a baroclinic structure with zonal wavelength 20° of longitude, moving westwards at approximately 10 m s^{-1} so that they overtake the westward moving air at low levels. The entrained air provides a source of moisture in a region of ascent, so that the major region of precipitation lies ahead of the axis of the wave. Figure 3.6, taken from Riehl (1979), illustrates the results of a composite study of such easterly waves observed during the GATE experiment.

3.7 Wave-wave Interactions

Waves do not occur in isolation. There have been many studies of the interactions of waves, for example Pedlosky (1975) investigated triads of baroclinic waves, and McWilliams (1983) studied the formation of modons (stable non-linear eddies) resulting from the interaction of barotropic vortices. These and other studies indicate the importance of wave-wave interaction for the dynamics of rotating fluids.

Fjørtøft (1953) derived a theorem which places strong constraints on the energy transformations which can be performed by waves. The quasi-geostrophic potential vorticity equation conserves both energy and (potential) enstrophy. In terms of the stream function the energy has the form $(\nabla\psi)^2$ (which includes both the potential and kinetic energies) while potential enstrophy takes the form $(\nabla^2\psi)^2$. Fourier analysis of the field onto wave components ψ_q (which are solutions of $\nabla^2\psi_q + (1/a_q)\psi_q = 0$) with amplitudes b_q results in the constraints

energy: $\sum H_q$ = constant

enstrophy $\sum a_q H_q$ = constant

where H_q represents the energy of component ψ_q. Large (small) values of $1/a_q$ correspond to long and deep (short and shallow) waves (from Sturm's oscillation

theorem, eg Ince 1956). Fjørtøft demonstrated that it was not possible for only two wave scales to interact and still conserve both energy and enstrophy. Denoting a change from the initial state by Δ and assuming that three waves interact ($q = r,s,t$) then

$$\Delta H_r + \Delta H_s + \Delta H_t = 0$$

and $$a_r\Delta H_r + a_s\Delta H_s + a_t\Delta H_t = 0$$

so that for a solution to be possible ΔH_r and ΔH_t must be of opposite sign to ΔH_s if $r<s<t$. Fjørtøft's theorem thus states:

(a) at least three scales must be involved in wave-wave interactions;

(b) no length scale can act as an energy source or sink for two other scales unless it is intermediate to them

and (c) the magnitude of the change in energy is greatest for the intermediate length scale.

3.8 References

Charney, J G, and Drazin, P G — 1964 Propagation of planetary scale disturbances from the lower into the upper atmosphere. Jour. Geophys. Res., 66, 83-109

Edmon, H J, Hoskins, B J, and McIntyre, M E — 1980 Eliassen-Palm cross-sections for the troposphere. Jour. Atmos. Sci., 37, 2600-2616 (see also Jour. Atmos. Sci., 38, 1115)

Fjørtøft, R — 1953 On the changes in the spectral distribution of kinetic energy for two-dimensional, non-divergent flow. Tellus, 5, 225-230.

Gill, A E — 1982 Atmosphere-ocean dynamics. Academic Press.

Golding, B 1984 A study of mid-latitude depressions in a numerical model using trajectory techniques. I. Development of ideal baroclinic waves in dry and moist atmospheres. Quart. Jour. Roy. Meteor. Soc., 110, 847-880

Holopainen, E O 1983 Transient eddies in mid-latitudes: observations and interpretation. pp201-234 of Hoskins, BJ, and Pearce, RP (ed): Large scale dynamical processes in the atmosphere. Academic Press

Hoskins, B J 1983 Modelling of the transient eddies and their feedback on the mean flow. pp169-200 of Hoskins, BJ, and Pearce, RP (ed): Large scale dynamical processes in the atmosphere. Academic Press

Hoskins, B J
James, I N, and
White, G H 1983 The shape, propagation and mean-flow interaction of large-scale weather systems. Jour. Atmos. Sci., 40, 1595-1612

Ince, E L 1956 Ordinary differential equations. Dover publications Inc.

McIntyre, M E 1970 On the non-separable baroclinic flow instability problem. Jour. Fluid Mech., 40, 273-306

McWilliams, J C 1983 Interactions of isolated vortices. II Modon generation by monopole collision. Geophys. and Astrophys. Fluid Dyn., 24, 1-22

Oort, A H — 1964 On estimates of the atmospheric energy cycle. Mon. Wea. Rev., 92, 483-493

Pedlosky, J — 1975 The amplitude of baroclinic wave triads and mesoscale motion on the ocean. Jour. Phys. Oceanog., 5, 608-614

Plumb, R A, and McEwan, A D — 1978 The instability of a forced standing wave in a viscous stratified fluid: a laboratory analogue of the quasi-biennial oscillation. Jour. Atmos. Sci., 35, 1827-1839

Simmons, A J and Hoskins, B J — 1978 The life cycles of some non-linear baroclinic waves. Jour. Atmos. Sci., 35, 414-432

Stone, P H — 1978 Baroclinic adjustment Jour. Atmos. Sci., 35, 561-571

3.9 Bibliography

In addition to the texts cited in this and the previous lecture, the reader may find the following text books useful.

Holton, J R — 1979 An introduction to dynamic meteorology. 2nd ed. Academic Press, New York.

LeBlond, PH and Mysak, L A — 1978 Waves in the ocean Elsevier Scientific Pub. Co.

Newell, R E, Vincent, D G, Dopplick, T G, Ferruzza, D, and Kidson, J W — 1969 The energy balance of the global atmosphere pp42-90 of Corby, G A (ed): The global circulation of the atmosphere. Roy. Meteor. Soc.

Pedlosky, J — 1979 Geophysical Fluid Dynamics. Springer Verlag. New York.

3.9 Figure Captions

Fig. 3.1 Momentum transport by waves. (a) Rossby wave. The correlation of meridional and zonal velocities is negative (positive) for waves sloping westwards (eastwards) with increasing latitude. (b) A wave on a curved mean flow may exhibit both northward and southward transport of momentum.

Fig. 3.2 Schematic representation of processes causing reversal of mean flow in Quasi-Biennial Oscillation analogue. (a) Initially the flow is at rest, and vibrating membranes create a standing wave pattern consisting of a pair of gravity waves with equal and opposite phase speeds. For convenience, the vertical propagation of the wave trains is shown on different sides of the vertical axis. (b) After a short time an asymmetry appears in the mean flow. One of the wave trains undergoes enhanced dissipation, and accelerates the mean flow. (c) The region of dissipation descends, while the upper flow is reversed by the other wave train. (d) As the wind maximum reaches the base of the container, boundary friction assists in its dissipation, and the other maximum continues to descend. (e) The process repeats.

Fig. 3.3 Energy conversions at middle latitudes. Subscripts T, MZ and ME refer to transient eddies, the time mean zonal flow, and time mean eddies respectively. Exchanges between stationary eddies and the zonal mean flow being omitted. From Holopainen (1983).

Fig. 3.4 E-P vectors and magnitude of $\nabla \cdot \mathbf{E}$ during the life cycle of an idealised baroclinic wave train. (a) At day 1 during rapid baroclinic growth. (b) At day 8 during the barotropic decay of the waves. Contour interval 4×10^{15}. From Edmon *et al.* (1980).

Fig. 3.5 E-vectors for the northern hemisphere during winter 19¿¿. Regions of convergence correspond to westerly acceleration of the mean flow by the eddies. From Hoskins *et al.* (1983).

Fig. 3.6 Structure of a composite easterly wave. Vvertical axes of (a) and (b) correspond to the latitudinal distance from the centre of the wave. Horizontal axes correspond to one zonal wavelength. Both horizontal flow at (a) 700mb and (b) 200mb; and vertical cross sections through the centre of the wave of (c) the meridional component of the flow and (d) the vertical velocity. Speeds are in: (horizontal) knots; (vertical) mb/hour.

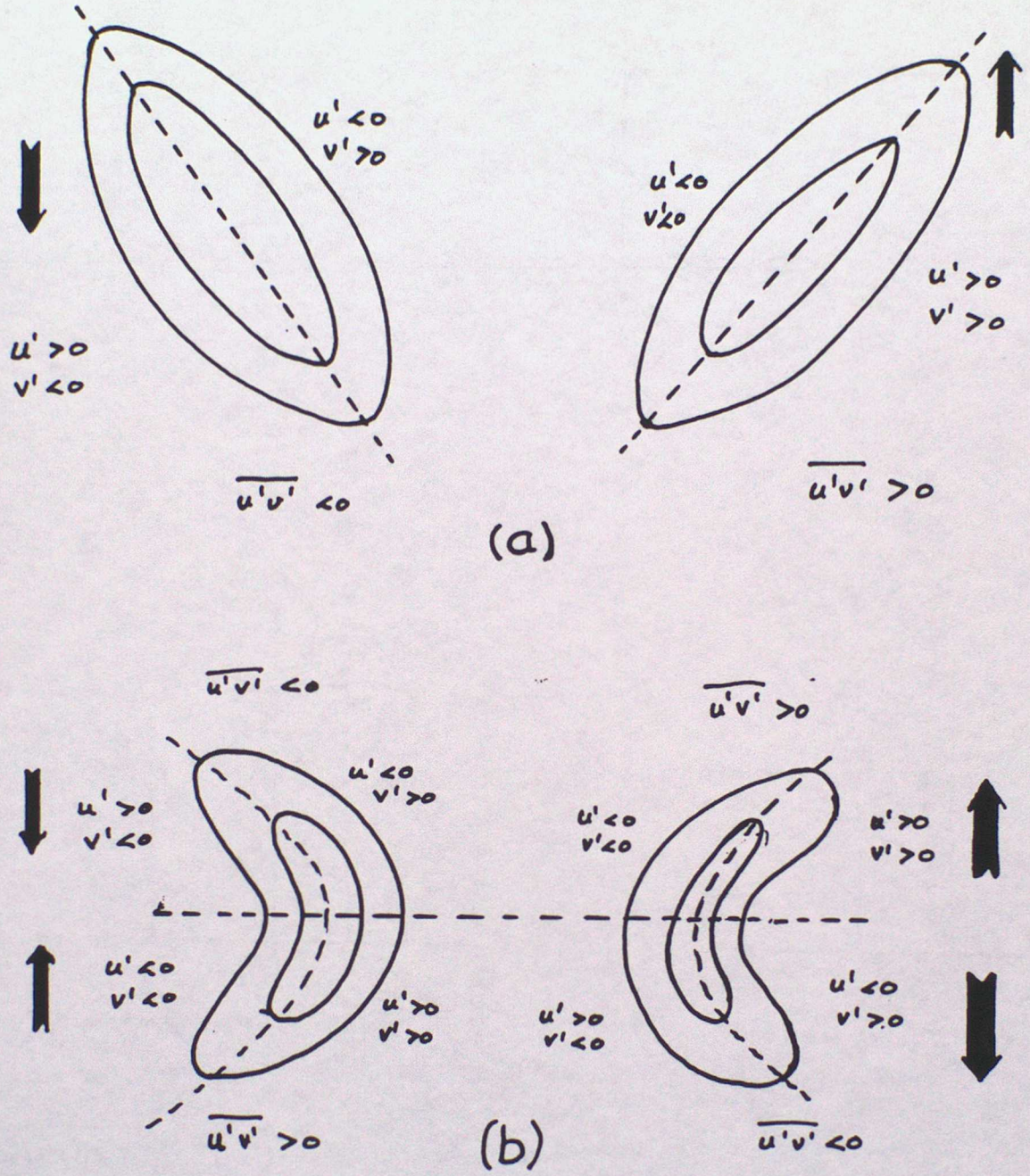
u' < 0
v' > 0
u' > 0
v' < 0
u'v' < 0
u' < 0
v' < 0
u' > 0
v' > 0
u'v' > 0
(a)
u'v' < 0
u'v' > 0
u' < 0
v' > 0
u' > 0
v' < 0
u' < 0
v' < 0
u' > 0
v' > 0
u' < 0
v' < 0
u' > 0
v' > 0
u' < 0
v' > 0
u'v' > 0
u'v' < 0
(b)

Figure 3.1

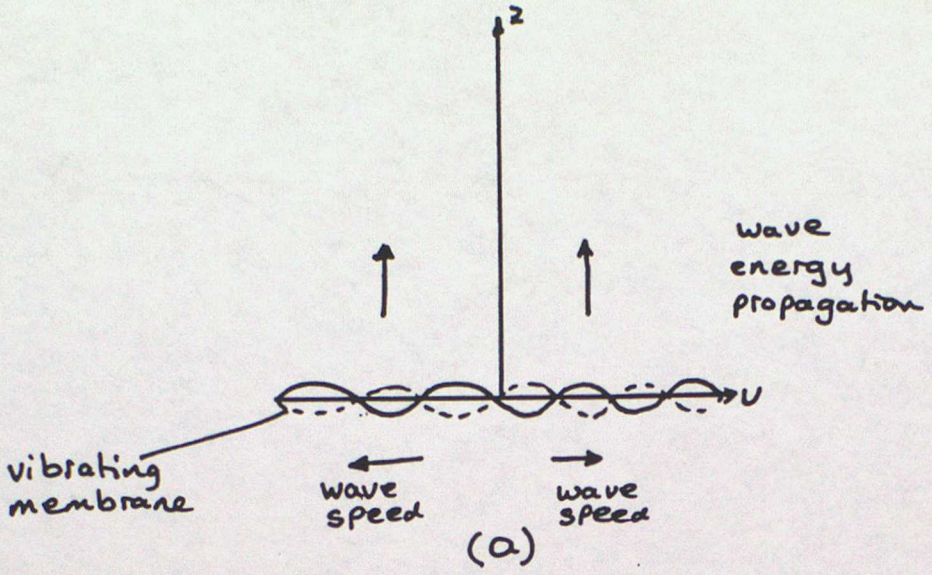
z
wave
energy
propagation
u
vibrating
membrane
wave
speed
wave
speed
(a)

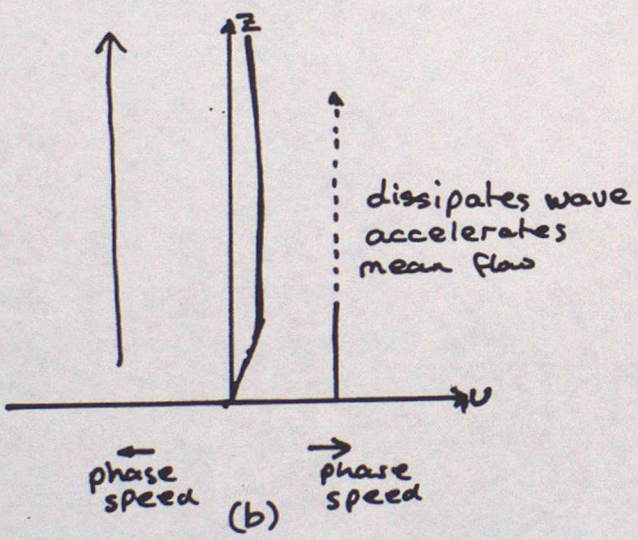
z
dissipates wave
accelerates
mean flow
u
phase
speed
(b)
phase
speed

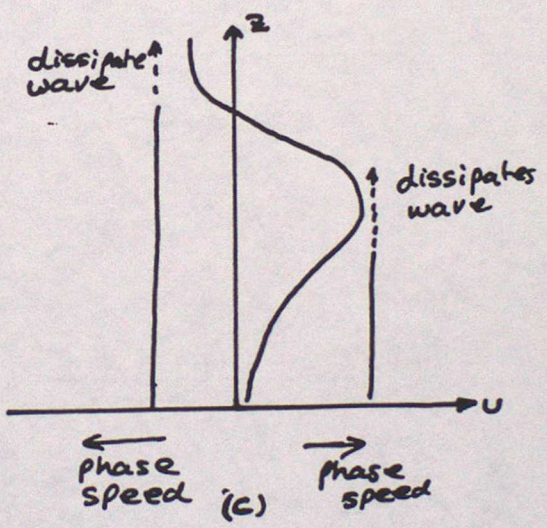
dissipate
wave
z
dissipates
wave
u
phase
speed
(c)
phase
speed

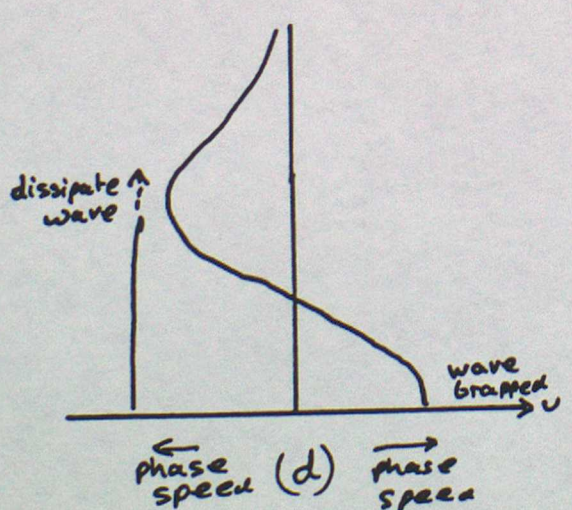
dissipate
wave
wave
trapped
u
phase
speed
(d)
phase
speed

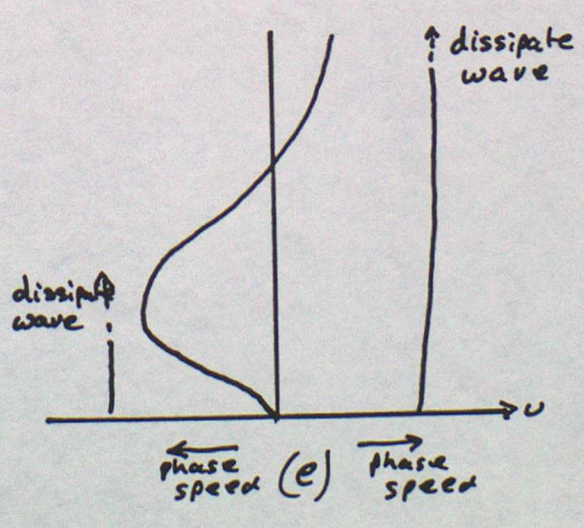
dissipate
wave
dissipate
wave
u
phase
speed
(e)
phase
speed

Figure 3.2

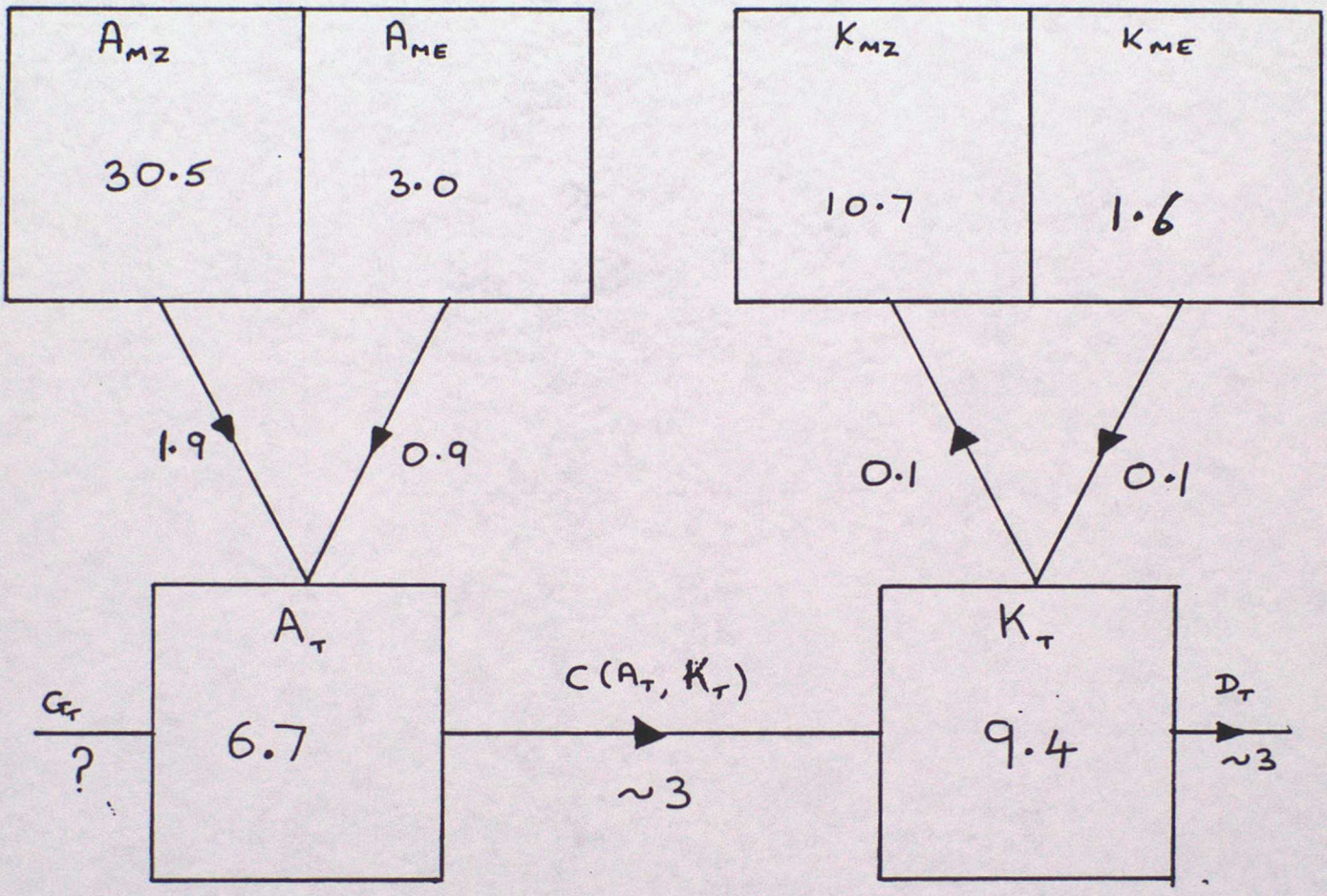

Figure 3.3

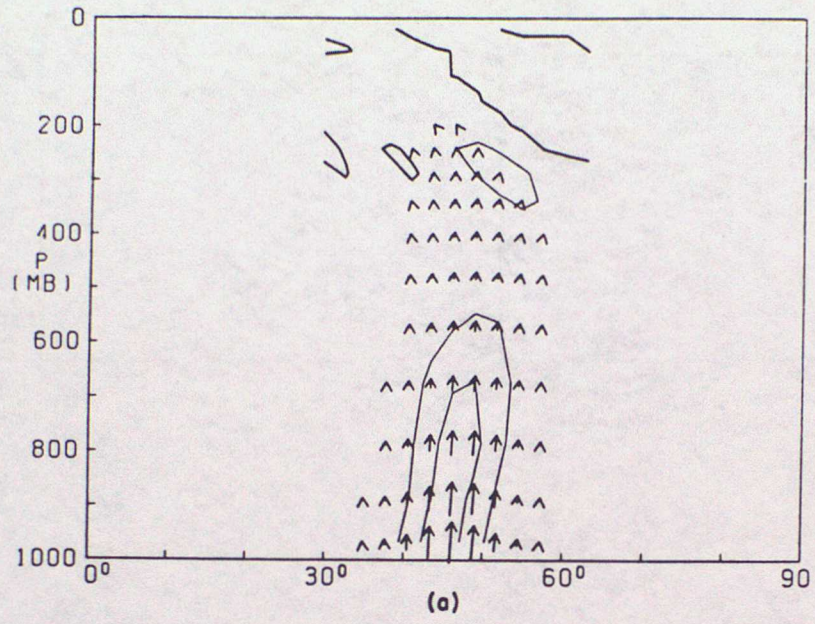
0
200
400
P
(MB)
600
800
1000
0°
30°
60°
90
(a)

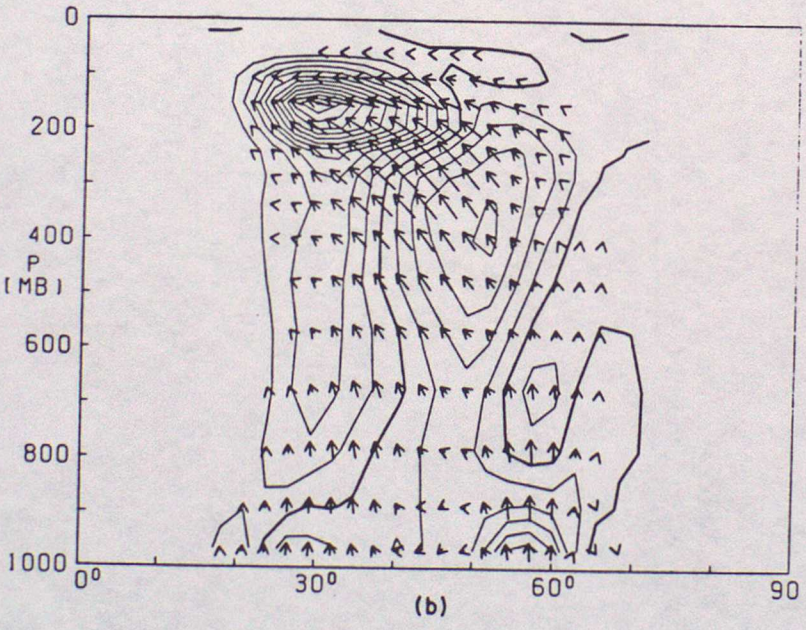
0
200
400
P
(MB)
600
800
1000
0°
30°
60°
90
(b)

Figure 3.4

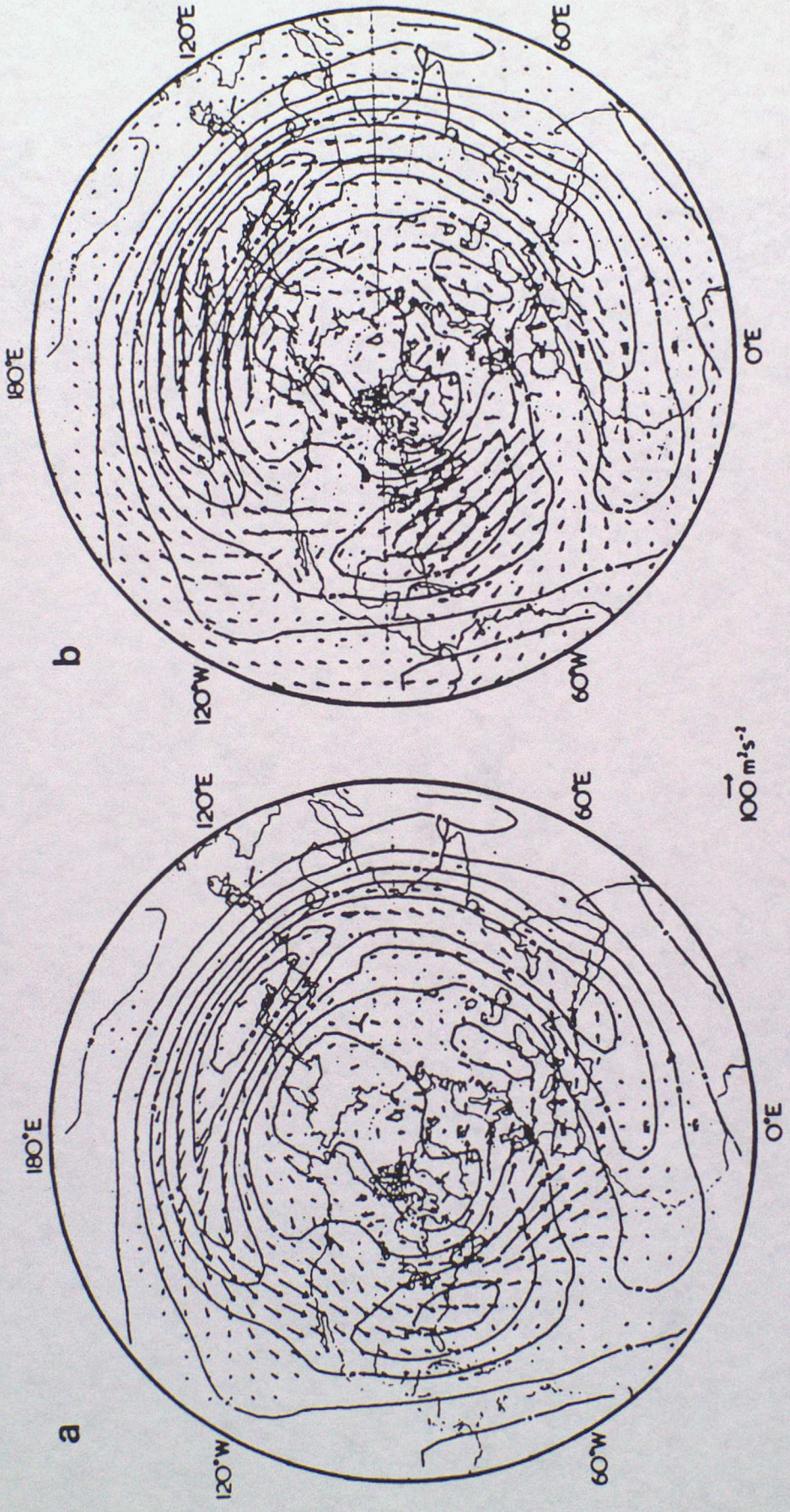

Figure 3.5

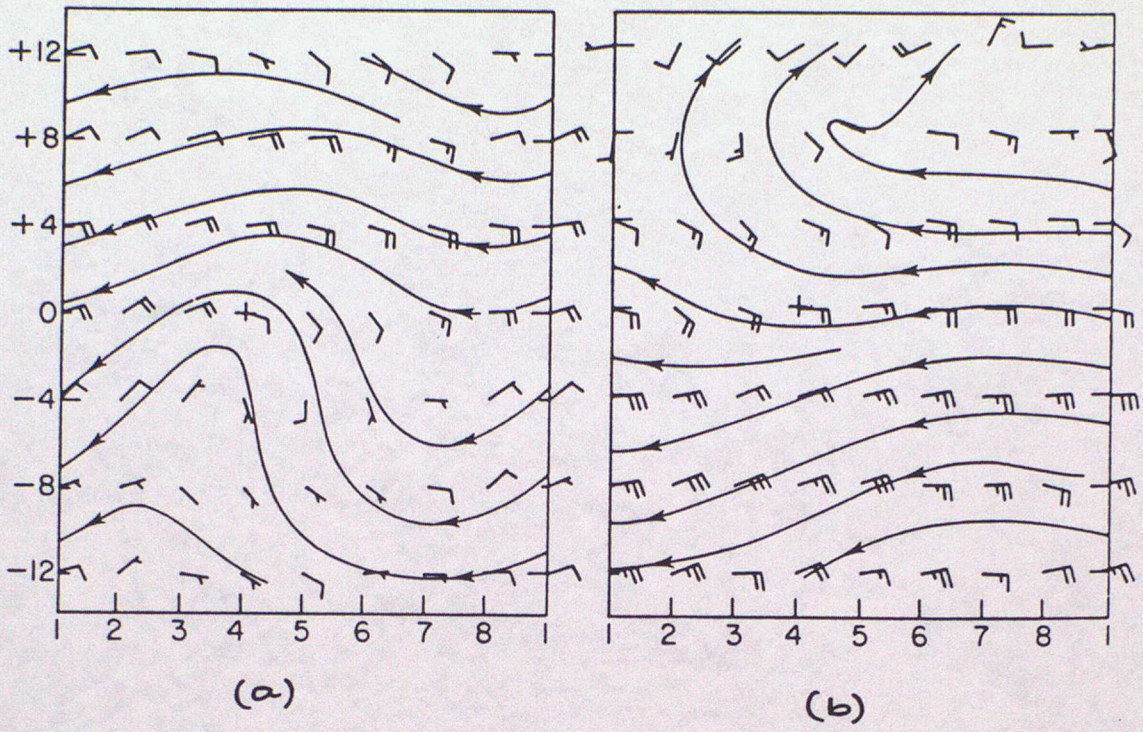
+12
+8
+4
0
-4
-8
-12
1 2 3 4 5 6 7 8 1
(a)
1 2 3 4 5 6 7 8 1
(b)

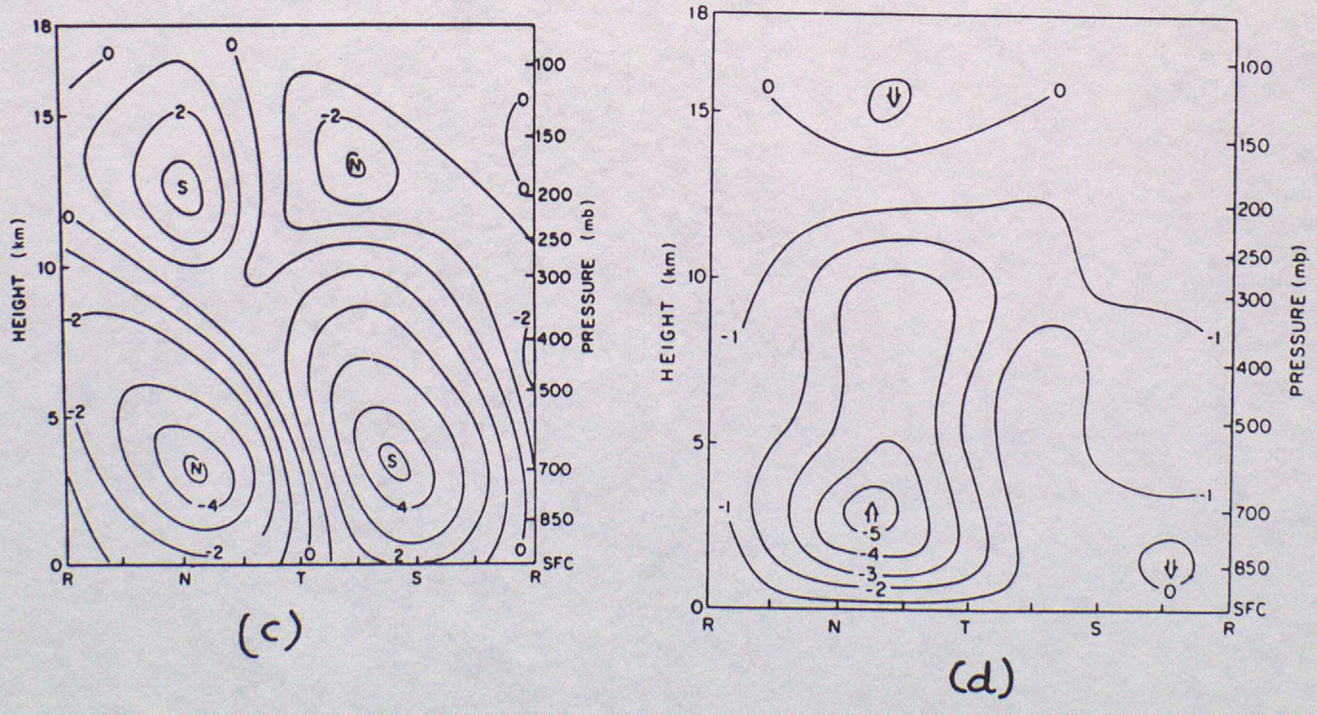
HEIGHT (km)
PRESSURE (mb)
R N T S R
SFC
(c)
(d)

Figure 3.6

THE PHYSICS AND DYNAMICS OF THE CLIMATE SYSTEM

ATMOSPHERIC RESPONSE TO ASYMMETRIC SURFACE FORCING

P R Rowntree
Met O 20, Meteorological Office, Bracknell

4.1 INTRODUCTION

In Lecture 1, I discussed the general circulation on a symmetric earth. The annual mean case (see the sequel (Part II to be published) to Williams (1988) for the seasonally varying case), was quite similar to the observed equinoctial circulation (e.g. March-May in Fig 4.1 from Oort and Rasmusson (1971)). Hadley and Ferrel cells appear in both hemispheres in the observed, though the intensities are less than half as large as in the Williams $\Omega_*=1$ case (the asymmetric solstitial circulations are closer to the intensity found by Williams). The differences may be attributable to the lack of seasonal variation which may tend to disperse the forcing from the equator, or to the geographical asymmetries of the forcing. In this lecture I shall focus on these asymmetries and discuss their role in determining the actual circulation.

4.2 FORCING BY TROPICAL OCEAN TEMPERATURES AND LAND / OCEAN CONTRASTS

4.2.1 Theory and observations

The earth's surface in the tropics is by no means uniform. Two major land masses lie across the equator, South America near 60°W and Africa near 20°E, with additionally a group of large islands (Indonesia and Papua - New Guinea) together with the Malaysian peninsula, centred near 120°E. Near this longitude also are the off-equatorial land masses of Australia and southern Asia. A consequence of this land - ocean distribution is another important asymmetry in the forcing, the sea surface temperature (sst) distribution. The January sst map (Fig 4.2) exhibits clearly the large sst gradients between the eastern and the western oceans, especially south of the equator. This contrast is particularly marked in the largest ocean, the Pacific, precisely because it is the largest. As will be discussed later, in the Climate of the World lecture series, the cool eastern oceans are regions of large variability, the eastern Pacific's El Nino being probably the most important source of interannual variability on the globe.

From what we have learned about the role of thermal forcing in the symmetric circulation, we can deduce some of the consequences of large-scale east-west

temperature gradients near the equator. We should expect heat transport from the warm to the cool regions to prevent barotropically unstable temperature gradients; this transport is not likely to be achieved by baroclinic waves because of the low latitude, so that vertical circulations should exist, with ascent over the warm waters of the west Pacific and descent over the cooler eastern ocean. The ascent will be associated with heavy precipitation and the descent with relatively rainless areas.

The December-February rainfall distribution (Fig 4.3) confirms these expectations. Prominent features are the dry zones over the cool southeastern oceans and the heavy rains over the warm west Pacific on both sides of the equator. Notice also the narrow belts of rainfall along the sst maxima north of the equator over the Atlantic and east Pacific. There are also major rainfall maxima over the continents south of the equator. These continental maxima should not surprise us. In Lecture 1, the lesser thermal capacity of the land compared with the ocean was noted; this allows the continents to respond more rapidly to the seasonal variations of the solar declination, and so act as heat sources relative to the surrounding oceans. We see the same in middle latitudes not only on a seasonal but also a daily basis (hence sea breezes). From the symmetric model we would expect descent in the winter subtropics; there is indeed a general aridity there, but it is broken by areas of moderate rain over the western oceans; these also are no doubt associated with asymmetries of the forcing, though it is not immediately obvious if they are of tropical or extratropical origin.

The ascent regions associated with the heat sources can also be seen on maps of the upper tropospheric velocity potential χ, whose gradient is proportional to the divergent wind. This parameter should be treated with caution, especially where wind data are sparse. However, with modern data assimilation techniques and the availability of wind estimates based on cloud motions observed from satellites, more confidence can be placed in them. As discussed in Lecture 1 for the Hadley cell, the divergent flows tend to be concentrated in shallow layers near the surface and in the upper troposphere, and the 200 HPa level is commomly used to analyse the upper divergence. The divergence is $\nabla^2\chi$, so a little imagination is required to estimate it. The map of χ for January 1979 (Fig 4.4), one of the FGGE special observing periods, emphasises the oceanic convergence zones of the west Pacific and Indian Ocean, with less evidence of the South American and, especially, the African convergence zones.

A striking feature is the anticipated divergent circulation between the Caribbean / east Pacific subsidence region and the west Pacific. This circulation is often called the Walker circulation after the meteorologist who did so much to document its existence through his attempts to predict the Indian monsoon (e.g. Walker, 1932). Equatorial upper westerlies lie above lower tropospheric easterlies and the two vary in intensity together according to the warmth of the equatorial east Pacific and the closely related phase of the 'Southern Oscillation'. These winds are not entirely divergent; the upper westerlies lie between troughs over the east Pacific, both north and south of the equator, while the easterlies which blow from the west Pacific to Africa are flanked by anticyclones (Fig 4.5 from Newell et al (1972)). When the central and east Pacific ssts are warmer than normal, the upper tropospheric rotational flow anomaly pattern features anticyclones north and south of the warm water (more precisely of the associated regions of increased rainfall) (Fig 4.6). These anticyclones are to be expected from the vorticity equation

$$D(\zeta+f)/Dt = -(\zeta+f)\,\nabla.\underline{V} \qquad (4.1)$$

with upper divergence generating anticyclonic vorticity ζ away from the equator until the absolute vorticity approaches zero.

4.2.2 The relative importance of tropical asymmetries

How dominant is the forcing of the tropics by tropical asymmetries or, expressed oppositely, how important are extratropical influences on the tropical circulation? Baroclinic eddies generated in middle latitudes propagate equatorward and may affect tropical rainfall distributions. There is relevant evidence from synoptic studies - for example of cold fronts extending close to the equator. One approach to the problem is to use numerical models to assess the importance of extratropical influences, simply by omitting them. We made some experiments with the Met Office 5 layer model to isolate the relative roles of tropical, extratropical thermal and orographic forcing. In the present context, it is instructive to compare the precipitation simulated by the model with full thermal and orographic forcing with that from an experiment in which only tropical forcing was retained (Fig 4.7, from Rowntree (1979)); specifically, all land was removed except between 21°N and 36°S, while in that belt coastlines and sst variations were retained but all mountains were omitted. Between 20°N and 30°S, the differences between the integrations are small, typically of the same order as expected between two sample periods from the same experiment. Much the same applies to the upper tropospheric flow fields from the two experiments (Fig 4.8).

In easterly wind regimes, trapping of wave energy at critical lines (where the wind speed equals the group velocity) is expected to limit the equatorward propagation of waves from higher latitudes. However, in the upper troposphere, Fig 4.5 shows westerly winds over much of the tropical western hemisphere (180-90-0°W) in northern winter. Webster and Holton (1982) investigated the propagation of waves from a source at 20°N with different zonal flow distributions. With a weak west wind region (Fig 4.9) there was only very limited propagation across the equator, whereas with more intense westerlies, typical of the real east Pacific atmosphere in some northern winter seasons, the waves reach the extratropics of the other hemisphere (Fig 4.10). The sign of the zonally averaged flow - still easterly in Fig 4.10 - clearly is not very relevant.

4.3 EFFECTS OF TROPICAL ASYMMETRIES ON THE EXTRATROPICS

Rossby waves generated at low latitudes may propagate poleward. Fig 4.9 showed one example with a wave train extending northeastward from the imposed wave source. Similar effects have been noted in GCM experiments with tropical Pacific sst anomalies (Fig 4.11, from Geisler et al, 1985) (see also Advanced Lecture 6 in the Climate of the World series), and in linear studies (Fig 4.12 reproduced from Webster (1983)). Observational studies of the flow in winters with a warm east Pacific confirm the relevance of the model results (e.g. Horel and Wallace, 1981), though the precise response varies. This may be due to random variations, or to differences in the basic zonal flow or in the detail of the sst anomaly. These responses show some similarity to the PNA (Pacific - North American) anomaly pattern which is a prominent feature of observed teleconnections in northern winter (Fig 4.13, from Wallace and Blackmon (1983), discussed further in Lecture 5). However, it appears that patterns like the PNA pattern can occur without excitation by asymmetries, tropical or otherwise, as found by Held (1983) in experiments with a flat globe covered by wet land.

There is uncertainty as to whether such propagation can occur from within the easterlies because of critical line absorption. Webster (1983) suggests that tropical sst anomalies affect higher latitudes only because they sometimes lie within the westerlies. However, it may be more relevant whether their upper tropospheric flow effects extend into the westerlies. The meridional scale of the anticyclonic anomaly patterns in Fig 4.6 (beyond 20°) is such that the equatorward limit of the westerlies in northern winter (Fig 4.5) (<15°) would always allow poleward propagation.

4.4 LAND SURFACE CONTRASTS

Contrasts in surface forcing are not confined to those due to sst gradients or land/ocean contrasts. Within land masses, there are variations in land surface characteristics; an obvious example is between forest and desert regions. Forests differ from deserts in several ways.

Firstly, the albedo is lower (0.12 compared with from 0.2 to 0.45 for deserts); with an incoming daily mean solar radiation of up to 300 W m^{-2} with clear skies, a difference of 0.2 reduces the absorbed solar radiation by 60 W m^{-2}; this cuts the net radiation at the surface by about a third. It also reduces the net radiation at the top of the atmosphere and the forcing of upward motion since, as discussed in Lecture 1, spatial variations in diabatic heating must be made good by heat redistribution through vertical circulations to avoid barotropically unstable flow gradients. This concept was used by Charney (1975) to develop a theory for the dynamical maintenance of deserts, based on the positive feedback mechanism implied:

dry land → high albedo → subsidence → less rain → dry land.

Charney's hypothesis has been well supported by GCM experiments (e.g. Mintz, 1984; Rowntree, 1984) which have invariably shown decreases of precipitation with increasing albedo, generally with decreases of moisture convergence also - the second result is not a necessary consequence of the first because an increase of albedo usually reduces the evaporation. (see also Lecture 4 in the Climate of the World series)

Secondly, over forests, there is readily available moisture for evaporation, either through transpiration or, if the canopy is wet, through direct evaporation at the potential rate. Typical water losses are 3 to 5 mm/day. Deserts typically have negligible (e.g. 0.1 mm/day) evaporation. An increase of 3 mm/day in evaporation can increase relative humidity by ≈12%/day in the tropics (see Lecture 4 in the Climate of the World series). Because a dry atmosphere inhibits precipitation, and the enhanced surface sensible heat flux does not penetrate beyond the middle troposphere, there is, as with increased albedo, a need for energy imports (leading to subsidence and so again a positive feedback) to balance the energy budget over arid regions. Surface aridity also contributes to the radiative deficit by two mechanisms: firstly, surface temperatures are higher in the absence of evaporative cooling so that longwave losses are increased; secondly, the drier atmosphere radiates less heat downwards and allows greater radiative loss to space direct from the surface. Both these again provide

positive feedbacks. On the other hand, cloudiness may be less, so reducing the planetary albedo and increasing surface solar heating, giving a negative feedback.

Again, there is ample evidence from GCMs of these effects. Experiments with reduced surface moisture availability give less rainfall. In an experiment with the Met Office model, the circulation over North Africa was considerably changed by increasing soil moisture over the Sahara. At 700 HPa, the usual easterly near 15°N was replaced by a westerly with cyclonic circulation centred near 20°N (Fig 4.14, from Cunnington and Rowntree (1986)). The associated ascent and rain (not shown) are consistent with the view that subsidence in the outer tropics and subtropics is not a function of latitude, as simplified pictures of the circulation can imply, but of the energy balance relative to surrounding areas.

Thirdly, surface roughness lengths (z_o) for forests are of order 1m, compared with less than 1cm for deserts. This has two effects. Firstly, with larger roughness, evaporation is increased from wet surfaces, accelerating the recycling of moisture, with possible consequent enhancement of precipitation over forested land during rainy periods. Note,however, that for dry, but still transpiring, surfaces evaporation decreases with increasing roughness(Rowntree, 1988). Secondly, frictional convergence is enhanced for the rougher surface. Sud and Smith (1985) found that a reduction of z_o over the Sahara reduced moisture convergence and rainfall in their (too wet) GCM (Fig 4.15). This is another possible positive feedback mechanism.

The effects on climate and the general circulation of changes in land surface characteristics have been explored in several GCM experiments (e.g. see Mintz (1984). In addition to the effects on precipitation stressed by Mintz, and those discussed above, changes in the tropics affect the tropical upper tropospheric flow (e.g. see discussion in Cunnington and Rowntree (1986)). The effects are of similar character to those obtained in sst experiments with anticyclonic (cyclonic) anomaly patterns with equatorial easterlies (westerlies) developing in response to heat sources (sinks). An example is the extensive tropical westerly anomalies in Fig 4.16 obtained in the experiment by Cunnington and Rowntree (1986) discussed earlier, in which a major source of latent heating over North Africa was eliminated. The discussion in section 4.3 above concerning the influence of tropical asymmetries on the extratropical flow refers equally to land surface characteristics and changes therein. The potential for positive feedbacks between the land surface and climate discussed earlier in this section could make this an important mechanism for climate change. However, as

discussed further in Lecture 4 of the Climate of the World series, there is little or no evidence that the suggested feedbacks have yet played a measurable role in any climate change.

There is also considerable scope for feedbacks between ocean and atmosphere. The ITCZ over the ocean is one possible example of a positive feedback:

- atmospheric convergence → light winds → weak fluxes → ocean warming

This topic will not be pursued here.

4.5 FORCING BY EXTRATROPICAL ASYMMETRIES

The extratropical circulation is forced by:

(i) tropical heat sources as discussed above;

(ii) extratropical thermal contrasts, as between warm oceans (land) and cool land (oceans) in winter (summer);

(iii) mountains.

The relative importance of these in forcing the major circulation features - winter longwave troughs, summer continental upper anticyclones and oceanic surface highs - can be assessed to a considerable extent using numerical models. We have already discussed the role of (i). Unfortunately, recent work on the separation of (ii) and (iii), while taking advantage of more powerful computing facilities to obtain more reliable results, has not attempted to separate the tropical (i) and extratropical (ii) thermal forcing.

As in the tropics, the thermal forcing in middle and high latitudes can be separated into the part due to the different thermal characteristics of land and sea, and that caused by spatial and temporal variations in ocean temperature. These will not necessarily have similar effects because of the different horizontal scales, and the different vertical atmospheric structures over cold surfaces (land in winter and ocean in summer) and warm surfaces. However, they have only been separated in a local context, as in sst anomaly studies on a scale of a few thousand kilometres or less (see Lecture 5 in Climate of the World series and Rowntree (1986)). The effect of thermal forcing is expected to be similar to that in the tropics: over warm surfaces, a lower tropospheric low and upper high, and the opposite over cold.

The effects of mountains on the flow can be considered in terms of the vorticity equation, using the schematic diagram of the flow over an extensive north-south barrier in Fig 4.17 (from Holton, 1979). The column of air M is confined between

the two potential temperature surfaces θ_0 and $\theta_0 + \delta\theta$. For adiabatic flow the low level air approximately follows the surface contours, whereas the air at upper levels experiences a smaller vertical deflection. As the initially zonal current (relative vorticity $\zeta = 0$) crosses the mountain, it therefore shrinks vertically and from equation (4.1) the relative vorticity must therefore become negative. This leads to anticyclonic curvature, so the column is deflected southwards. Beyond the mountain the air column returns to its original depth, but because the air is now further south than before, f is smaller and ζ must therefore become positive to satisfy equation (4.1). Cyclonic curvature is produced which remains until the air is back at its original latitude. The air now overshoots northward and experiences an increasing coriolis parameter which returns the air to the south. This oscillatory behaviour continues as the air moves away from the mountain. Such a barrier therefore induces a ridge over the mountain and a lee trough to the east, followed by a train of forced Rossby waves. As Charney and Eliassen (1949) found in surprisingly successful early numerical research on this problem, the effect of surface friction is to reduce the amplitude of these waves progressively as the air moves downstream.

The effects of the total thermal forcing and also the orographic forcing have been analysed by Held (1983) using the results of a 15 year run with the GFDL model. It is clearly important for the credibility of such an analysis that the simulation with full forcing be realistic; this is demonstrated for 45°N by the vertical cross sections for 45°N in Fig 4.18 (from Wallace (1983), Held (1983) and Charney and Eliassen (1949) in order from the top). This figure allows comparison of the relative importance of the thermal and orographic contributions; the maximum amplitudes are similar, though the thermal pattern is of larger scale, with only a weak effect from North America, whereas the Rockies and Asia are of similar orographic importance at this latitude. The horizontal picture (Fig 4.19 from Held (1983)) gives a similar impression. The Atlantic warm ridge and east Asian cold trough dominate the thermal effects, the Rockies ridge and the Asian massif's downwind trough the orographic. A curious feature is the broad similarity of the orographic and thermal components at this level.

Held points out that the downwind response to the Rockies suggests wavetrains propagating southeastward from Alaska to the Caribbean; this is more obvious in the streamfunction field (Fig 4.20) because the weighting by f is removed. A corresponding feature is evident emanating from the Asian massif. This is reminiscent of Charney and Eliassen's work discussed above. A similar pattern is obtained by Held (1983) in a linear barotropic steady-state model (similar to

Charney and Eliassen's but two-dimensional) and explained in terms of Rossby wave ray tracing.

The summer circulation has had less analytical effort devoted to it. Wallace (1983) notes the large response at 25°N (Fig 4.21), and its generally thermal character - i.e. opposite responses in the lower and upper troposphere, with the summer monsoon heat source over southern Asia dominating at this latitude. At higher latitudes, the patterns are weaker, though the trough near 70°W with downstream Scandinavian ridge are interesting. Wallace considers the suggestion that their equivalent barotropic character (i.e. same phase at all levels) and the orientation of the features imply a wave train propagating from the Rockies ridge (Fig 4.22).

Finally, the effects of the Antarctic continent on the southern hemisphere circulation deserve discussion. The 200 HPa stationary wave structure in January and July are quite similar, so we will discuss only the winter pattern (Fig 4.23 from Wallace (1983)). The high latitudes are dominated by a strong wave 1, with a ridge in the Pacific sector and trough south of the Indian Ocean. James (1988) has used the non-linear barotropic vorticity equation, with the addition of a term to relax the solution towards a mean zonal flow, to calculate the steady state response of the flow to a circular mountain of radius 10° displaced 10° from the pole (Fig 4.24). There is considerable similarity to the observed circulation, not only in the features mentioned above, but also in the high east of southern Africa and the trough near southwestern Australia (120°E). It is interesting that in the run with relaxation to the northern hemisphere zonal mean flow (Fig 4.24 (lower)), the response was confined to the poles - a good illustration of the difficulties of understanding the global circulation!

The relative roles of tropical and extratropical forcing have not been assessed in recent analyses. The spectral analysis for 18° wide latitude belts (Fig 4.25) from Rowntree (1979) shows the dominance of extratropical forcing poleward of 36° latitude for the first three wavenumbers, especially in the upper troposphere. The tropical effects which are equivalent barotropic outside the tropics are relatively more important near the surface in middle latitudes and tend to be dominant at both levels in the tropics.

4.6 REFERENCES

Arkin, P. A., Kopman, J. D. and Reynolds, R. W., 1983, 1982-1983 El Nino / Southern Oscillation event quick look atlas. Climate Analysis Center, NOAA, Washington, D.C.

Charney, J. G., 1975, Dynamics of deserts and drought in the Sahel. Quart J R Met Soc, 101, 193-202.

Charney, J. G. and Eliassen, A. 1949, A numerical method for predicting the perturbations of the middle latitude westerlies. Tellus, 2, 184-195.

Cunnington, W. M. and Rowntree, P. R., 1986, Simulations of the Saharan atmosphere - dependence on moisture and albedo. Quart J R Met Soc, 112, 971-999.

Geisler, J. E., Blackmon, M. L., Bates, G. T. and Munoz, S., 1985, Sensitivity of January climate response to the magnitude and position of equatorial Pacific sea surface temperature anomalies. J Atmos Sci, 42, 1037-1049.

Held, I. M., 1983, Stationary and quasi-stationary eddies in the extratropical troposphere: theory. In: Large-scale dynamical processes in the atmosphere (Ed. Hoskins, B. J. and Pearce, R. P.), Academic Press, pp. 127-168.

Holton, J. R., 1979, An introduction to dynamic meteorology. (Second edition), Academic Press, 391 pp.

James, I. N., 1988, On the forcing of planetary-scale Rossby waves by Antarctica. Quart J R Met Soc, 114, 619-637.

Mintz, Y., 1984, The sensitivity of numerically simulated climates to land surface boundary conditions. In: The global climate (Ed. Houghton, J. T.), Cambridge University Press, pp. 79-105.

Newell, R. E., Kidson, J. W., Vincent, D. G. and Boer, G. J., 1972, The general circulation of the tropical atmosphere and interactions with extratropical latitudes, Vol. 1. MIT Press, 258 pp.

Oort, A. H. and Rasmusson, E. M., 1971, Atmospheric circulation statistics. NOAA Professional Paper 5, NOAA, U.S Department of Commerce, 323 pp.

Rowntree, P. R., 1979, Numerical prediction and simulation of the tropical atmosphere. In: Meteorology over the tropical oceans, (Ed. Shaw, D. B.), Royal Met Soc, pp. 219-249.

Rowntree, P. R., 1984, Review of general circulation models as a basis for predicting the effects of vegetation change on climate. Met O 20 Tech. Note II/225.

Rowntree, P. R., 1986, A survey of ocean surface temperature anomaly experiments. Met O 20 Tech. Note II/220 (Revised edition).

Rowntree, P. R., 1988, Estimates of the sensitivity of climate to vegetation changes using the Penman-Monteith equation. (In preparation).

Sud, Y. C. and Smith, W. E., 1985, The influence of surface roughness of deserts on the July circulation (a numerical study). Boundary Layer Met, 33, 15-49.

Walker, G. T. and Bliss, E. W., 1932, World weather V. Mem R Met Soc, IV, 53-84.

Wallace, J. M., 1983, The climatological mean stationary waves: observational evidence. In: Large-scale dynamical processes in the atmosphere (Ed. Hoskins, B. J. and Pearce, R. P.), Academic Press, pp. 27-53.

Wallace, J. M. and Blackmon, M. L., 1983, Observations of low-frequency atmospheric variability. In: Large-scale dynamical processes in the atmosphere (Ed. Hoskins, B. J. and Pearce, R. P.), Academic Press, pp. 55-94.

Webster, P. J., 1983, Large-scale structure of the tropical atmosphere. In: Large-scale dynamical processes in the atmosphere (Ed. Hoskins, B. J. and Pearce, R. P.), Academic Press, pp. 235-275.

Webster, P. J. and Holton, J. R., 1982, Cross equatorial response to middle latitude forcing in a zonally varying basic state. J Atmos Sci, 39, 722-733.

Williams, G. P. 1988, The dynamical range of global circulations - I. Climate Dynamics, 2, 205-260.

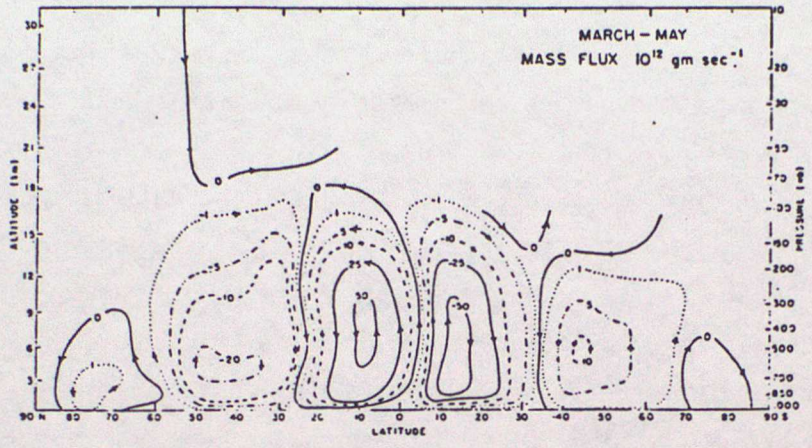

Figure 4.1 Observed March to May mean meridional mass flux latitude-height cross section (10^{12} g s^{-1})

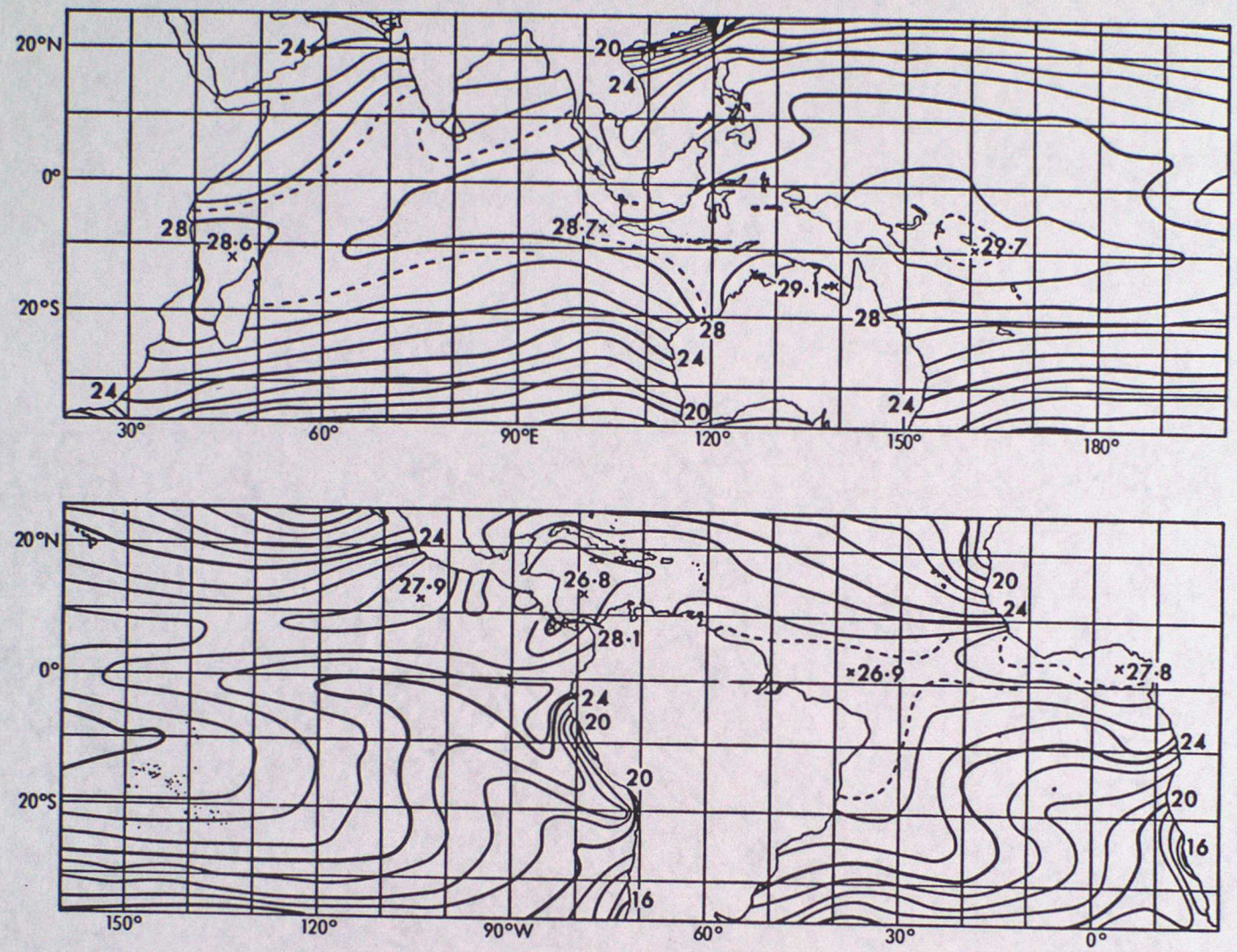

Figure 4.2 Normal January sea surface temperatures used in the experiments. Solid contours at 1°C intervals with some dashed 0.5°C contours.

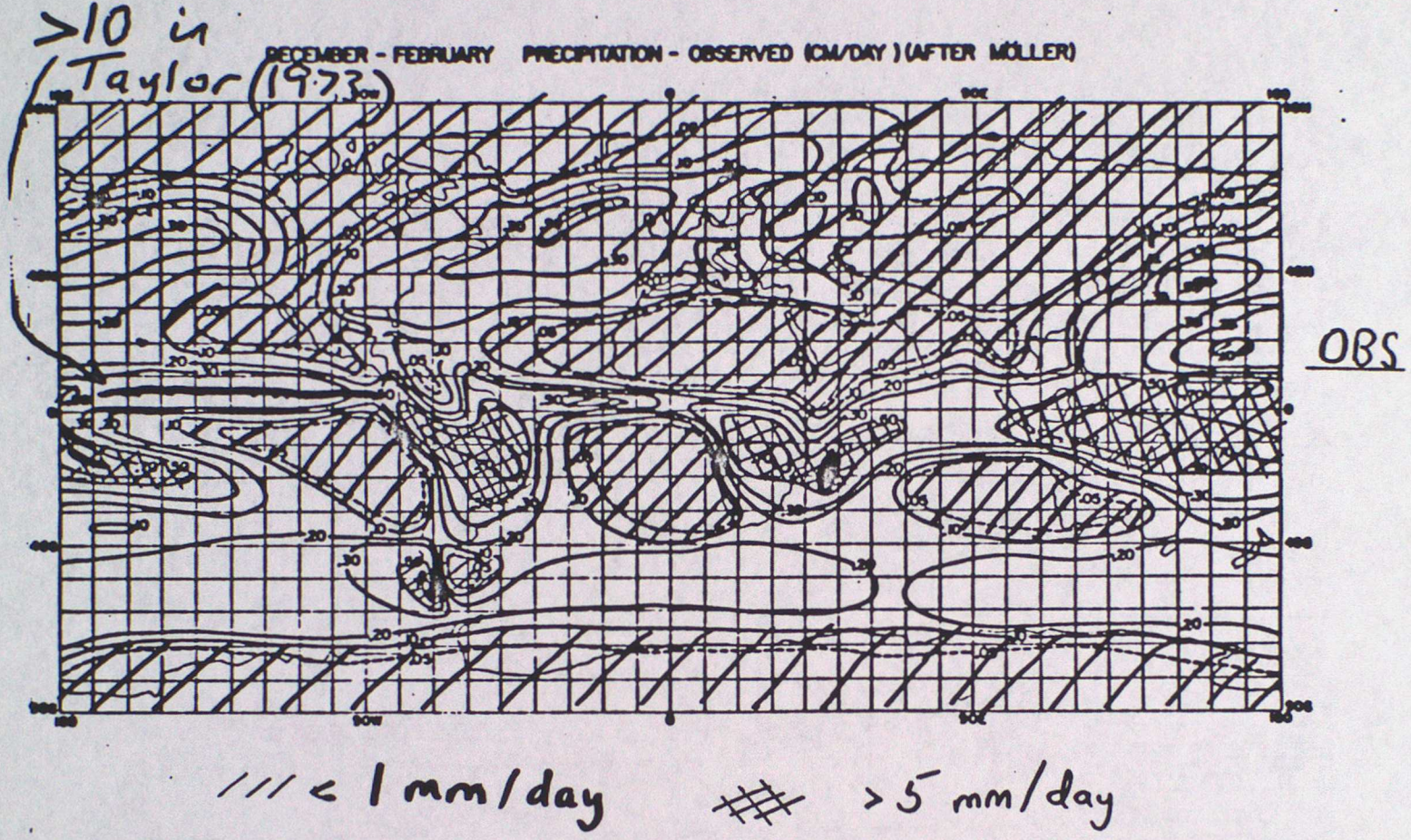
>10 in Taylor (1973)
DECEMBER - FEBRUARY PRECIPITATION - OBSERVED (CM/DAY) (AFTER MÖLLER)
OBS
/// < 1 mm/day
>5 mm/day

Figure 4.3

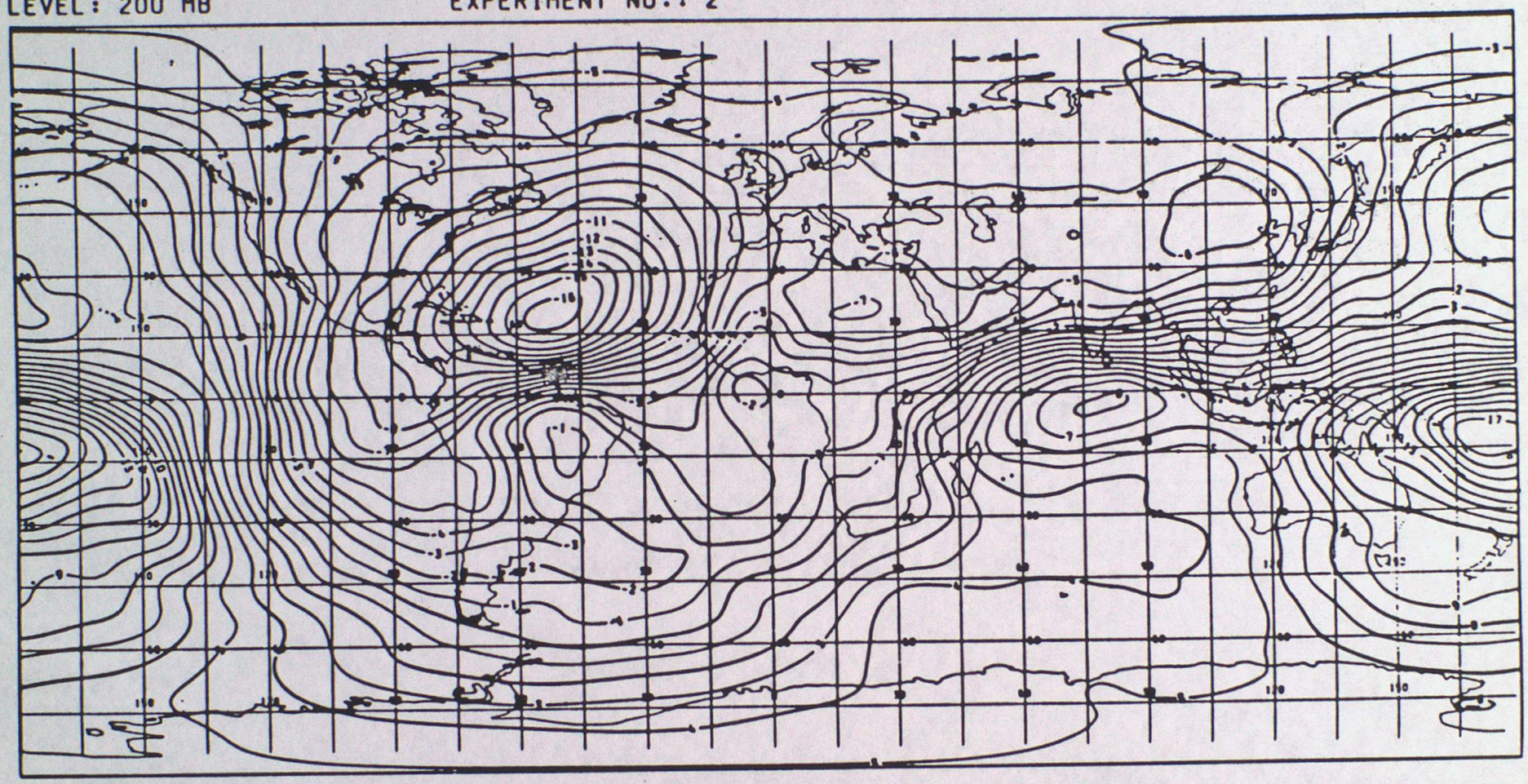

Figure 4.4

(Units: $10^6 m^2 s^{-1}$)

Figure 4.5 (from Newell et al, 1972)

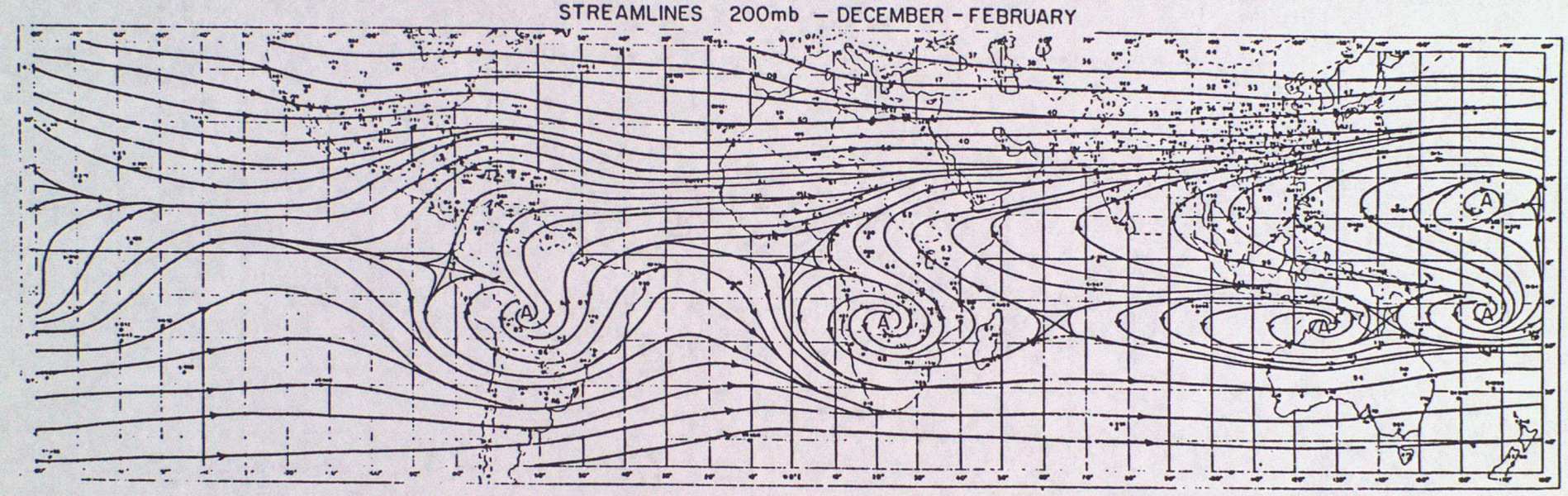

Figure 4.6

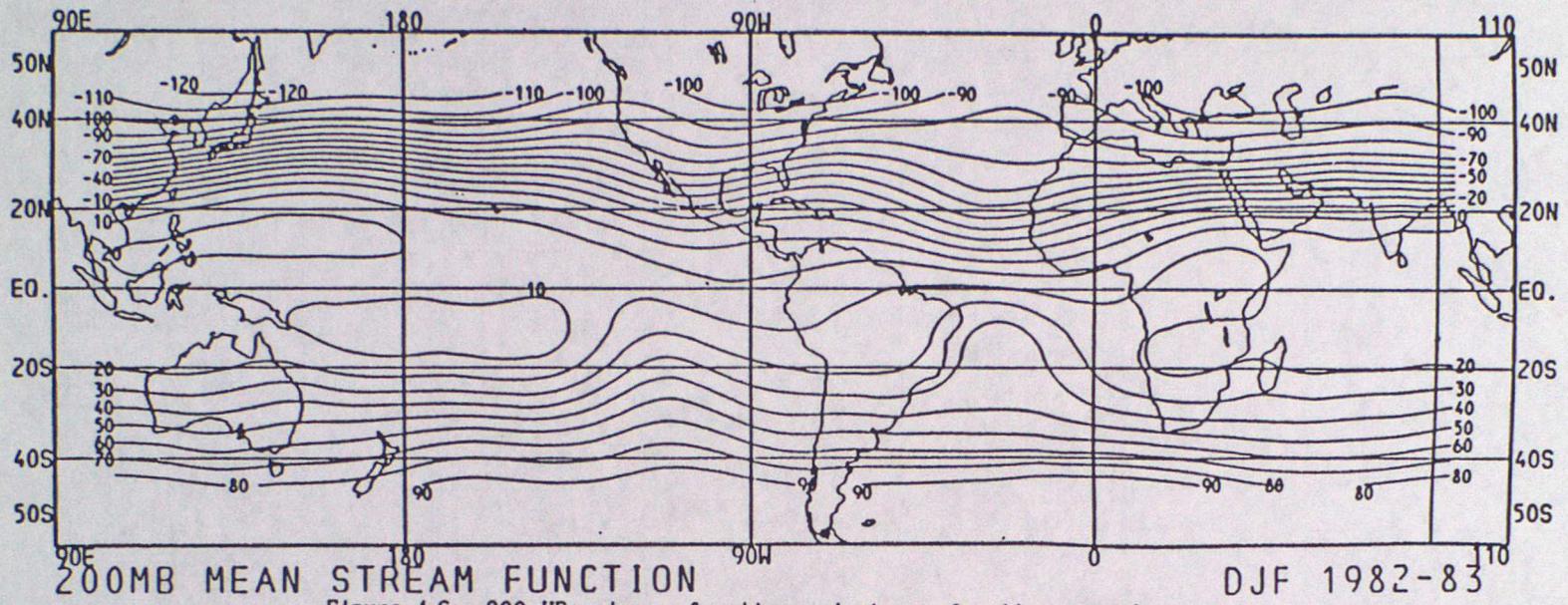

Figure 4.6: 200 HPa stream function and stream function anomaly for December - February 1982-83 from Arkin et al (1983).

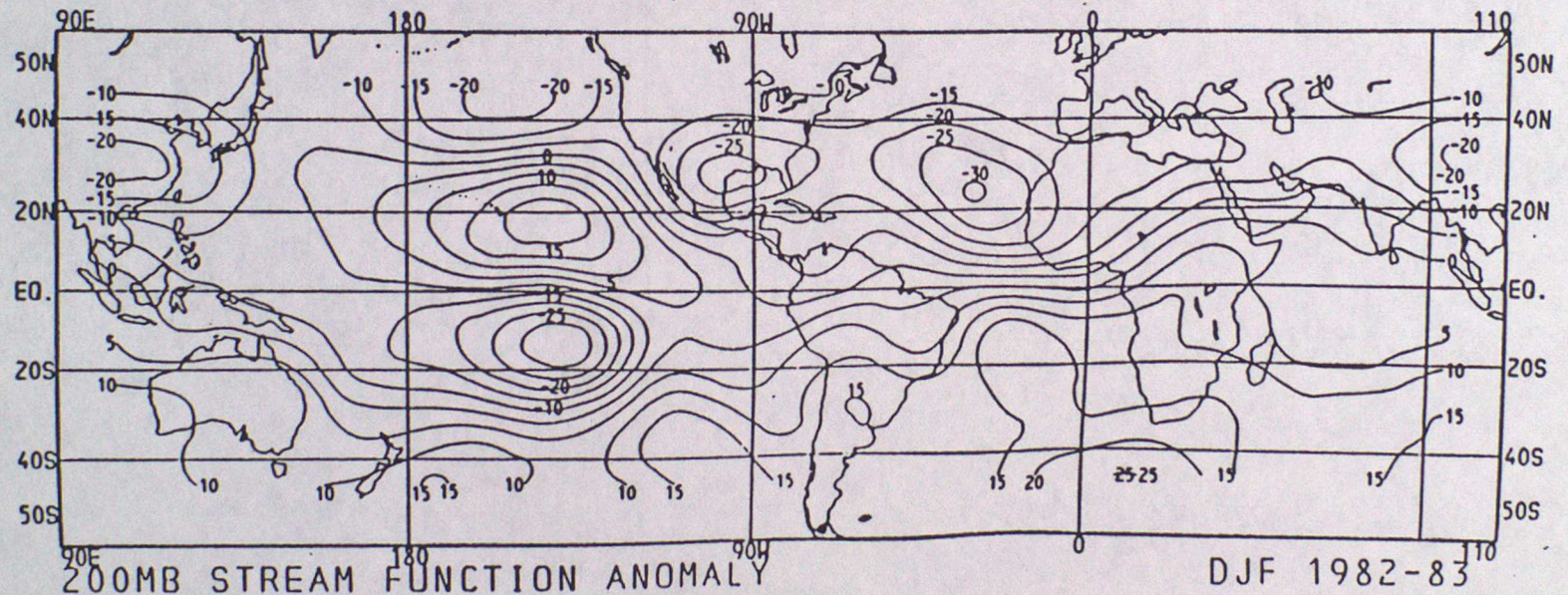

Figure 4.7

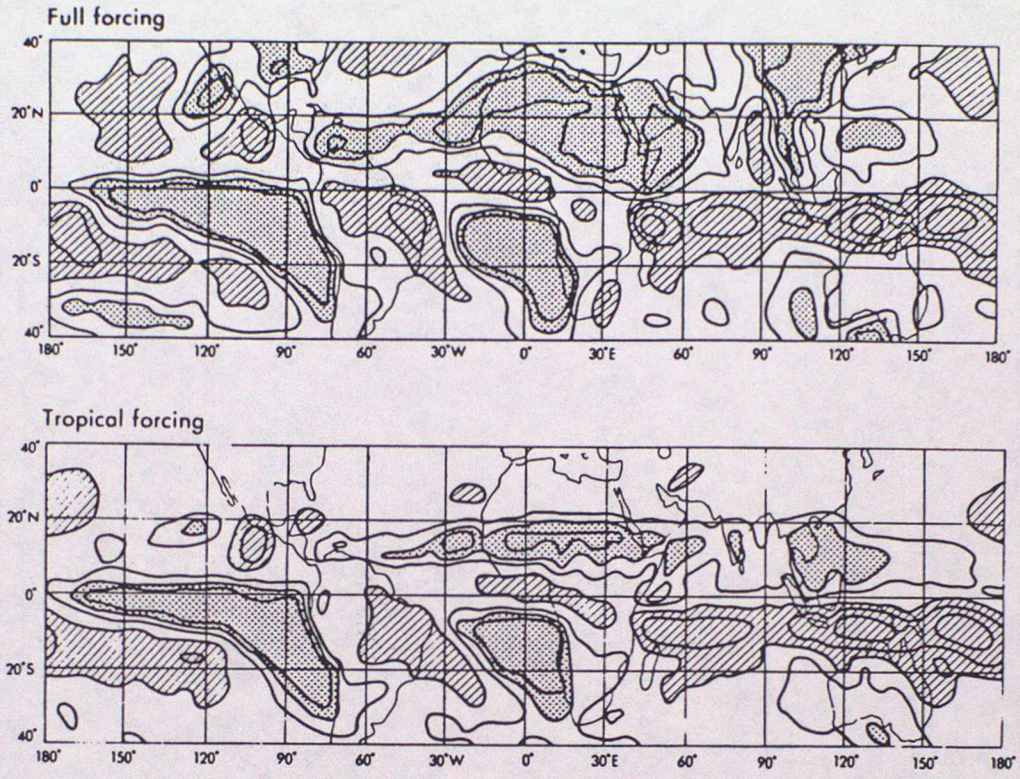

Precipitation for the day 41–80 mean of experiments with (a) full forcing and (b) only tropical forcing. Contours at 0·5, 1, 2, 5, 10, 20 mm d^{-1}. Areas with less than 1 mm d^{-1} stippled and more than 5 mm d^{-1} hatched.

Figure 4.8

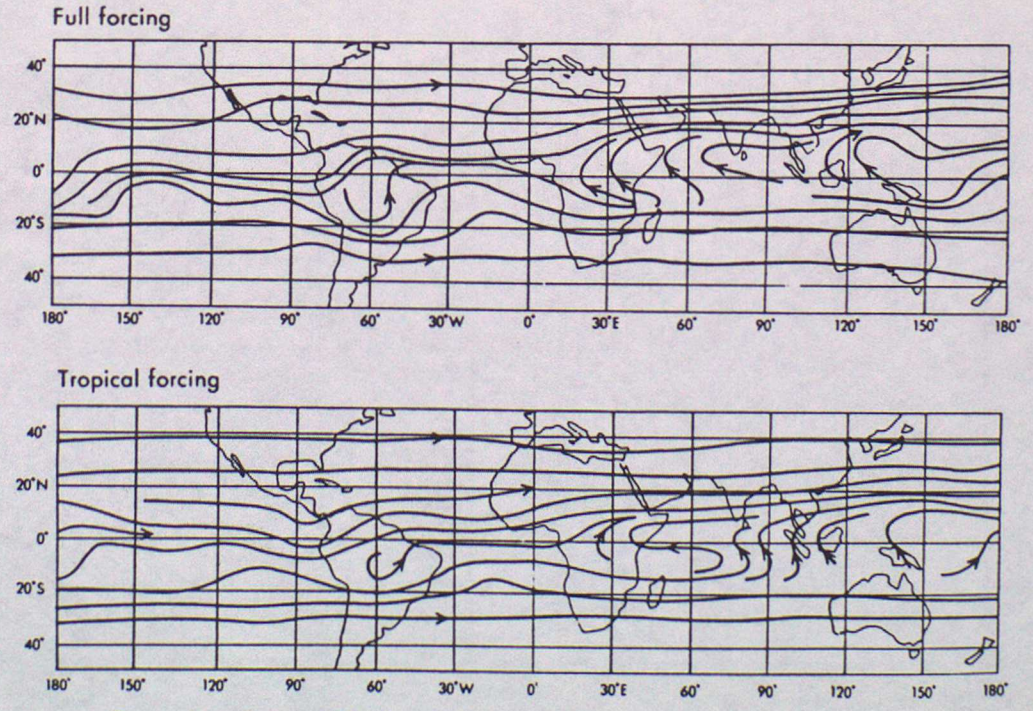

Stream lines for $\sigma = 0{\cdot}3$ (about 300 mb) for the day 41–80 mean of experiments with (a) full forcing and (b) only tropical forcing.

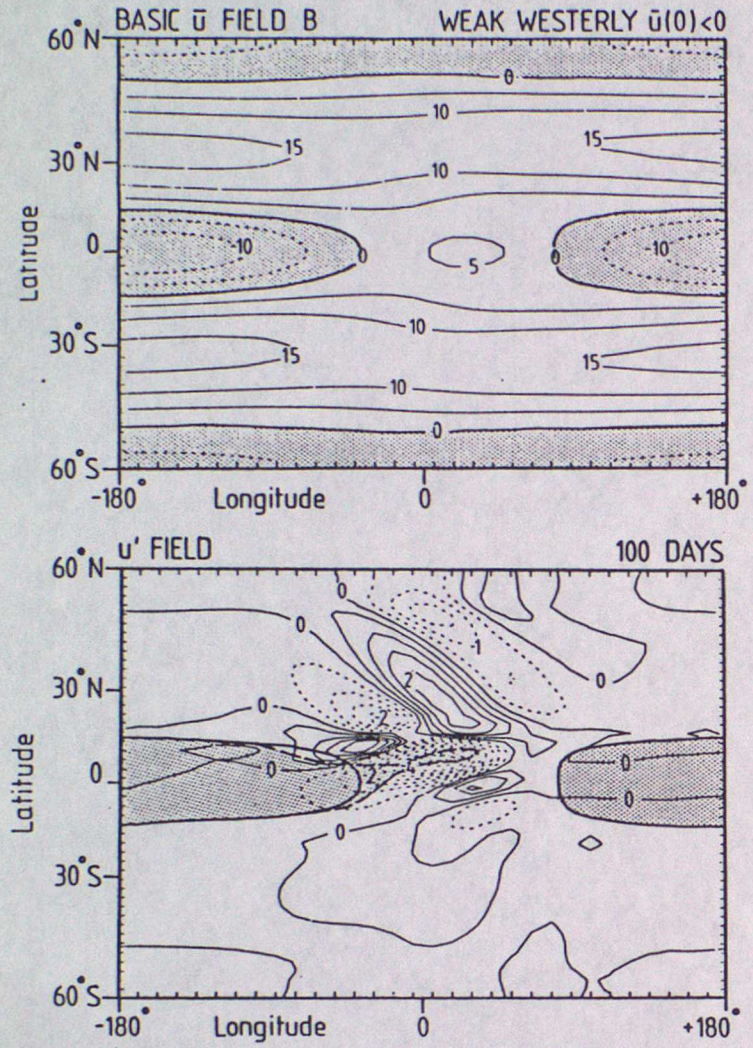

Wave propagation of modes forced in mid-latitudes in a zonally varying basic state possessing a weak westerly maximum at the equator. The zonally averaged state is easterly. Upper panel shows the initial basic state and the lower panel the perturbation zonal velocity component after 100 days of integration. Shaded area denotes the location of the zonal easterlies after 100 days. (From Webster and Holton, 1982.)

Figure 4.9

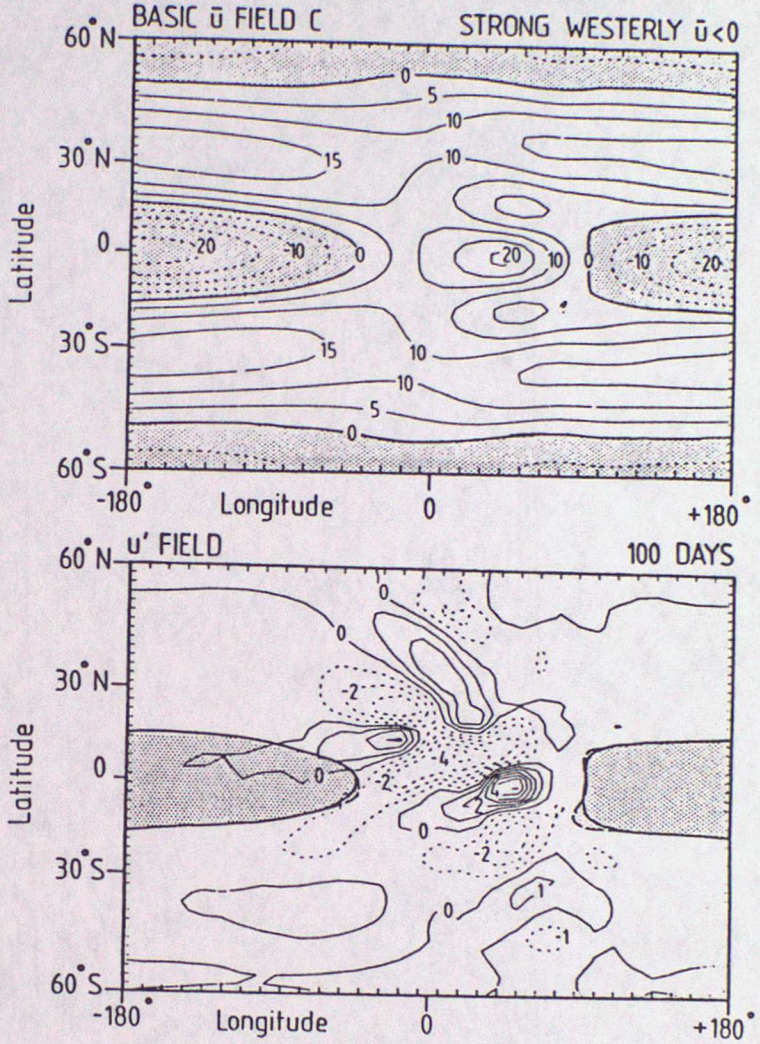

Same as Fig. 9.20 but for a basic state with a strong westerly region at the equator. Zonally averaged state is still easterly. (From Webster and Holton, 1982.)

Figure 4.10

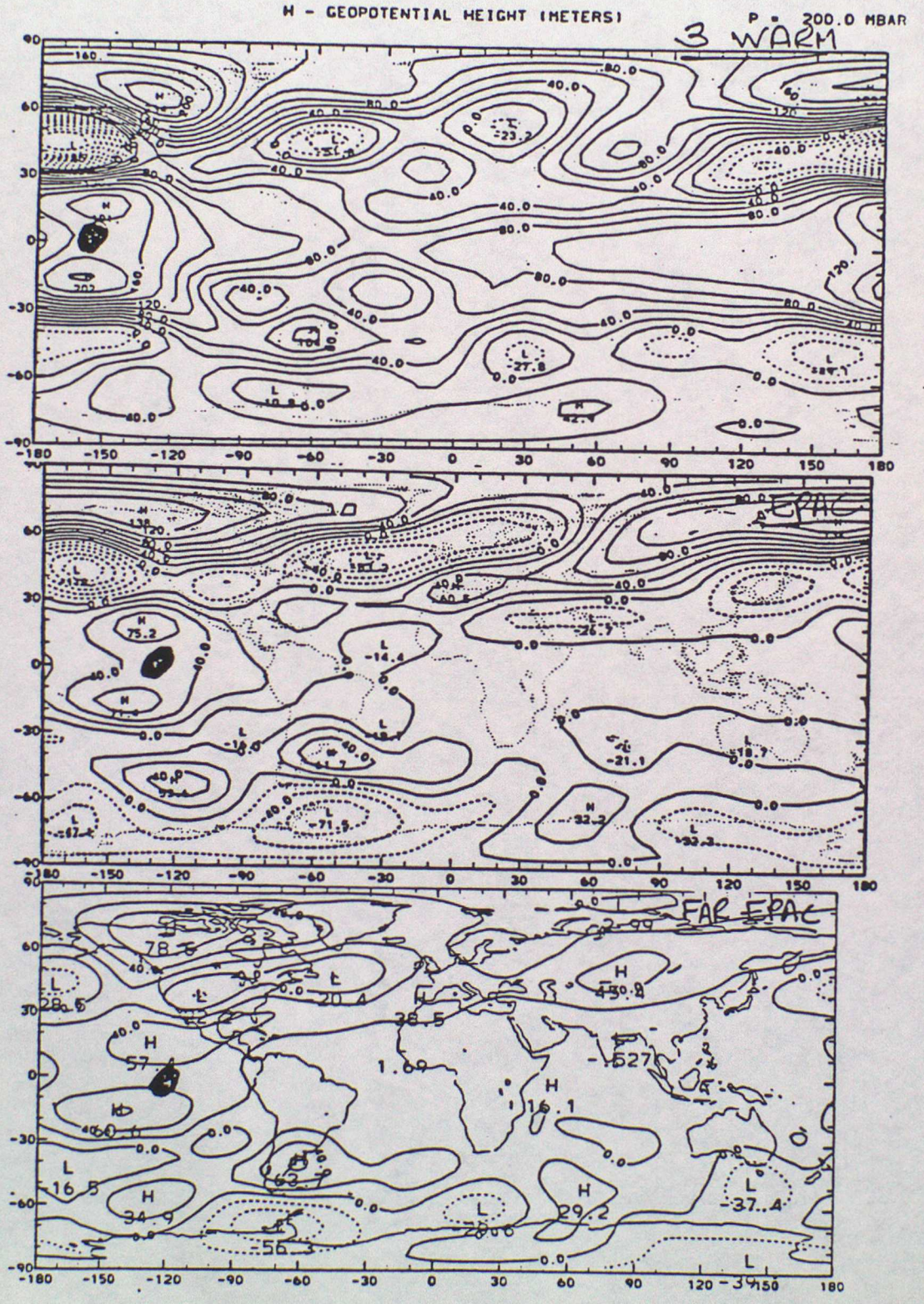
H - GEOPOTENTIAL HEIGHT (METERS)
P = 200.0 MBAR
3 WARM
EPAC
FAR EPAC

Figure 4.11

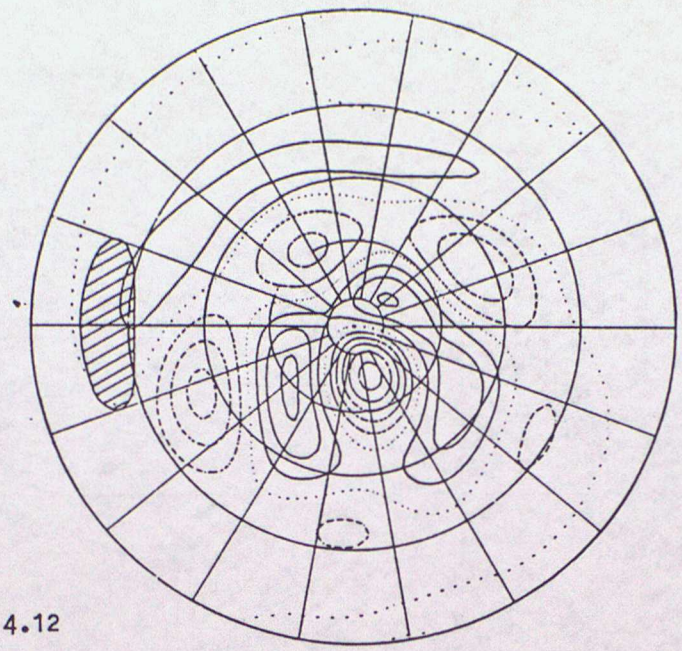

Figure 4.12

The 300 mb height field perturbation for a steady state, linear solution of a five layer baroclinic model with a heat source in the hatched region perturbing the Northern Hemisphere winter zonal flow. The vertical distribution of the source is of the form sin $\pi\sigma$. Positive contours are continuous. If the depth averaged heating maximum is 2.5 K day^{-1} then the contour integral is 2 dam. (From Hoskins and Karoly, 1981.)

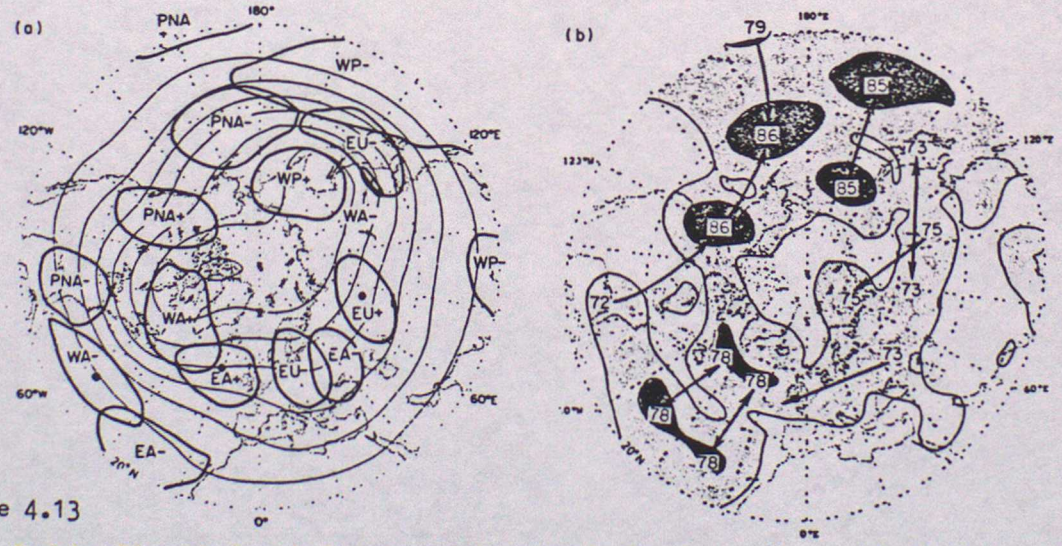

Figure 4.13

.. Depiction of the predominant simultaneous correlation patterns in winter-time monthly mean 500 mb height data. (a) Areas enclosed by heavy lines represent centres of the five strongest patterns identified in the correlation statistics: PNA—the Pacific/North American pattern; WA—the West Atlantic pattern; EA—the East Atlantic pattern; EU—the Eurasian pattern; and WP—the West Pacific pattern. The plus and minus signs denote the sense of the correlations within each pattern; centres of like (unlike) sign are positively (negatively) correlated with one another. The lighter contours show the wintertime mean 500 mb height pattern. (b) Shading denotes regions that exhibit strong negative correlations with distant gridpoints (light shading, stronger than -0.6; and heavy shading, stronger than -0.75). Arrows indicate the region with which they are strongly negatively correlated. For example, gridpoints over the southeastern United States show strong negative correlations (up to -0.72) with gridpoints in western Canada and those gridpoints show even stronger negative correlations (up to -0.86) with gridpoints in the Central Pacific. After Wallace and Gutzler (1981). For confirmation of these results based upon methods of factor analysis, see Horel (1981). Small circles in (a) denote gridpoints for which lag correlation statistics are shown in the following three figures.

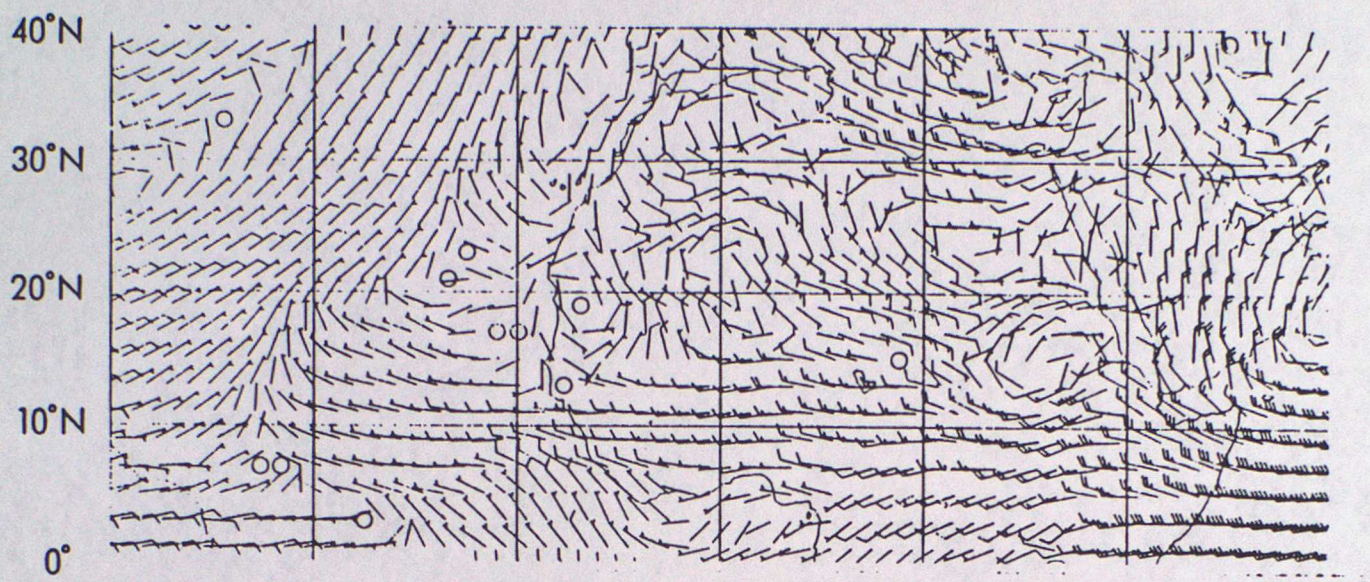

(a) I1

Figure 4.14: Winds at 700 HPa averaged for last 30 days of 50 day July simulations with (a) wet and (b) dry initial atmosphere over North Africa.

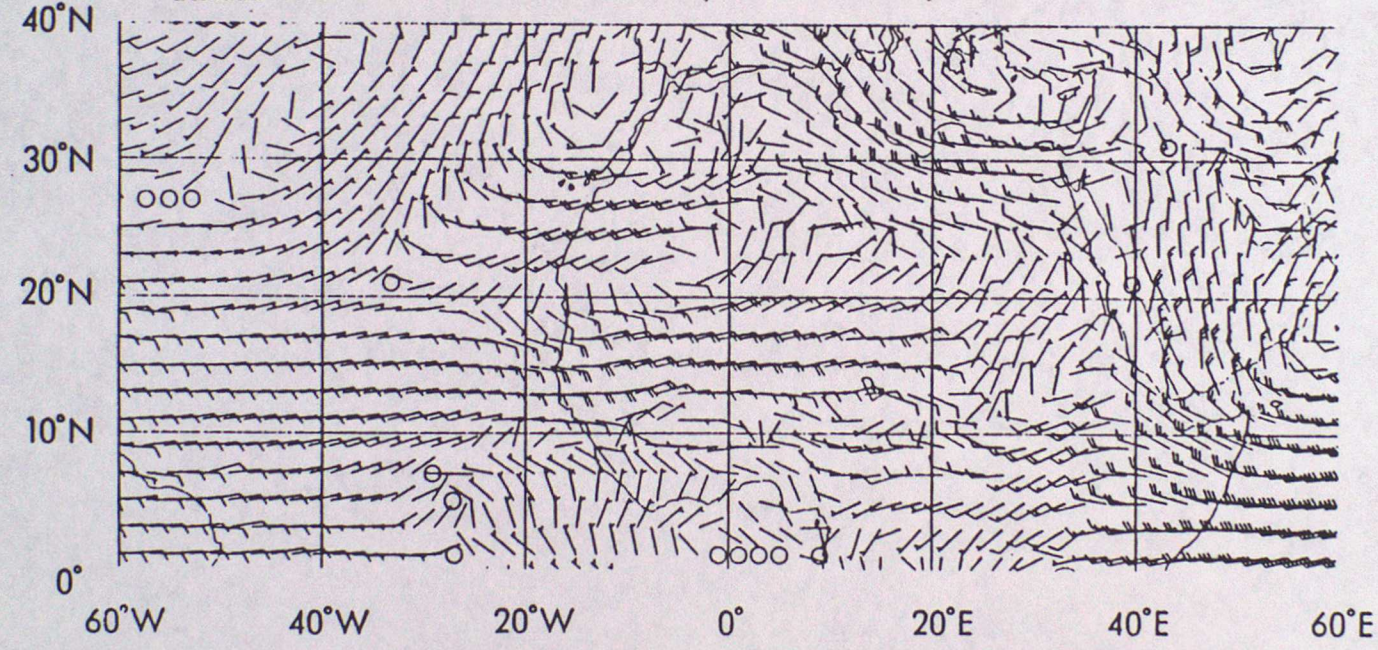

(b) I2

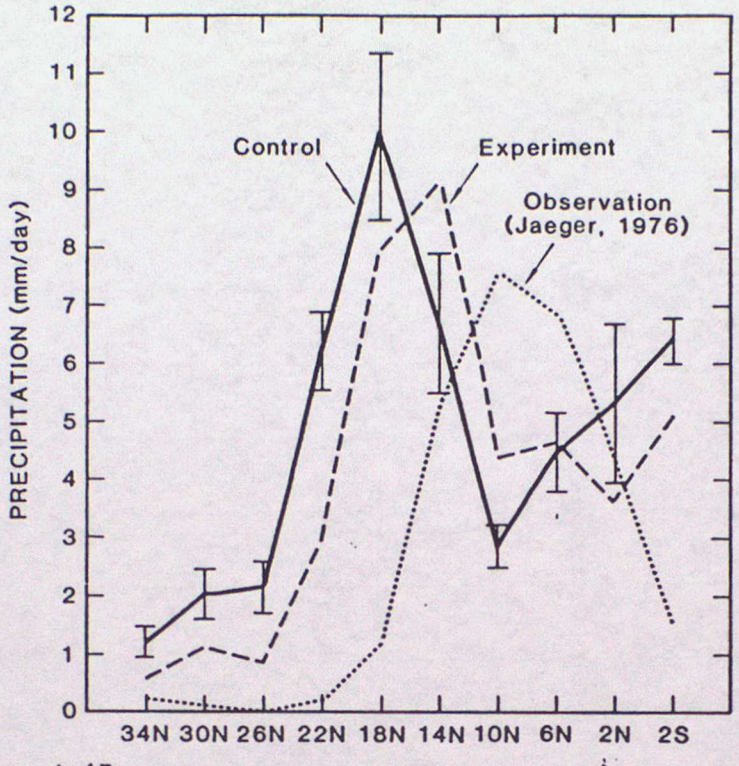

Figure 4.15

Mean Zonal July Precipitation (mm/day) over the Sahara Region for Control and Experiment simulations, and for Jaeger's (1976) Observations. (Error Bars for the Control case represent the standard deviation).

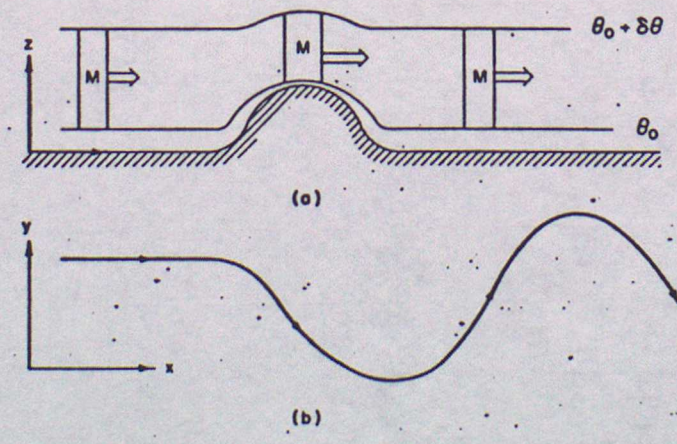

Westerly flow over a topographic barrier: (a) the depth of a column as a function of x, (b) the trajectory of a parcel in the x, y plane.

Figure 4.17

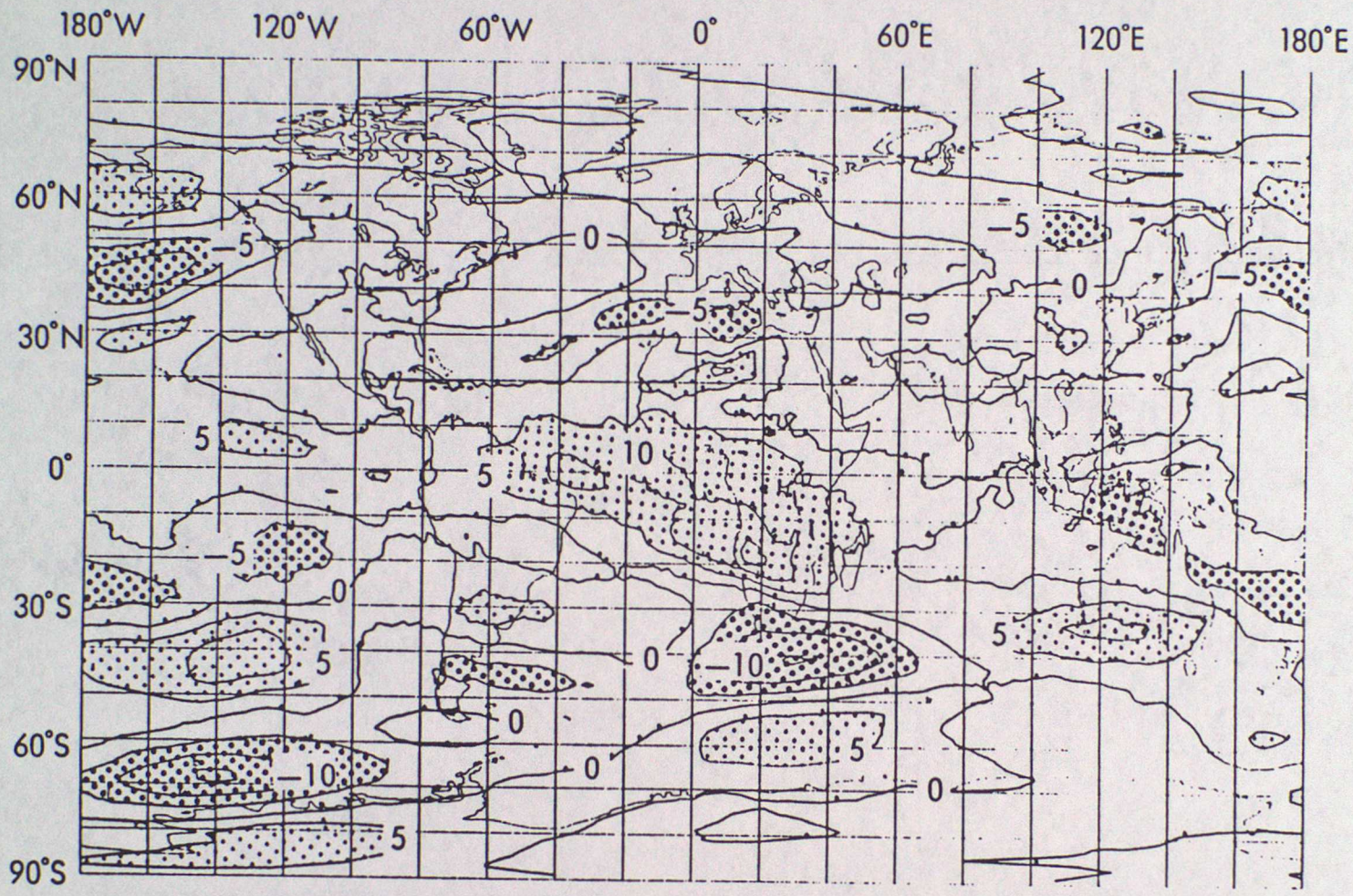

Figure 4.16: Differences in zonal winds at 200 HPa of dry relative to wet North African experiments as in Fig 4.14. Light stippling for increases in westerly component by >5 m/s, heavy stippling for decreases of >5 m/s.

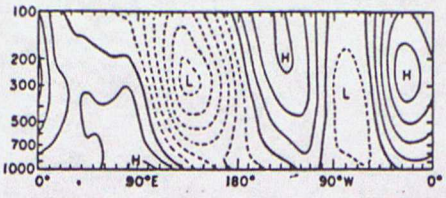

Longitude–height cross-sections of stationary-wave geopotential height Z^* for the winter season, derived from 11 years of NMC operational analyses, adapted from Lau (1979). 45°N Contour interval 50 m; the zero contour is thickened.

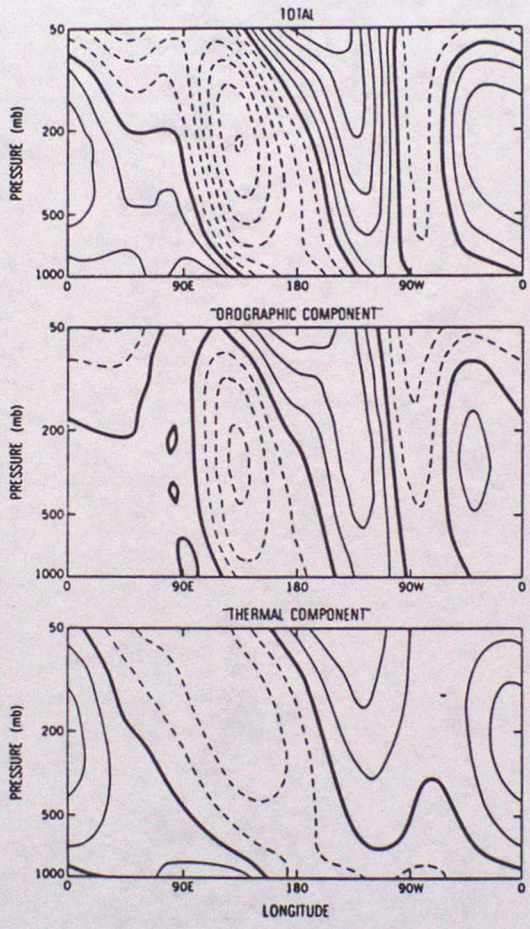

The eddy geopotential height as a function of longitude and pressure at 45 N for the mountain model ('total'), the mountain minus no-mountain flow ('orographic component') and the no-mountain model ('thermal component'). The contour interval is 50 m with negative contours dashed. Model fields in Figs. 6.19–6.23 are averaged over the three winter months in each of the 15 model years.

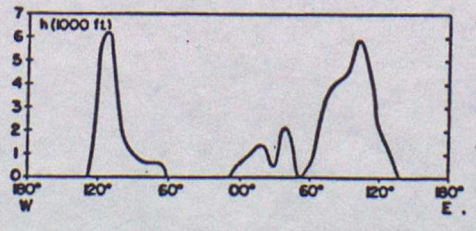

Topographical profile at 45° N. The elevations represent the mean height of the earth's surface, averaged for the interval 40° N to 50° N, as a function of longitude.

Figure 4.18.

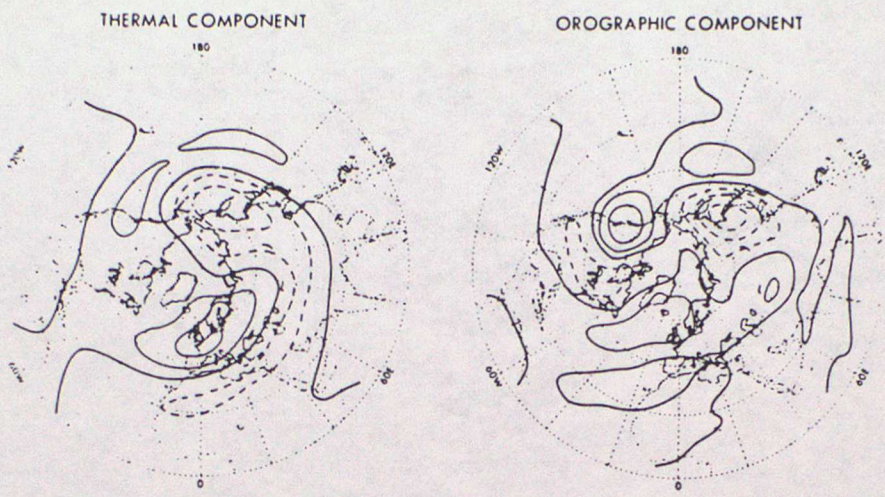

The stationary eddy geopotential field of Fig. 6.21 split into its 'thermal' and 'orographic' components.

Figure 4.19

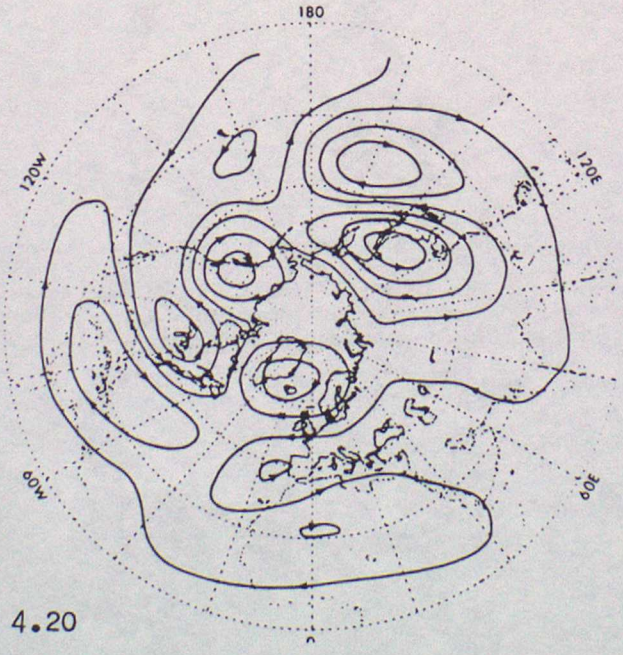

Figure 4.20

The streamfunction for the mountain minus no-mountain flow at 300 mb. Contour interval is 4×10^6 m^2 s^{-1}.

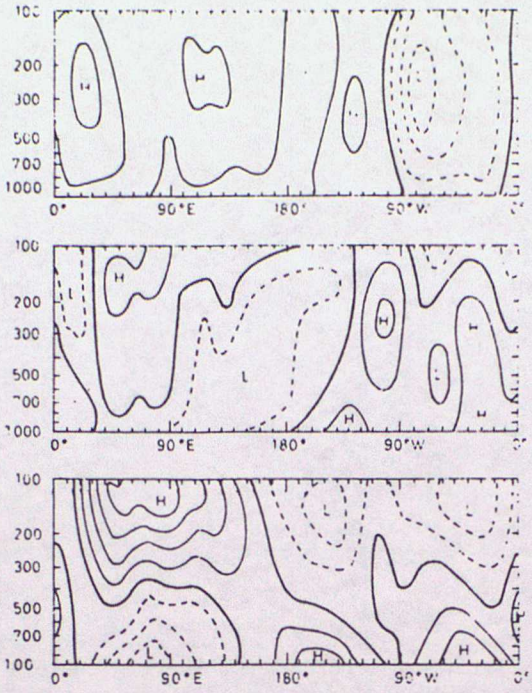

Longitude–height cross-sections of stationary wave geopotential height $\bar{Z}^*$ for the summer season, derived from 12 years of NMC operational analyses, adapted from White (1982a). (a) 60°N; (b) 45°N; (c) 25°N. Contour interval 30 m. The zero contour is thickened.

Figure 4.21

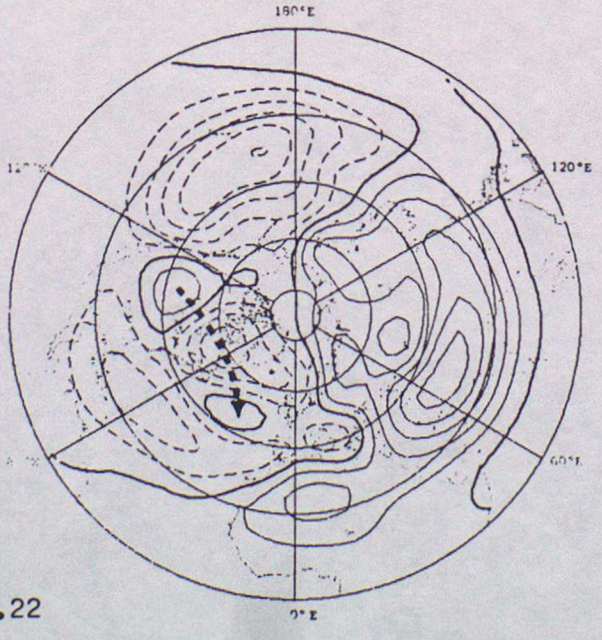

Figure 4.22

Climatological mean July distribution of stationary wave geopotential height at the 200 mb level. Data source, and plotting conventions as in Fig. 2.2, except that the contour interval is 30 m. For comparable distributions based on different data sets, see Holopainen (1970) and White (1982a) or Lau *et al.* (1981). The arrow shows the wavetrain discussed in the text. The outer latitude circle is the equator.

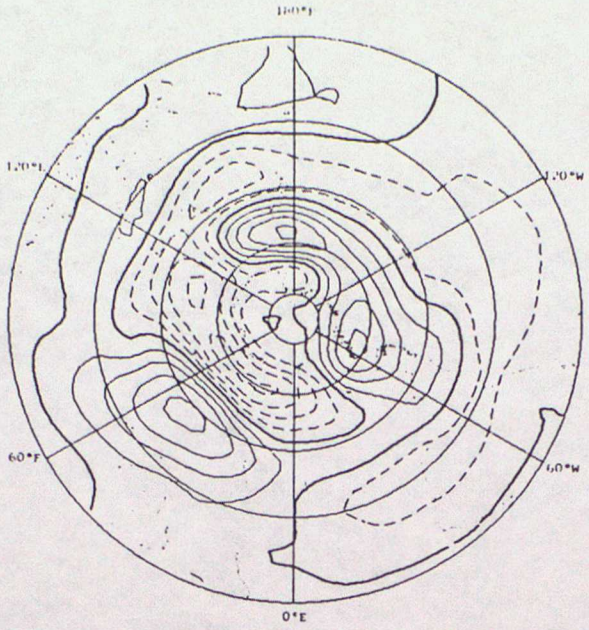

Figure 4.23

Southern Hemisphere climatological mean July distribution of stationary wave geopotential height $\bar{Z}^*$ on the 200 mb level, based on the atlas of Taljaard *et al.* (1969) digitized, spatially and temporally smoothed, and archived on magnetic tape in the NCAR data library. Contour interval 30 m. The zero contour is thickened; positive contours are solid and negative ones are dashed. For comparison with the 500 mb $\bar{Z}^*$ field derived from Australian operational analyses, see Trenberth (1980). The outer latitude circle is the equator.

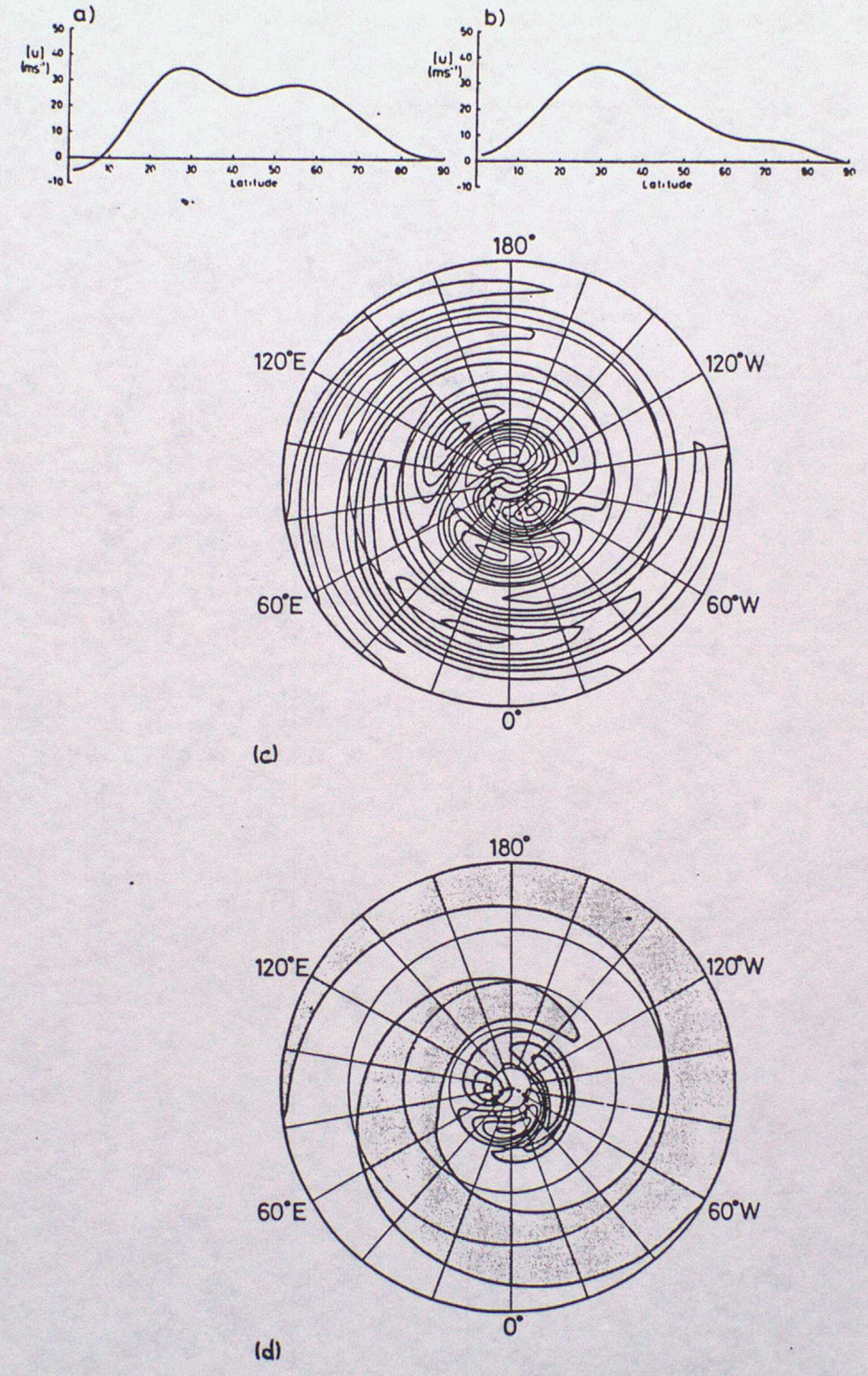

Figure 4.24 Showing the steady zonal vorticity anomaly when the nonlinear barotropic vorticity equation model was run to a steady state with forcing by a circular mountain displaced 10° of latitude from the pole (c) Southern hemisphere case, with the flow relaxed to the zonal flow shown in [illegible] a). (d) Northern hemisphere case, in which the zonal flow is relaxed towards the profile shown in [illegible] (b). The contour interval is $1{\cdot}82\times10^{-6}s^{-1}$ and anticyclonic values are shaded. The dashed circle near the pole indicates the edge of the mountain. For ease of comparison, both integrations have been carried out on the southern hemisphere

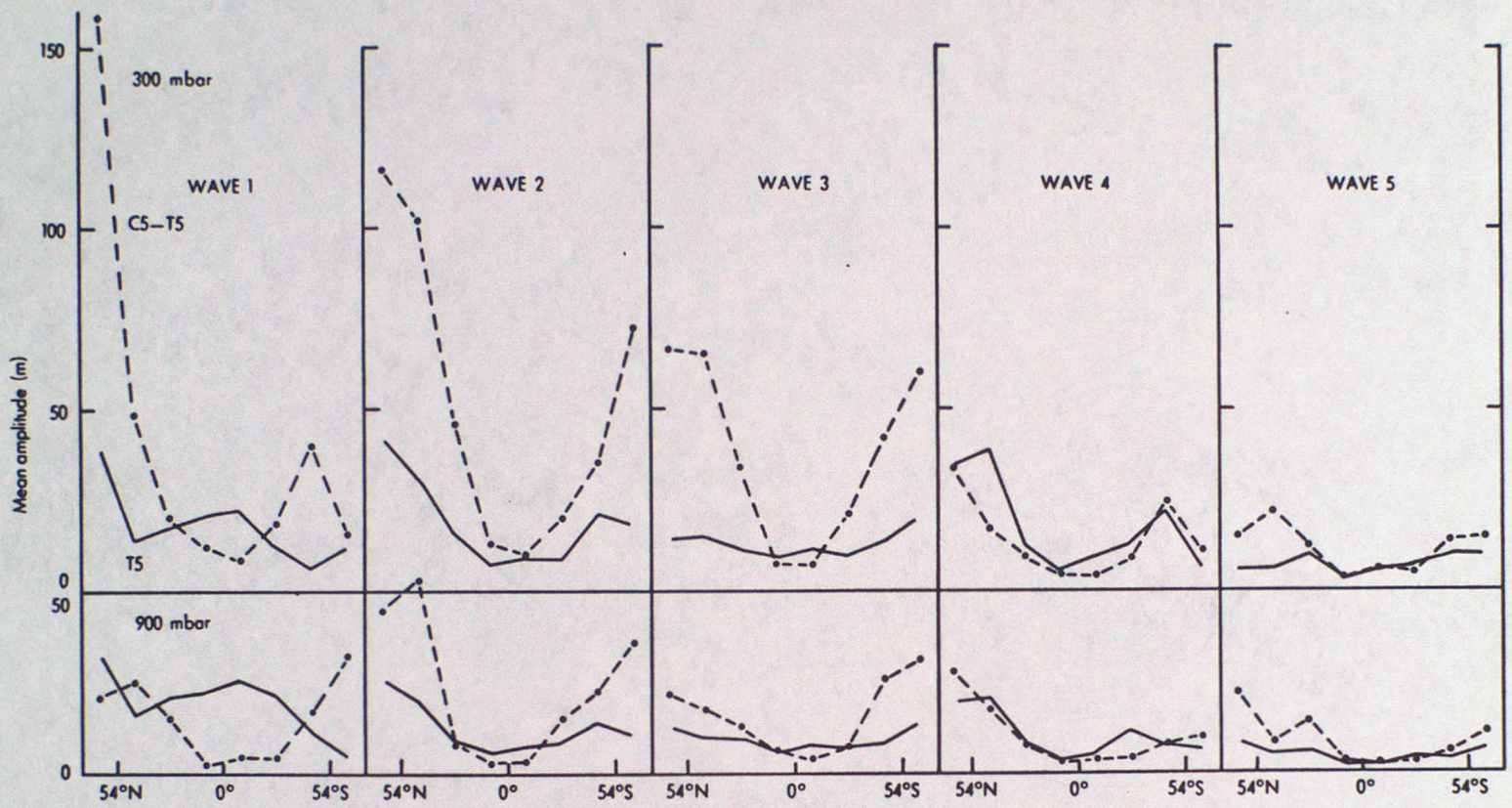

Figure 4.25 Mean amplitudes for 72°-54°N, 54°-36°N, - - - - - -, 54°-72°S for waves 1 to 5 for tropical (T5) and all other (C5–T5) forcing.

PHYSICS AND DYNAMICS OF THE CLIMATE SYSTEM

OBSERVED ATMOSPHERIC CIRCULATION

P R Rowntree

Met O 20, Meteorological Office, Bracknell

5.1 INTRODUCTION

In the first lecture of this series, I considered the forcing of the global circulation with some emphasis on the symmetric case, and in Lecture 4 I discussed asymmetries in the forcing of the circulation. This lecture is aimed at an overall appreciation of what the mean circulation is (5.2), how variable it is (5.3), how it transports energy and momentum (5.4), and how its energy is maintained (5.5). In the space available, it is impossible for the lecture to be comprehensive. Some of the topics missing or almost missing here may be found in the Climate of the World series.

5.2 THE MEAN CIRCULATION

5.2.1 The tropics

(i) Divergent circulation and rainfall In Lecture 4, I showed precipitation (Fig 4.3, see also Fig 5.3(a)) for December-February (DJF) and velocity potential χ (Fig 4.4) for January. Fig 4.4 showed the northward divergent flow expected if the Hadley cell exists, the χ gradient being generally in the required sense at 0-15°N, indicating ascent near or south of the equator and descent near 20°N, consistently with the rainfall distribution. There was little evidence of a second Hadley cell south of the equator, the southward outflow from the west Pacific ascent region being at least partly compensated by flow in the opposite direction south of the eastern Pacific and Atlantic sectors. The climatological estimates of the zonally averaged meridional circulation (Fig 5.1(a) from Oort (1983)) confirm this impression, with a single dominant Hadley cell centred near 10°N, several times stronger than a weak southern hemisphere Hadley cell centred just south of 20°S.

The corresponding June-August (JJA) picture (Fig 5.1(c)) shows a comparably dominant single cell with ascent concentrated between 0 and 10°N and descent strongest near 15°S. As in DJF, the JJA χ map (Fig 5.2) shows a dominance of three outflow regions, the west Pacific again being the strongest but with significant contributions from Central America and west Africa. The Walker circulation is again evident with downgradient flow from the northwest to the

southeast Pacific, and the main χ minima over the south Atlantic and southern Africa, with an extension to the southeast Pacific. The climatological rainfall map (Fig 5.3(c)) is consistent with this, with maxima exceeding 10 mm/day over eastern Asia and the northwest Pacific, and near the other χ minima, Central America and west Africa. The oceanic ITCZs, clearly evident in the rainfall, do not show up well in χ, perhaps because of their small latitudinal scale.

(ii) Vertical velocity in JJA An alternative depiction of the distributions of convergence and divergence is provided by vertical velocity at 500 HPa (Fig 5.4, from Oort (1983)), in the middle troposphere between the strongly divergent and convergent flows in the boundary layer and upper troposphere. The agreement with precipitation is generally good; the three major rainfall areas referred to above all appear, with ascent of around -0.6 μbar/s (-0.06 Pa/s) or, perhaps more intelligibly, just over 50 HPa (or mbar) /day. Even the east Pacific ITCZ has not been wholly eliminated by the smoothing used to "better exhibit the large scale patterns". The descent regions also emerge clearly with intensities as large as or larger than the ascents; mostly they coincide well with the dry (<1 mm/day rainfall) zones; the ascent west of Australia interrupts the dry zone near 20°S, while other oddities include the ascent west of North Africa and the descent near S W India. These are all in or near areas of sparse data.

(iii) Data sparsity Sparsity of data is not of course a problem confined to the wind field, but the data distribution maps shown by Oort (1983) are a greater discouragement to the use of the vertical velocity analyses than is suggested by the above comparison with rainfall, especially south of the equator. Between 40°S and 30°N there are four data gaps more than 20° of latitude north to south and as wide as the North Atlantic (from Newfoundland to France) east to west: the Indian Ocean from Australia almost to Madagascar, the south Atlantic from Africa to South America, the North Atlantic from the Cape Verde Islands to the Caribbean and finally the enormous data void of the east Pacific, which at its extreme dimensions measures 90° of longitude and 55° of latitude. Even land areas are not necessarily well represented at least above the level reached by pilot balloons; on the two sample maps printed by Oort, for January of 1966 and 1971, the 1966 map has no data at 500 HPa over inland South America or Africa south of the equator; in 1971, South America is much better, but Africa is still vacant inland from about 0 to 15°S.

Rainfall data are usually quite adequate over land, being an inexpensive ground-based observation of general interest. Over oceanic areas, however, there are no

data at sea except observations of frequency from ships, whose interpretation involves problems of subjectivity - is heavy rain the same intensity to a North Sea fisherman as to a sailor in Indonesian waters, or even to the same person after several months in each of the two environments? There are island data, but much doubt has been expressed about the representivity of islands with local thermal and orographic influences; probably small low atolls provide acceptably reliable data, judging by their coherence (see Taylor, 1973). These problems are highlighted by the contrasts between analyses of rainfall over the oceans, such as two for the Pacific published in the same year, Dorman and Bourke (1979) and Reed and Elliott (1979); these differ by more than a factor of two in places, notably the east Pacific ITCZ (up to 1400mm in the first and 700mm in the second) and southeast of the Phillipines (1000 and 300 mm) in June to August.

(iv) Use of satellite data It is therefore desirable to supplement the ground-based data with the global cover offered by satellites. The best estimates to date are probably those from satellite observations of the outgoing longwave radiance, effectively showing the emitting temperature of cloudtops. These data are now available for long enough to allow preparation of a climatology such as that in Fig 5.5 for 1974-1983 (from Janowiak et al, 1985). Comparison with Fig 5.3(c) shows generally good agreement over land; for example, the patterns over Africa from 5°S to 20°N are similar in many respects, though the critical might note the different locations of the peak rainfall and minimum radiance near the Cameroons (8° and 20°E respectively). The radiances suggest that the wettest places in JJA are over the N E Bay of Bengal and the adjacent land and the southwest tip of west Africa near Sierra Leone, both below 200 W m^{-2}; the climatologist would probably not argue with this.

How then do the radiances and rainfall estimates compare over the oceans? Again, the comparison is encouraging; the ITCZs north of the equator stand out clearly, the bulge of the Indian Ocean rainfall south of the equator is supported, and also the locations of the dry zones. The South Pacific Convergence Zone extending southeast from east of New Guinea is evident though maybe less clear in the radiances. However, the quantitative conversions from satellite radiances to rainfall in millimetres cannot be made with confidence over the oceans because of (a) the lack of 'ground truth' and (b) the likely inapplicability of calibrations derived from land data due to the different responses to the diurnal cycle and the likely persistence of daytime cloud over land. What these comparisons do allow is greater confidence in the oceanic rainfall patterns and their use as surrogates for the divergent circulation.

(v) Radiation as a forcing factor The radiances are important not only as a diagnostic tool but also, as discussed in 4.4, for their role as forcing factors for the circulation. However minima in the outgoing radiance due to deep convective cloud tend to coincide with maxima in the reflected solar radiance (Fig 5.6, from Winston et al (1979)). The eastern tropical Pacific is an instructive region in this respect. The albedo and radiance maps for JJA match well in most respects: the minima in radiance near and over Central America and over the east Pacific ITCZ coincide with maximum albedos, and the areas with albedo below 20% coincide well with radiances exceeding about 260 W m^{-2}. However, strong albedo maxima off the Peru coast and near 20°N 130°W are associated with only weak minima in the radiance field. These are regions of low cloud with little rain, and lead to marked minima in the field of net radiation at the top of the atmosphere (Fig 5.7, from Winston et al (1979)). The deep convection regions on the other hand barely show up in the net radiation. Before leaving Figs 5.6 and 5.7, the reader should note the high albedos, large radiances and minima in the net radiation generated by the hot, highly reflective bare surfaces of the Sahara desert.

(vi) Role of land and oceans in seasonal variations We have already seen in Lecture 4 that the tropical circulation in southern summer is dominated by the surface thermal features which force areas of precipitation, ascent and upper tropospheric divergence and anticyclonic vorticity. How does this forcing vary through the year, and what aspects of the forcing are responsible for the seasonal variations?

The sea surface temperature patterns in the tropics (Fig 5.8, from Alexander and Mobley (1974)) vary seasonally to a significant extent. Despite the large thermal inertia of the ocean, the depth affected by seasonal variations can be limited to a few tens of metres because of the stability produced by surface heating and because wind mixing can be quite weak. I shall not trespass further on the ocean but merely note that the regions of warmest water transfer northwards between late southern summer and late northern summer. The extent of the shift is about 15° of latitude in the west Pacific, 10° in the west Atlantic and even less than this, perhaps 5°, in the Indian Ocean and in the narrow bands of warm water associated with the inter tropical convergence zones (ITCZs). These regions, especially the warmest in the west Pacific, are of great significance for atmospheric convective activity because they help to determine the upper tropospheric temperatures throughout the tropics and hence limit the depth of convection in regions with cooler surface water.

It is misleading to look only at January and July sst. Firstly, because of the lag of ocean temperatures behind the solar intensity, the oceans outside the equatorial belt (where of course the solar intensity is a maximum at the equinoxes) tend to have extremes of temperature in February or March and August or September. Secondly, there are considerable variations in wind speed and direction in association with the seasonal cycle and especially the monsoons. For example, note in Fig 5.8(b) the warmth of the Indian Ocean in April before the Asian summer monsoon circulation transforms the ocean circulation. (May sst which is even warmer in the north Indian Ocean with no water below 27°C, would make the point even better but April is shown for consistency with the seasons available for illustrating the atmosphere.) Otherwise the change from January to April is not large, as is to be expected with extremes in February-March. Similarly, October is rather like July.

The implications of this seasonal cycle in sst for the atmosphere are that insofar as it is forced by the ocean we would expect March - May (MAM) to be like December - February (DJF) and September- November (SON) to resemble June - August (JJA). However, the sun's declination differs by about 30° between SON and JJA, but only by about 13° between SON and DJF, so if the thermal forcing by the land is important, the patterns of similarities will be quite different. Examination of Fig 5.1 confirms that the meridional circulation in MAM is like that of DJF in pattern but only about half the intensity. There is an important difference of pattern near 10°S, with the ascent disappearing completely in MAM, reflecting the retreat of the summer rains from the southern tropical continents (Fig 5.3 (a,b)). Fig 5.3 confirms that the oceanic rainfall pattern has changed little from DJF to MAM. Similarly, the SON pattern in Fig 5.1 resembles JJA but is less than half as intense; also the northern winter Hadley cell is much more prominent than in JJA and shifted south. Maps of ω at 500 HPa (not shown) reveal that this change is mainly due to a reversal over southern Asia from the ascent of the summer monsoon season to descent in SON. This is consistent with the rainfall changes (Fig 5.3). The detailed month to month variations in Oort and Rasmusson (1971) show that the mean meridional circulation reaches its extreme states between July and August and between February and March. These suggest a domination by land forcing in northern summer and ocean forcing in southern summer; this is consistent with the asymmetric distribution of land between the hemispheres.

(vii) <u>The rotational circulation</u> In discussing the northern winter circulation (Fig 4.5) in Lecture 4, we noted that both the mean flow and the variations in

the rotational flow associated with warming of the east Pacific were closely related to the heat sources. The change to the northern summer circulation (Fig 5.9, from Newell et al (1972)) can similarly be related to the changes in heating, particularly the heating over land. The anticyclones over the tropical Pacific persist, consistent with the continuing heavy rainfall (Fig 5.3). However, the southern summer upper anticyclones over the three southern continents are replaced by northern summer anticyclones, over southern Asia with a ridge to North Africa, and near Central America. The locations of these features close to the desert regions of central and southwest Asia, Africa and southwestern North America might suggest a link with the hot lower troposphere of desert regions. This is unlikely because: (a) deserts are heat sinks as seen in Fig 5.7; (b) the southern summer highs are associated with the rainfall maxima not minima; (c) these southern summer highs are located just poleward of the rainfall maxima, whilst just equatorward of the highs near Mexico and India are respectively the Central American and southeast Asia rainfall peaks. On the other hand, the two northern summer highs are close to high topography; there is good evidence that the elevated heat source of Tibet plays an impoortant role in the development of the south Asian summer high (Hahn and Manabe, 1975), and it is possible that the Rockies have a similar role.

A more quantitative impression of the flow is provided by the 200 HPa zonal wind magnitudes (Fig 5.10, from Oort (1983)).

(Lest the reader forget the cautionary remarks on data sparsity, particularly over the east Pacific, it is worth comparing the DJF map with the analysis of the January climatology made by Sadler (1977) (Fig 5.11), using aircraft reports to supplement the ground-based radiowind data. The differences approach 20 m/s near the equator at 120°W. Analyses in recent years for operational forecasts, using wind data derived from satellite observations of cloud motions, show similar intensities of equatorial westerlies to those analysed by Sadler. Aside from the eastern tropical Pacific, the Oort and Sadler analyses are in good agreement with each other, and Oort's are used here because they are global.)

JJA has more easterly 200 HPa equatorial winds than DJF; this may be due to the greater intensity of the main northern summer heat source. All seasons are similar however in having winds that are more easterly over the west Pacific and Indian Ocean and Africa than elsewhere. As indicated earlier, this apparently reflects the strength of the heat sources in this sector (see also Fig 4.16). The intensity of the Indian Ocean easterlies is stronger in SON than in DJF and MAM, consistently with the precipitation differences discussed earlier.

(viii) Tropical upper tropospheric troughs and easterly waves The influence of heat sinks can also be detected in Fig 5.9 in the cold upper troughs over the northern tropical oceans near 20°N. These features, together with the similar

southern summer troughs south of the equator (Fig 4.5), can also be explained in terms of the vorticity equation (equ. (4.1)), cyclonic vorticity being generated by the upper tropospheric convergence. The associated vertical circulation provides the convergence of energy flux needed to balance the atmospheric radiative cooling (as discussed in Lecture 1). They are not quiescent stationary troughs but active features with strong horizontal shears and waves which usually move westward; they are, at times, sufficiently extensive in the vertical to generate rain-producing synoptic systems (see Sadler (1975) for references). As discussed by Rowntree and Cattle (1983), westward-moving waves observed in the Atlantic upper tropospheric trough can be in or out of phase with the lower tropospheric easterly waves which move west from Africa; the development of the latter over Africa has been studied extensively (e.g. Norquist et al, 1977) and found to be associated with both baroclinic and barotropic instabilities caused by the lower tropospheric thermal contrasts which result from the gradient of surface dryness between the Sahara and the moister land south of 10°N. Some of these waves develop into tropical cyclones and even hurricanes over the warmer water of the west Atlantic; others may reach the east Pacific and either develop into more intense systems there or progress further west to the central and west Pacific. Hurricanes (typhoons, etc) also develop over other areas with water warm enough to generate deep convection to near the tropopause, notably the west Pacific. Note that there is no absolute critical surface temperature for their development, only relative ones for given atmospheres, though theory suggests that intensity will increase with increasing temperature (Emanuel, 1987).

5.2.2 The subtropical jet

(i) Observations A prominent feature of any depiction of the global circulation is the subtropical jet (STJ). As discussed in Lecture 1, in models of a zonally symmetric earth it occurs just poleward of the Hadley cell near 30°N. Its location on the real earth is similar in the zonal mean (Fig 5.12 from Newell et al (1972)) in winter of both hemispheres, with a maximum near 30°. Analyses of the southern hemisphere are plagued by data inadequacies, such as the biassing of averages by loss of data with strong winds, and the large unobserved areas. However, careful early analyses using additional data (e.g. from aircraft), and more recent analyses based on operational work, so taking account of height data through the geostrophic relation and of cloud motion derived winds, do indicate substantially stronger winds in the winter STJ than Newell et al (1972); Sadler (1977)'s maximum is 36 m/s.

The emphasis here will be on the northern hemisphere, where the winds are generally well observed. The zonal means show the STJ to weaken slightly from winter to spring and then almost collapse in summer, with maximum of less than 20 m/s, about half the winter intensity, and a location much further north near 40-45°N. The maps confirm the much larger change from MAM to JJA than from DJF to MAM. Indeed the pattern hardly changes from DJF to MAM, with the three major jet maxima persisting over south Japan, the eastern USA and the Middle East. The northward movement of the Asian jet to near 40°N in JJA is not a gradual development but occurs quite suddenly at the time of the onset of the Asian monsoon, usually in June. Lorenc (1982)) illustrated this development for June 1979, and Kershaw (1988) depicts the extension of the southwesterlies across the Indian Ocean at 850 HPa in June 1979. The southward return of the jet across the Himalayas in October is also fairly abrupt.

(ii) Explanations of subtropical jet maxima Poleward of the subtropical jets are the troughs and ridges of middle latitudes (Fig 5.13(a), from Moffitt and Ratcliffe (1972)). Each of the northern winter troughs, including that over eastern Europe, is close to the longitude of an STJ maximum. It is generally considered that this is because the troughs force the STJ maxima, and there can be little doubt that their role is important. However, there is evidence that tropical forcing also plays a part. Each of the STJ maxima lies poleward of a maximum in the tropical rainfall, associated, as discussed in Lecture 4, with tropical thermal forcing - specifically, the intense Japanese jet is north of the major rainfall maximum near Indonesia, the eastern USA maximum north of the South American peak and the Middle East maximum north of the African peak.

(iii) Evidence from models Effects of tropical forcing on the subtropical flow were evident in the tropical forcing experiment discussed in 4.2.2 (see also Fig 4.25). Fig 5.13(b) compares the 300 HPa geopotentials from that experiment for two tropical latitudes, of which 10½°S is closest to the latitude of forcing, for 31½°N just north of the STJ, and for higher latitudes. The troughs at 31½°N are close to the longitudes of maxima in the STJ, located near 60°W (30 m/s), 40°E (35 m/s) and 150°E (45 m/s), and so close to the observed longitudes (Fig 5.10). These maxima are all at about 21°N, at which latitude the minimum speeds are 15-20 m/s near West Africa. The observed maxima and those in the control experiment with full forcing are further north, near 30°N, except the Middle East maximum in the control which was at 22½°N. The observed stationary wave amplitudes increase rapidly northwards from 30°N, and by 49½°N are far in excess of those in Fig 5.13(b). It appears from this experiment that the tropical

forcing generates STJ maxima at longitudes close to those observed, but nearer the equator, while the middle latitude forcing is mainly responsible for the intensity of the standing waves there, except perhaps the east European trough, which has no obvious middle latitude explanation and may well be due to the African rainfall maximum.

In the southern hemisphere, the winter (also fall and spring) STJ maximum is located over Australia (Fig 5.10), poleward of the major Indonesian heat source (Fig 5.3). A significant role for tropical latent heat release in forcing this maximum has been claimed by Nogues-Paegle and Mo (1988). However, as discussed in 4.5, the asymmetric forcing by Antarctica may contribute to this feature.

5.2.3 Middle and high latitudes

The features discussed in the previous lecture (see 4.5) are dominant here - in winter, low pressure over the oceans and high pressure over the continents with a tendency for westward shift with height so that the upper ridges lie over the west coasts of the continents and the troughs near the east coasts. In these latitudes, the variations on timescales from a few days to months are the main interest. These are discussed for the winter circulation in the following section, and also in lectures in the Climates of the World series.

5.3 VARIABILITY OF THE CIRCULATION

How constant are these circulation features? A measure of this is obtained by use of time filters to estimate the variance on different timescales. A 3 to 6 day bandpass filter is useful for identifying regions of large 'synoptic-scale' variability; these can usually be identified with depression tracks. Longer period filters, such as the low-pass filter used to isolate variations on timescales of over 10 days (Wallace and Blackmon, 1983) reveal planetary scale teleconnections such as the PNA or Pacific - North American pattern referred to in Lectures 3 and 4 (Fig 4.13). It may be a surprise to learn how much of the day-to-day variance is on the longer time scales; Fig 5.14, from Wallace and Blackmon (1983), shows the variances obtained with these two filters and also those for monthly mean data. The low-pass filter and monthly mean data give similar patterns, explaining about 80% and 60% of the total respectively.

The depression tracks can be explained in terms of baroclinic instability due to surface forcing - e.g. the generation of eddy APE on the east coasts of the winter continents. The longer period variations are more of an enigma. A list of proposed mechanisms from Wallace and Blackmon reads like chapter headings for a

text on dynamics: - forcing by oceans and cryosphere; vacillation phenomena; transitions between different climatic regimes; gyres, solitons and modons; wave interactions; forcing by high-frequency transients.

What do these variations on the monthly scale look like? Fig 5.15, from Ratcliffe (1986), compares a recent pair of adjacent months, with contrasting circulation anomalies in the Atlantic sector, but rather similar ones in the Pacific. Though not located at the maxima of Fig 5.14, the peak anomalies are over the oceans, consistently with the low variances in the climatology over land. Wallace and Blackmon also show the correlation maps for a few points. Fig 5.16 corresponds to Fig 5.14 but for 55°N 20°W. The band-pass map shows the typical scale of 'synoptic scale' features over the east Atlantic, about 50°. For the longer timescales, the horizontal scales are much larger; note the strong inverse north-south relation with 25°N. They also studied lag correlations for times two days earlier and later. The maps for 55°N 20°W (Fig 5.17(a) resemble Fig 5.16 (a) but with, naturally, some weakening. On the other hand, the maps for 55°N 75°E (Fig 5.17) show strong evidence of propagating Rossby waves: - large upstream correlations with the pattern 2 days earlier and downstream correlations with that 2 days later. With a ridge slow moving near this point, troughs evidently propagate from Scandinavia two days before to east China two days later.

In summer, the northern hemisphere is relatively less active, though not to the extent that many general circulation models suggest. Indeed there is little difference between the transient eddy K E in winter and summer at 300mb at 60°N (229, 199 m^2s^{-2} respectively) (Oort and Rasmussen, 1971); at lower altitudes and latitudes the contrast is much larger however.

5.4 ENERGY BUDGETS AND TRANSPORTS

(i) Different forms of energy As discussed in Lecture 1, there is a need for poleward energy transfer to compensate for the uneven distribution of energy input over the globe. This topic was investigated thoroughly in the 1970s by Oort and co-workers (e.g. Oort, 1971; Oort and Vonder Haar, 1976). Oort (1971) analysed the atmospheric contents and transports of energy. Four forms of energy were considered :

potential energy gz	(24.6%)	(345.4)	(10^{20} cal)
internal energy c_vT	(72.6%)	(1018.4)	
latent heat Lq	(2.8%)	(38.9)	
kinetic energy $(u^2 + v^2)/2$	(0.05%)	(0.72)	

The percentage that each form is of the whole and its total quantity (1 cal = 4.18 J), each averaged over the northern hemisphere for 1000 to 75 HPa are indicated in parentheses.

(ii) Energy fluxes by mean meridional circulation The horizontal flux of energy passing through a latitudinal wall can be written (Oort, 1971) as

$$F = F_{PE} + (F_{IE} + W) + F_{LH} + F_{KE}$$

Here $W = \int\int pv\ dx\ dz$ is the work done by the air south of the wall on the air north of it through the action of pressure forces. The bracketed terms combine into the flux of sensible heat (c_pT). Oort considered separately the fluxes by mean meridional circulations (mmc), by transient eddies and by standing eddies. The fluxes by the meridional circulation (Fig 5.18) illustrate the near compensation between the different forms of energy, due to their opposite vertical variations in the tropical atmosphere (Fig 5.19) (from Oort, 1971). Note that as an estimate for a typical point, the vertical profile in Fig 5.19 underestimates values near the surface because part of the layer is missing due to the presence of mountains. The typical surface value is near 3.6 in the units of Fig 5.19 (see also 1.3.2).

(iii) Eddy fluxes Whilst the mmc dominates the transports in the tropics, the eddies are generally more important poleward of about 20°N. Figure 5.20 (from Oort, 1971) reiterates the lack of seasonal variation of transient eddy intensity relative to that of standing eddies. Another feature is the contrast between the latent heat fluxes by standing eddies in summer when a strong peak is evident near 25°N associated with the monsoons, and winter when transports are weak. The lack of moisture in the winter atmosphere is probably mainly responsible as the corresponding sensible heat flux is of similar sign throughout the year but much larger. There is some sign of a like contrast between the transient fluxes with the winter peak further south for the latent fluxes. The eddy fluxes of potential energy are negligible in comparison to the sensible and latent heat fluxes. This is to be expected from geostrophy since

$$\int v\varphi\ dx = \int (\partial\varphi/\partial x)\varphi\ dx = \int (\partial(\varphi^2)/\partial x)\ dx$$

which is zero when integrated around a latitude circle.

(iv) Contribution required from ocean The total atmospheric flux of energy does not vary through the year (Fig 5.21, from Oort, 1971) quite as one would expect from the observed imbalance of top of the atmosphere (TOA) energy input (Fig 5.22, from Oort and Vonder Haar (1976)) . One obvious discrepancy is that flux convergence is absent south of 50°N, whereas TOA energy requirements are for

convergence north of about 35°N. The explanation must lie in the transport of energy by the oceans. Oort and Vonder Haar (1976) used the balance equation

$$F_{TA} = S_A + \nabla.T_A + F_{BA}$$

where the first and last terms are the energy fluxes at the top and bottom of the atmosphere, S_A is the storage term and T_A is the atmospheric transport (diagnosed above), to calculate the last term. They then assumed the transport across the land surface to be negligible (correct in the annual mean though perhaps in error by up to ± 10 W m^{-2} in higher latitudes in spring and autumn), calculated the storage in the ocean and so deduced the transports by the ocean needed to balance the ocean energy budget (Fig 5.23, from Oort and Vonder Haar (1976)). Comparison with Fig 5.21 indicates that the ocean provides perhaps more than half the flux at 20°N decreasing to a small fraction at 50°N.

(v) Global budgets - energy Before leaving the energy balance, it is worth noting the constraints on the global budgets. For heat, the atmospheric global balance is:

$$C\partial T/\partial t = H + LP + (R_{NT} - R_{N*}) - [PE \rightarrow KE] + Q_F. \qquad (5.1)$$

The last two terms are defined below and otherwise notation is as in 1.2.1 (C is heat capacity). This equation is dominated by the latent heat release (≈80 W m^{-2}) and the radiative imbalance (≈100-110 W m^{-2}) (see also Fig 1.4, interpreting 100% as 343 W m^{-2}). The sensible heat flux makes up the balance while the last two terms, the conversion from potential to kinetic energy ($x\omega T/p$) familiar from the thermodynamic equation and the generation by friction roughly balance. Note that the last term is commonly omitted from models because it is not clear how to formulate it and obtain its spatial distribution. Its magnitude deduced from ($x\omega T/p$) is about 2 to 3 W m^{-2} (see Fig 5.26(a)), and so its omission introduces a spurious cooling of about 0.03 K/day. The latest Met O 20 GCM represents it simply by calculating the imbalance in the energy budget and distributing the compensation uniformly.

(vi) Moisture budget For moisture, the global balance is

$$M_A \partial q/\partial t = E-P.$$

where M_A is the atmospheric mass per unit area and q is specific humidity. The component terms E and P are of order 0.3 g/cm^2/day or 3 kg/m^2/day as required by the energy balance equation (5.1). For the land surface in the absence of snowmelt, we have almost as simple a balance:

$$M_G \partial w/\partial t = P - E - R$$

where M_G is the mass of the hydrologically active soil layer per unit area, and w is fractional soil moisture content. Since runoff R represents the horizontal

advection, this equation is valid locally as well as globally and implies the general constraint that except in rivers, P>E in the longterm mean - i.e. more cannot be evaporated than is precipitated. It follows that the land must be a net sink of moisture for the atmosphere and the oceans a net source. Runoff estimates indicate that, averaged over all land, runoff is about 40% of precipitation (Korzun et al, 1978).

(vii) Atmospheric angular momentum budget The eddies and the mmc both play a role in the transport of angular momentum. Angular momentum per unit mass m has two components:

$$m = \Omega a^2 \cos^2\varphi + ua \cos\varphi$$

only the second of which depends on the atmosphere (here Ω is earth's rotation rate, a is earth radius, φ is latitude and u is zonal wind). However, the atmospheric angular momentum

$$M = \Sigma\Sigma\Sigma\ m\ p_* (a^2/g) \cos\varphi\ \Delta\sigma\ \Delta\lambda\ \Delta\varphi$$

involves a multiplication by p_*, and so both the components can contribute to variations in time (here λ is longitude, σ is the vertical coordinate (p/p_*), p is pressure and p_* is surface pressure).

The rate of change of angular momentum is

$$Dm/Dt = \partial m/\partial t + \partial(m\omega)/\partial p + \nabla_H.(m\underline{V}) = -\partial\Phi/\partial\lambda - g\ (\partial\tau/\partial p)\ a \cos\varphi \qquad (5.2)$$

where Φ is geopotential and τ is the vertical momentum flux. Here, the vertical and horizontal flux convergences are separated on the left hand side, while on the right are the terms which, when integrated vertically and zonally, lead to the mountain torque and frictional torque terms:

$$-\int_o^{p^*} \frac{\partial\Phi}{\partial\lambda} \frac{dp}{g}$$

and

$$-(a \cos\varphi)\ \tau_*$$

(τ_* is surface stress). The sources and sinks of angular momentum have been analysed by Swinbank (1985) using FGGE data for January and June 1979, based on the assimilations using the Met O 20 11 layer model, as it was at that time. In his results for January (Fig 5.24), the dashed line shows the sum of the two source terms, and the symbols show the separate contributions. Generally the two contributions have the same sign and similar orders of magnitude in the northern hemisphere while the mountain torque is relatively insignificant south of 20°S. Of particular interest is the large discrepancy between the sum of the two source terms and the source as diagnosed from the integral of the left hand side of (5.2), i.e. from the analysed time change and horizontal flux convergence. This

is believed to be due to underestimation of the effects of orography in the model; introduction of enhanced representations of the earth's topography, so-called envelope orography, or of drag due to mountain-induced gravity waves (see Slingo and Pearson, 1987) should have helped to correct this imbalance in current models though the calculations have not, I think, been repeated.

Are mean or transient circulations responsible for the fluxes whose convergence is shown in Fig 5.24? Data from Oort (1983) show that in northern winter, the mmc has an important role in the tropics, transient and stationary eddy fluxes share the transport in middle latitudes whilst stationary eddies are most important, providing an equatorward flux, in high latitudes. Stationary eddies are less important in the other seasons. The magnitudes of the total eddy fluxes (Fig 5.25, from Oort and Rasmusson (1971)) show that the region of equatorward fluxes has a similar extent in all seasons. There are variations of about a factor of 2 between summer and winter in both maxima. Note that the direction of the eddy fluxes has little relation to the direction of the zonal wind gradient (Fig 5.12), with countergradient fluxes south of the subtropical jet near 30°N and north of 55°N. An interesting feature of the equatorial region (see Oort and Rasmusson, 1971, p. 126) is the large flux by the mmc into the summer hemisphere near 200 HPa.

5.5 MAINTENANCE OF THE CIRCULATION

In lecture 3, the concepts of energy conversions between zonal and eddy forms of available potential energy (APE) and kinetic energy were introduced. Fig 5.26(a) (from Oort and Peixoto (1974)) shows a 5 year mean energy box diagram for the northern hemisphere. Zonal available potential energy (P_Z) is generated and converted at a rate of 1.5 W m^{-2} to P_E. This together with 0.7 W m^{-2} generated directly as P_E (through heating of warm or cooling of cold air, is converted to eddy kinetic energy (K_E) and then mostly dissipated, though there is a small conversion to K_Z. There is considerable seasonal variation, with extremes in January and July (Fig 5.26(b)), with the zonal energies four and the eddy energies two times greater in January. The January conversions are similar to the annual mean pattern; however, in July generation of APE is mainly as P_E, eddy conversions are much weaker, and dissipation is only double the conversion to K_Z.

The interactions between waves of different wave number and between waves and the mean flow have been analysed by Kanamitsu (1980). Fig 5.27 shows the results at 200-250 HPa for three sectors of the globe. Two conclusions are that

the major K_E source outside the tropics is in waves 7-10 (the baroclinic scale) and that these waves maintain the ultralong waves in the northern hemisphere but the zonal flow in the southern hemisphere. (see also Lorenc (1982))

5.6 REFERENCES

Alexander, R. C. and Mobley, R. L., 1974, Monthly average sea-surface temperatures and ice-pack limits on a 1° global grid. Rand, Santa Monica, Report ARPA 189-1, 30 pp.

Dorman, C. E. and Bourke, R. H., 1979, Precipitation over the Pacific Ocean, 30°S to 60°N. Mon Weath Rev, 107, 896-910.

Emanuel, K. A., 1987, The dependence of hurricane intensity on climate. Nature, 326, 483-485.

Hahn, D. G. and Manabe, S., 1975, The role of mountains in the south Asian monsoon circulation. J Atmos Sci, 32, 1515-1541.

Heasman, C. C., 1984, Climatological precipitation fields available in Met O 20. Met O 20 Internal Note 19 (not to be quoted).

Jaeger, L., 1976, Monatskarten des Niederschlags fur die ganze Erde. Bericht Deutscher Wetterdienst, 18, No 139, 38pp.

Janowiak, J. E., Krueger, A. F., Arkin, P. A. and Gruber, A., 1985, Atlas of outgoing longwave radiation derived from NOAA satellite data. NOAA Atlas No. 6, U. S. Department of Commerce, 44 pp.

Kanamitsu, M., 1980, Some climatological and energy budget calculations using the FGGE-b analysis during January 1979. ECMWF Seminar on Data Assimilation Methods, 399-454.

Kershaw, R., 1988, The effect of a sea surface temperature anomaly on a prediction of the onset of the south-west monsoon over India. Q J R Meteorol Soc, 114, 325-345.

Korzun, V. I. and others (Editors), 1978, World water balance and water resources of the earth. UNESCO (English translation, original 1974).

Lorenc, A., 1982, Lecture 6 - Budget calculations. In: Advanced Lectures 1982 - General circulation of the atmosphere. Met O 20 Tech Note II/181.

Moffitt, B. J. and Ratcliffe, R. A. S., 1972, Northern hemisphere monthly mean 500-millibar and 1000-5000-millibar thickness charts and some derived statistics (1951-66). Met. Office Geoph Mem, 117, 61 pp.

Newell, R. E., Kidson, J. W., Vincent, D. G. and Boer, G. J., 1972, The general circulation of the tropical atmosphere and interactions with extratropical latitudes, Vol. 1. MIT Press, 258 pp.

Nogues-Paegle, J. and Mo, K. C., 1988, Transient response of the southern hemisphere subtropical jet to tropical forcing. J Atmos Sci, 45, 1493-1508.

Norquist, D. C., Recker, E. E. and Reed, R. J., 1977, The energetics of African wave disturbances as observed during Phase III of GATE. Mon Wea Rev, 105, 334-342.

Oort, A.H., 1971, The observed annual cycle in the meridional transport of atmospheric energy. J Atmos Sci, 28, 325-339.

Oort, A. H., 1983, Global atmospheric circulation statistics, 1958-1973. NOAA Professional Paper 14, U.S. Department of Commerce, 180 pp.+fiche.

Oort, A. H. and Peixoto, J. R., The annual cycle of the atmosphere on a planetary scale. J Geoph Res, 79, 2705-2719.

Oort, A. H. and Rasmusson, E. M., 1971, Atmospheric circulation statistics. NOAA Professional Paper 5, NOAA, U.S Department of Commerce, 323 pp.

Oort, A. H. and Vonder Haar, T. H., 1976, On the observed annual cycle in the ocean-atmosphere heat balance over the northern hemisphere. J Phys Ocean, 6, 781-800.

Reed, R. K. and Elliott, W. P., 1979, New precipitation maps for the North Atlantic and North Pacific Oceans. J Geoph Res, 84, 7839-7846.

Ratcliffe, R. A. S., 1986, Atmospheric circulation review, January and February 1986. J Climatology, 6, 228-231.

Rowntree, P. R. and Cattle, H. (Editors), 1983, The Meteorological Office GATE modelling experiment. Met Office Sci Pap No. 40.

Sadler, J. C., 1975, The upper tropospheric circulation over the global tropics. Rep. UHMET-75-05, Hawaii Institute of Geophysics, 35 pp.

Sadler, J. C., 1977, The upper tropospheric circulation over the global tropics: Part II - Statistics. Rep. UHMET-77-02, Hawaii Institute of Geophysics.

Slingo, A. and Pearson, D. W., 1987, A comparison of the impact of an envelope orography and of a parametrization of orographic gravity-wave drag on model simulations. Q J R Meteorol Soc, 113, 847-870.

Swinbank, R., 1985, The global atmospheric angular momentum balance inferred from analyses made during the FGGE. Q J R Meteorol Soc, 111, 977-992.

Taylor, R. C., 1973, An atlas of Pacific islands rainfall. Rep. HIG-73-9, Hawaii Institute of Geophysics, 7 pp + 13 figures.

Wallace, J. M. and Blackmon, M. L., 1983, Observations of low-frequency atmospheric variability. In: Large-scale dynamical processes in the atmosphere (Ed. Hoskins, B. J. and Pearce, R. P.), Academic Press, pp. 55-94.

Winston, J. S. and others, 1979, Earth-atmosphere radiation budget analyses derived from NOAA satellite data, June 1974-February 1978, Vols. 1 and 2, NOAA, U S Department of Commerce.

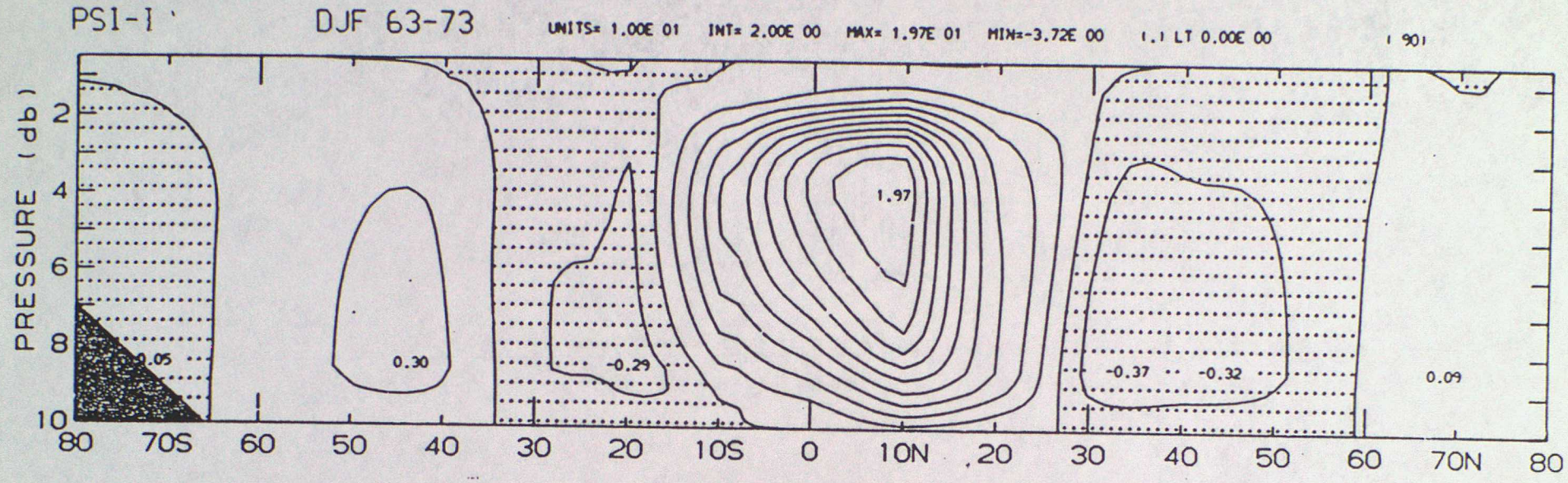

Figure 5.1a

Figure 5.1: Stream function of the mean meridional circulation for the seasons based on 1963-73 data. (units: 10^{10} kg/s; contour interval $0.5*10^{10}$)

Figure 5.1b

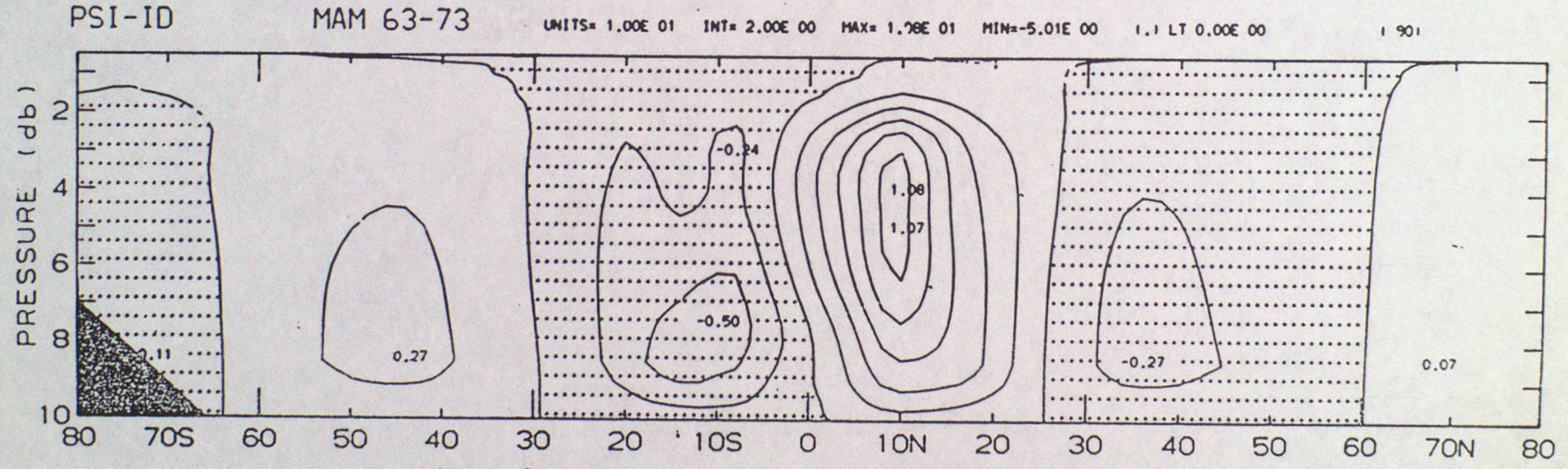

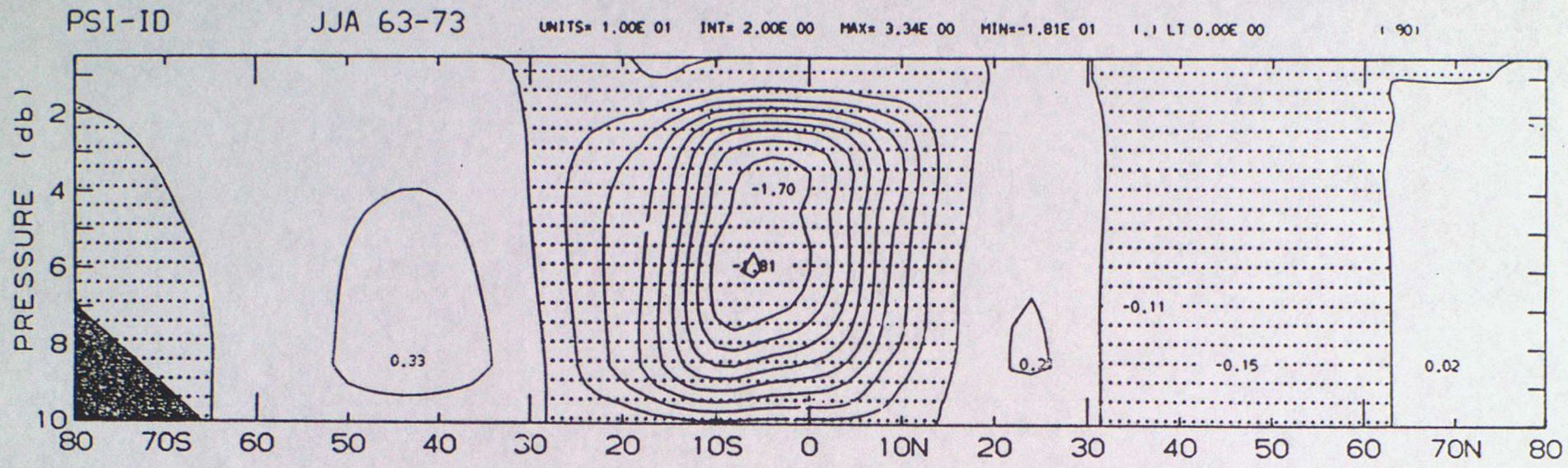

Figure 5.1c

Figure 5.1d

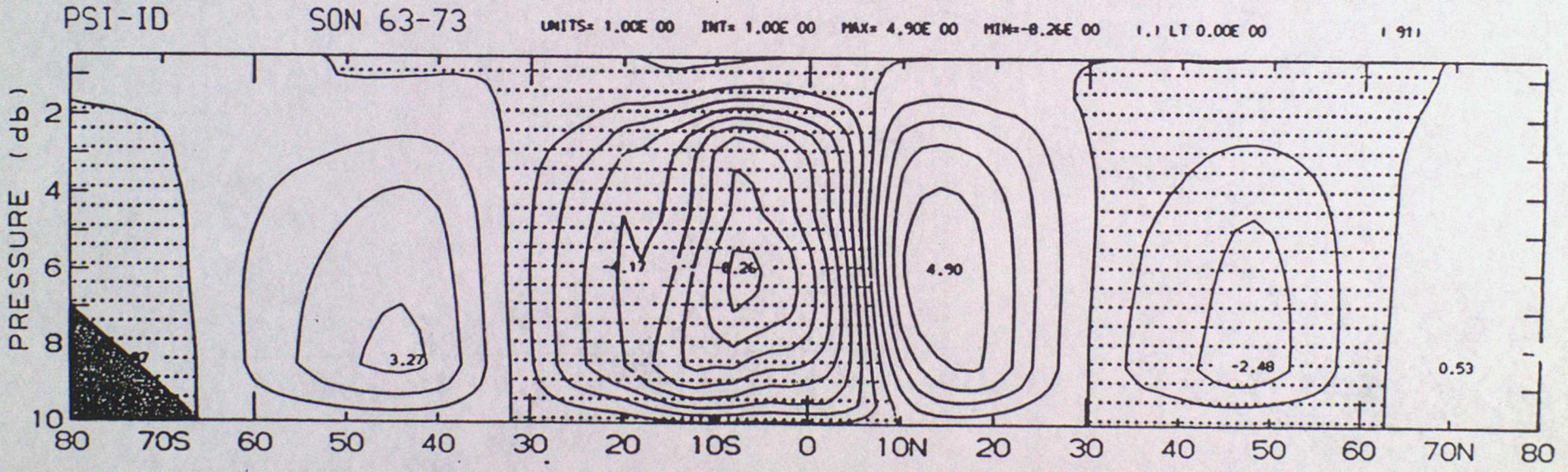

FGGE JUL
VELOCITY POTENTIAL
FROM 0Z ON 1/7/79 DAY 182 TO 12Z ON 31/7/79 DAY 212
LEVEL: 200 MB EXPERIMENT NO.: 3

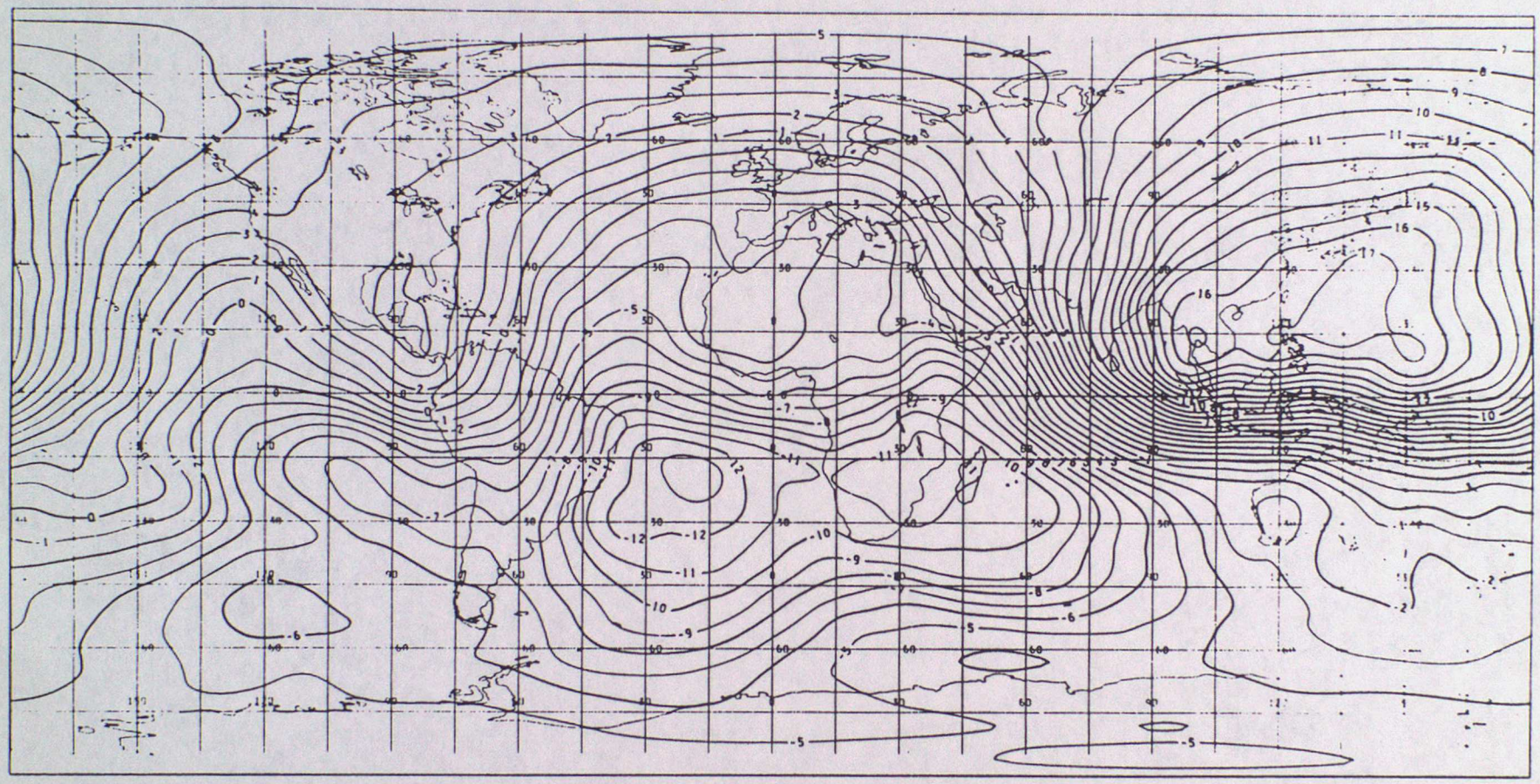

Figure 5.2 (Units: 10^6 m^2 s^{-1})

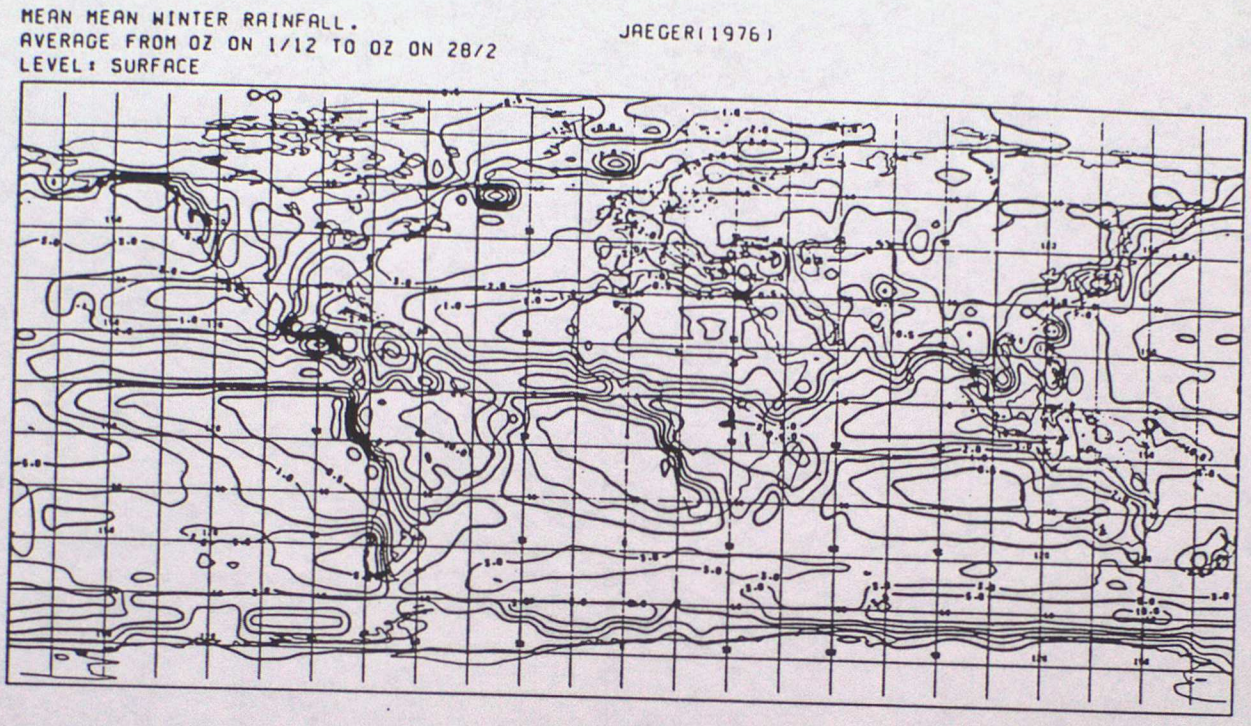

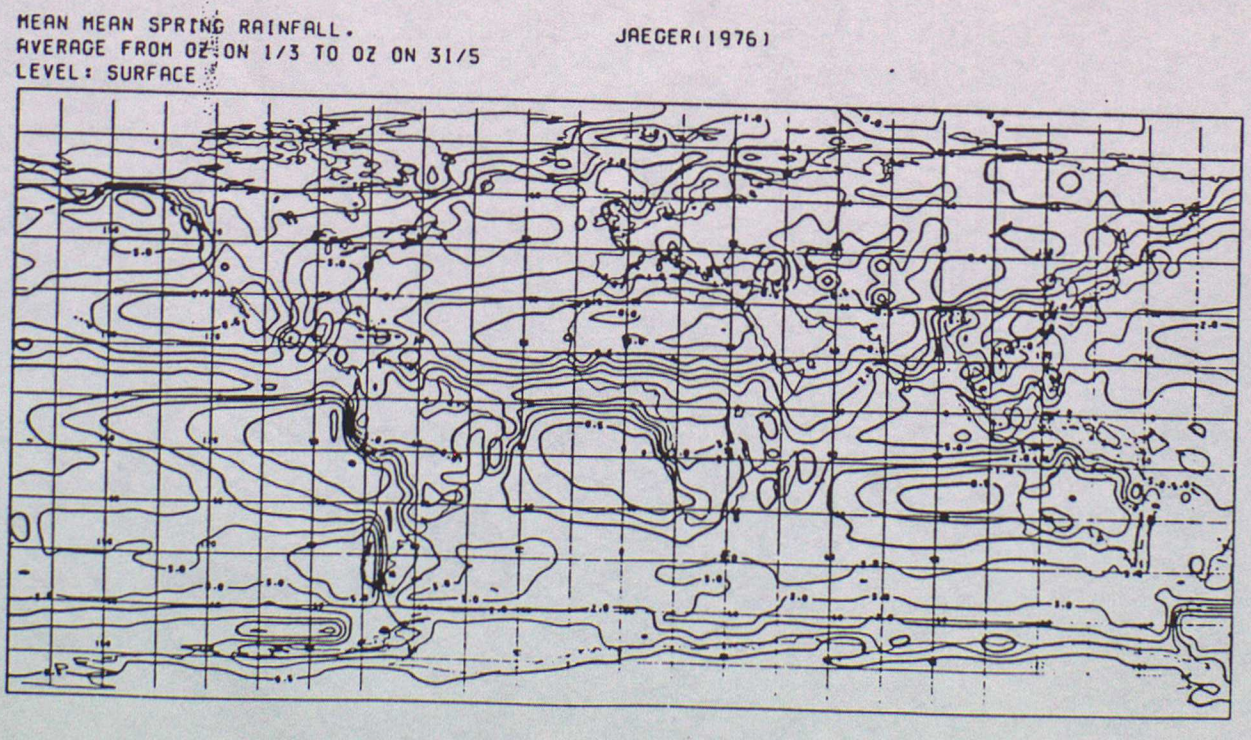

Figure 5.3: Seasonal precipitation from Heasman (1984) after Jaeger (1976). Contours at 0, 0.5, 1, 2, 3, 5, 10 mm/day, underlined contours being thickened. (a) Winter (DJF), (b) Spring.

MEAN MEAN SUMMER RAINFALL.
AVERAGE FROM OZ ON 1/6 TO OZ ON 31/8
LEVEL: SURFACE

JAEGER(1976)

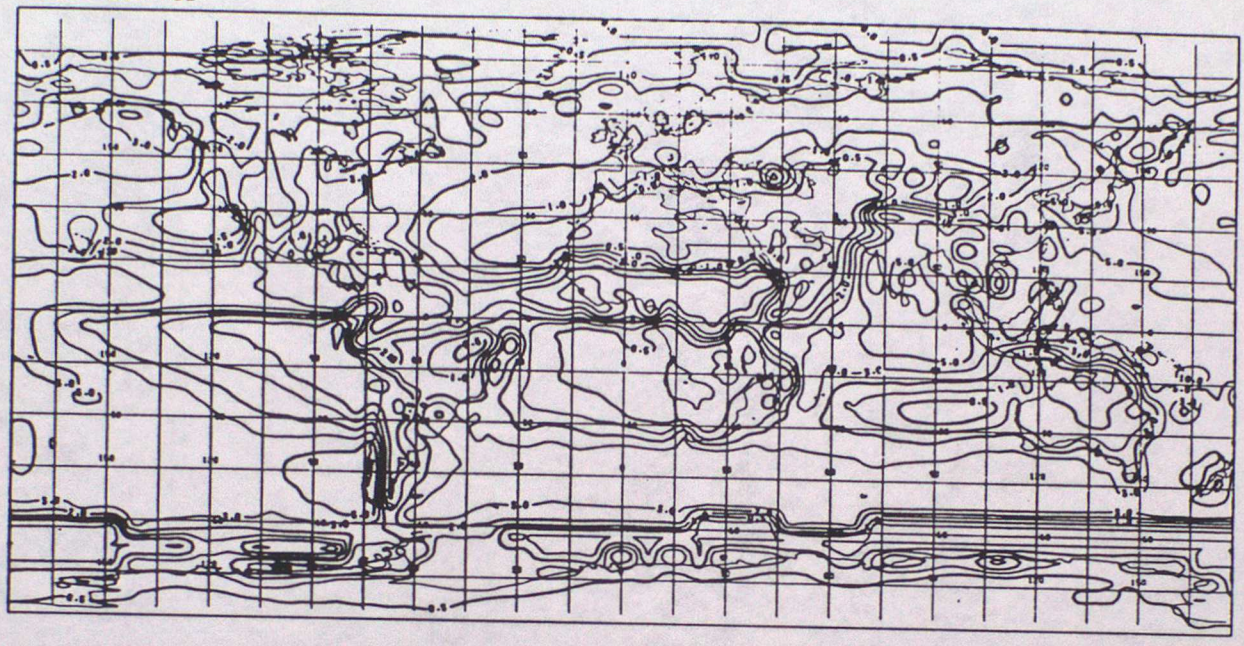

MEAN MEAN AUTUMN RAINFALL.
AVERAGE FROM OZ ON 1/9 TO OZ ON 30/11
LEVEL: SURFACE

JAEGER(1976)

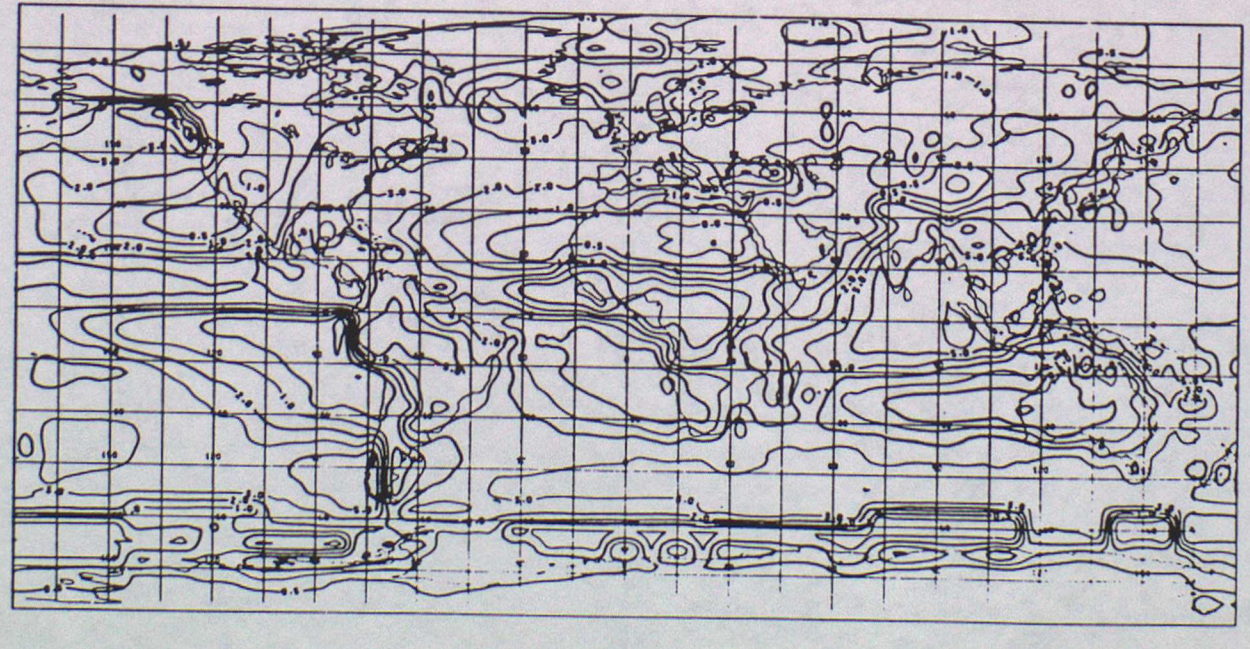

Figure 5.3

Climatological rainfall (mm/day), c) Summer, d) Autumn.

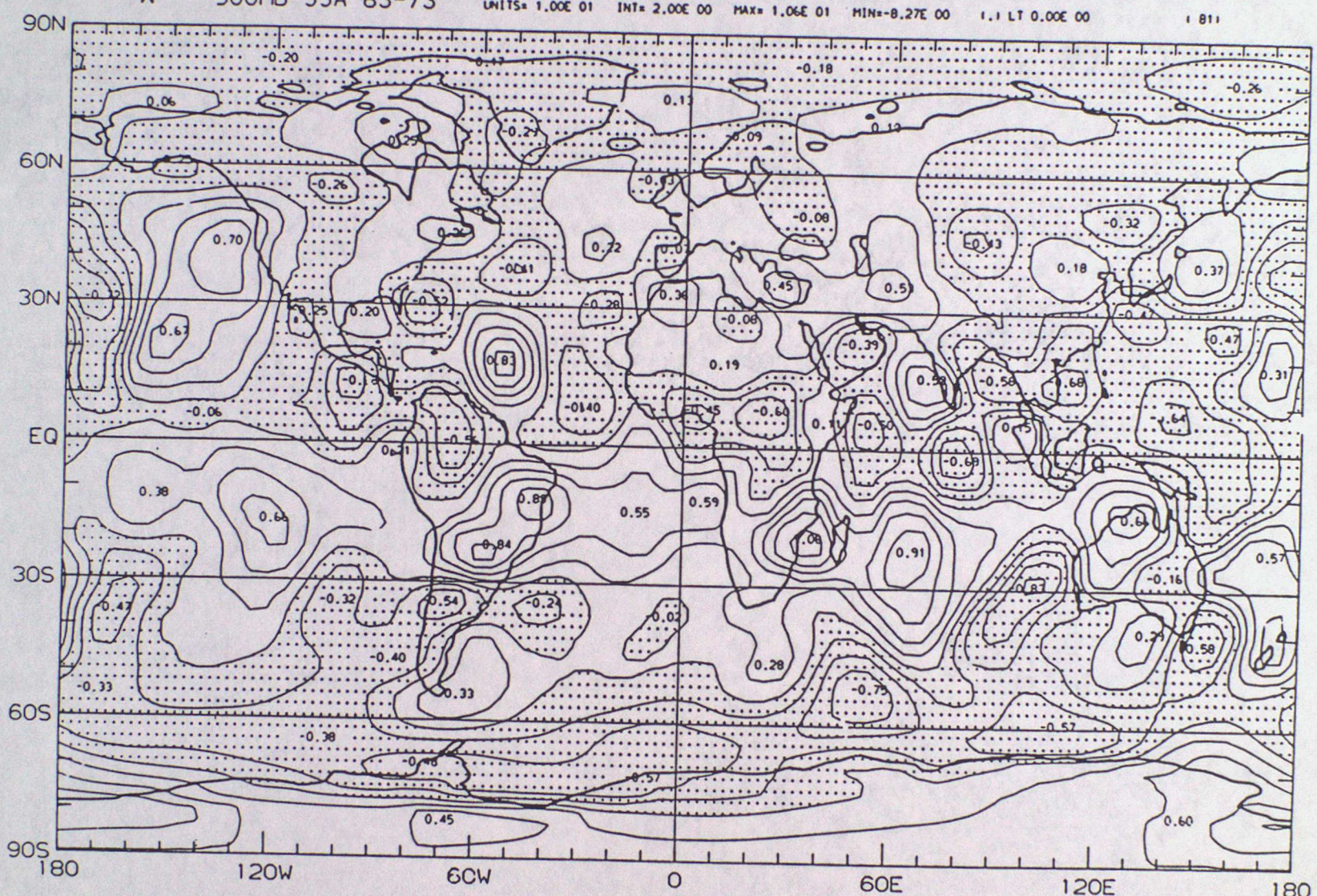

Figure 5.4 (Units: μbar/s)

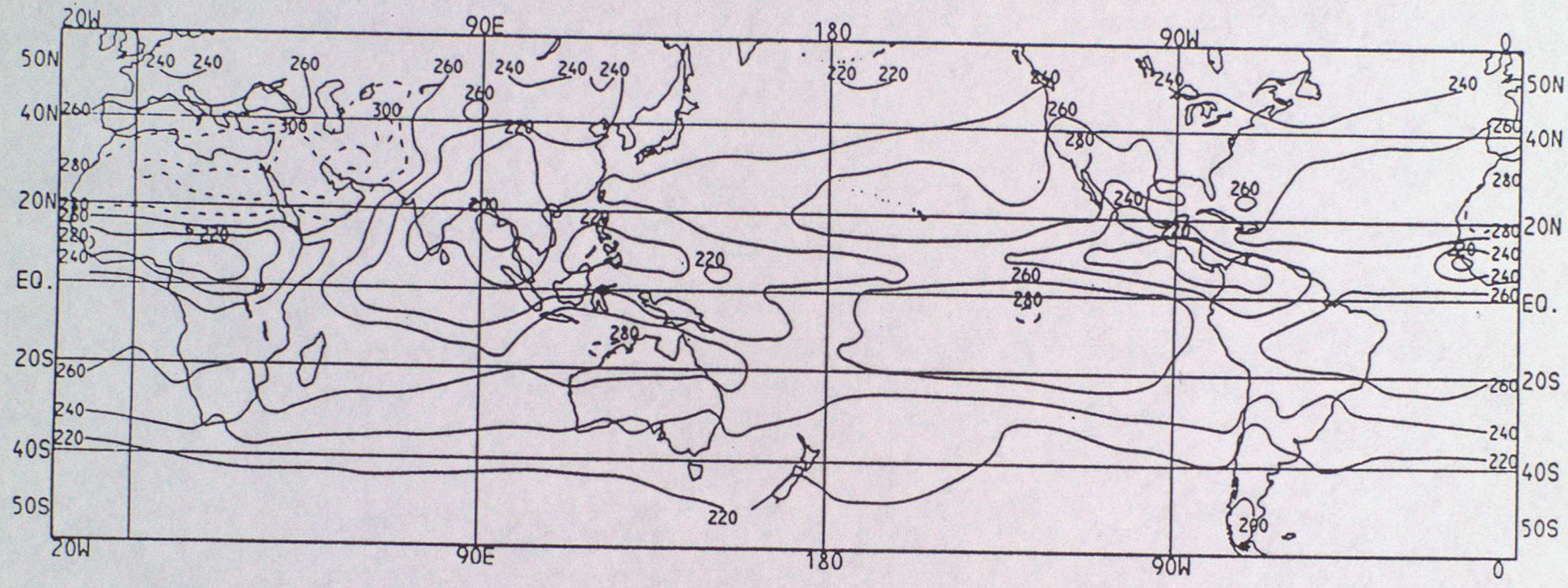

Figure 5.5: Outgoing longwave radiance for DJF (Units: W m^{-2})

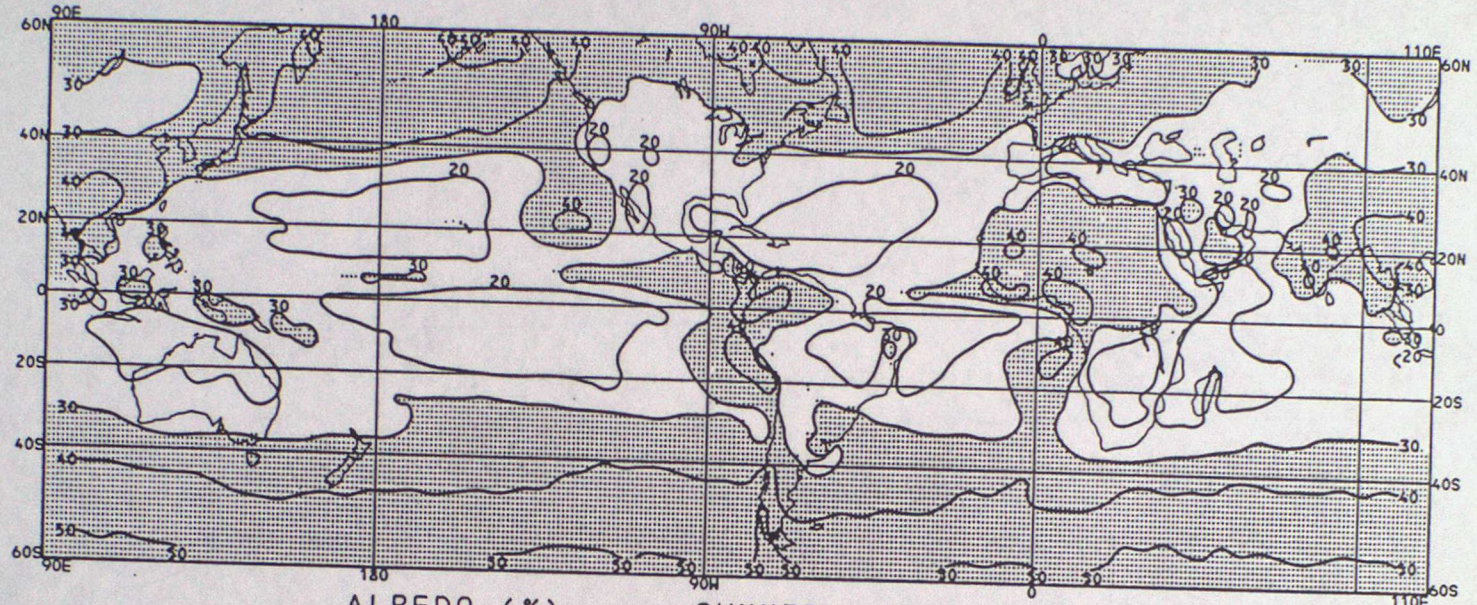

Figure 5.6

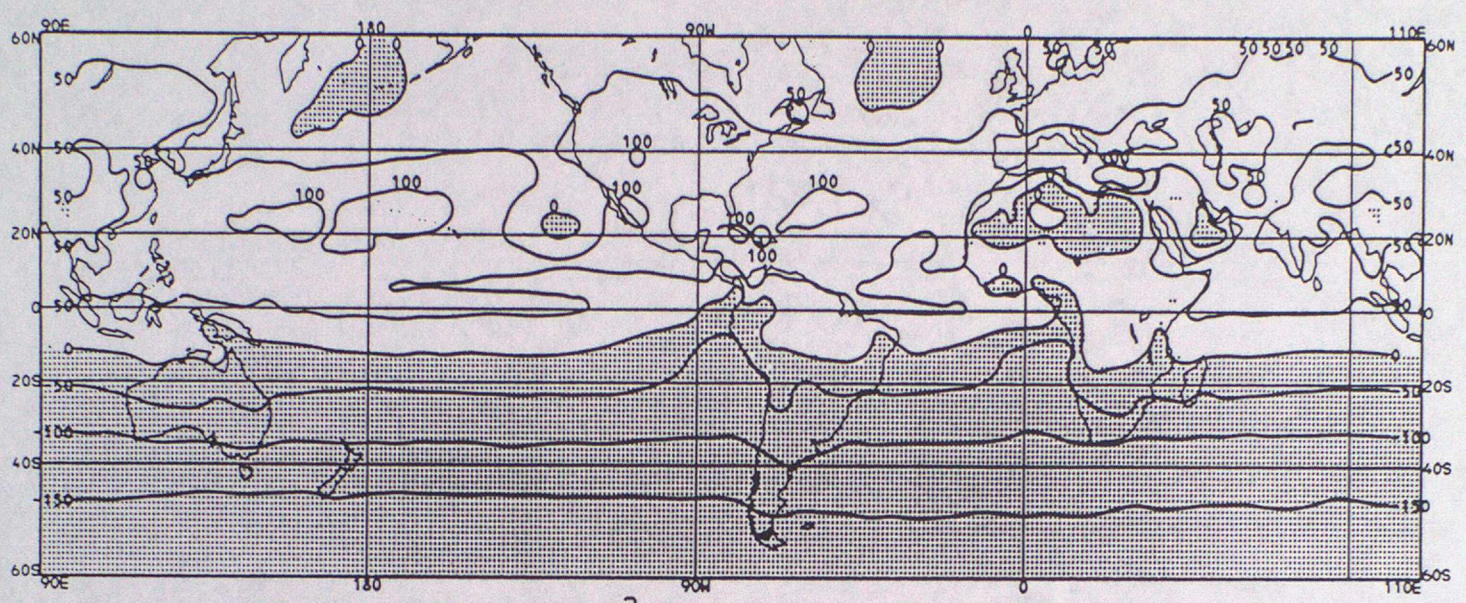

Figure 5.7

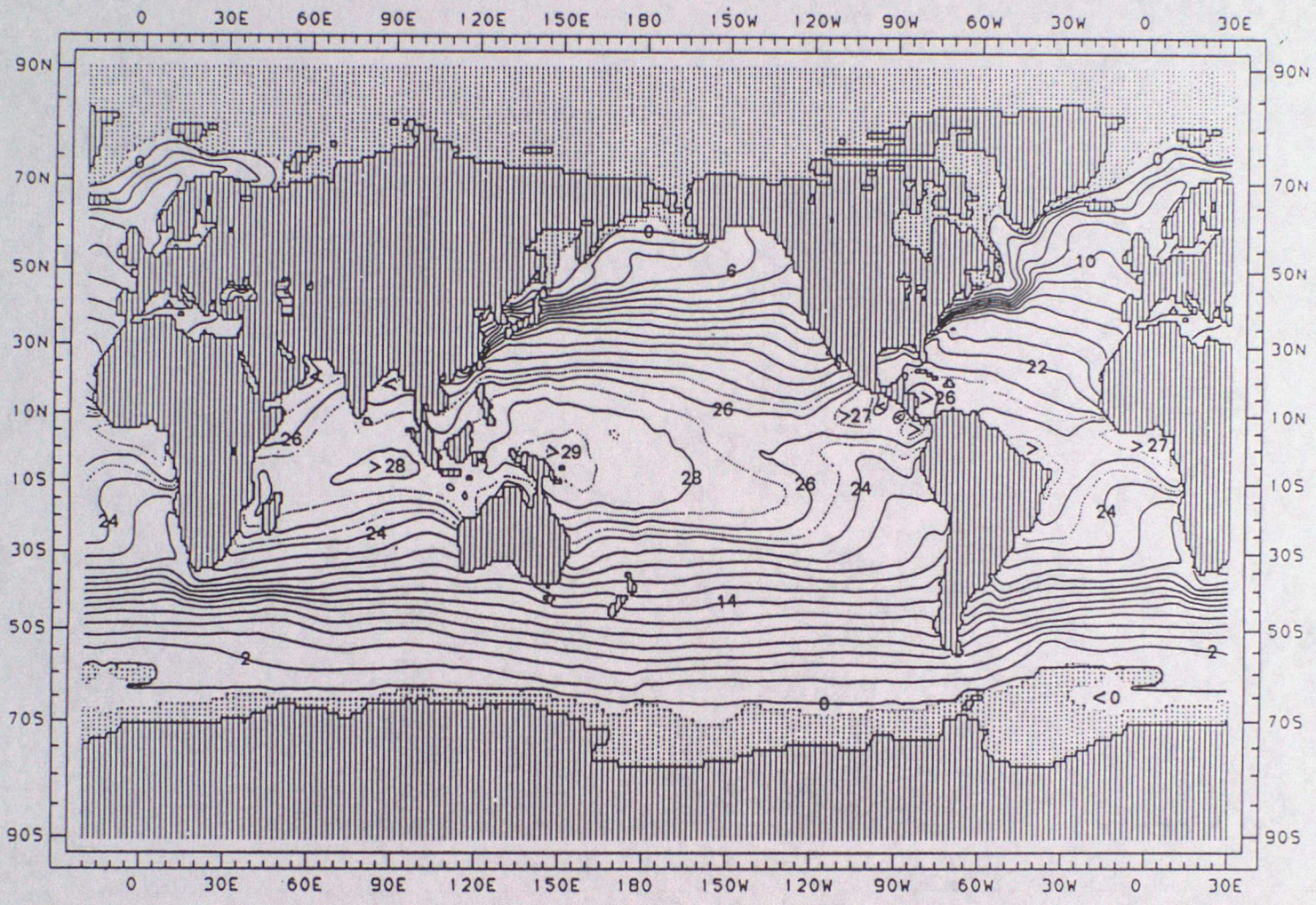

January average ocean-surface temperatures (°C) and ice-pack distributions (broken hash marks). Solid isolines denote 0°, 2°, 4°, 6°C . . . . Dotted isolines in low latitudes denote 25°, 27°, and 29°C.

Figure 5.8a

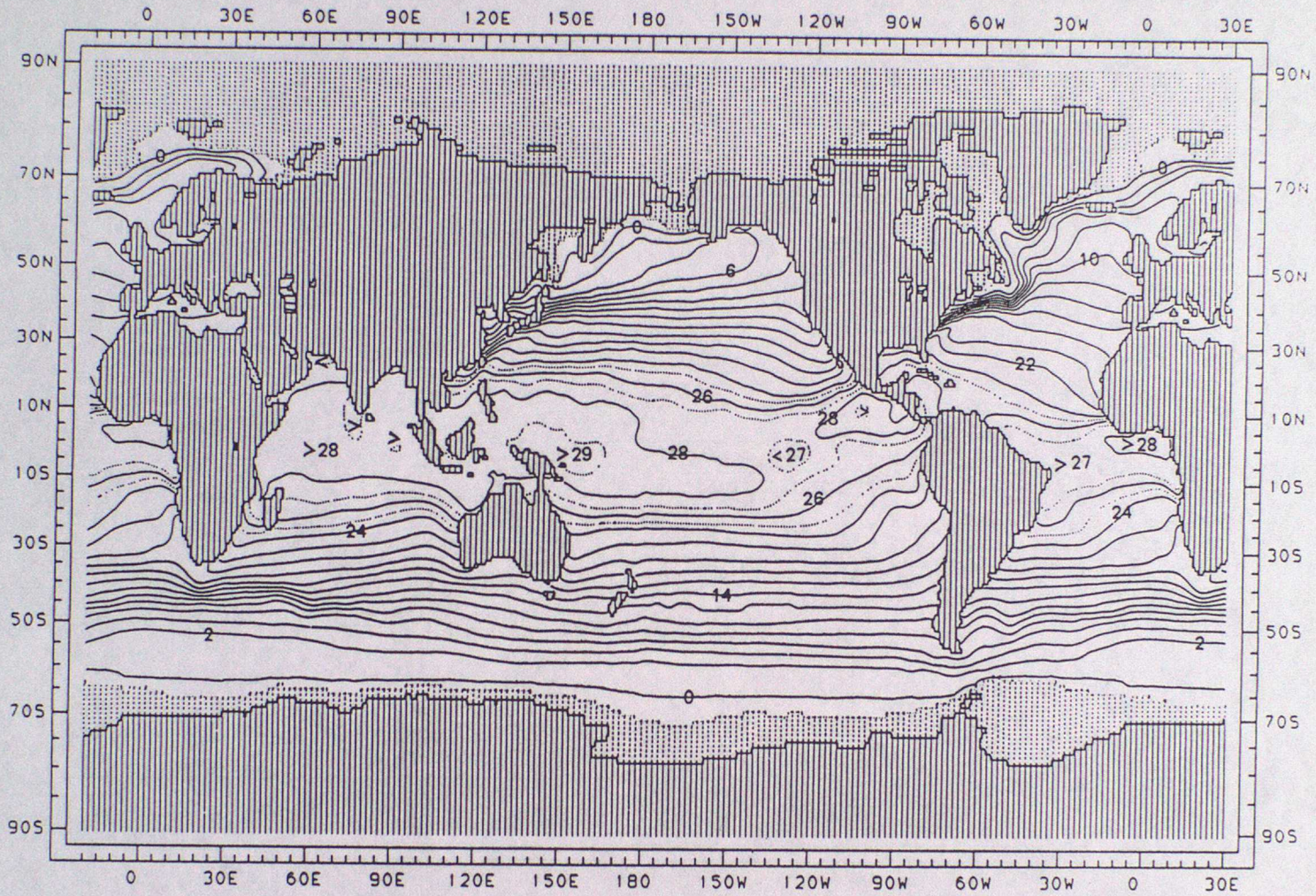

April average ocean-surface temperatures (°C) and ice-pack distributions (broken hash marks). Solid isolines denote 0°, 2°, 4°, 6°C . . . . Dotted isolines in low latitudes denote 25°, 27°, and 29°C.

Figure 5.8b

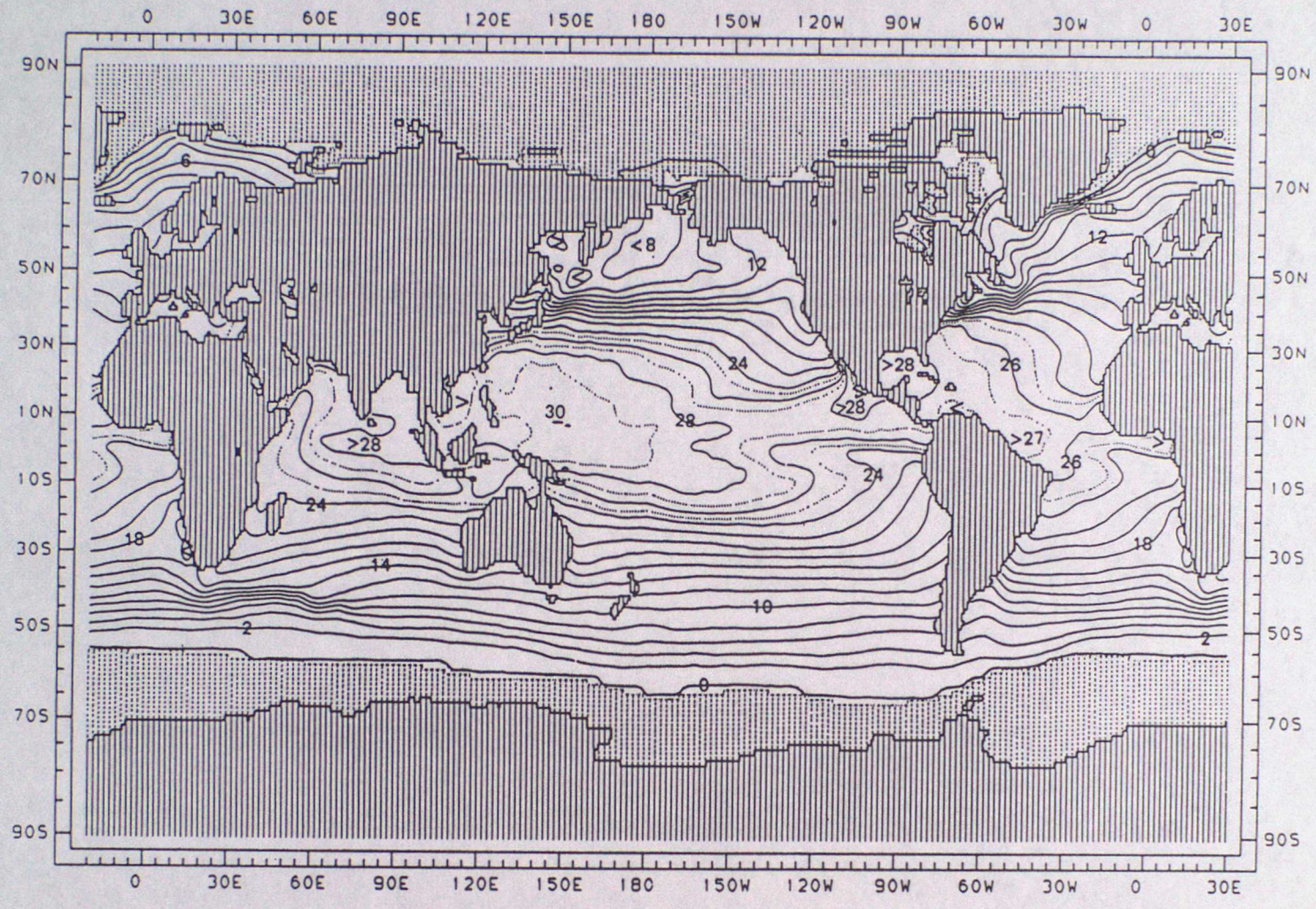

July average ocean-surface temperatures (°C) and ice-pack distributions (broken hash marks). Solid isolines denote 0°, 2°, 4°, 6°C . . . . Dotted isolines in low latitudes denote 25°, 27°, and 29°C.

Figure 5.8c

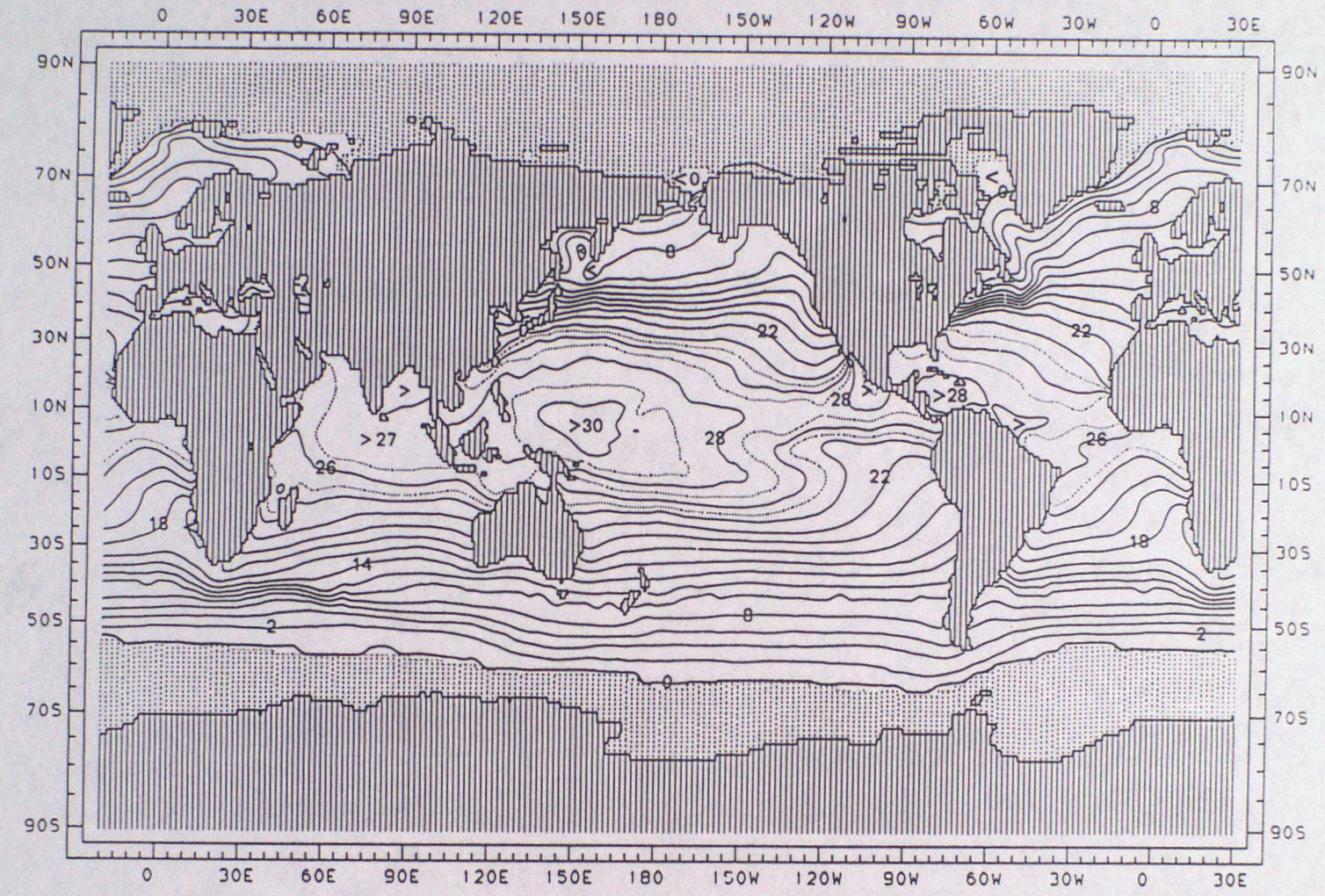

October average ocean-surface temperatures (°C) and ice-pack distributions (broken hash marks). Solid isolines denote 0°, 2°, 4°, 6°C . . . . Dotted isolines in low latitudes denote 25°, 27°, and 29°C.

Figure 5.8d

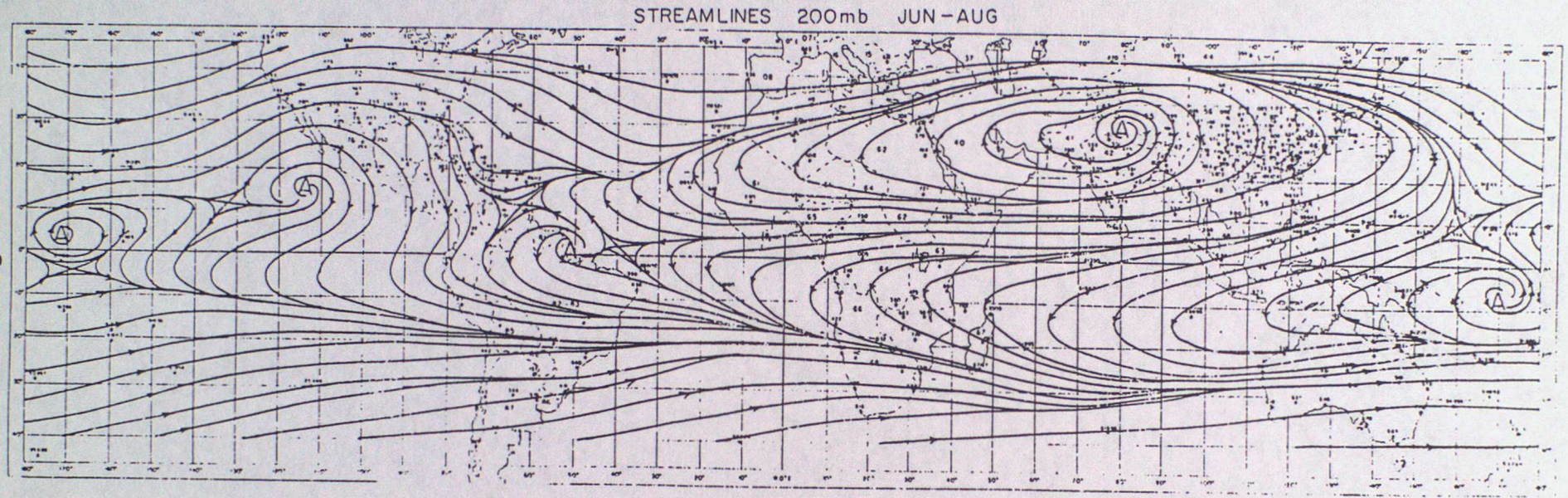

Figure 5.9

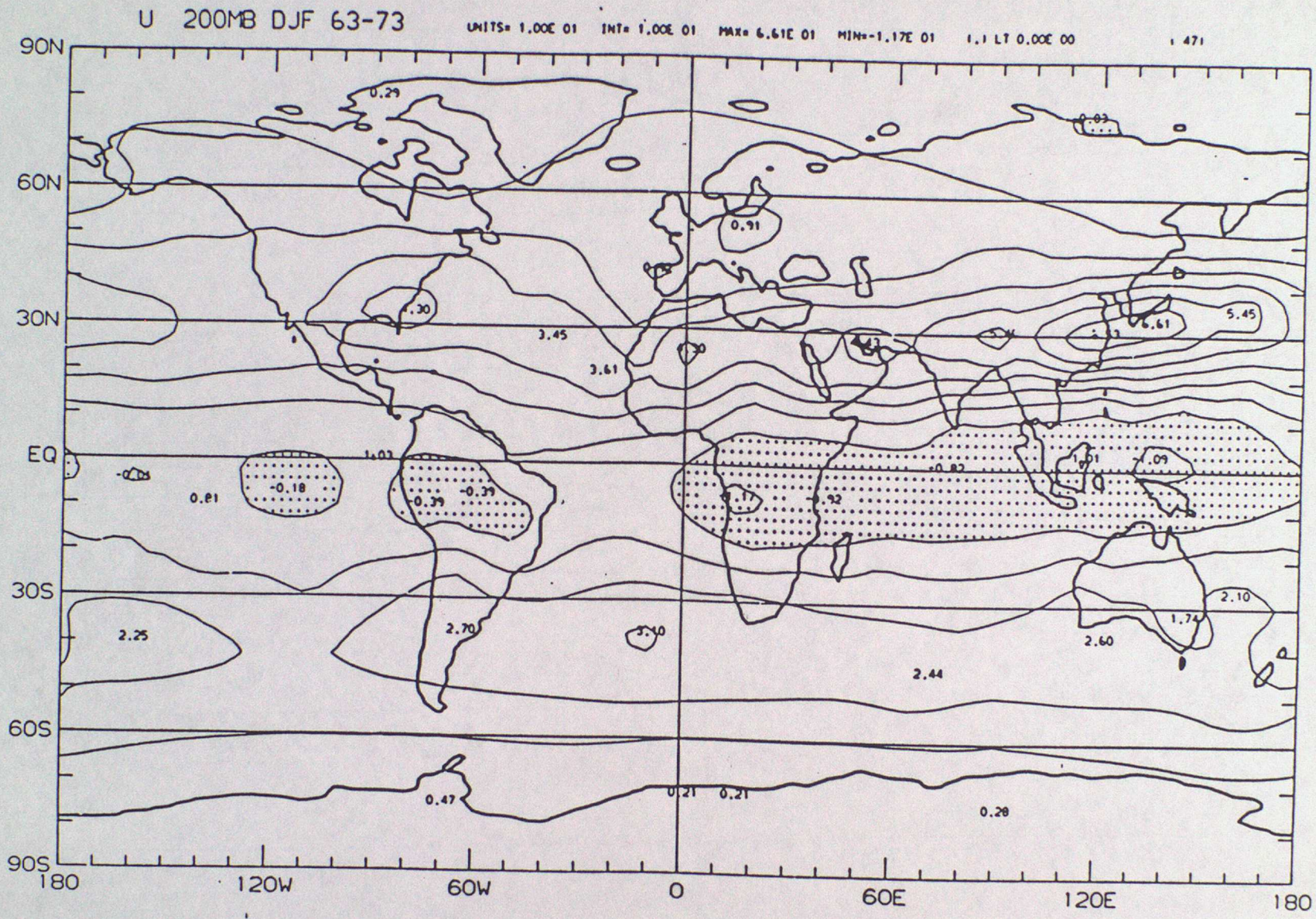

Figure 5.10a (Units: 10 m/s)

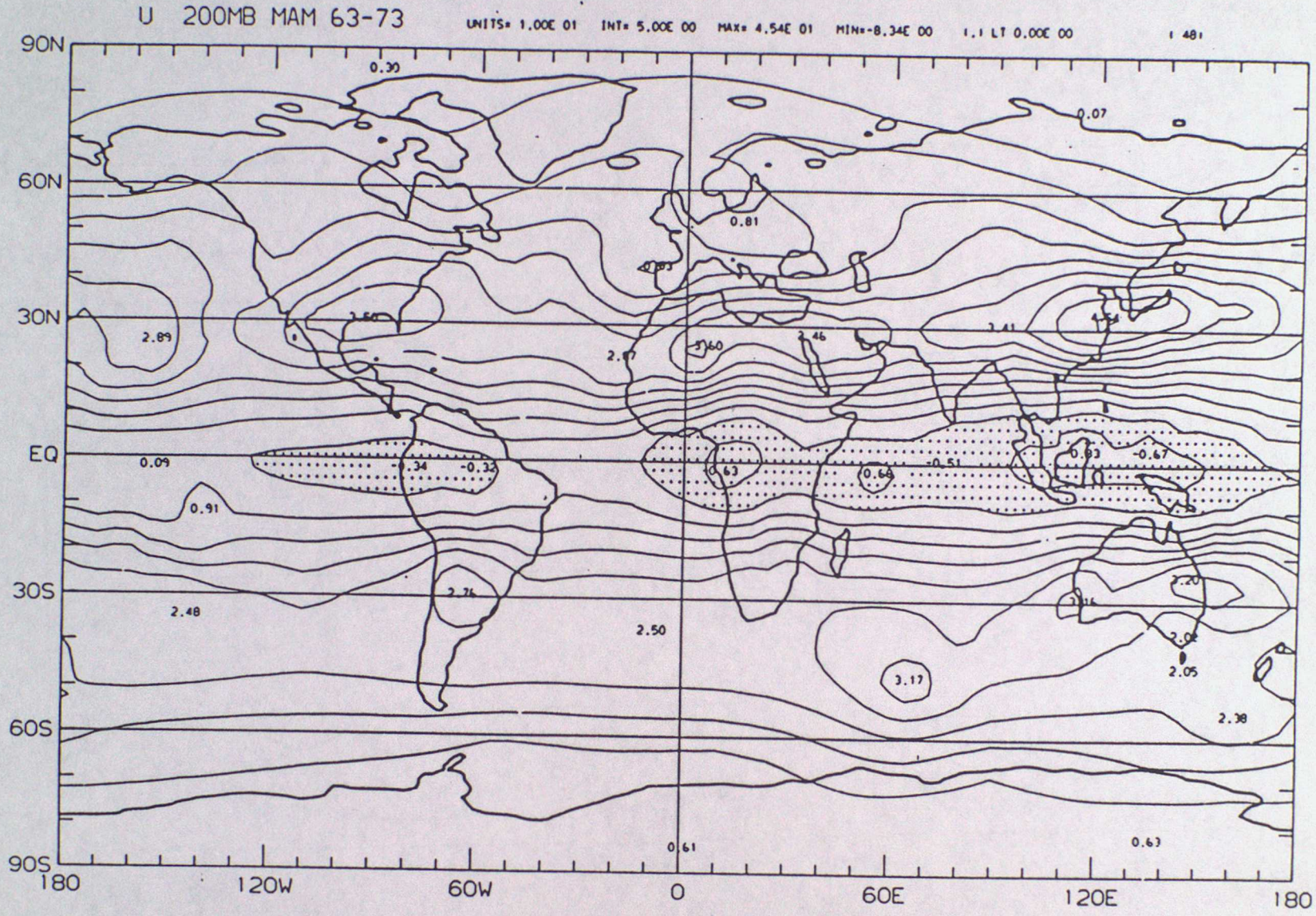
U 200MB MAM 63-73
UNITS= 1.00E 01 INT= 5.00E 00 MAX= 4.54E 01 MIN=-8.34E 00 I,J LT 0.00E 00 1 481
90N
60N
30N
EQ
30S
60S
90S
180
120W
60W
0
60E
120E
180
0.30
0.07
0.81
2.89
2.60
2.46
2.41
0.09
-0.34
-0.32
0.63
0.66
-0.51
0.93
-0.67
0.91
2.48
2.76
2.50
3.17
2.05
2.38
0.61
0.63

Figure 5.10b

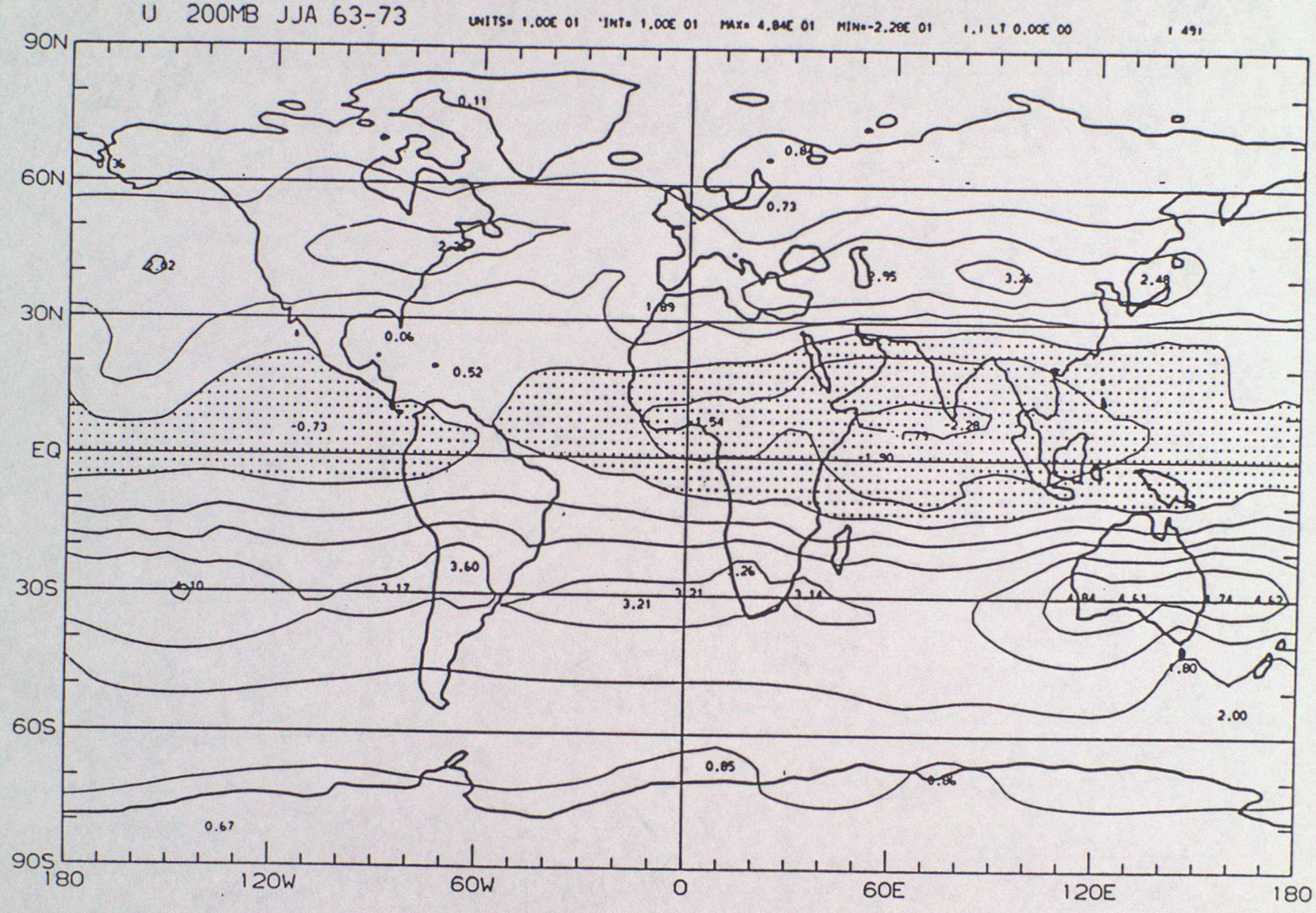
U 200MB JJA 63-73
UNITS= 1.00E 01 'INT= 1.00E 01 MAX= 4.84E 01 MIN=-2.28E 01 (.) LT 0.00E 00
90N
60N
30N
EQ
30S
60S
90S
180
120W
60W
0
60E
120E
180
0.11
0.73
0.06
0.52
-0.73
3.60
3.21
2.00
0.85
0.67

Figure 5.10c

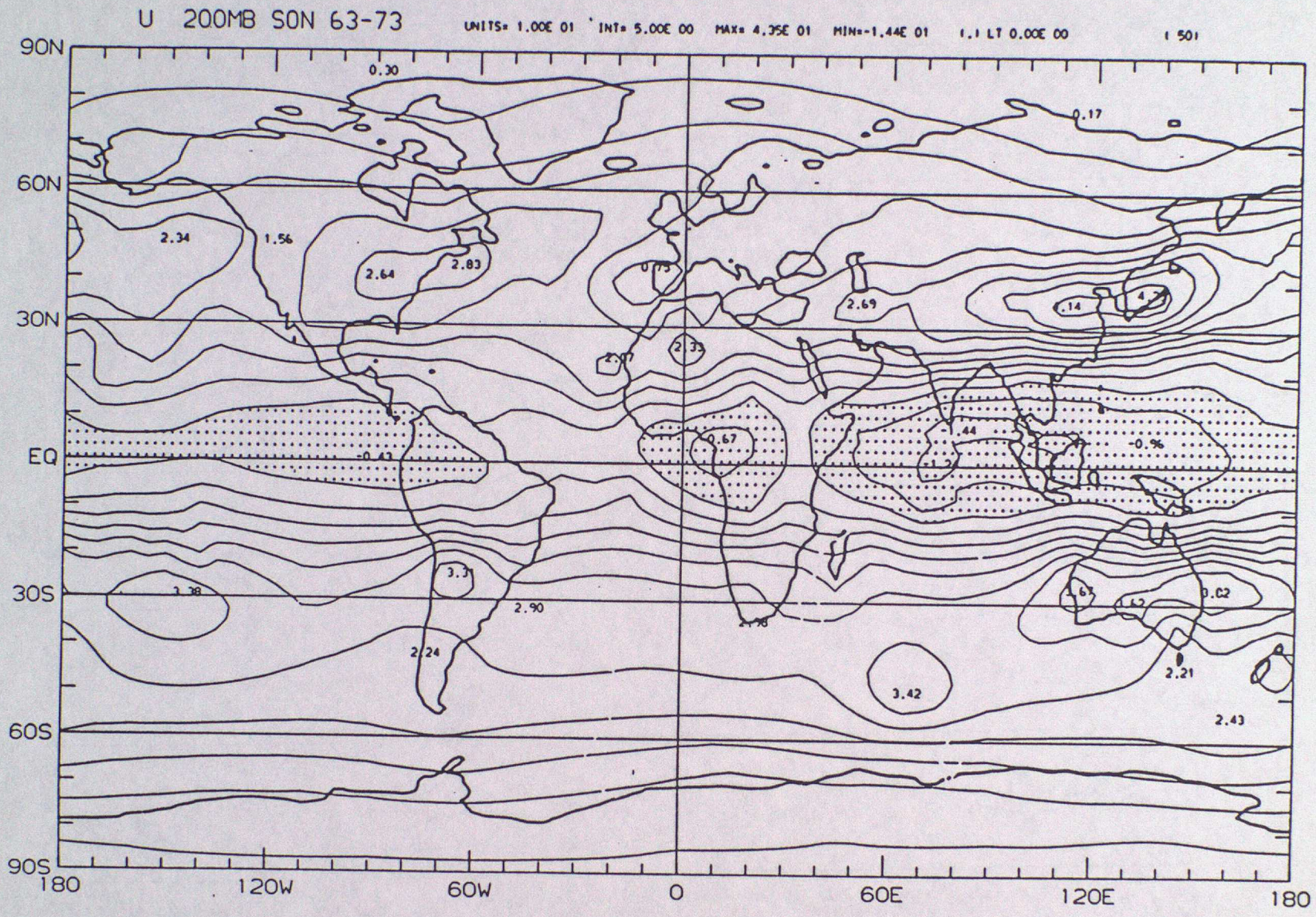
U 200MB SON 63-73
UNITS= 1.00E 01 INT= 5.00E 00 MAX= 4.35E 01 MIN=-1.44E 01 (.) LT 0.00E 00 (50)
90N
60N
30N
EQ
30S
60S
90S
180
120W
60W
0
60E
120E
180
0.30
0.17
2.34
1.56
2.64
2.83
2.69
2.33
0.67
-0.43
-0.96
3.38
3.31
2.90
2.24
3.42
2.21
2.43

Figure 5.10d

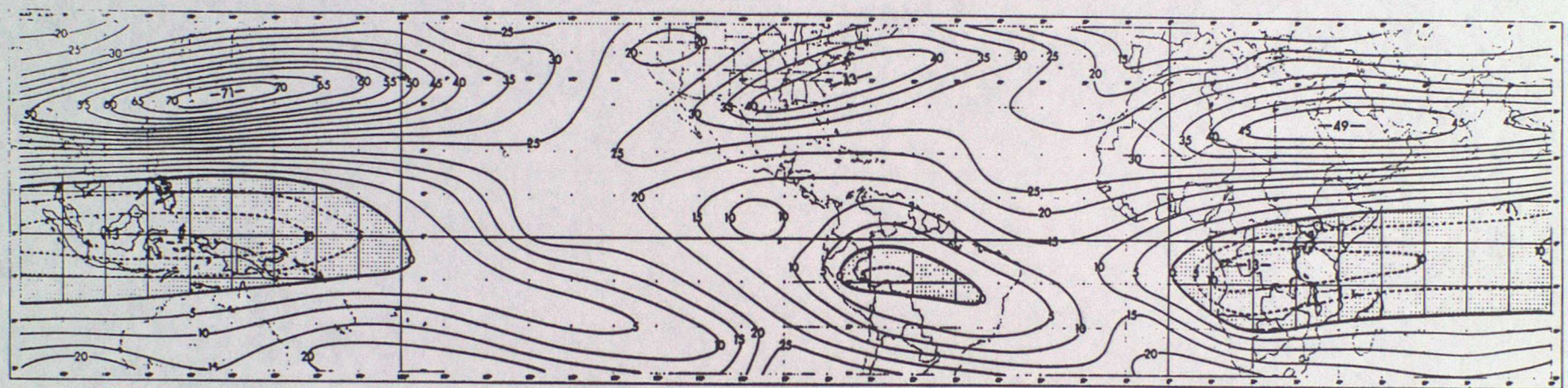

Figure 5.11

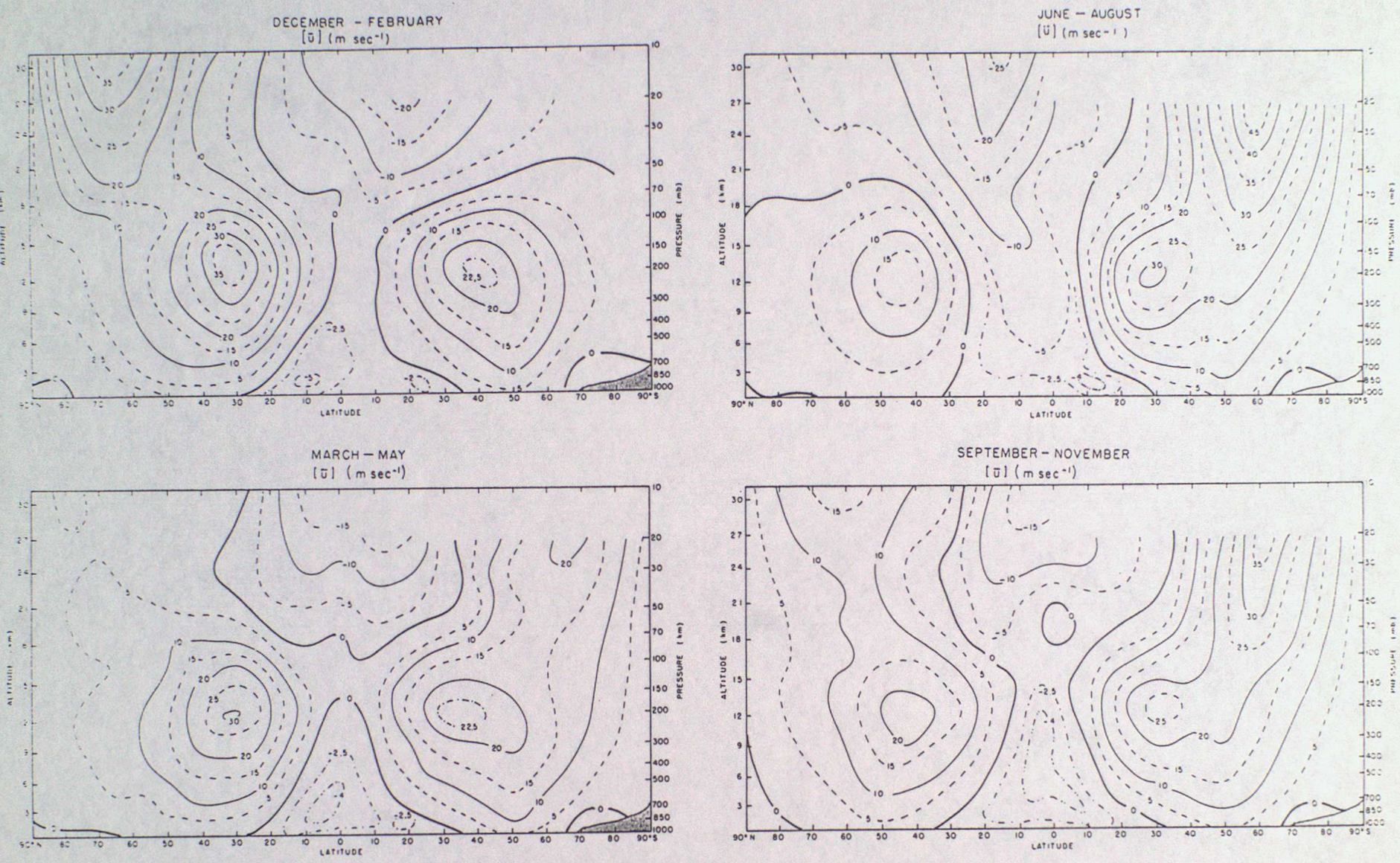
DECEMBER - FEBRUARY
[ū] (m sec⁻¹)
JUNE - AUGUST
[ū] (m sec⁻¹)
MARCH - MAY
[ū] (m sec⁻¹)
SEPTEMBER - NOVEMBER
[ū] (m sec⁻¹)
ALTITUDE (km)
PRESSURE (mb)
LATITUDE
90°N
90°S

Figure 5.12

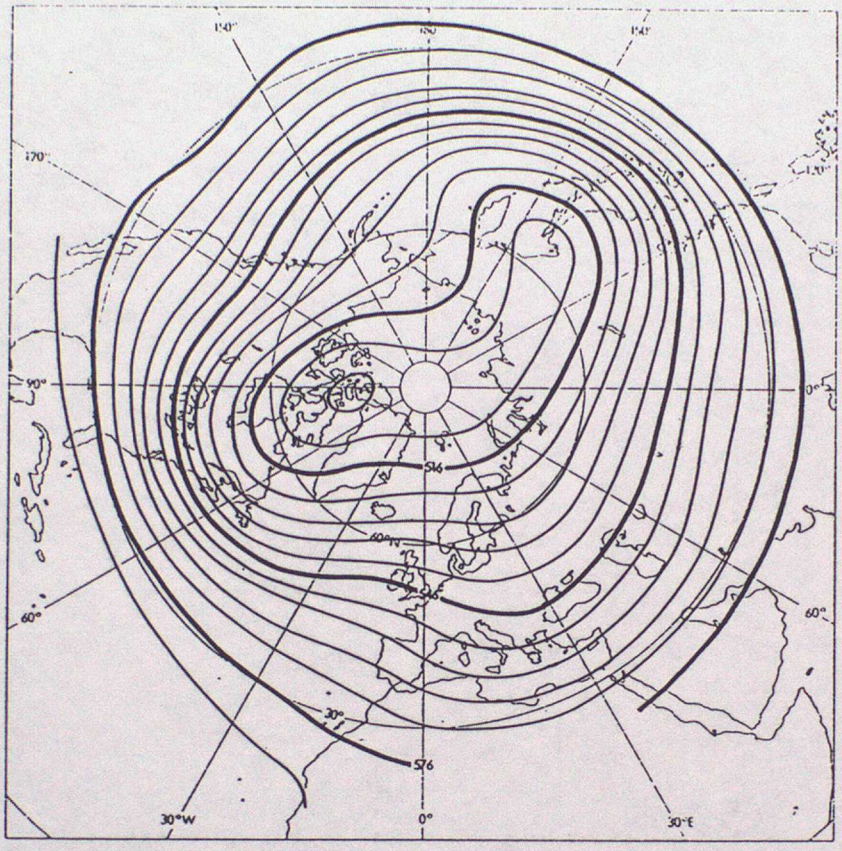

MONTHLY MEAN 500-MILLIBAR CONTOURS FOR JANUARY 1951–66
Isopleths are at intervals of 6 geopotential decametres

Figure 5.13a

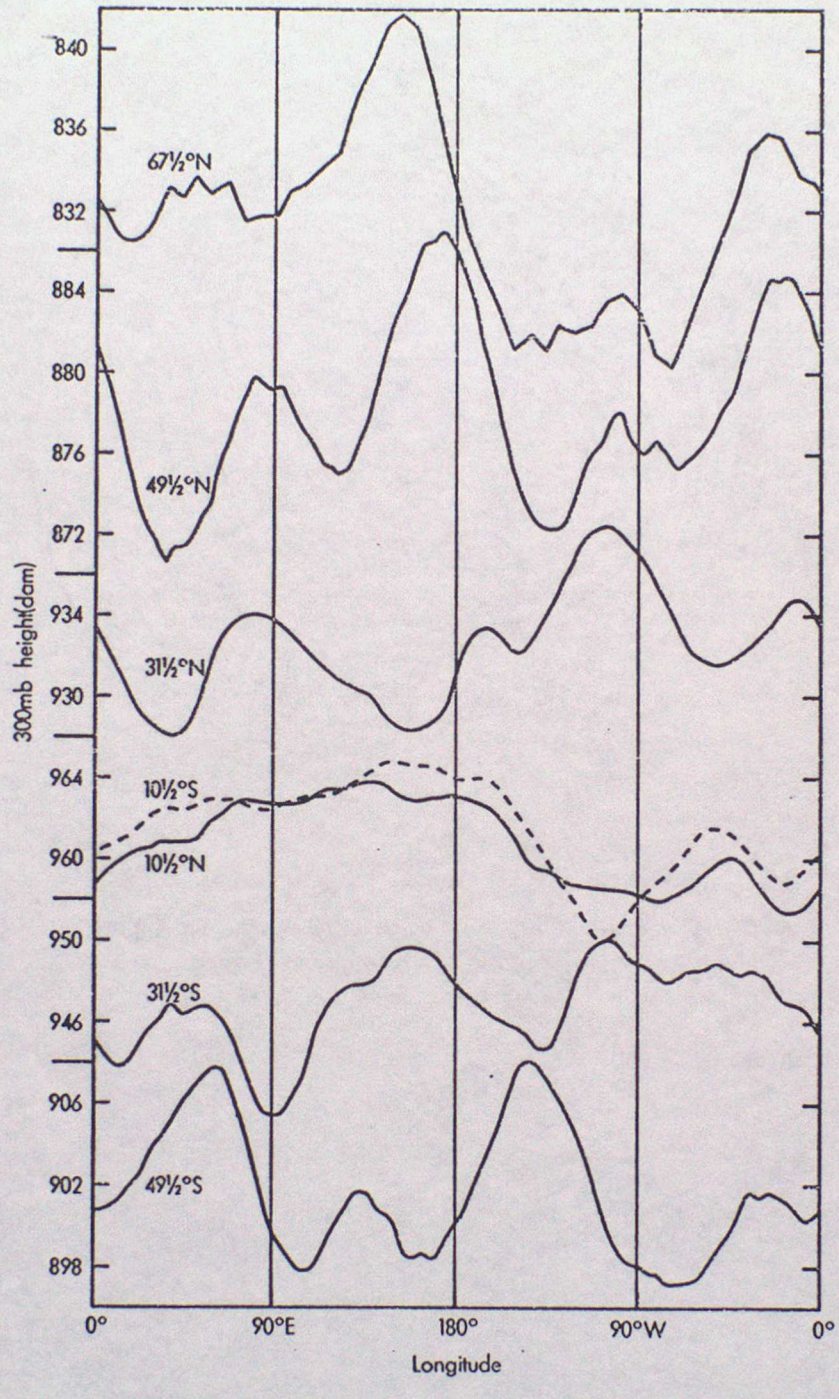

Figure 5.13b

Day 41-80 average longitudinal profiles of 300 mbar height for experiment T5 for selected latitudes.

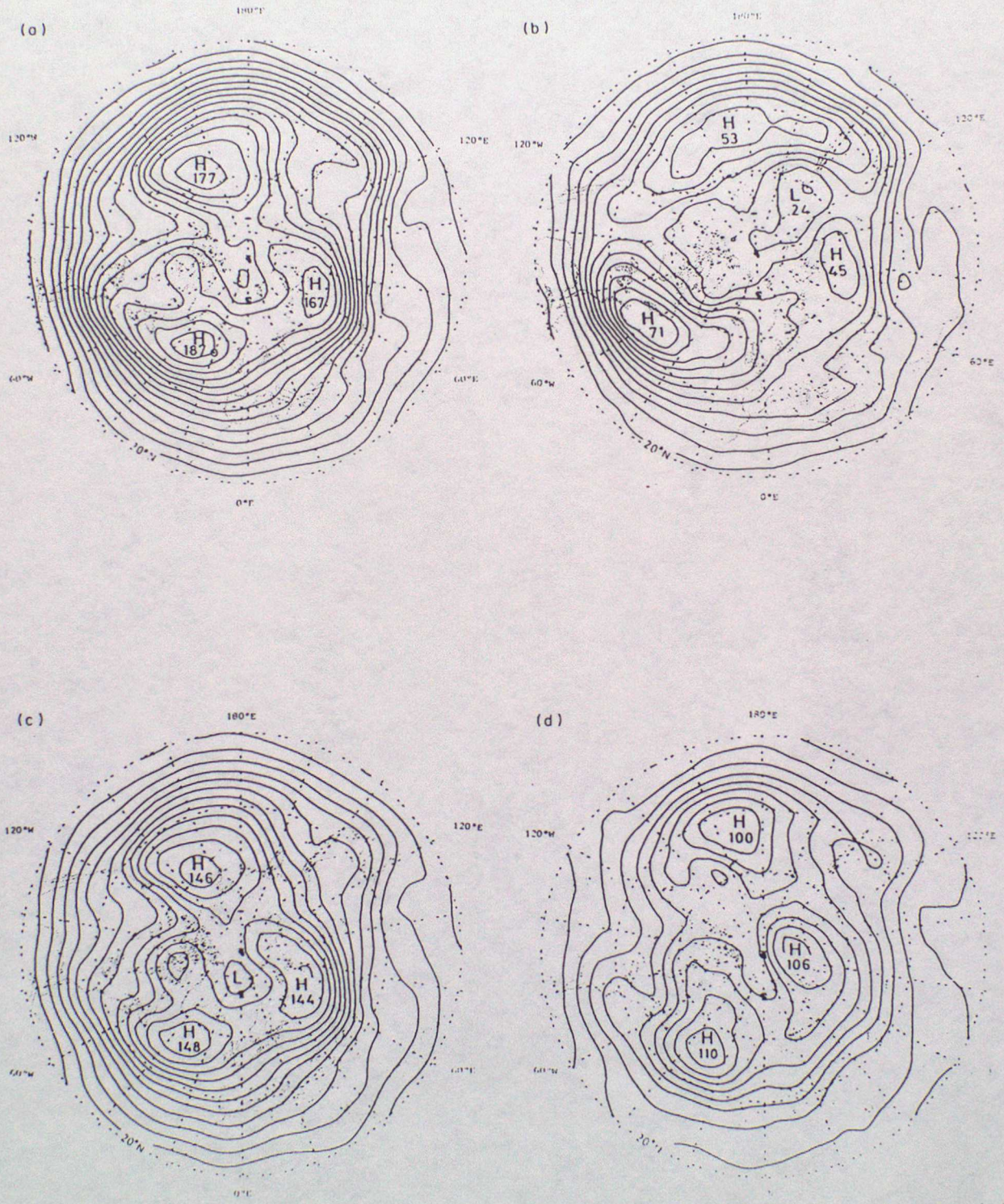

Variance of 500 mb height based on NMC analyses for 18 winter seasons (1962–63 to 1979–80, inclusive) where winter is defined as the 90 days beginning 1 December. The contribution from the climatological mean annual cycle has been removed. (a) Unfiltered twice daily data; contour interval 10 m. (b) Band-pass filtered data emphasizing fluctuations in the 2.5–6 day period range; contour interval 5 m. (c) Low-pass filtered data emphasizing fluctuations with periods longer than 10 days; contour interval 10 m. (d) 30-day mean data; contour interval 10 m. Lines of latitude and longitude are drawn every 20°, the outer latitude circle being 20° N.

Figure 5.14

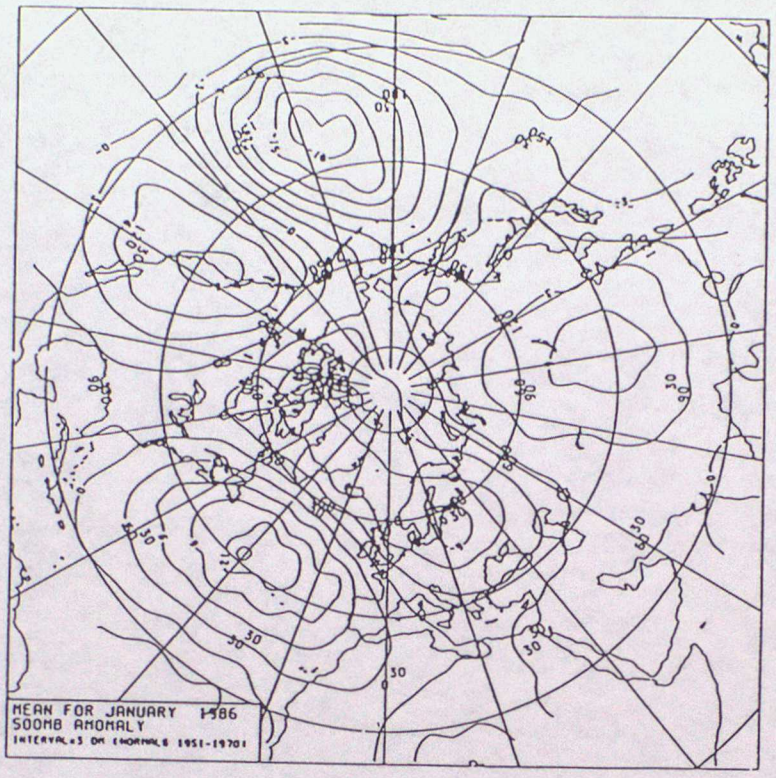
MEAN FOR JANUARY 1986
500MB ANOMALY
INTERVALS ON ENORMALS 1951-1970

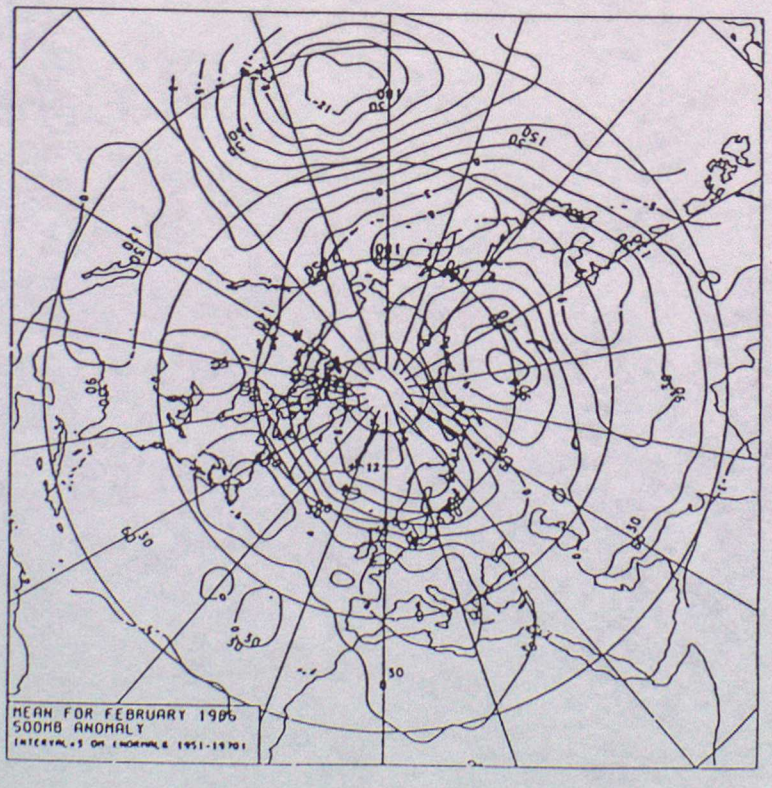
MEAN FOR FEBRUARY 1986
500MB ANOMALY
INTERVALS ON ENORMALS 1951-1970

Figure 5.15

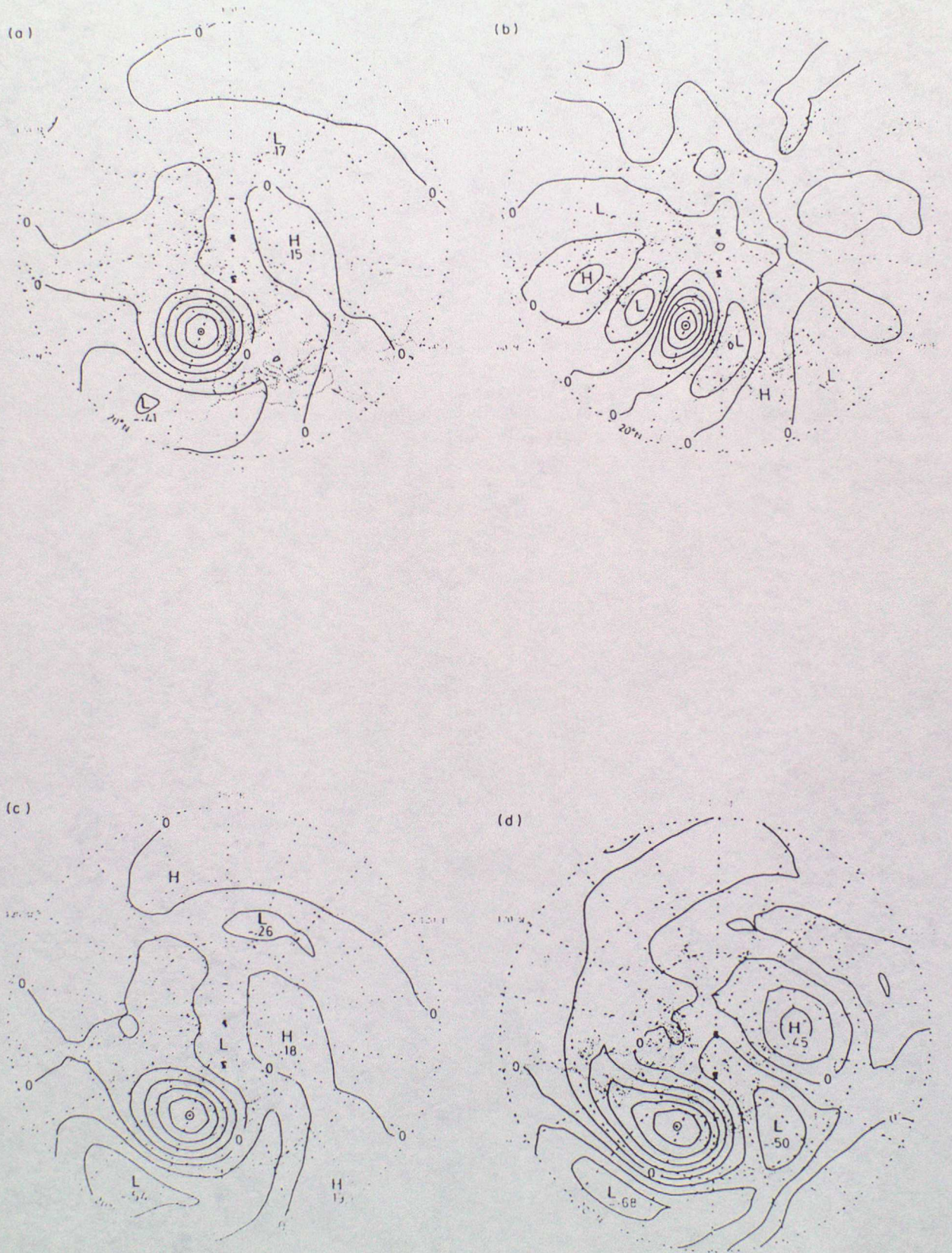

Simultaneous temporal correlations between 500 mb height fluctuations at 55 N, 20 W and other Northern Hemisphere locations during wintertime, based on the same data set as Fig. 5.14, contour interval 0.2. (a) Unfiltered twice daily data. (b) Band-pass filtered data emphasizing fluctuations in the 2.5–6 day period range. (c) Low-pass filtered data emphasizing fluctuations with periods longer than 10 days. (d) Monthly mean data. For further details, see Blackmon *et al.* (1983a).

Figure 5.16

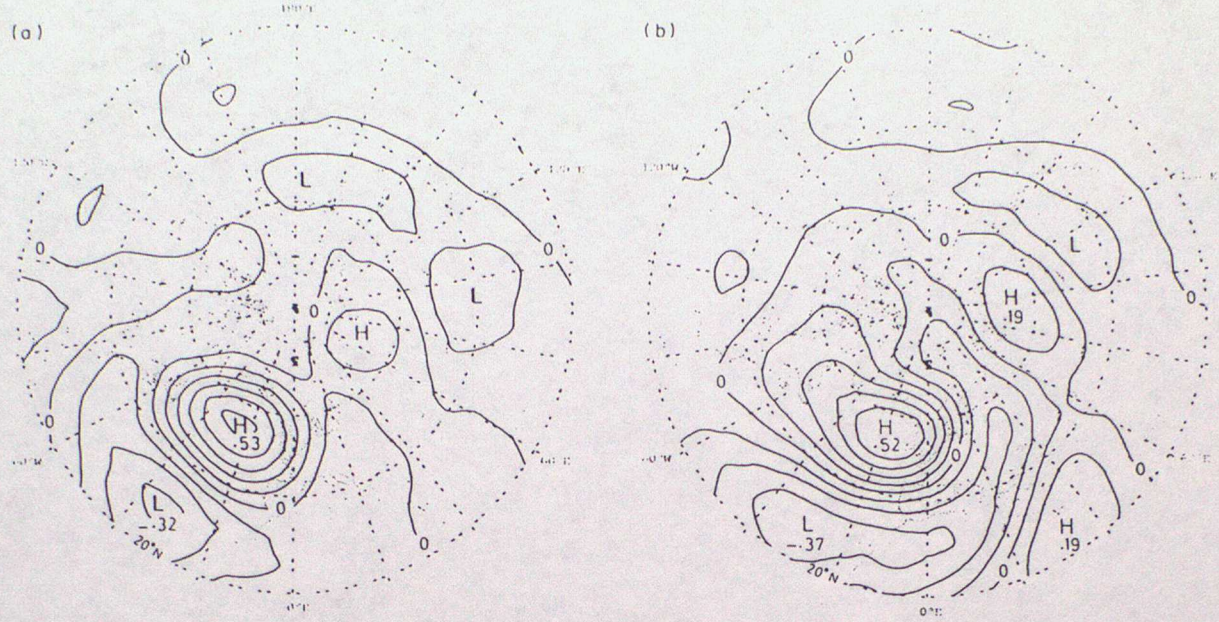

Lag correlations between 500 mb height at (55°N, 20°W) and 500 mb height throughout the hemisphere (a) 2 days earlier and (b) 2 days later, based on the unfiltered daily data set described in the caption of Fig. 5.14. Contour interval 0.1.

Figure 5.17(a)

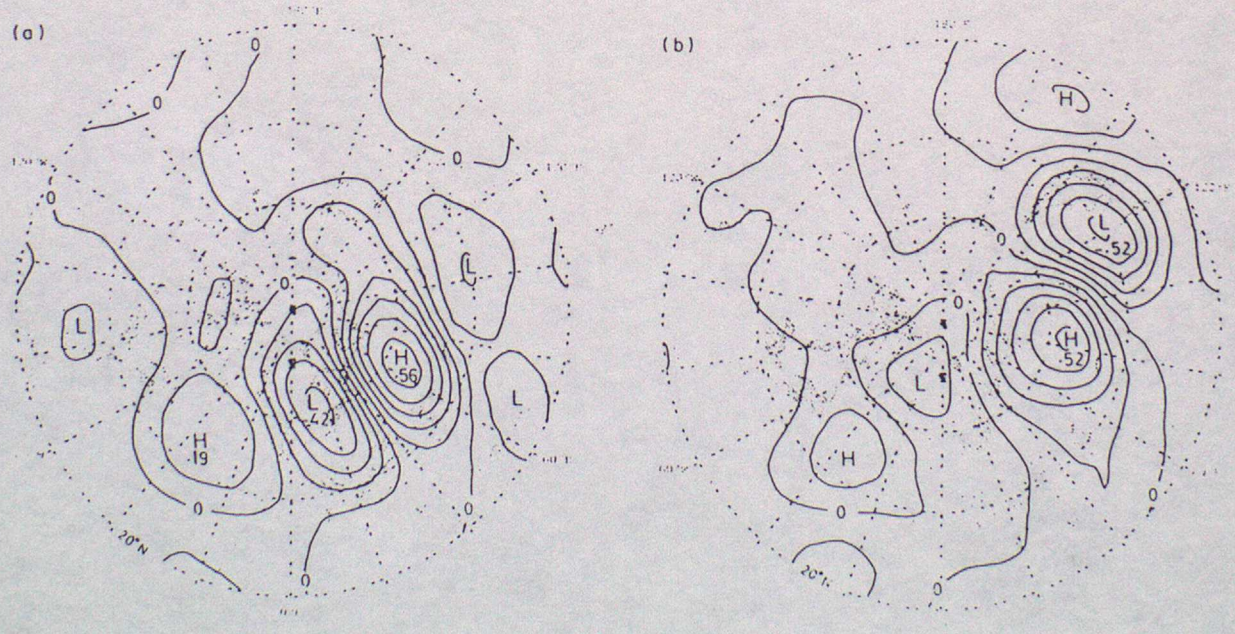

As in (a) but for the gridpoint (55°N, 75 E).

Figure 5.17(b)

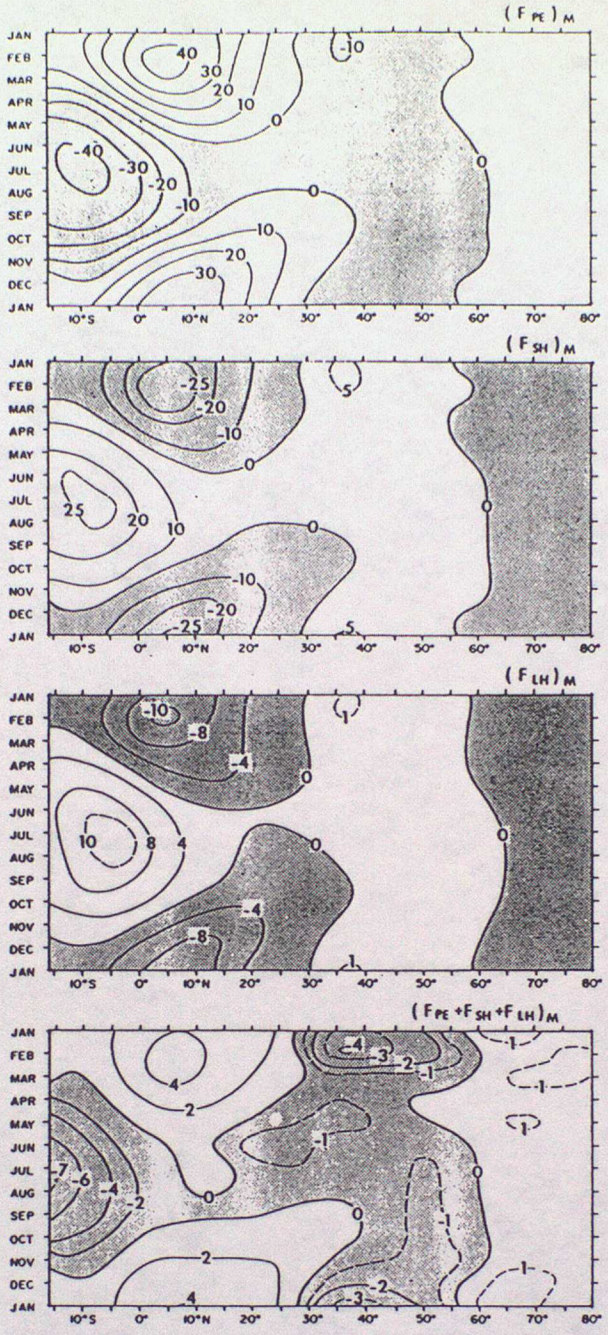

Figure 5.18

The annual variation of the meridional fluxes of potential energy, sensible heat and latent heat by the mean meridional circulation: all units 10^{19} cal day^{-1}.

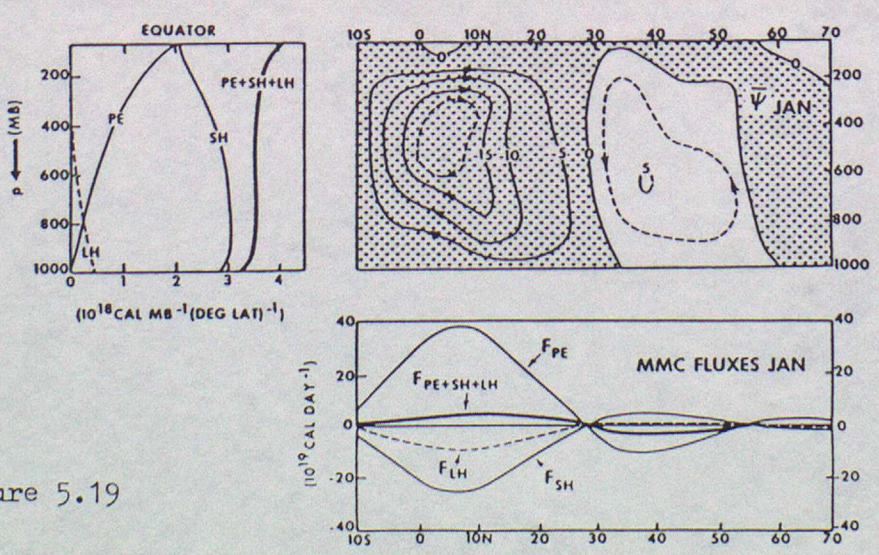

Figure 5.19

Vertical distribution of potential energy, sensible and latent heat at the equator integrated over a latitude strip 1° wide and 1 mb thick (upper left); streamlines of the mean meridional circulation (10^{13} gm sec^{-1}) for January (upper right); and corresponding vertically integrated energy fluxes (10^{19} cal day^{-1}).

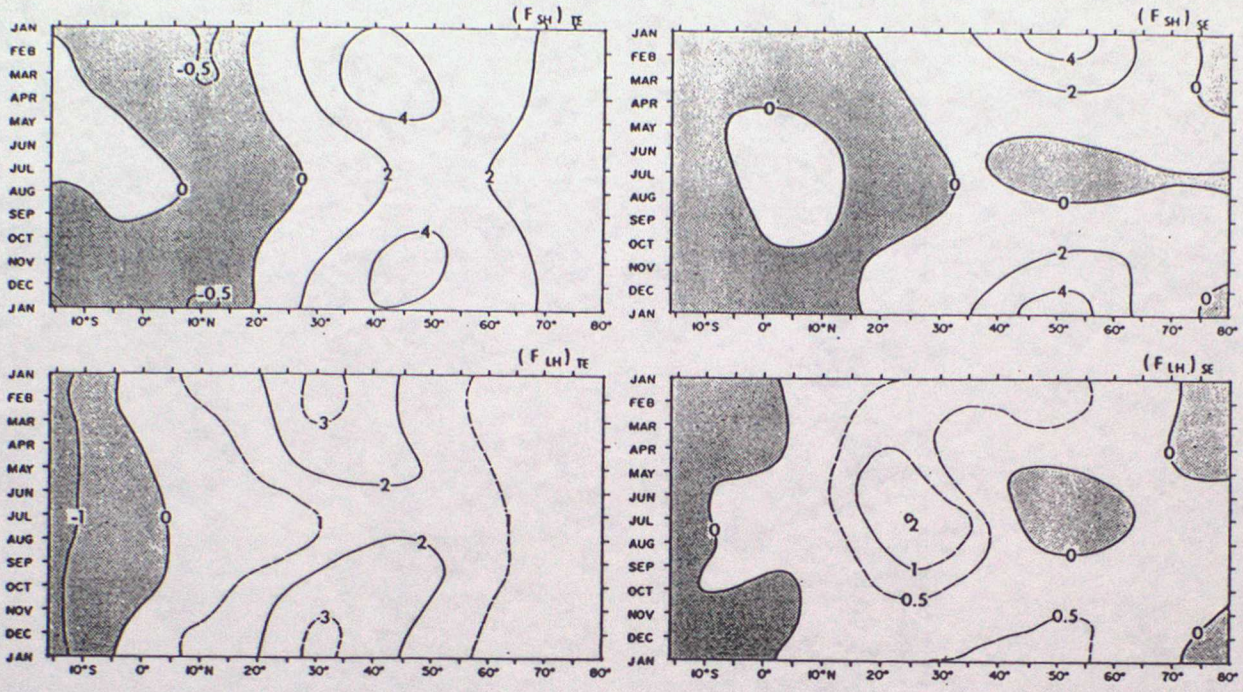

The annual variation of the transient and standing eddy fluxes (10^{19} cal day^{-1}) of sensible and latent heat.

Figure 5.20

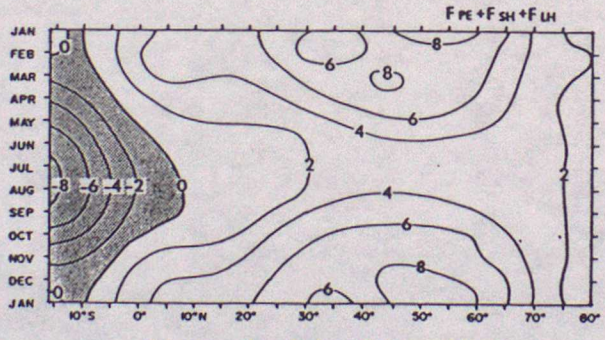

The annual variation of the meridional flux of total energy (10^{19} cal day^{-1}).

Figure 5.21

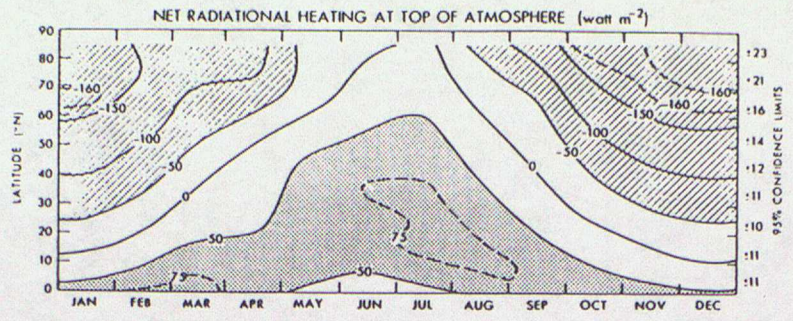

Figure 5.22

Net incoming radiation flux at the top of the atmosphere (F_{TA}) based on satellite data as a function of latitude and month of the year. Annual mean 95% confidence limits are shown on the right hand side of the diagram (see Appendix for further information.) Units are in W m^{-2}.

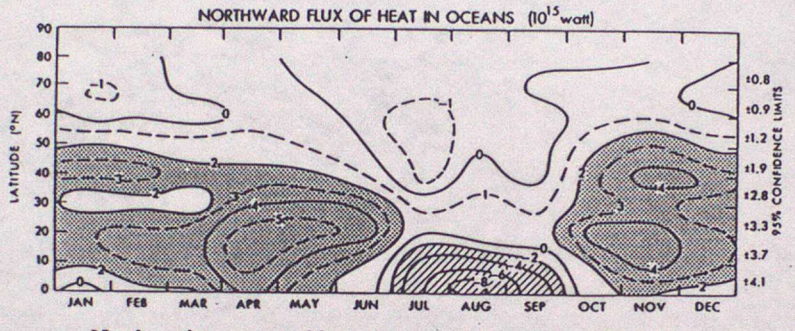

Figure 5.23

Northward transport of heat due to oceanic motions (T_O) computed as a residual term in the earth's heat balance. Units are in 10^{15} W.

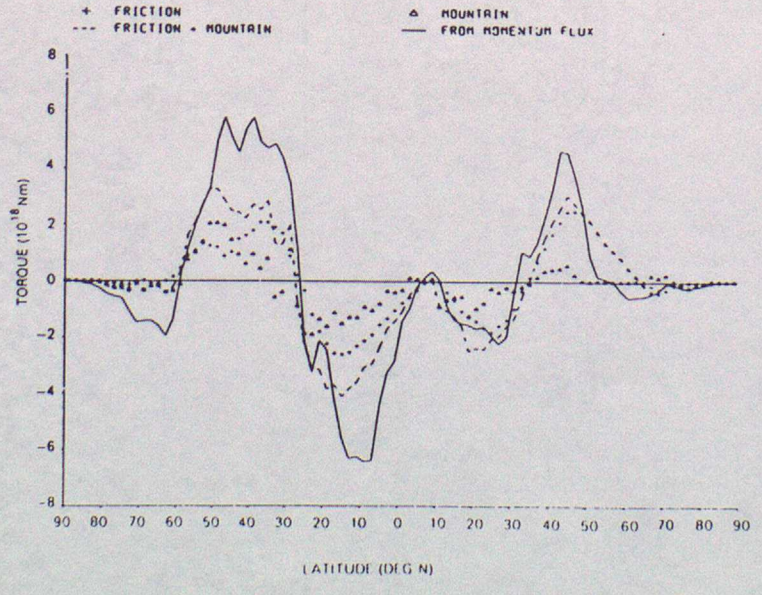

Figure 5.24

Mountain and friction torque for January 1979, compared with the total torque inferred from the atmospheric angular momentum budget.

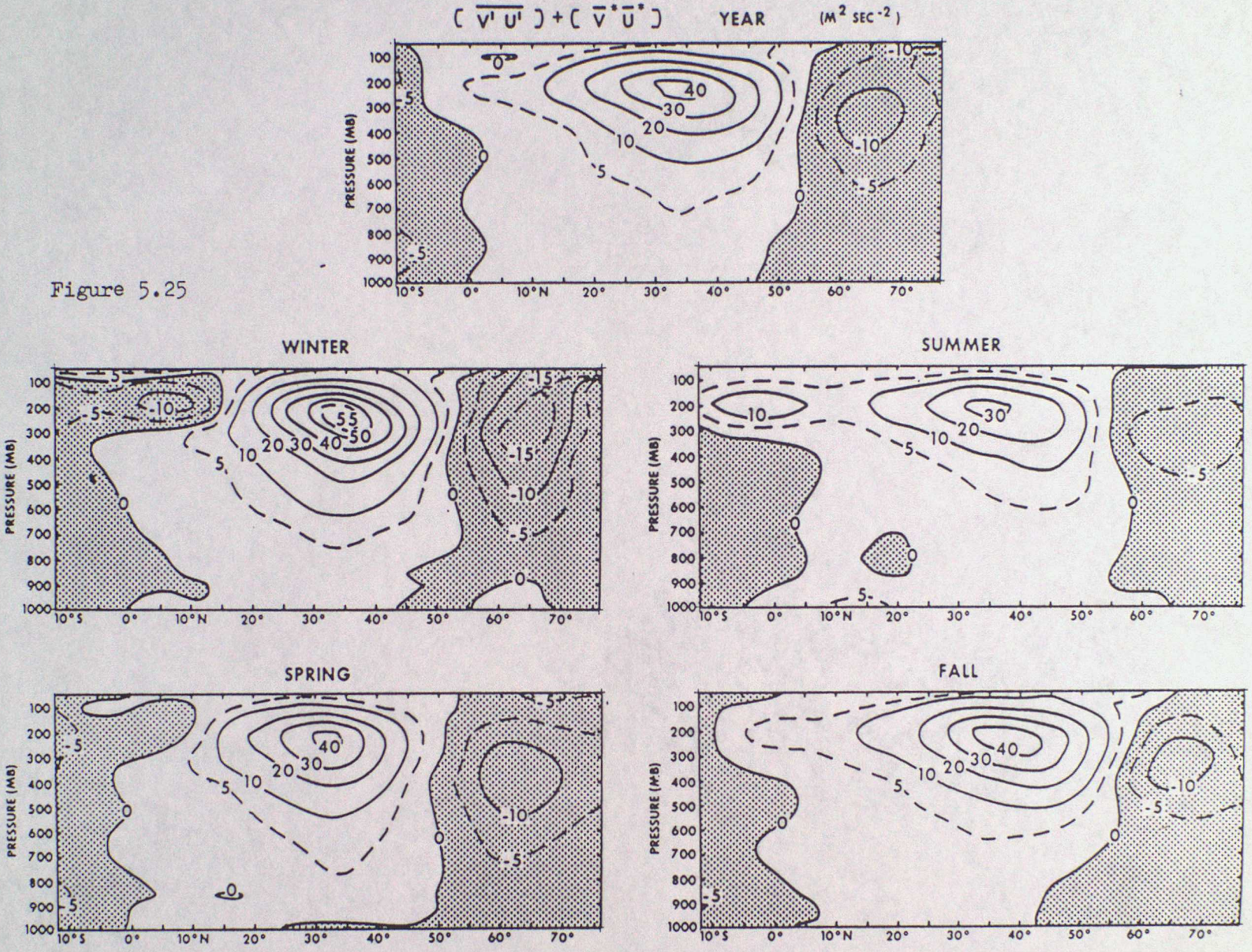

Figure 5.25

Northward transport of westerly momentum by all eddies $[\overline{v'u'}]+[\bar{v}^*\bar{u}^*]$ for year and seasons. (Units in m^2 sec^{-2}.)

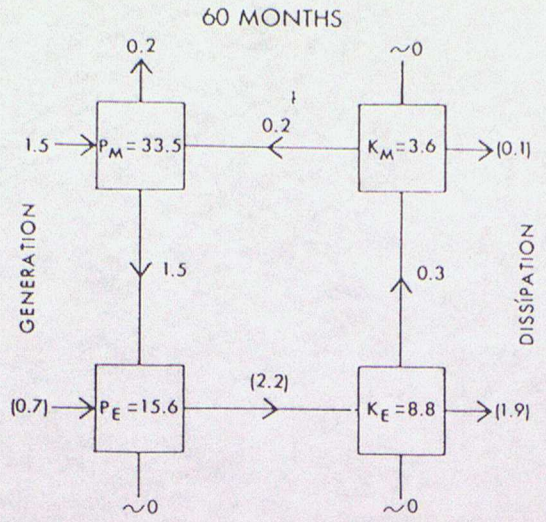

(a) Tentative diagram of northern hemispheric energy cycle in the mixed space-time domain for the long-term mean. Energy amounts are in units of 10^5 J m^{-2}; transformation rates are in units of watts per square meter.

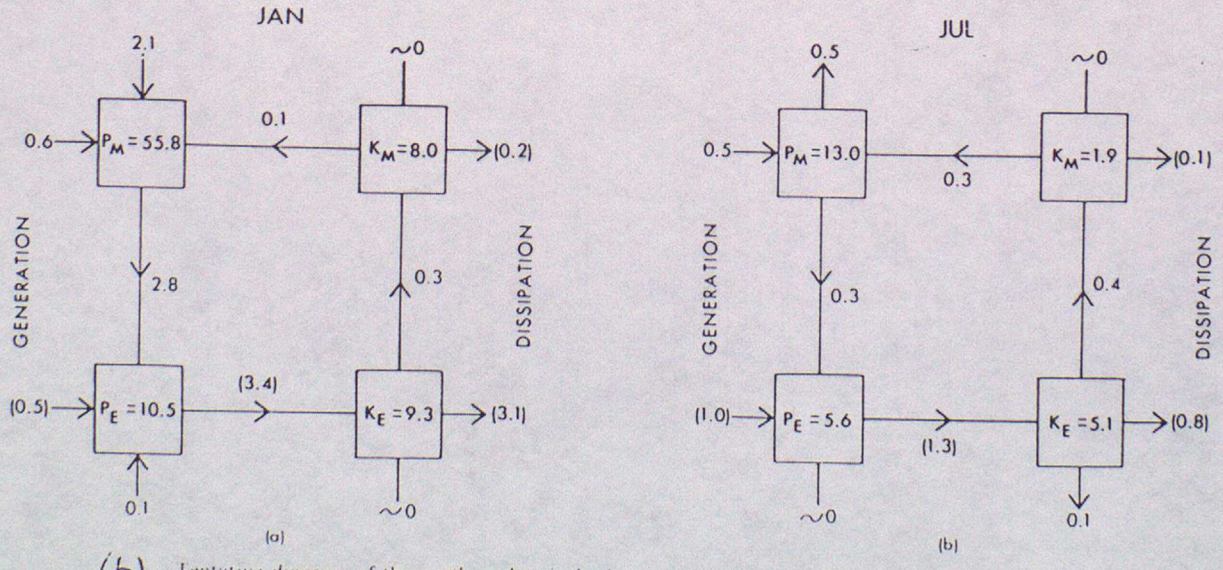

(b) Tentative diagram of the northern hemispheric energy cycle in the mixed space-time domain for a typical January (left) and a typical July (right). Energy amounts are in units of 10^5 J m^{-2}; transformation rates are in units of watts per square meter.

Figure 5.26

ENERGY DIAGRAM (GLOBAL) JANUARY 1979 250 mb–200 mb

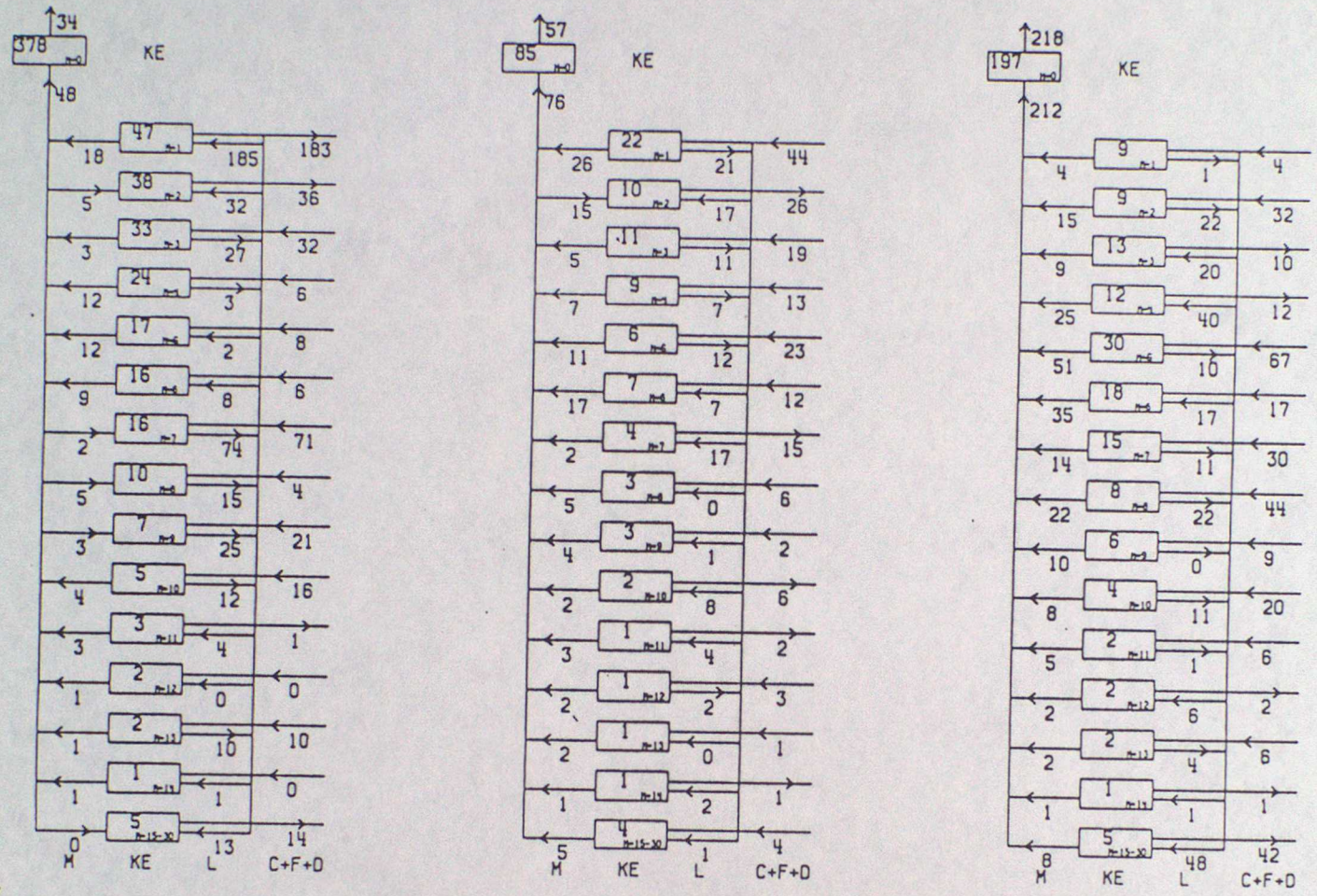

90°-20°N 20°N-20°S 20°-90°S

Figure 5.27

Energy diagram for the northern hemisphere (left) tropics (centre) and southern hemisphere (right) in the layer between 200 and 250 mb during January 1979 obtained from ECMWF anlyses. The large numbers in the boxes are the area averaged kinetic energies of the zonal Fourier component m indicated by the small number. The box at the top of the diagram is for the zonal mean field (m=o). The arrows and lines at the left side of the diagram connecting the boxes with the one at the top indicate zonal-wave interactions (M) and their directions. Similarly the lines connecting the boxes on the right side of the diagram indicate wave-wave exchanges (L). The other lines on the right and at the top indicate the residuals (the sum of conversion from potential energy, boundary fluxes, dissipations, etc). Units are in m^2 sec^{-2} for energies, m^2 sec^{-3} for the conversions.